FUNDAMENTAL STUDY OF THE AUSTENITE FORMATION AND DECOMPOSITION IN LOW-Si, Al ADDED TRIP STEELS

by

Jose Enrique Garcia-Gonzalez

B.S. Materials Engineering, Instituto Tecnologico de Saltillo, 1999

M.S. Materials Science and Engineering, University of Pittsburgh, 2002

Submitted to the Graduate Faculty of

School of Engineering in partial fulfillment

of the requirements for the degree of

Doctor of Philosophy

University of Pittsburgh

2005

UNIVERSITY OF PITTSBURGH

SCHOOL OF ENGINEERING

This dissertation was presented

by

Jose Enrique Garcia-Gonzalez

It was defended on

April 15, 2005

and approved by

Dr Judith Yang, Materials Science and Engineering

Dr Calixto I. Garcia, Materials Science and Engineering

Dr Dennis Haezebrouck, US Steel Laboratories

Dr Michael Lovell, Industrial Engineering

Dr Anthony J. DeArdo, Materials Science and Engineering
Dissertation Director

FUNDAMENTAL STUDY OF THE AUSTENITE FORMATION AND DECOMPOSITION IN LOW-SI, AL ADDED TRIP STEELS

Jose Enrique Garcia-Gonzalez, PhD

University of Pittsburgh, 2005

TRIP (Transformation Induced Plasticity) steels are under development for automotive applications that require high strength and excellent formability. Conventional TRIP steels consist of a multiphase microstructure comprised of a ferrite matrix with a dispersion of bainite and metastable retained austenite. The high ductility exhibited by these steels results from the transformation of the metastable retained austenite to martensite during straining. In conventional TRIP steel processing, the multiphase microstructure is obtained by controlled cooling from the $\alpha+\gamma$ region to an isothermal holding temperature. During this holding, bainite forms and carbon is rejected out into the austenite, which lowers the Ms temperature and stabilizes the austenite to room temperature.

In this research project, a fundamental study of a low-Si, Mo-Nb added cold rolled TRIP steel with and without Al additions was conducted. In this study, the recrystallization of cold-rolled ferrite, the formation of austenite during intercritical annealing and the characteristics of the decomposition of the intercritically annealed austenite by controlled cooling rates were systematically assessed. Of special interest were: (i) the effect of the initial hot band microstructure, (ii) the formation of epitaxial ferrite during cooling from the intercritical annealing temperature to the isothermal holding temperature, (iii) the influence of the intercritically annealed austenite on the formation of bainite during the isothermal holding temperature, and (iv) the influence of the processing variables on the type, amount, composition and stability of the retained austenite. During this research study, techniques such as OM, SEM, EBSD, TEM, XRD and Magnetometry were used to fully characterize the microstructures. Furthermore, a Gleeble 3500 unit at US Steel Laboratories was used for dilatometry studies and to simulate different CGL processing routes, from which specimens were obtained to evaluate the mechanical properties.

TABLE OF CONTENTS

LIST OF TABLES

LIST OF FIGURES

ACKNOWLEDGEMENTS

I would like to express my appreciation and gratitude to my advisors Dr. A.J DeArdo and Dr. C.I. Garcia for their guidance and encouragement throughout the course of this research project.

I would also like to thank Dr. Hua for his guidance with the TEM and STEM during the last years. I want to thank all BAMPRI and graduate students for their friendship, support, and stimulating discussions during my years here at the University of Pittsburgh. Also, I want to express my gratitude to all the faculty and staff in the MSE department. Thanks to Jinghui Wu for his help and training on the IQ analysis and to Andreas Kulovits for his help with the magnetometer. Special thanks to Dr. K. Goldman for all his advises and patient proof-reading, as well as for making corrections to my drafts.

I would like to thank US Steel and Dr. Dennis Haezebrouck for his help with the Gleeble testing, as well as for the hot and cold rolling of steel specimens. Similarly, I want to thank POSCO for their help with additional hot and cold rolling, and for the use of their simulation facilities.

Gratitude is expressed to National Council of Science and Technology in Mexico (CONACYT) for their financial support during the course of my PhD.

Furthermore, I would like to thank my parents, relatives and friends in Mexico, for their constant support and encouragement.

Finally, I would like to thank my wife Nadia, and my son Dante, for their constant praying and love, without whom this could not have been achieved. They have been my inspiration and I dedicate this work to them.

1.0 INTRODUCTION

High strength sheet steel grades have attracted the interest of the automotive industry because of the necessity to reduce car weight and to improve the safety of cars. A very promising approach to increase the ductility of high strength steels grades are TRIP (Transformation Induced Plasticity) steels. In these grades metastable austenite is transformed into martensite during deformation processes such as forming and stretching, thus yielding an outstanding uniform elongation and formability at a very high strength level.

In low alloyed TRIP steels, the retained austenite is mainly stabilized by carbon, C. The carbon enrichment in the austenite and the prevention of precipitation of iron carbides are achieved by lowering the activity of carbon in cementite, by the addition of alloying elements such as Si and an appropriate heat treatment of the cold-rolled sample.

Figure 1 shows a relationship between the fuel mileage and automotive weight[1]. The weight reduction directly contributes to the improvement of the fuel consumption of automobiles. In order to succeed in car weight reduction, it is necessary to develop sophisticated high strength steels. Unfortunately, there are various factors that hinder the application of high strength steels sheets for automotive parts, such as high production costs, poor formability, poor shape fixability, weldability problems, and hot dip Zn coating. The latter is a problem that is due to the high Si content in conventional TRIP steels, which results in surface defects and decreases

the adherence of the Zn coating to the steel sheet. Therefore, the reduction of the C and Si content and a partial or complete substitution of Si by other elements is a major importance for the industrial application of low alloyed TRIP steels.

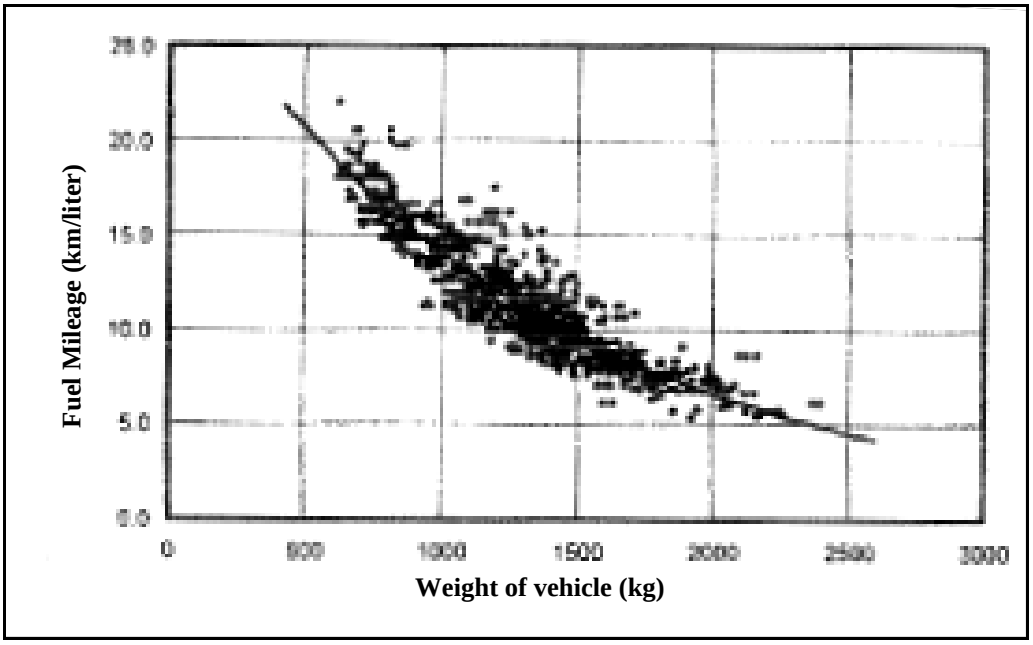

Figure 1 Relationship between fuel mileage and automotive weight

2.0 BACKGROUND

TRIP steels are known to combine high strength levels with high ductility and therefore are very attractive for the automotive industry, in particular for stretch forming applications and crashworthiness. The high ductility of this type of steel results from the transformation of metastable retained austenite to martensite under straining. This transformation is accompanied by a volume expansion and results in a localized increase of the strain hardening coefficient during straining, which delays the onset of necking and ultimately leads to a higher uniform and total elongation. TRIP steels consist of a multiphase structure consisting of an intercritical ferrite + "new" ferrite matrix with a dispersion of bainite, metastable retained austenite, and martensite.

The TRIP effect improves strength and ductility by helping to maintain a high work-hardening rate during straining. This can be explained due to two mechanisms[(2)]:

the stress assisted nucleation of martensite variants favorably oriented with respect to the applied stress, and the plastic straining of the surrounding phases due to the volume and shape changes associated with the displacive transformation.

2.1 PROCESSING OF TRIP STEEL

There are two principal thermomechanical methods for TRIP processing:

a) Intercritical annealing of a cold rolled product, combined with a holding period in the bainitic field, to obtain cold-rolled TRIP steel, and

b) Austenitic hot rolling, combined with a holding period in the austenite + ferrite field, followed by coiling in the bainitic range, to obtain a hot-rolled TRIP steel.

The chemical composition and processing routes of the TRIP-assisted multiphase steels are designed for the retention of austenite within a multiphase microstructure. In hot rolled TRIP steels, thermomechanical processing is employed to control the microstructural evolution, in order to optimize the characteristics of retained austenite. TMP is comprised of five stages: a) deformation in the austenite recrystallization region, b) deformation in the austenite non–recrystallization region: c) holding in the two phase, austenite + ferrite region, d) cooling during the transformation (run-out table), and e) coiling. Coiling takes place in the temperature range of the austenite to bainite transformation, thus, the final microstructure is strongly affected by the coiling conditions.

In the case of cold-rolled and annealed steels, the TRIP-aided steels are obtained at the end of a two-stage heat treatment. The first stage consists in an intercritical annealing (as for Dual-Phase steels) during which a controlled volume fraction of austenite is formed together with the intercritical ferrite. This intercritical annealing is followed by a fast cooling rate (15-25°C/sec) to an isothermal holding stage in the bainite transformation temperature range of 350°C to 450°C.

During this holding, part of the austenite transforms to bainite, whereas residual austenite (i.e. non-bainitically transformed austenite) may become sufficiently stabilized by carbon rejection from bainitic ferrite as to not transform to martensite during the final quenching to room temperature. As a consequence, the high carbon content in this residual austenite brings the Ms temperature below room temperature[2,3,71]. It is worth pointing out that the bainite transformation is accompanied by the carbon redistribution from the bainitic ferrite to the surrounding residual austenite. The bainite morphology appears to be in the form of upper bainite (ferrite laths) above 350°C. Below this temperature, the carbide precipitation characteristics of bainitic ferrite changes to lower bainite. All these variations in the bainite characteristics can affect the state of the retained austenite and the final mechanical properties[4].

2.1.1 Intercritical annealing

During intercritical annealing of cold rolled TRIP-assisted steel, new equiaxed ferrite is formed, and the remaining untransformed austenite is available for further transformation. Next, the steel is cooled at approximately 15-25°C/sec to an isothermal bainitic temperature (IBT) of 350°C - 450°C. Here the bainite is formed, which in turn, stabilizes the remaining austenite even down to room temperature. Most of the studies are focused on the second stage of the thermal scheme, despite the fact that intercritical annealing itself offers a significant contribution to the final microstructure and properties. Two distinct transformations take place during the intercritical annealing stage: the deformed ferrite matrix recrystallizes and austenite forms. Only part of that austenite is retained at room temperature as metastable austenite, while the other part transforms to new or equiaxed ferrite and bainite.

Samajdar et al.[5] have characterized the transformations during intercritical annealing in a Fe-0.11C-1.53Mn-1.5Si steel, and they reported that the initial formation of austenite was observed inside pearlite colonies. They claimed that the transformation may be divided in two stages: spheroidization of cementite and formation of austenite from the spheroidized cementite particles. Below 1 min annealing, they observed the austenite structure to be very fine. When the intercritical soaking time increased, a general coarsening of the austenite particles was observed while the volume fraction of the austenitic phase leveled off. Also, the Ms temperature determined by dilatometry was found to increase with longer soaking time. Even after a few seconds annealing, about 5% of retained austenite could be detected, and the measured carbon content of the retained austenite steadily dropped with longer annealing times. The rate of austenite formation was much slower than that of ferrite recrystallization, the completion of the latter being observed within about 5 seconds at 750°C. Pure austenite grain coarsening was observed for prolonged holding, beyond 4 minutes at 750°C. Austenite, in general, was less stable at long intercritical annealing times. This was in part interpreted by the influence of grain size on the stability of austenite. For a given chemical composition, larger austenite grains are expected to be less stable. Also, the high stability of intercritical austenite in the very beginning of the soaking treatment was a direct consequence of its formation process from spheroidized cementite, i.e., high C austenite. By this, the new austenite particles resulted with a high carbon content leading to a considerable stability.

The decrease in the carbon content of the retained austenite for long holding times was a direct consequence of the carbon homogenization process[5]. At the initial stages of intercritical annealing, the relative high carbon content of the austenite domains may strongly influence its stability.

Garcia and DeArdo[6] have established in previous work that the nucleation of austenite from ferrite-Fe_3C structures occurs at the interface between the α and the Fe_3C. In addition, the formation of austenite was characterized by a three stage mechanism: a) preferential nucleation of austenite at pearlite colony intersections or grain boundary cementite particles, followed by a rapid growth of austenite accompanied by cementite dissolution, b) spheroidization of the cementite particles due to their continuing dissolution and diffusion of the carbon from these particles towards the growing austenite, c) very slow growth of the austenite into the ferrite. The very final step involves the equilibration of ferrite and austenite which is controlled by Mn diffusion in austenite.

Park and Eldis[7] observed in a Fe-0.11C-0.55Si-(0.09-0.18)Mo steel that there were no undissolved carbides in specimens annealed at 760°C for 30 seconds, indicating that dissolution of carbides was complete within a short time. After complete dissolution of the carbides, the initial austenite formed would be high in carbon. As more austenite forms at the expense of ferrite, the average carbon content of the austenite decreases. The decomposition behavior of the austenite cooled at several cooling rates can be seen from the CCT diagram of these steels, Figure 2, constructed from an intercritical annealing temperature of 790°C for 90 seconds. At high Mo contents, the hardenability increased, and at all cooling rates, the austenite transformed to ferrite (α), acicular ferrite(α') and M-A, while no bainite nor pearlite was formed. At low Mo contents, it was reported that bainite (B) formed at low cooling rates.

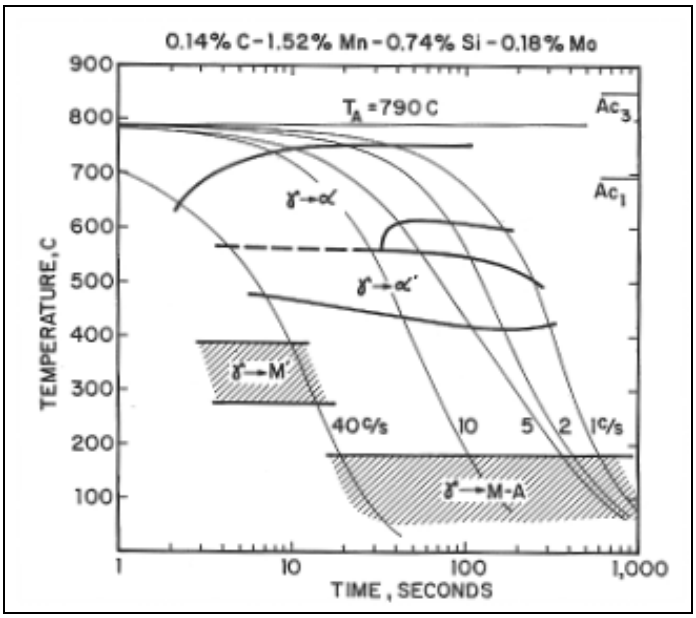

Figure 2 Continuous cooling transformation diagram of a Fe-0.11C-0.55Si-0.18Mo steel intercritically annealed at 790 C for 90 seconds

The variations in the fraction of retained austenite with respect to intercritical annealing temperature and the isothermal treatment temperature and time have been found to be quite substantial in a study by Lee et al[8]. In the case of an intercritical annealing temperature of 810°C and isothermally treated at 450°C (in a Fe-0.1C-1.5Mn-0.94Si steel), the fraction of retained austenite was close to 10% when the isothermal treatment time was 1 minute, but was reduced to 2% when isothermally treated for 10 minutes. When intercritically annealed at 780°C, it was slightly over 10% at the initial stage of isothermal treatment, and then decreased to about 4% after 10-minute isothermal treatment; this case thus showed the higher fraction of retained austenite overall than the 810°C case. Isothermal treatment at 450°C also resulted in the higher fraction of retained austenite in comparison with 470°C. Therefore, lowering both the intercritical annealing temperature and the isothermal treatment temperature worked more

favorably for the increased fraction of retained austenite and the subsequent improvement in strength and elongation.

Microstructures and fractions of retained austenite of cold-rolled steels substantially vary with the intercritical annealing conditions due to the redistribution of solute elements, particularly carbon. At a high intercritical annealing temperature, the austenite fraction increases, but a large amount of retained austenite (after the IBT) cannot be obtained because the carbon content in austenite decreases. At low intercritical annealing temperatures, the carbon content in austenite can increase, but the obtainable amount of retained austenite is also reduced because of the initially low austenite fraction. It has been reported[8] that the intercritical annealing temperature to obtain the higher fraction of retained austenite is $(Ac_1+Ac_3)/2$, however, this may not always be the best choice. The intercritical annealing should be conducted at a temperature at which the stability of austenite can be raised by increasing the concentration of alloying elements in austenite by lowering the fraction of austenite formed during the intercritical annealing. When the intercritical annealing temperature is set too low, the mechanical properties do not improve much because the fraction of retained austenite is reduced due to the reduction of the absolute amount of austenite and because retained austenite with higher stability than an appropriate stability level is formed. It is often believed that the appropriate temperature is the one at which the fraction ratio of ferrite and austenite is 50:50[8]. Furthermore, it has also been reported that the bainitic isothermal treatment at Ms+(20-30°C) produces the highest fraction of retained austenite and excellent mechanical properties.

2.1.2 Isothermal Bainitic Transformation (IBT)

The bainite transformation can be described as both diffusionless as well as a short range diffusion transformation in which the growth of a sheaf occurs by the martensitic propagation of subunits, and redistribution of carbon from these subunits to the residual austenite mainly occurs after the actual transformation has taken place. Hence, austenite is retained due to a lowered Ms point by the enrichment of carbon even after cooling to room temperature[4,9,33,38,65]. The stabilization of austenite at room temperature is due to its carbon enrichment all along the thermal scheme. Firstly, carbon concentrates within austenite during the intercritical annealing. Secondly, the bainite transformation is accompanied by carbon redistribution from bainitic ferrite to the surrounding residual austenite[2,3,9,10].

The carbide phase associated with upper and lower bainite, precipitates from the carbon enriched austenite, and is always cementite. If the carbon concentration of the remaining austenite exceeds the value given by the extrapolated $\gamma/(\gamma+\theta)$ phase boundary shown in Figure 3, then cementite precipitation from the enriched austenite lying adjacent to the platelets of bainitic ferrite, becomes possible. The shaded area in this figure represents austenite which is unstable with respect to the precipitation of cementite. Similarly, bainite growth stops when the carbon concentration of the remaining austenite exceeds the T'o phase boundary. This "stasis" between the T'o phase boundary and the extrapolated $\gamma/(\gamma+\theta)$ phase boundary, Tc, results in carbon enrichment in the remaining austenite, thereby assisting austenite stabilization. Furthermore, carbide precipitation is expected to accompany the continuation of the growth of upper bainite from the remaining austenite, if the transformation temperature is below Tc or the holding time

being long enough for the carbon concentration of the remaining austenite to reach the extrapolated $\gamma/(\gamma+\theta)$ phase boundary.

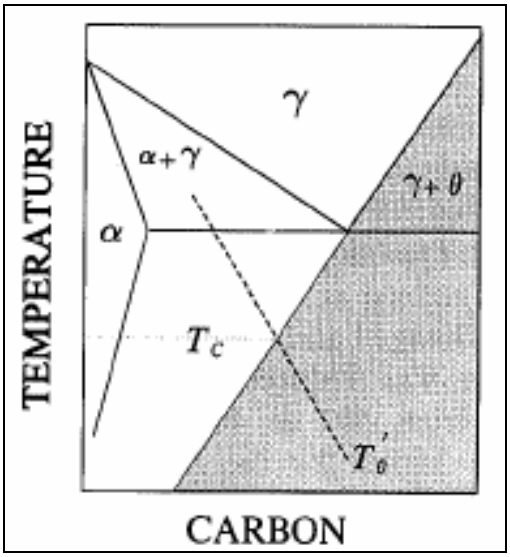

Figure 3 Schematic illustration of the condition which has to be satisfied before cementite may precipitate from the remaining austenite

The evolution of volume fraction and C content of retained austenite in TRIP steels can be explained by the possible reaction phenomena occurring during isothermal bainitic transformation. These are shown schematically in Figure 4, where three cases can occur[11]:

a) Bainite formation can proceed at the expense of austenite, which eventually disappears. For high Si additions, the reaction will never be completed, and an amount of retained austenite will be retained in the final microstructure. After long holding times, the austenite can be decomposed into a secondary ferrite and carbide phase.

b) For C-Mn-Si TRIP steels, the reaction behaviour corresponds to the "incomplete reaction phenomenon", where the retained austenite increases to a maximum, which is maintained during further holding.

c) For Al-alloyed TRIP steels, the reaction corresponds to the fully completed bainite transformation. This is because the retained austenite volume fraction increases to a maximum and then decreases while the C content still grows larger.

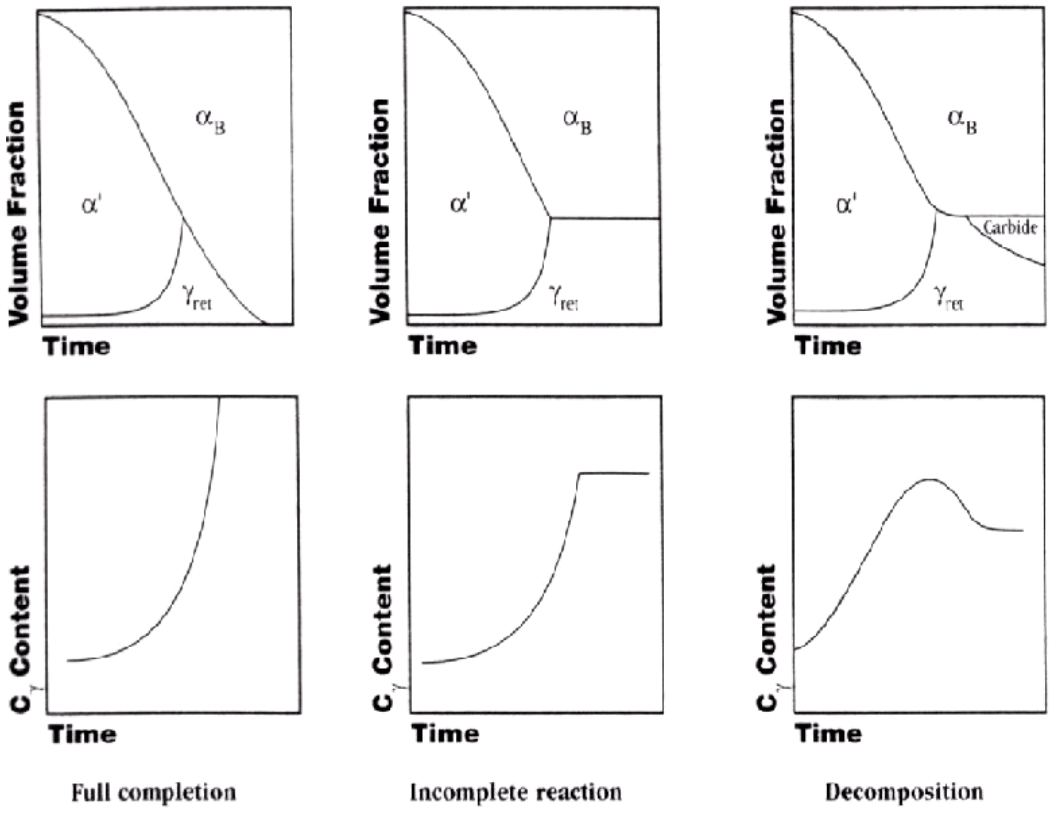

Figure 4 Room temperature phase composition and Cγ content are shown as a function of isothermal transformation

2.2 MECHANISMS OF BAINITE TRANSFORMATION

2.2.1 Continuously cooled transformed bainite

In commercially important steels, typical CCT diagrams features the polygonal ferrite transformation region shifted rightwards to regions of very slow cooling rate, exposing a broad, flat bainite transformation region. This has the advantage of an almost constant transformation start temperature for bainite over a wide range of cooling rates. However, this situation is complicated because of the wide variations in bainite microstructures that can be observed. The transformation in the bainite region does not produce a single microconstituent despite the uniformity in the transformation temperature range. The microstructures produced in this region are very complex and result from the growth of an acicular ferrite phase associated with a second constituent which may consist of carbides, martensite and/or austenite depending upon supersaturation of carbon in the austenite, the kinetics of carbon diffusion, steel compositions, etc. Acicular bainite will form at fast cooling rates, whereas granular bainite appears at slow cooling rates. At fast cooling rates within the bainitic region, a steep carbon concentration gradient is developed in the austenite, with a high carbon supersaturation at the ferrite/austenite interface. As a consequence, cementite precipitation can occur at the ferrite/austenite interface during the growth process. At slow cooling rates, the carbon gradient extends over a greater distance into the austenite and the carbon concentration is lower at the interface, making the cementite precipitation process very difficult. This increased carbon concentration in the remaining austenite can stabilize the austenite from further transformation, resulting in retained austenite which leads to the formation of a granular bainite morphology.

2.2.2 Isothermally transformed bainite

From an industrial point of view, many types of steel are processed under continuous cooling conditions and it is rare that steel is processed under isothermal conditions in the bainitic region. In conventional TRIP steels, bainite is formed by isothermal treatment. The mechanism of isothermal bainitic transformation has been the subject of numerous investigations and three distinct models have been proposed so far, and these are[12], a) displacive, b) diffusional, and c) coupled diffusional/displacive models. In the displacive model for the transformations from austenite to ferrite, it is assumed that, although the product ferrite nucleates with carbon partitioning, its growth involves a full carbon supersaturation as in the case of martensite, the alloy partitioning occurring mostly after transformation. In the case of diffusional (reconstructive) transformation, it has been reported that one-to-one atomic site correspondence at the coherent parent/product interfaces as expected in the case of ledge mechanism can produce surface reliefs similar to those in displacive transformation. The other model in an intermediate case is the coupled diffusional/displacive transformation mechanism. In this case, as far as substitutional atoms are concerned, the bainitic transformation is assumed to be in a displacive fashion but the partition of interstitial atoms is thought to occur at the advancing product/parent interfaces. This implies that bainitic reaction in interstitial-free steels should be the same as that of martensite.

The formation of surface reliefs has often been referred to as an evidence of displacive transformation. However, surface reliefs can also be formed by the diffusional ledge mechanism[12]. In the latter case, if the elastic strain due to the phase change by the ledge mechanism were built up, the progress of phase transition would be stopped by the strain energy

which consumes the driving force in the early stage of transformation, producing rather small surface reliefs. While, if such an elastic strain were relaxed also by a diffusional process, very sharp surface reliefs at higher temperatures would not be expected and the surface rumpling due to the volume change would be produced.

Both Widmanstatten structures and upper bainite in steels are lathlike. Lower bainite in ferritic steels, however, is platelike. According to Ohmori[12], the orientation relationship between the parent austenite and upper bainite is always close to that of Kurdjumov-Sachs. The habit plane and the growth direction of each lath are parallel to $\{223\}_\gamma//\{451\}_\alpha$ and $<1\text{-}10>_\gamma//<1\text{-}11>_\alpha$. This is also quite similar to that observed in lath martensite. Such a situation is difficult to explain by a direct application of the theory of martensite crystallography, but can be explained by considering the relaxation of the shape strain within the austenite matrix. Here it is assumed that the lattice invariant shear must be chosen to make the direction of the shape strain as parallel as possible to the slip direction in the matrix as well as the condition minimizing the magnitude of shape strain. In addition, a bainitic lath is assumed to be formed by the coalescence of the needlelike ferrite subunits lying parallel to the invariant line close to $<110>\gamma//<111>\alpha$ within a slip band almost parallel to $\{111\}\gamma//\{110\}\alpha$. A similar approach can be made also for upper bainite as illustrated in Figure 5. Figure 5a shows the nucleation of a needlelike ferrite subunit, the growth direction close to the invariant line being normal to this figure. Dislocations are generated also in the parent austenite at the side-edge of it where the largest elastic stress is concentrated by the shape deformation. Catalytic effects of dislocations will induce many needlelike bainite subunits within this slip band as shown in Figure 5b. The coalescence of them will produce a lathlike bainite lying almost parallel to the slip band as in Figure 5c. It should be

noted that the growth direction of a lath is normal to the figure and only the sidewise growth direction can be recognized in Figure 5c.

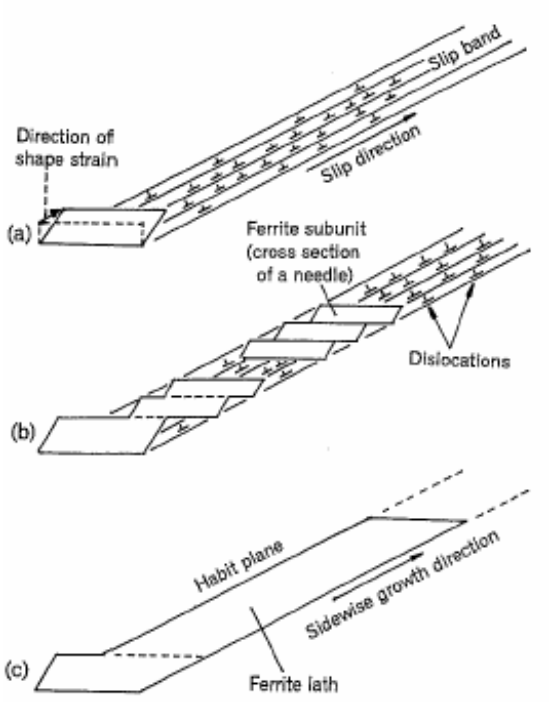

Figure 5 A model of upper bainite formation. The growth direction of either the bainite subunits or the bainitic lath which lies close to the invariant line is normal to this figure. Thus, these figures show the cross sections normal to the growth direction for either the bainite subunits or the laths. (a) nucleation of bainite subunit, (b) autocatalytic nucleation of ferrite subunits and (c) the lath formation by the coalescence of them.

Bhadeshia and Edmonds[18,19] have measured the extent of isothermally transformed bainite at the point where the bainite reaction ceases, and found that this approximately conformed with the To line, but was in disagreement with the Ae_3 composition. This effect, is known as the "incomplete reaction phenomenon", and implies that bainite does grow with a supersaturation of carbon. They pointed out that exact agreement with the To line cannot be expected since the

distribution of carbon in the austenite was not uniform. This should lead to a greater than expected volume fraction of transformation even if bainite formation involved full carbon supersaturation. Therefore, the existence of an inhomogeneous distribution of carbon is an important factor in the development of the bainite transformation.

Bhadeshia[18] demonstrated this existence of the non-uniform distribution of carbon in the austenite retained after bainitic transformation, where the carbon concentration in many cases exceeded that given by the To curve. The results, however, could be interpreted to be in accord with the contention that bainite initially forms with a full supersaturation of carbon, despite the apparent disagreement with the To criterion. This becomes clear when it is realized that austenite can continue to accumulate carbon from suitable sources, up to a maximum corresponding to the Ae3 limit, although it cannot then transform to fully supersaturated ferrite. A small region of austenite which has already been affected by the dumping of carbon from a bainite plate may become isolated by the formation of further supersaturated platelets in close proximity. The subsequent rejection of carbon from the latter can then raise the carbon content of entrapped austenite to levels beyond the To curve. The probability of such a sequence of events is high because of the nature of bainite sheaf development. An inhomogeneous distribution of carbon is also to be expected under these circumstances, since the local carbon content of any isolated region of austenite must depend on the state of isolation, the morphology and the exact sequence of transformation.

An alternative interpretation could arise if bainite growth, at all stages of transformation, involved only a partial supersaturation, the remainder being pushed ahead of the transformation interface, giving diffusion controlled kinetics. It might be assumed that the level of carbon in the

ferrite during growth must have been less than $\bar{x}$ (avg. alloy carbon content) although greater than the corresponding equilibrium concentration. It is possible to calculate the interface tie-line compositions for growth involving partial supersaturation, as shown in Figure 6. If $\bar{x}$ is the average alloy carbon concentration, the tie line X_α^1 - $X\gamma^1$ refers to the formation of bainitic ferrite with a carbon excess of (X_α^1 - $X_\alpha^{\alpha\gamma}$), with reaction termination occurring when the austenite carbon level reaches X_γ^1. Figure 6 properly depicts the conditions involved in Bhadeshia's work, since $\bar{x}$ falls to the left of the intersection of the alpha and gamma free energy curves. If the supersaturation in the ferrite is now allowed to approach $\bar{x}$, then $X\gamma^1$ tends towards X_γ^m. In the limit that $X_\alpha^1 = \bar{x}$, we obtain the unexpected result that growth involving partial supersaturation must have a minimum terminal carbon level in the austenite, given by X_γ^m. Clearly, an austenite tie-line composition less than X_γ^m., i.e., $X\gamma^2$, is physically unreasonable since it corresponds to a ferrite supersaturation exceeding $\bar{x}$. It should be pointed out, that if growth does involve the formation of partially supersaturated ferrite, it is not obvious as to why the level of supersaturation should vary as it does. It would also appear that growth under these circumstances of partial supersaturation would be unstable, and should rapidly degenerate to that involving a zero excess of carbon in the ferrite. While it seems reasonable that the hypothesis of ferrite growth involving supersaturations less than $\bar{x}$ - $X_\alpha^{\alpha\gamma}$ can be discounted, there is yet another possible interpretation. In this, the sub-units of bainite may first grow martensitically, with subsequent carbon rejection into the residual austenite, until the carbon content of the latter reaches the To line. At this point, the bainite could start growing with a lower carbon content than the now enriched remaining austenite. However, such an interpretation seems unsatisfactory since there is then no clear reason why the bainite-ferrite should not continue to grow with

successively decreasing levels of excess carbon, until reaction stops when the austenite carbon content reaches the Ae3 line. The latter does not occur, and it is believed that bainite growth involving full supersaturation is still the most reasonable interpretation of the incomplete reaction phenomenon, with the apparent discrepancy between the measured austenite carbon contents and To curves arising due to kinetic factors.

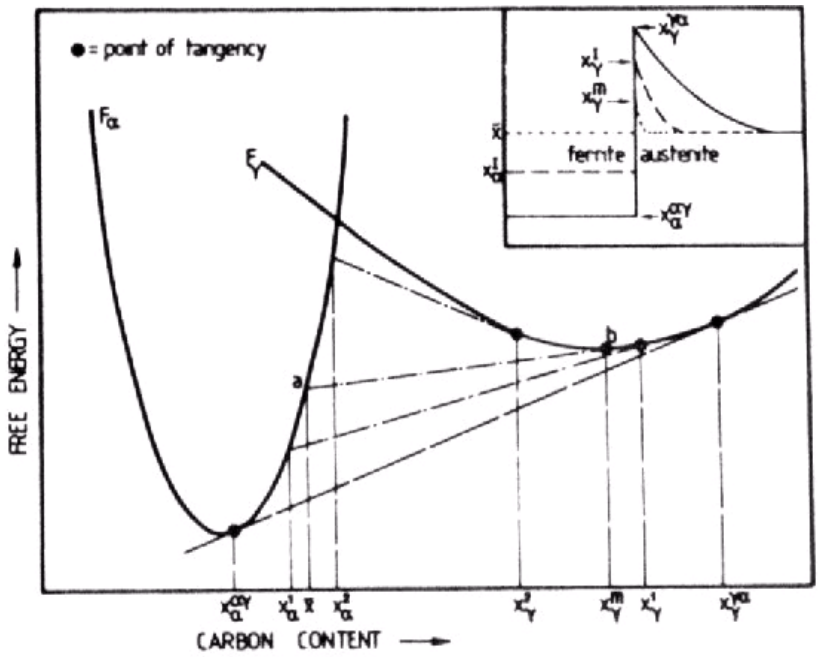

Figure 6 Schematic free energy curves for the analysis of ferrite growth involving partial-supersaturation. This illustrates the sort of composition profiles to be expected across the transformation interface, under conditions of steady-state growth, with carbon content and position relative to the interface plotted on the ordinate and abscissa respectively. Lines such as *ab* mark the tie-line compositions involved in difussion controlled growth (the general corresponding set of compositions linked by a tie line such as *ab* are labeled X_α^1 and X_γ^1)

2.2.3 Alloy partition during the bainite transformation

Carbon atoms are enriched in the untransformed austenite during the progress of bainite transformation in steels. The stage where such partition of carbon atoms occurs has been the subject for numerous arguments. In the diffusional and the coupled diffusional/displacive models, the partition is expected to occur during the progress of bainitic transformation, whereas in the displacive mechanism martensitic structure supersaturated in interstitial atoms forms first at temperatures below To and then carbon atoms are depleted from martensite.

Bainite and enriched austenite are in thermodynamical equilibrium, if the To carbon concentration is reached, which is a function of chemical composition, temperature and stress state of the austenite[13,14,21,22], Figure 3. Also, cementite precipitation in the austenite during bainite holding can occur, if the carbon concentration is situated in the extrapolated γ+θ field. The kinetics of cementite precipitation can be reduced when lowering the temperature due to slower diffusion processes. The addition of graphitizing elements, will also slow the nucleation and growth of cementite embryos.

Similarly, the bainite transformation kinetics decrease when lowering the temperature due to a slower diffusion of the carbon out of the bainite sheaves and an obstruction of the plastic accommodation of the surrounding austenite caused by its strengthening.

Matsumura et al[15] have expressed the kinetics for the bainite transformed 0.4C-1.5Si-0.8Mn steel in the form of :

$$\frac{1}{V_\gamma} - \frac{1}{V_{\gamma 0}} = \left(\frac{k_p}{p}\right)\varepsilon^p$$

where Vγ is the volume fraction of austenite, $V\gamma_0$ is the initial austenite volume fraction, k_p is a constant relating to the stability of retained austenite against deformation, and *p* is the strain exponent concerning auto-catalytic effect. The strain exponent *p* was assumed to be 1 for dual-phase steel as well as for C, Si, Mn TRIP steels. The product of tensile strength × total elongation (TSxEl) increases with the decrease in k_p as shown in Figure 7. Since k_p is a constant relating to the plastic stability of retained austenite, the fact that k_p decreases with the increase in bainite transformation time suggests that the retained austenite becomes more plastically stable by increasing bainite transformation time.

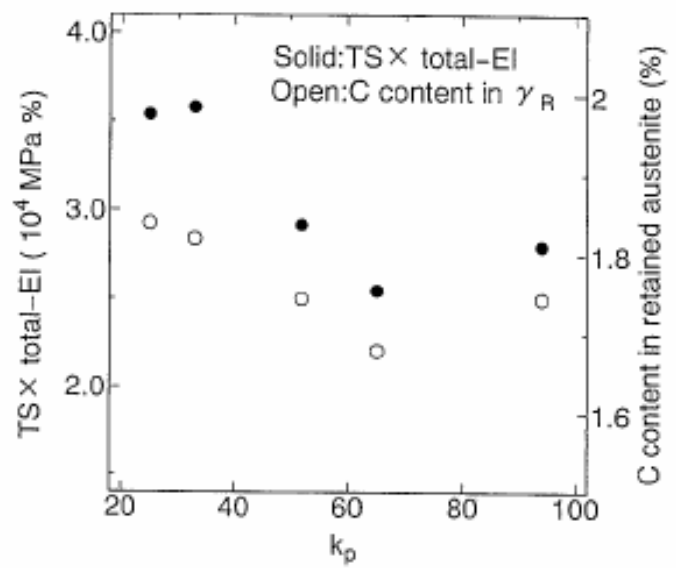

Figure 7 Effect of k_P on the TS*El and C content in retained austenite of bainite transformed 0.4%C-l.5%Si-0.8%Mn steels. The properties only in the case of k_P=94 have longer bainite transformation time than the time which gives the maximum TS*El.

Experimental evidence indicate that the kinetic properties and the partition of alloying elements in bainitic structures arise definitely out of a reconstructive phase change and are difficult to be explained by a displacive mechanism. The crystallographic properties, however, are much easily understood in terms of a displacive theory. In order to interpret these observations comprehensively, a model where the lattice change from the parent to the product phase occurs via a reconstructive mechanism and then the elastic strain due to the lattice change is partially relaxed by shear has been devised[16]. As an example for the reconstructive phase change from the parent ferrite to the product austenite with the Kurdjumov-Sachs orientation relationship, the migration of a coherent interphase boundary is illustrated in Figure 8, schematically. The plane on which the atomic sites of substitutional elements are projected is the $(-1-12)\delta//(11-2)\gamma$. The atoms on successive three atomic layers in ferrite and the corresponding two layers in austenite are projected on one plane. The open and the solid symbols are iron and substitutional alloying elements, respectively. The broken line shown in Figure 8a indicates an interphase boundary. Within the parent ferrite, the atomic exchange between iron atoms and alloying elements may occur quite frequently by thermal fluctuation. If such an exchange occurs in the parent phase in contact with the product phase into the direction favorable for the phase transformation, the interphase boundary will migrate via a small atomic displacement less than an atomic distance as in Figure 8b, the alloying elements being partitioned partially without losing the interface coherency. The repetition of these processes will lead to the successive migration of the interphase boundary, Figures 8b,c. That is, the mutual exchange of atomic sites prior to the interphase boundary migration, which leads to the alloy partition, and the individual atomic displacements at the interphase boundary will result in the lattice change with keeping the interface coherency. In the fcc to bcc transformation, the coherent interphase boundary migration

produces a large elastic strain and either considerably large atomic diffusion or shear deformation should take place to reduce it. If the elastic strain is relaxed by diffusion, the surface reliefs similar to those of martensite will not be produced and only surface rumpling due to the volume change will be observed. Whereas if the elastic strain is partly relaxed by a lattice invariant shear with forming an invariant plane, the phenomenological theory of martensite can also be applied to bainitic transformation. In the latter case, of course, the elastic strain due to the phase change with atomic site correspondence can not be completely relaxed, and the residual strain is recognized as the shape strain which is 0.2~0.3 in magnitude in the case of ferrous martensite and can be observed as surface reliefs. This model of transformation has been referred to as "Shear-Assisted Diffusional Transformation model"[16].

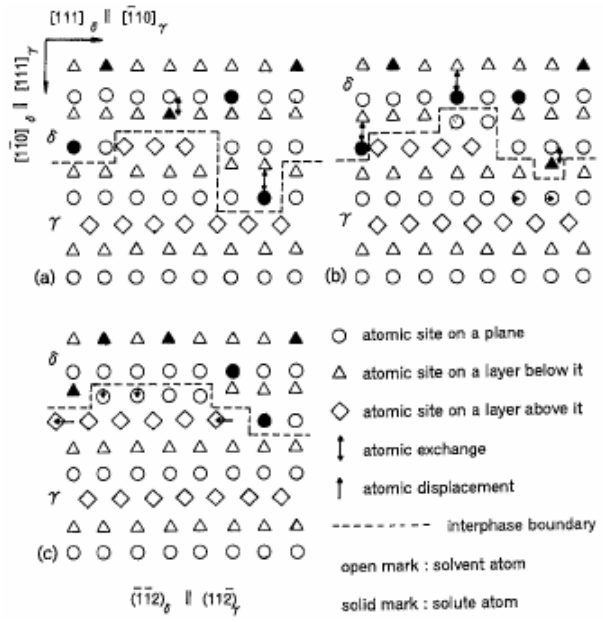

Figure 8 Diffusional migration of an interphase boundary with keeping coherency at the interface; (a) exchange of lattice sites, (b) migration of interphase boundary and slight displacements of atomic sites, and (c) further migration of the interface and the enrichment of alloying elements in the vicinity of the interface.

2.3 AUSTENITE STABILITY

Two main directions for austenite formation and stabilization have been followed in investigations performed by several researchers. The first approach concerns with austenite formation and stabilization during intercritical annealing, and the second approach is concerned with austenite stabilization during the isothermal bainitic transformation (IBT) stage.

Haidemenopoulos[23,24] studied the austenite stabilization during the bainitic transformation in triple-phase microstructures in a low alloy steel. The aim was the enhancement of uniform ductility and formability through the transformation plasticity of the metastable austenitic dispersion in ferrite/bainite/austenite mixtures, which resulted from the isothermal bainite transformation. The heat treatment schedule consisted as the following: the first step was an intercritical annealing at 770°C for 5 min to form approximately 50% austenite and 50% ferrite. Intercritical annealing was followed by isothermal transformation in the upper or lower bainite range (500 to 400°C). Following the isothermal treatment the specimens were water quenched. The isothermal transformation temperatures that were studied were 500°C, 450°C, and 400°C, while the heat treatment times were 1,2, 5 and 10 minutes. It was found that the strength properties are mostly determined by the transformation temperatures and are not significantly affected by the transformation time. Higher uniform elongation values were associated with lower bainite isothermal temperatures, with the maximum values at the second minute for a Fe-0.260C-1.48Si-0.8Mn-0.04Al and fifth minute for a Fe-0.1C-0.98Si-1.78Mn-0.03Al of isothermal transformation. In contrast with the strength properties, the uniform elongation was more strongly influenced by the holding time. The total elongation results indicated that total elongation was strongly influenced by both bainitic isothermal transformation

(BIT) time and temperature. The higher total and uniform elongation were associated with the lower transformation temperatures. Retained austenite was found to increase first and then decrease with BIT time, regardless of temperature. This behavior was attributed to the variation of austenite stability with BIT time.

At short times, the growing bainite rejects carbon to the austenite, and the carbon enrichment stabilizes the austenite. At longer times, carbide precipitation starts and carbon content of the austenite decreases and its stability drops. The maximum in the amount of retained austenite coincides with the maximum of uniform elongation, indicating a strong influence of transformation plasticity of retained austenite in plastic flow stabilization.

Itami et al[20] investigated the influence of stability of retained austenite on tensile properties in a Fe-0.14C-1.66Mn-1.94Si. Only the bainite transformation time during the IBT in the continuous annealing process was varied in order to change the C content in retained austenite. No significant difference in microstructures was detected for the specimens bainite transformed for 10, 60 and 480s, and the second phases seem to be located in grain boundaries and in ferrite matrices. Tensile strength and elongation increased with the increase in bainite transformation time. The strength-ductility balance deteriorated with the decrease in bainite transformation time. YP and yield ratio (YP/TS) become remarkably low when the bainite transformation time was short. On the other hand, the observed volume fraction of retained austenite increased from 9.5, 12.7 to 13.2% when the bainite transformation time is 10, 60 and 480s, respectively, showing the effect of austenite stabilization at longer holding times. Short bainite transformation treatment times are considered to result in unstable austenite which will transform to martensite during air-cooling after the bainite transformation treatment, therefore

decreasing the total amount of retained austenite. Figure 9 shows that the volume fraction of retained austenite decreases with the increase in strain, the behavior of which depends on bainite transformation time. The longer the bainite transformation time, the higher the volume fraction of retained austenite remains.

Work hardening occurs when the retained austenite transforms to martensite. Since the plastically unstable retained austenite transforms in the early stage of deformation, it leads to the high 'n' value only at this deformation stage. Therefore, this kind of austenite is not thought to improve the strength-ductility balance. A local neck is avoided by work hardening of ferrite, bainite and retained austenite before the critical stress when the martensitic transformation takes place. After the critical stress, 'n' value increases due to the martensitic transformation of retained austenite, and the strength-ductility balance is improved. The strength-ductility balance and plastic stability of retained austenite are improved with the increase in C content in retained austenite after optimizing the bainite transformation time. Martensitic transformation is considered to occur from the plastically unstable retained austenite with low C content.

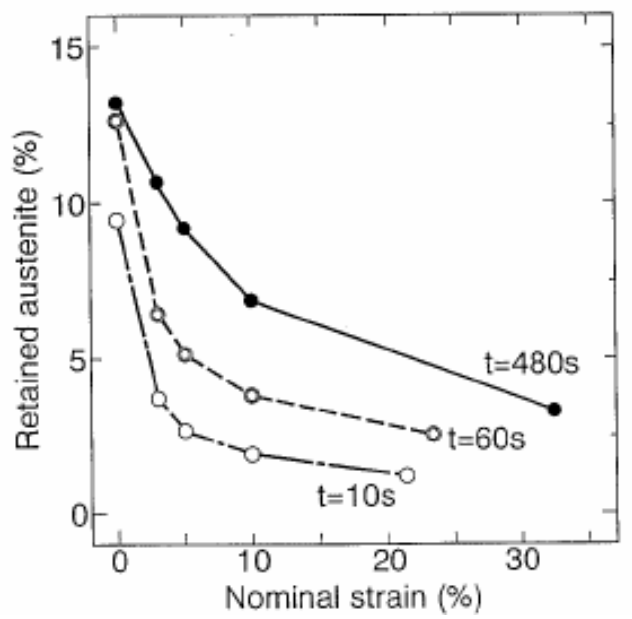

Figure 9 Effect of bainite transformation time (t) on change in volume fraction of retained austenite with deformation

Figure 10 shows the typical variation in retained austenite content with tempering treatments for 600 sec at 400°C[21]. The retained austenite is completely stable against the tempering below a given critical temperature T_H, and above this temperature T_H the volume fraction decreases drastically (T_H is therefore defined as the decomposition temperature of the retained austenite to bainite). A relationship was observed between Ms and T_H temperatures, as observed in Figure 11, for two different BIT holding times. It is found that the temperature T_H increases linearly with an increase in the Ms temperature, and these are related as:

$$T_H = 395\text{-}Ms$$

The retained austenite content $f\gamma$ reduces with an increase in tensile strain ε as the following equation:

$$\log f\gamma = \log f\gamma_0 - k\varepsilon$$

where k is a constant above zero and the value is small when the strain induced transformation of retained austenite is suppressed. The variation in k-value is summarized as follows:

(1) k-value becomes minimum at temperatures between 100 and 200°C for all the steels.

(2) The minimum value k_{min} linearly reduces with a decrease in Ms temperature of retained austenite.

(3) The temperature corresponding to k_{min}, Ts, decreases with decrease in the Ms temperature when Ms≥20C, while it is nearly constant (about 120°C) when Ms<20°C.

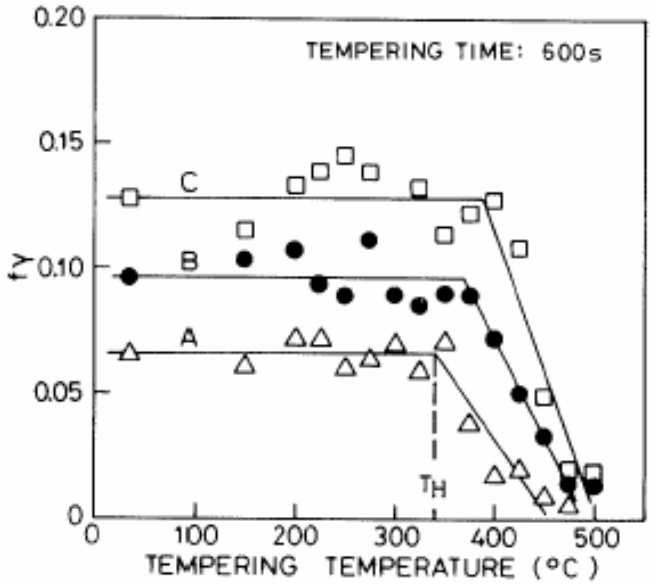

Figure 10 Variation in volume fraction of retained austenite fv with tempering temperature for various steels. T_H in the figure represents critical temperature at which retained austenite starts to decompose to bainite

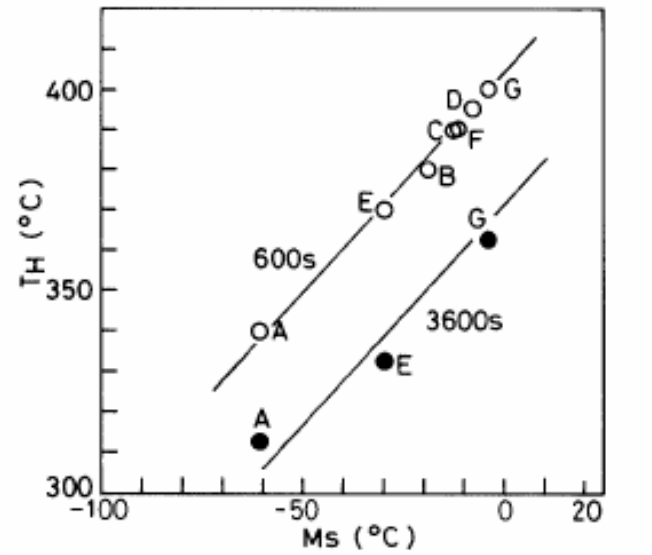

Figure 11 Relationship between critical decomposition temperature of retained austenite to bainite T_H and Ms temperature of retained austenite for unstrained steels. Numerals in the figure represent tempering time.

A reason why the temperature Ts varies with Ms temperature is considered as follows: the strain induced bainite transformation occurs preferentially instead of the strain induced martensite transformation above 200°C. From these experimental facts, the temperature Ts is considered to increase with an increase in the temperature at which the strain induced bainite transformation of retained austenite starts. In the case of Ms<20°C, at which the temperature Ts is held constant, it is estimated that there is a critical temperature below which the strain induced bainite transformation hardly occurs.

Spontaneous martensitic transformation can occur during cooling below the Ms temperature. At temperatures just above Ms, the nucleation of the transformation can be stress-assisted at the same sites at increasingly higher stress for increasing temperatures (Figure 12a). In this regime, the transformation can be modelled by incorporating the thermodynamic effect of the applied stress in the theory developed for the cooling transformation, Figure 12b. Above the Ms temperature, when the transformation stress exceeds the yield stress of the austenite, plastic yielding occurs before the transformation (Figure 12a). In this regime, the nucleation is strain-induced on potent sites created by plastic strain. The driving force for the austenite to martensite transformation can be written as a sum of chemical and mechanical contribution. The chemical driving force for the martensitic transformation is a function of the chemical composition of the austenite (C,Mn,Si, Al…). The chemical stabilization of the retained austenite can be easily estimated from the Ms temperature.

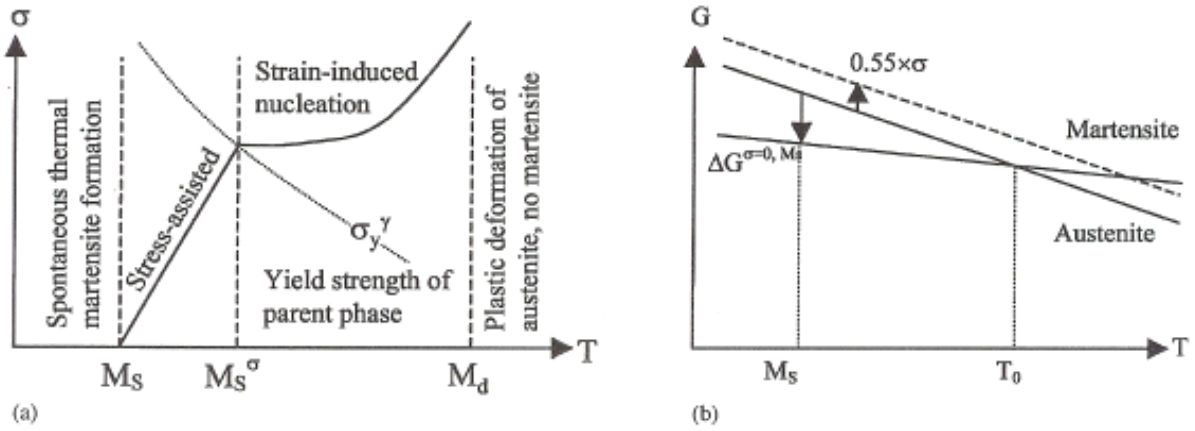

Figure 12 (a) Evolution of the martensitic nucleation stress with temperature, (b) Gibbs free energy curves versus temperature and effect of an applied stress σ

Strain induced transformation of retained austenite can be suppressed considerably with an increase in temperature, as in warm forming. Warm deformation is expected to be connected with retained austenite stability, Ms temperature, and strain induced transformation behavior.

Sugimoto et al[21,25] also found that the testing temperature dependence of total elongation differs among different steels with varying silicon and manganese content, and the largest total elongation ca be obtained at a given temperature between 23 and 175°C, i.e., a peak temperature. The peak temperature T_P(°C) increased with increase in silicon and manganese contents (which in turn affects the carbon concentration in retained austenite) and is related to Ms temperature of retained austenite as:

$$T_P=3.04Ms+187$$

The strength-ductility balance at the peak temperature was found to increase linearly with increase in the initial retained austenite content. Also, an increase in silicon content was concluded to be effective to obtain a larger strength-ductility balance. It is in the form of solute in the ferrite and strengthens the ferrite matrix while at the same time results in a small decrease in the ductility. The maximum total elongation was obtained at a given temperature between Ms and M_d, at which the strain induced transformation was suppressed moderately.

While it is known that the improvement of mechanical properties is primarily related to the initial volume fraction and the stability of retained austenite, little is known on the possible influence of the other phases surrounding retained austenite. Jacques et al[2,3,10] investigated the resistance of the dispersed retained austenite to mechanically induced martensitic transformation on two steels which differed by their silicon content. The high silicon TRIP steel contained 1.5% Si, whereas the low silicon TRIP steel contained 0.38% Si. The different specimens presented the same volume fraction of austenite with identical grain size, but different phases surrounding the austenite grains. In fact, these specimens differed by the carbon content of retained austenite and by the nature and volume fractions of the phases constituting the "matrix" in which the austenite grains are dispersed. In the case of the low silicon steel, the second phases changed only as a consequence of the change of the bainitic holding time. Also, only these steels contained some martensite. These differences influence in a large way the true stress-true strain curves, as well as the evolution of the incremental work hardening exponent (Figure 13, 14).

Furthermore, even though all specimens contained about the same initial content of retained austenite, the rate of austenite transformation during plastic straining was different, since the retained austenite content decreased faster for the specimens with the low silicon content. An interpretation of the mechanisms by which the interactions between the various

phases constituting the microstructure affect the austenite stability is as follows. The present microstructures can be considered to consist of a discontinuous composite in which the austenite grains constitute the reinforcing phase dispersed in a ferrite-based matrix that globally presents a lower flow strength than the reinforcement particles. Also, the presence of hard martensite grains in the matrix can be assimilated to a strengthening of the matrix that leads to a change in the partition of the stress between the constitutive phases. The strengthening of the matrix by martensite, brings about a sort of “shielding” effect that causes a decrease of the austenite transformation rate. This stronger matrix leads to a smaller mean-stress level within the austenite grains and thus, a postponed triggering of the martensitic transformation. Another important observation is that, the film-type austenite located between bainitic ferrite laths cannot easily transform during straining.

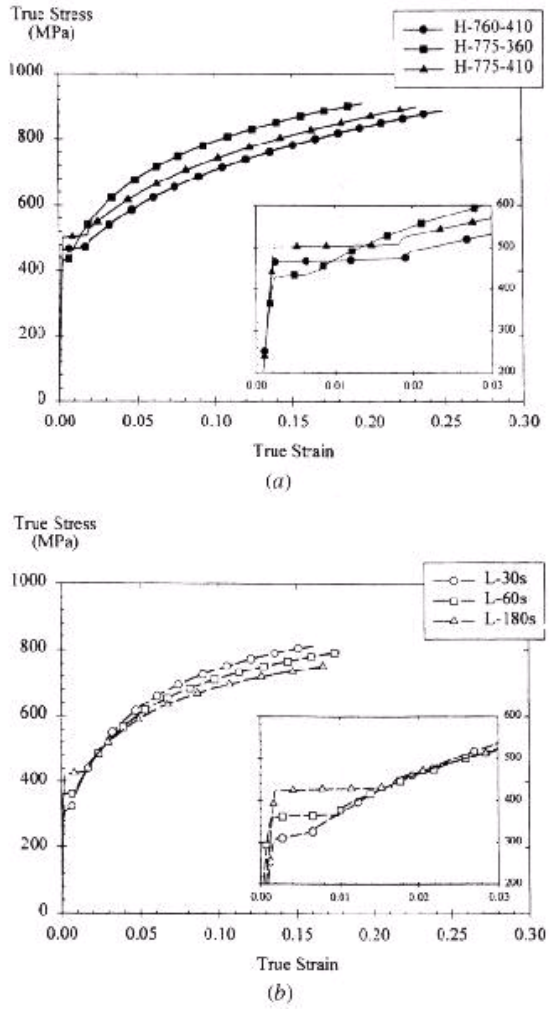

Figure 13 True stress-true strain curves of a) specimens of high silicon and b) specimens of low silicon

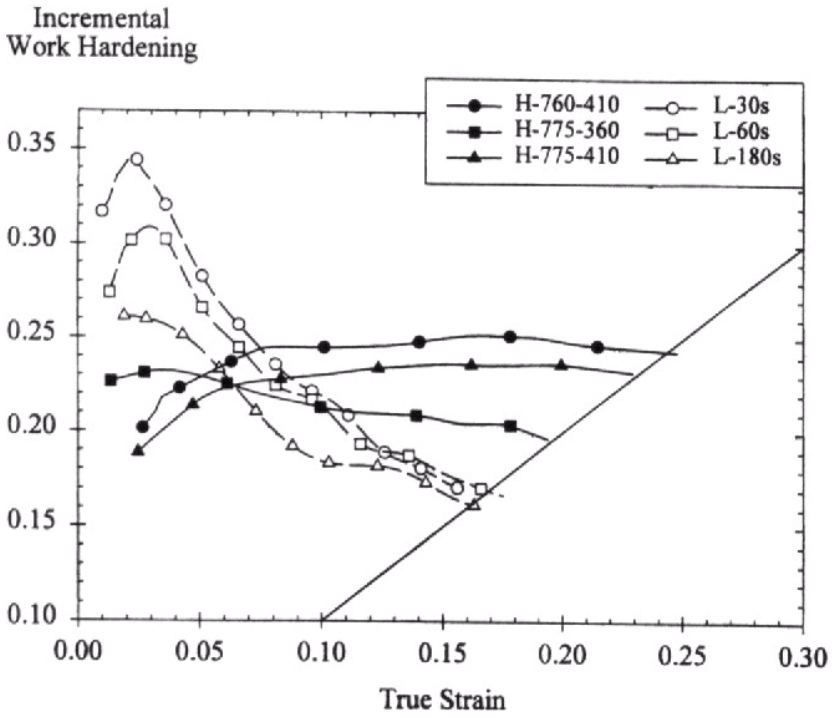

Figure 14 Incremental work-hardening curves (n_{incr}) of the different specimens of high and low Si steels

2.3.1 Effect of Austenite Morphology

In general, retained austenite morphology in TRIP steels is classified into two groups by the type of phase surrounding it as follows[25].

(Type 1) Isolated retained austenite islands, and granular retained austenite, lying in a soft ferrite matrix or on the grain boundary, adjacent to or away from the other hard second phases such as bainite or martensite.

(Type 2) Retained austenite thin films existing along martensite or bainite lath boundary, or blocky retained austenite in these hard second phases.

The Ms temperature of the retained austenite is expected to be mainly affected by hydrostatic pressure as well as carbon concentration. Hydrostatic pressure constrains a volume expansion and shear deformation accompanied with strain induced martensite transformation. If an isotropic transformation strain expressed as $\varepsilon^* = 0.0058 + 0.0045C\gamma$ occurs on the martensite transformation, the resultant hydrostatic pressure σ_p can be estimated using the following equation[25]:

$$\sigma_P = \frac{2}{3}\left[Y_0 + 2H_0\varepsilon^*\right] + \frac{2}{3}Y_0 \ln\left[E\varepsilon^* / (1-\upsilon)Y_0\right]$$

where Y_0, H_0 are yield stress and strain hardening rate of a given phase surrounding retained austenite particle, respectively. E and ν are respectively Young's modulus and Poisson's ratio, and are assumed to be equal for all constituents. From this equation, high hydrostatic pressure of about 1560Mpa occurs in retained austenite films of type 2 (γ_r-type 2), if Y_0= 1000 Mpa and H_0=5000 Mpa for bainite phase, Cγ=1.34 mass%, E=206000 and ν=0.28.

On the other hand, lower hydrostatic pressure of about 900Mpa arises in the retained austenite islands of type 1 (γ_r-type 1), if Y_0=400 MPa and H_0=1000 MPa for ferrite phase and Cγ= 1.26 mass%. According to the work of Radcliffe and Schatz[26] using plain 0.3-1.2%C steels, the Ms temperature decreases by about 6°C per hydrostatic pressure of 100 MPa. Therefore, Ms temperature of retained austenite in γ_r-type 2, should be estimated to be reduced by 40°C due to hydrostatic pressure, compared to γ_r-type 1.

The effects of second phase morphology on volume fraction, stability and morphology of retained austenite in a 0.17C-1.41Si-2.0Mn TRIP-aided dual phase steel was investigated by Sugimoto and Misu[25]. They found that when the second phase morphology was a network

structure along the ferrite grain boundary or an isolated fine and acicular one along previous martensite lath boundary, a large amount of carbon-enriched isolated austenite particles retained in the ferrite matrix, adjacent to or away from bainite. On the other hand, a small amount of retained austenite thin film was observed along bainite lath boundaries, when the second phase had an isolated coarse structure. The Ms temperature of the retained austenite films was estimated to decrease by 70 to 110°C compared to isolated retained austenite particles due to higher carbon concentration and higher hydrostatic pressure.

Also, a steel with a network structure or an isolated fine and acicular of second phase, resulting in γ_r-type 1 had lower flow stress and greater ductility compared to a steel with an isolated coarse structure of second phase, which results in γ_r-type 2. The excellent ductility in the former was concluded to be caused by the TRIP effect of the retained austenite as well as the network effect or the fine grain size effect of second phase morphology itself. On the other hand, retained austenite films (γ_r-type 2) in the later type of microstructure hardly influenced deformation behavior.

The formation processes of stabilized granular γ_R are explained as follows. As heating in intercritical range is performed after cold rolling, extremely fine granular austenite grains, in which C enriches rapidly to nearly equilibrium state at that temperature, are formed along ferrite grain boundaries. If the steels with such fine austenite grains surrounded by untransformed recrystallized ferrite matrix are quenched to and held at the bainite transformation temperature, the growth of equiaxed ferrite could have an advantage in view of energy compared to that of lath ferrite. The similar phenomenon of ferrite lath growing to its transverse direction was previously observed at the later stage of bainite transformation. Besides that, it is to be noted that

some recovery goes on simultaneously with transformation. A sequence of forming stabilized granular γ_R could be explained as mentioned above.

Similarly, Hanzaki and Yue[28,43], also carried out a systematic investigation on the ferrite formation characteristics and their effects on the state of the retained austenite. To determine the effect of ferrite quantity on the amount of retained austenite, the specimens were held at a temperature below the Ar_3 (650°C) for various times, followed by quenching into a salt bath. All the specimens before air cooling to room temperature were held isothermally at 400°C in the salt bath for 2min. The variation of retained austenite quantity with the amount of ferrite for steels with and without Nb, for similar prior austenite grain sizes, is shown in Figure 15. It seems that, there may be an optimum volume fraction of ferrite (i.e., an optimum volume fraction of untransformed austenite) which maximizes the amount of retained austenite, although for large amounts of ferrite (hence, low amounts of untransformed austenite) the retained austenite falls significantly. The existence of an optimum ferrite fraction which leads to a maximum amount of retained austenite appears to be repeated for all austenite grain sizes. The observed changes in the retained austenite characteristics, mainly volume fraction, with ferrite quantity and with the combined effects of prior austenite grain size and ferrite fraction (Figures 15, 16), can be rationalized from a morphological and compositional variation point of view. According to a geometrical configuration, the only way to stabilize the remaining austenite is by trapping the austenite through the impingement mechanism during growth of polygonal ferrite. The remaining austenite has a smaller particle size (smaller than r_{crit} for the austenite to martensite transformation), thereby assisting in its stabilization. In general, an increase in V_{RA} would be expected with increasing ferrite quantity, and decreasing austenite grain size. However, these

factors also influence the compositional variations in the remaining austenite during ferrite formation. This can be rationalized as follows: during the formation of ferrite, carbon diffuses in the austenite ahead of the α/γ interface. Figure 17a shows a portion of the Fe-Fe_3C diagram, and Figure 17b shows a plot of carbon concentration normal to the α/γ boundaries. In this case, since equilibrium is assumed to be attained only at the α/γ interface, the carbon concentrations in α and γ at this interface, denoted by $C_\alpha^{\alpha\gamma}$ and $C_\gamma^{\gamma\alpha}$, respectively, correspond to those of the equilibrium phase diagram. As can be seen in Figure 17c, by increasing the holding time or ferrite volume fraction at a given temperature, the remaining austenite becomes more homogeneous with respect to carbon. Also the average carbon concentration of the untransformed austenite is increased.

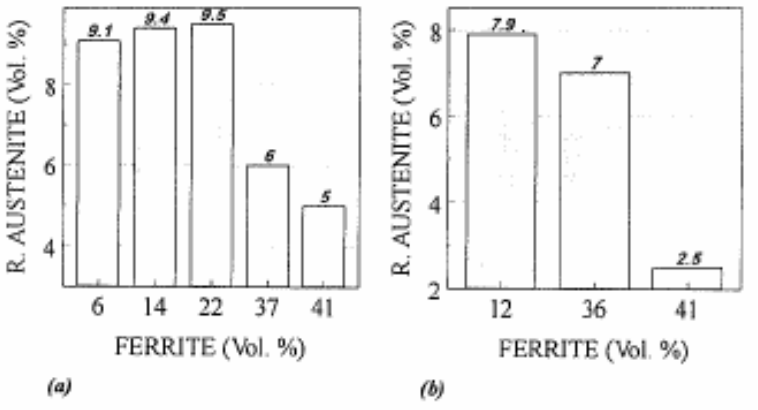

Figure 15 Variation of the retained austenite volume fraction with the amount of ferrite; (a) steel A with the prior austenite grain size of 40 um and (b) steel B with the prior austenite grain size of 45um

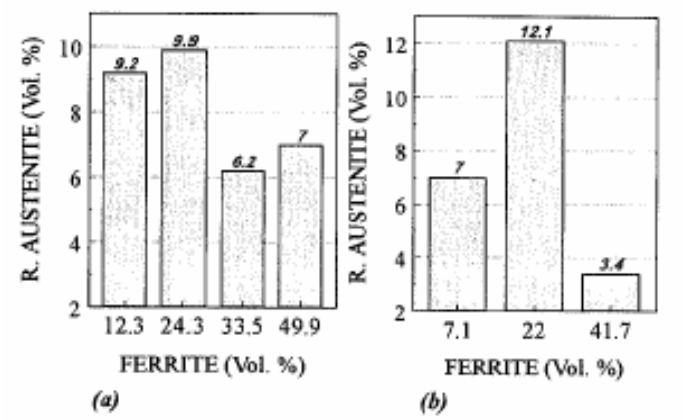

Figure 16 Variation of the retained austenite volume fraction with the ferrite quantity of steel A for different prior austenite grain sizes; (a) 70 um and (b) 230 um

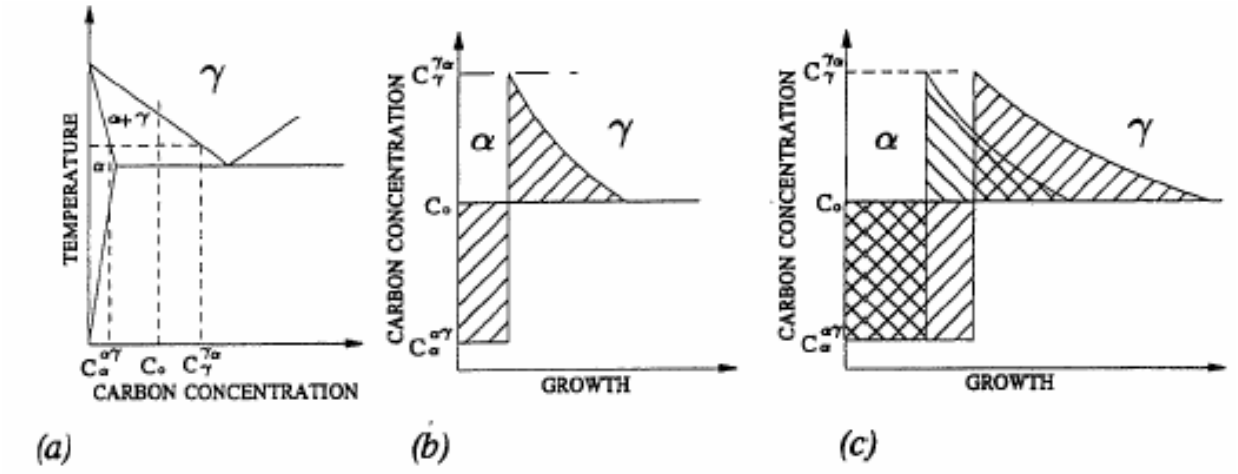

Figure 17 (a) A portion of the $FeFe_3C$phase diagram, (b) carbon concentration profile along a direction perpendicular to the austenite/ferrite interface, (c) carbon concentration profile in front of growing ferrite at different time intervals or different volume fractions of ferrite.

It was found that a decrease in the ferrite grain size by pancaking does not increase the retained austenite quantity. On the other hand, refining the grain size by dynamic transformation, i.e., deforming isothermally at a temperature below Ar_3 (the two phase region), has the effect of retaining more austenite compared to pancaking. Ferrite grain refinement increases the total area of the austenite/ferrite interface. This, in turn, increases the rate of carbon and Mn diffusion during the ferrite growth, leading to faster partitioning of alloying elements. By straining in the two phase region (during transformation) the rate of transformation is much increased, thereby decreasing the ferrite grain size significantly more than pancaking. It also introduces dislocations in the ferrite, increasing the rate of diffusion and thus accelerating C and Mn partitioning into the remaining austenite.

Furthermore, to study the effect of ferrite morphology, Hansaki and Yue[4,28] generated acicular ferrite in addition to polygonal ferrite. To achieve this, the isothermal hold in the two phase region and the quench in the salt bath stages were substituted by continuous cooling in the furnace (in the two phase region) and with compressed air and argon (from the two phase region to the bainite holding temperature). The presence of acicular ferrite in the Nb added steel resulted in a significant increase in the quantity of retained austenite. The opposite is, however, observed in the steel without Nb addition. In both steels, the retained austenite is mostly enclosed by fine acicular ferrite or coarse granular bainite. Essentially, the prior austenite grains have been fragmented by these phases, and the distributions of the retained austenite is dictated by this grain fragmentation. Therefore, these smaller particles of austenite tend to be retained through the geometric effect.

The results of the steel without Nb addition are contradictory because of the presence of pearlite in its microstructure. This is because the pearlite transformation start temperature of this steel is higher than that of the Nb-added steel, and the same continuous cooling procedure was used regardless of this effect. The formation of pearlite decreases the carbon in the remaining austenite, leading to a reduction in the retained austenite volume fraction.

2.4 EFFECT OF PRIOR PROCESSING HISTORY

Although much work has been generated on cold-rolled and annealed TRIP steels, little attention has been paid to the effect of prior hot rolling of these steels. It is usually assumed that the subsequent processing after hot rolling radically alters the microstructure, presumably much reducing any effect of the prior microstructure.

Jiao et al[29] studied a Si–Mn TRIP steel microalloyed with Mo and Nb which was subjected to heat treatments (no effect of rolling schedule was studied) designed to create several different types of ferrite microstructures. These were then subjected to cold rolling and TRIP annealing, and the subsequent tensile properties and retained austenite characteristics were then determined. The heat treatments, are shown schematically in Figure 18. The main difference in the resulting microstructures is a variation in the respective volume fractions of bainite and proeutectoid ferrite. At 650°C, longer times led to increased levels of proeutectoid ferrite. The true tensile strain-stress curves from tensile test after intercritical annealing are shown in Figure 19. In general, the specimens that had prior microstructures that were predominantly bainitic had significantly inferior ductility. Also, the steels with the highest fractions of prior proeutectoid

ferrite exhibited much superior strengths. The retained austenite volume fractions were all similar, whereas the retained austenite carbon concentrations exhibited more variability. A higher carbon concentration resulted in superior ductility.

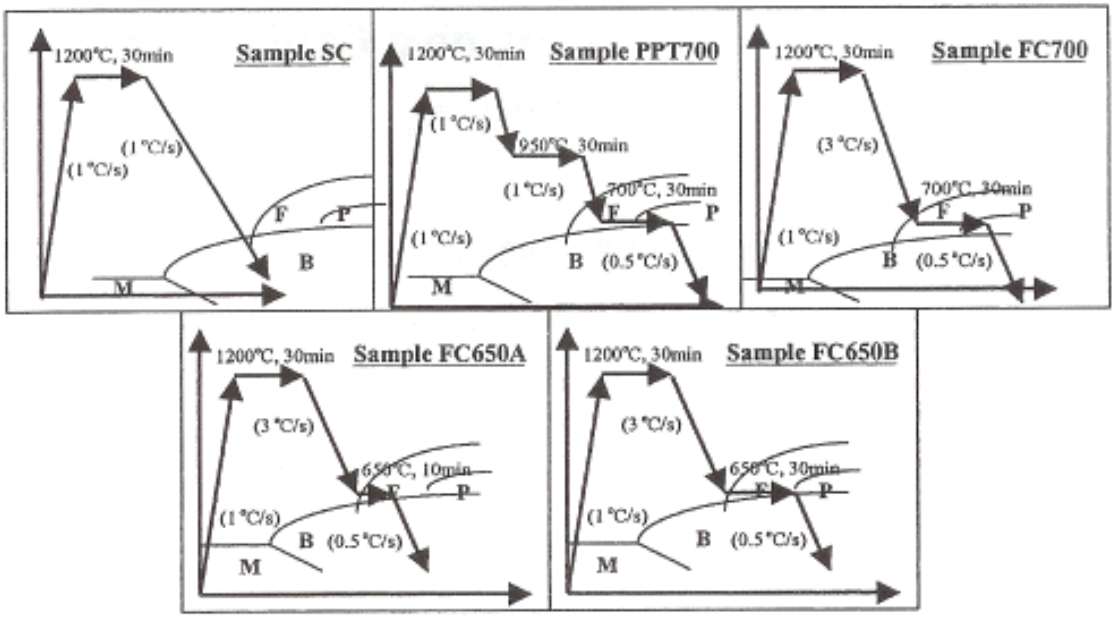

Figure 18 Heat treatments routes to achieve different hot band microstructures

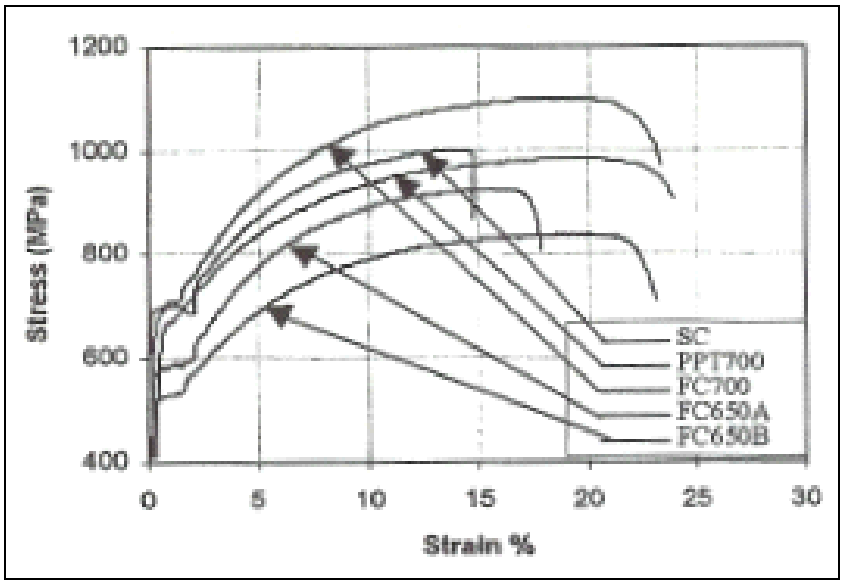

Figure 19 True strain-stress curves of tensile test for the samples in Figure 18 after the intercritical annealing treatment

The variation in enrichment level of retained austenite for different samples was reported to be due to the different proeutectoid ferrite volume fractions in the microstructures. It also appeared that good mechanical properties did not always coincide with high fraction of retained austenite, while on the other hand, the variation of carbon concentration in retained austenite corresponded far better with the mechanical properties. The stability of the retained austenite increased with increasing retained austenite carbon concentration and decreasing retained austenite particle size.

2.5 ALLOYING EFFECTS

2.5.1 Si and Mn

Silicon is known to inhibit cementite formation in steels. This is explained by the relative insolubility of silicon in cementite requiring the diffusion controlled rejection of silicon at the transformation front which in turn results in a silicon concentration build-up during an early stage of growth. This locally increases the activity of carbon so that the carbon flux is reduced and further development of the cementite embryos is inhibited[29]. A significant amount of austenite is retained in steels containing about 2%Si when cooled to room temperature through the bainite transformation region. While it has been established that carbon is one of the most beneficial elements for retaining austenite, sheet steels with a high carbon content (over 0.2%) are disadvantageous in applications which require spot welding.

Sugimoto and Usui[21] investigated the effects of silicon and manganese content on the volume fraction and stability of retained austenite particles in a cold rolled Fe-0.2C-(1.0-2.5)Si-(1.0-2.5)Mn TRIP steel. The BIT was 400°C for 1000 seconds followed by cooling in oil. The cooling rate from the intercritical annealing to 400°C was 120 C/sec (which is very high compared to the 5-25°C/sec in continuous galvanizing lines). They observed that the volume fraction of second phases increases with increasing manganese or silicon content, and the initial volume fraction of retained austenite increases with increasing silicon and manganese content, up to a 2.0%Mn. On the other hand, the carbon concentration $C\gamma$ reduces with increase in silicon and manganese contents.

Matsumara et al[31] investigated in three steels with varying silicon content, the variation in carbon content in the retained austenite during BIT, as well as the evolution of phases and morphology. They found that, in general, 1) Cγ increases with isothermal holding time to its largest ($C\gamma_{max}$) followed by decreasing., 2) In steels held at 350°C, Cγ remains 1-1.20/0 as early in the holding times as unstable γ_R co-exists with martensite. The above value, therefore, can be regarded as the lowest of Cγ($C\gamma_{min}$), 3) With a rise in holding temperature, the curve of Cγ vs holding time shifts to shorter times, while $C\gamma_{max}$ itself becomes slightly lower, and 4) The curve of Cγ vs holding time shifts to longer times with an increase in Si additions.

According to Takahashi[32], manganese addition may lower Ar_3 and To temperatures, so that the carbon concentration in austenite at To temperature reduces relatively although the volume fraction of austenite phase increases. On the other hand, an excess adding of manganese can lower so much the carbon concentration in austenite at the To temperature that the bainite transformation starts preferentially prior to formation of carbon-enriched austenite. Therefore, the volume fraction of bainite increases considerably resulting in the decrease in volume fraction and carbon concentration of retained austenite. This theory cannot be applied to explain the effect of silicon content on retained austenite because silicon hardly influences To temperature.

Baik et al[33] analyzed the effect of alloying elements on the volume change of transformed phases and the relation between the phase transformation and the mechanical properties in cold rolled TRIP steels. Figure 20 shows the change of strength and elongation as a function of the intercritical annealing temperature for 0.14C steels containing various contents of Mn, Si and Nb. The volume fraction of second phases is strongly influenced by the chemical

composition. The volume fraction of bainite was increased when the content of Mn was increased, because the volume of austenite was increased during intercritical annealing with the content of austenite stabilizing element, Mn. The volume fraction of bainite was increased with decreasing the content of Si, a ferrite stabilizing element. This indicated that the strength was more strongly influenced by the change of the bainite volume fraction than the solid solution hardening effect. The bainite volume was slightly increased by the addition of Nb. Figure 21 compares the tensile properties of the experimental steels for various BIT. The highest balance of (TS*El) in the steel was observed when BIT was 450°C. In regard to the volume changes of bainite, ΔV_B, as a function of BIT time at various temperatures, it was found that the formation of bainite was retarded above the holding time of 300s. Holding at 450°C, resulted in the lowest bainite volume fraction regardless of steel composition. ΔV_B was increased when Mn content was increased, which was due to the fact that Mn retarded the transformation during cooling for BIT and, hence, a large amount of austenite was transformed to bainite during BIT.

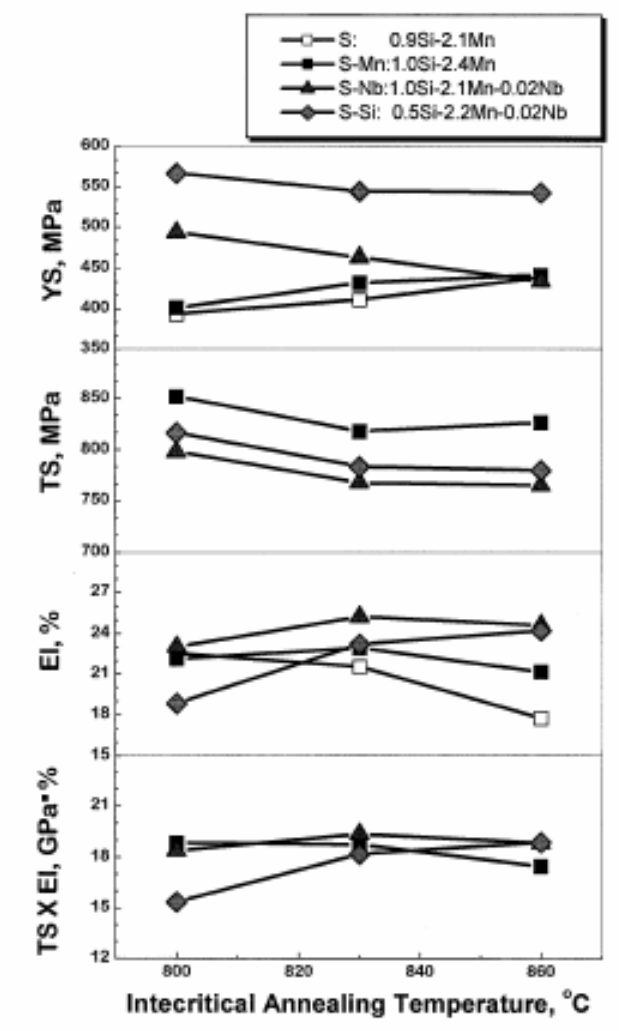

Figure 20 Mechanical properties as a function of annealed temperature for the steels annealed at various temperatures for 51 s, followed by austempering at 450°C for 300 sec.

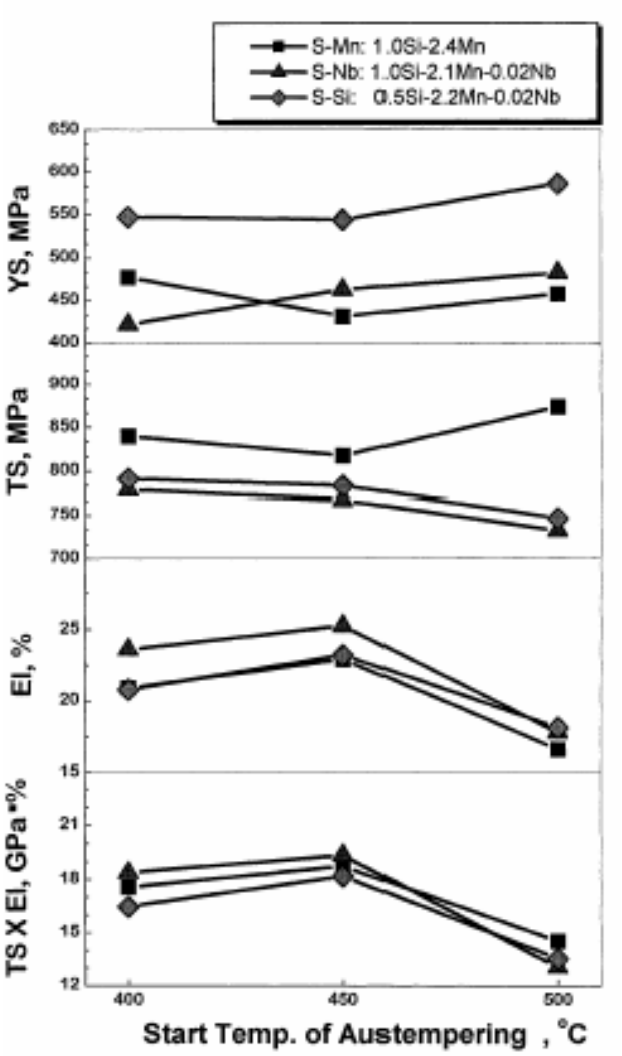

Figure 21 Mechanical properties as a function of austempering start temperature for the steels obtained by annealing at 830°C for 51 s, followed by austempering at various temperatures for 300s

In a 1.0Si-2.4Mn steel, it was observed that Ms linearly decreased with increasing ΔV_B, exhibiting a maximum rate of the Ms decrease when the BIT was 450°C, Figure 22. The volume fraction of retained austenite as a function of ΔV_B is shown in Figure 23. It can also be observed that the maximum rate of volume fraction of retained austenite is obtained at 450°C, which coincides with the observed largest elongation.

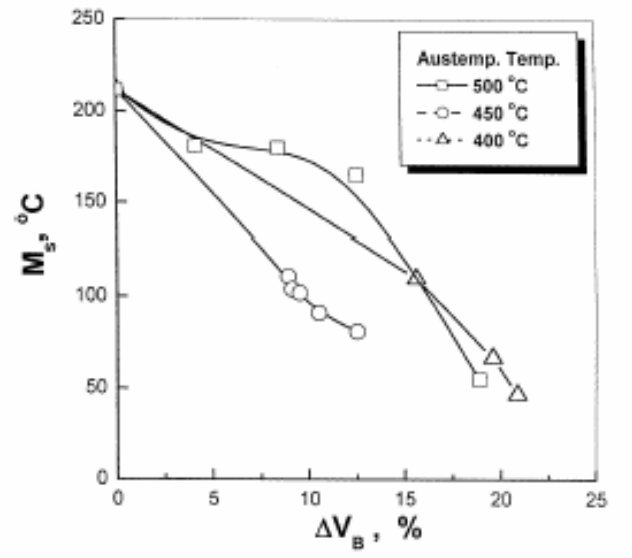

Figure 22 Martensite start temperature, Ms, for a 1.0Si-2.4Mn steel as a function of the volume fraction of bainite transformed during austempering, ΔV_B , at various temperatures.

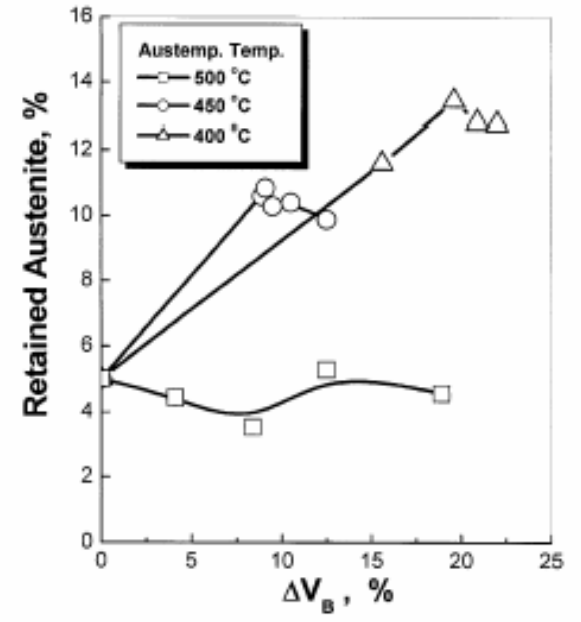

Figure 23 Volume percentage of retained austenite for a 1.0Si–2.4Mn steel as a function of the volume fraction of bainite transformed during austempering, ΔV_B, at various temperatures.

Tsukatani et al[34] examined the effects of silicon and manganese content on mechanical properties in 0.2C hot rolled steel. The finish-rolling temperature was about 780-800°C. The hot-rolled sheets were air-cooled to 740C, rapidly cooled at a cooling rate of 50-60C/sec for 5sec, and held at 400°C for 30min, followed by furnace cooling or air-cooling, simulating the thermal history of the coiling process. Figure 24 shows the change in volume fraction of retained austenite as functions of silicon and manganese content in steels processed at an isothermal holding temperature of 400°C for simulating the coiling process. In low silicon and manganese content steels, lower volume fractions of retained austenite are formed in furnace-cooled samples than those air-cooled ones. The addition of silicon increases the volume fraction of retained austenite in 1.5-2.0% manganese steels. Silicon addition over 1.0% results in a significant increase in the volume fraction of retained austenite. The volume fraction of retained austenite is also affected by the manganese content, even at high silicon content of 2.0%. A large increase in the volume fraction of retained austenite is also observed when the manganese content is increased from 1.0 to 1.5%. In high silicon and manganese content steels, the volume fraction of retained austenite maintains a high value even in the furnace-cooled sheets.

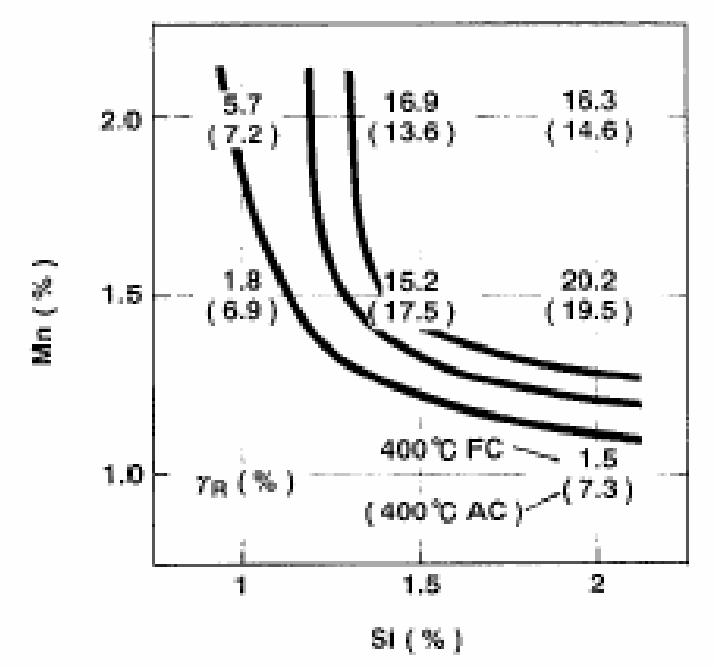

Figure 24 Change in volume fraction of retained austenite as functions of silicon and manganese content in steels at an isothermal holding temperature of 400C for simulating coiling process.

Figure 25 shows the change in CCT diagrams from a temperature of 1000°C as a function of silicon and manganese content. The transformation to pearlite from austenite is delayed by increasing silicon content, and was considered to have arisen from the increase in carbon activity of ferrite and the inhibition of carbide precipitation due to silicon. The increase in manganese content from 1.5 to 2.0% shifts the $\gamma \rightarrow \alpha$ transformation region to the right side and decreases the cooling rate necessary to produce the same amount of ferrite. It as also observed that the volume fraction of retained austenite increases with lowering the finishing temperature. The volume fraction of retained austenite is slightly affected by the amount of slow-cooling time after hot-deformation which depends on the starting temperature of rapid-cooling in the present experiment. The finishing temperature which gives rise to high volume fractions of retained

austenite is nearly coincident with the Ar_3 temperature. The transformation from austenite to bainitic ferrite is assumed to be highly promoted at temperatures of 350 to 400°C. The prevention of carbide formation correspondingly leads to a high concentration of carbon in residual austenite and, in consequence, a large amount of retained austenite was obtained at the isothermal holding temperatures of 350 to 400°C.

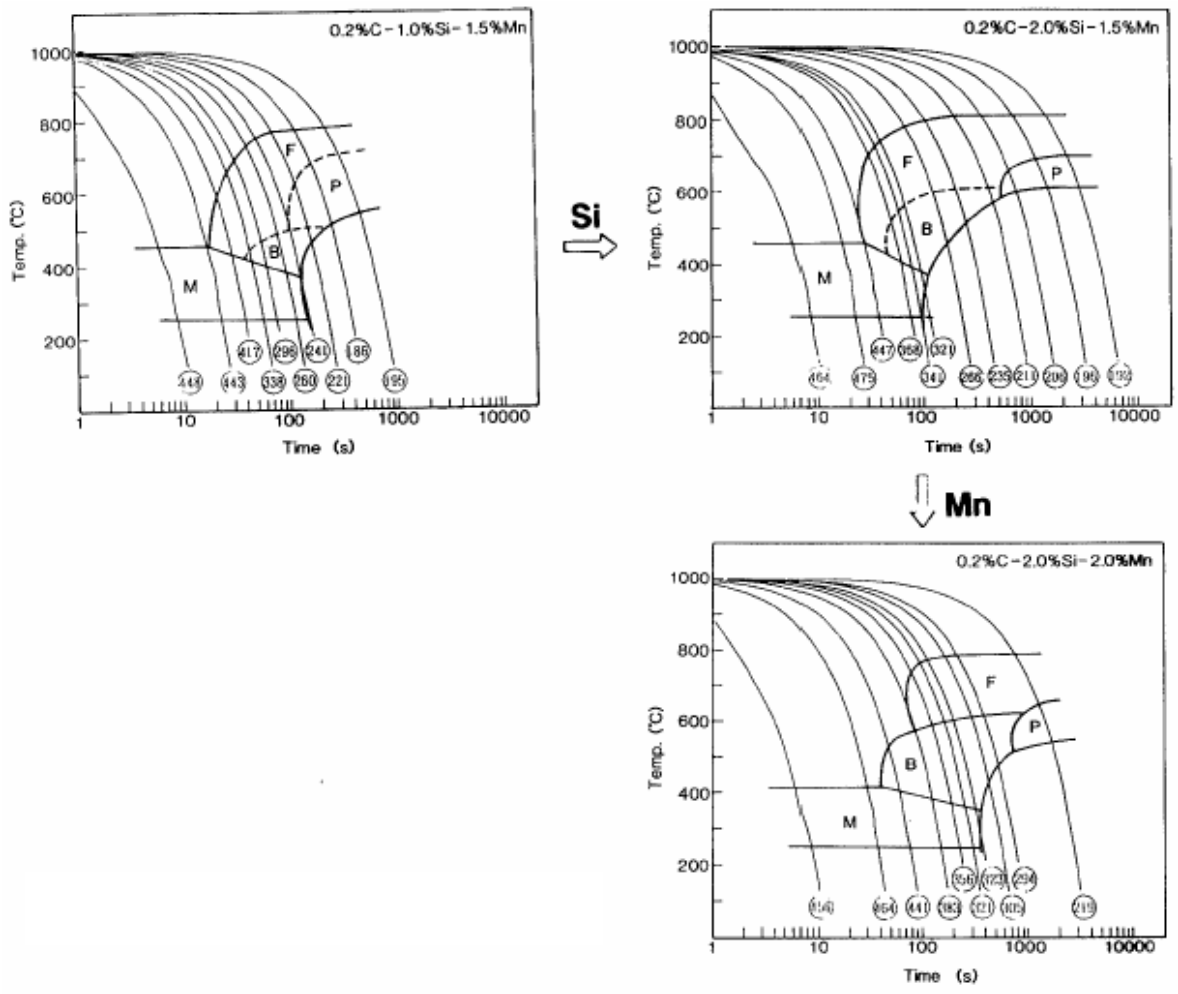

Figure 25 Change of CCT diagrams as function of Si and Mn content

Figure 26 shows the changes in tensile strength, yield strength, total elongation and (TS*El) value as functions of silicon and manganese content. The tensile strength increases, while the yield strength decreases with increasing silicon and manganese content. The total elongation and the product value (TS*El) sharply increase with increasing the silicon content from 1.0 to 1.5% and the manganese content from 1.0 to 1.5%. It was also observed that changes in total elongation and the (TS*El) value have the same tendency as that of retained austenite. The decrease in manganese content is assumed to bring about instability of austenite and consequently acceleration of ferrite transformation during the hot rolling and cooling process.

The microstructure changes due to increasing the manganese content is mainly the increase in volume fraction of martensite. The increase in volume fraction of martensite and the consequential decrease in volume fraction of ferrite deteriorates the (TS*E1) product in spite of a given volume fraction of retained austenite. Furthermore, the difference in slip deformation caused by the changes in silicon and manganese content may influence the transformation behavior of retained austenite to martensite. The increase in silicon content of ferrite phase promotes planar slip and brings about a random array of dislocation. This result in a gradual strain-induced transformation. On the other hand, the increase in manganese content promotes cross-slip deformation and the cell structure formation of dislocation in the ferrite phase immediately surrounding the retained austenite particles. Therefore, retained austenite may be locally stressed and rapidly transforms to martensite in sheets having high manganese content, probably deteriorating the total elongation[(34)].

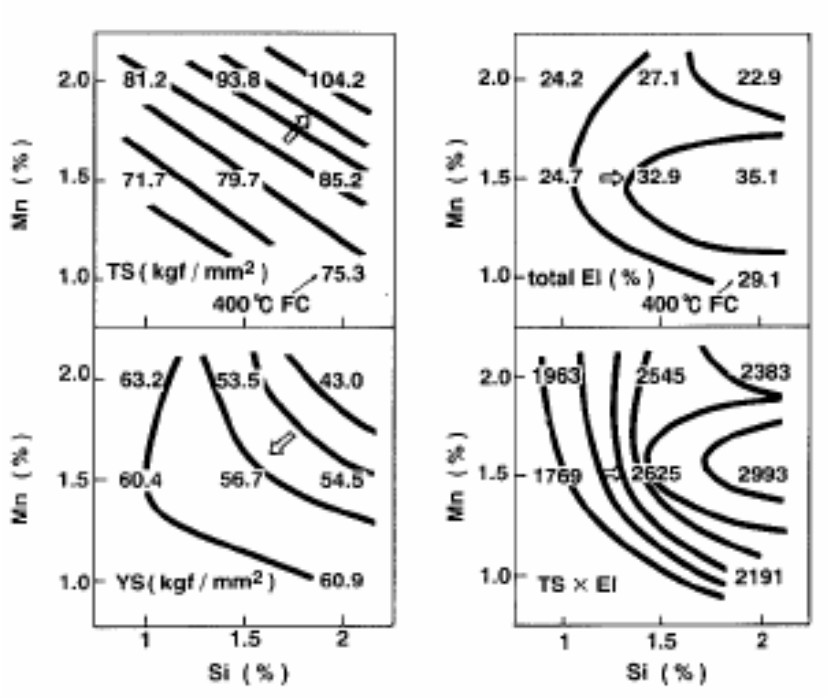

Figure 26 Changes in tensile strength, yield strength, total elongation and TSxEl value as functions of silicon and manganese content.

2.5.2 Al

Some research now is focused on the investigation of the use of other alloying elements as an alternative for Si[35,36,38,40,65]. Al and P, in addition to being strong ferrite stabilizers, retard the tempering reaction and inhibit the formation of cementite. Al is also an element which is not soluble in cementite, Little is known about the effect of small Al additions on the galvanizing of sheet, but as a solute element Al does not segregate. Hence, Al additions are not expected to influence the coatability adversely[35,40,41,68].

DeMeyer and Vanderschueren[35,36] investigated the effect of the partial substitution of Si by Al on the microstructure and mechanical properties of cold rolled and two stage annealed TRIP steels. Steel A is a conventional Fe-0.2C-1.5Mn-1.5Si TRIP steel, while steel B is a Fe-0.3C-1.5Mn-0.3Si-1.2Al steel. After soaking in the intercritical region, the samples were quenched in a salt bath at a lower temperature and isothermally held for several minutes. The substitution of Si by A1 is favorable since high-Si contents result in poor surface conditions and low ductility. From the calculations shown in Figure 27, obtained by using Thermo-Calc software, it can be seen that the substitution of Si byA1 extends the intercritical region. For a C content of 0.2%, the austenitic phase region even disappears for a total substitution of Si by Al. Therefore, the Si content can only be partially replaced by Al.

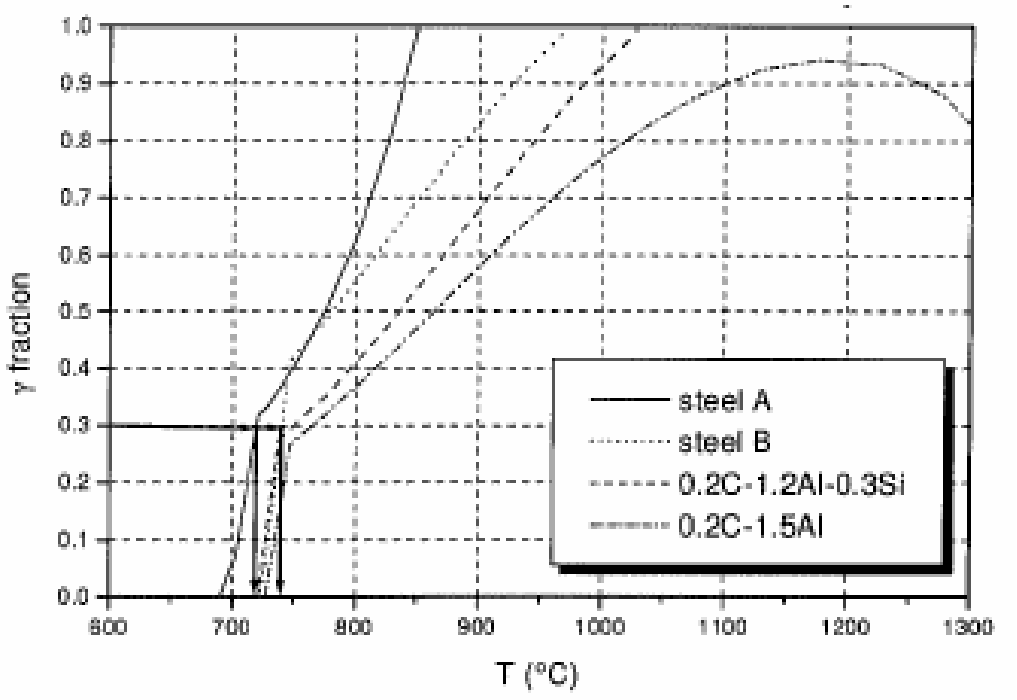

Figure 27 Equilibrium austenite fraction as a function of the temperature

Figure 28 is a calculated TTT diagram for the conventional C-Mn-Si TRIP steel composition. The evolution of the Ms temperature corresponds to an isothermal holding at 400'C, which results in a phase distribution as shown in Figure 29 on the left side. On the right side of Figure 29**,** the evolution of the C content in the retained austenite is shown when a low C bainite is formed. For both steels the yield stress increased with increasing bainitic transformation time, and the yield stress was higher in practically all cases for steel B than for steel A. The tensile strength decreased with increasing bainitic transformation time. After a 240 secs isothermal holding, the C enrichment of the austenite phase is such that the transformation to martensite during air cooling is unlikely. This explanation based on the formation of martensite, was suggested to be responsible for the decrease of tensile strength with increasing bainitic holding time.

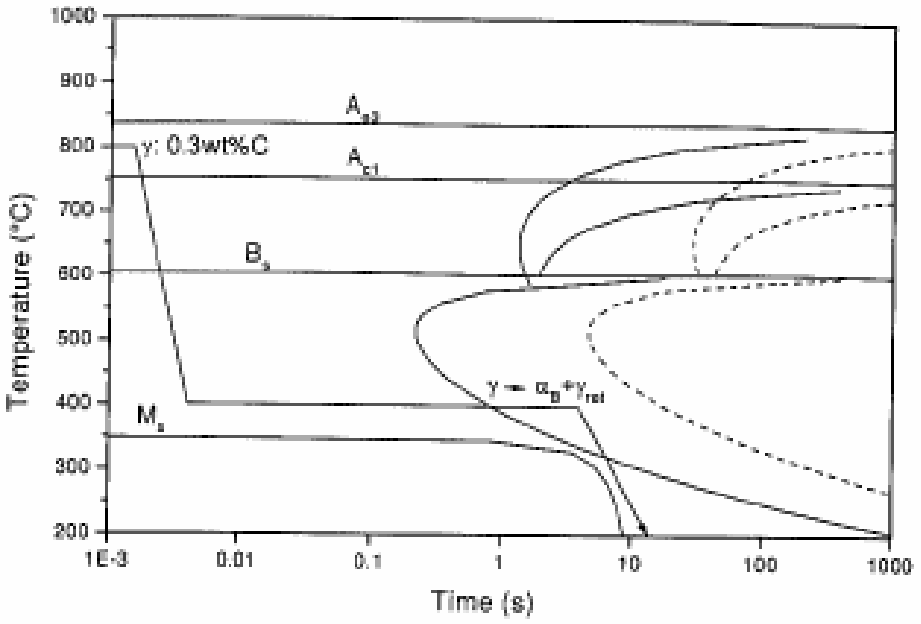

Figure 28 Calculated TTT diagram for the Fe-0.2%C-1.5%Mn-1.5%Si TRIP steel

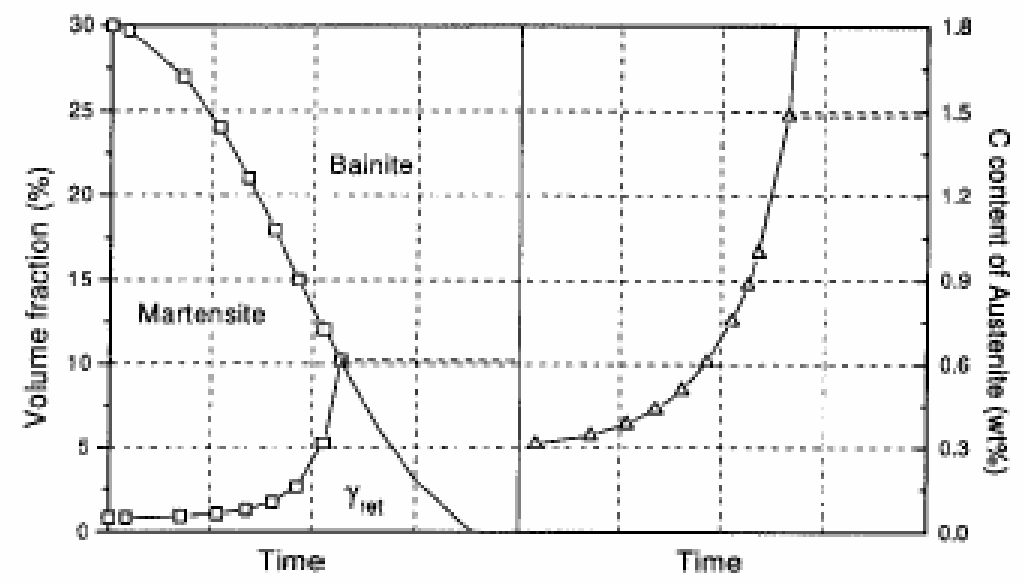

Figure 29 Calculated phase distribution and evolution of carbon content for the Fe-0.2%C-1.5%Mn-1.5%Si TRIP steel

For the same heat treatment, the ductility was clearly higher for the Al alloyed TRIP steel (B) than for the C-MnSi TRIP steel (A). Since TRIP steels combine high strength and high ductility, their mechanical properties are often characterized by the product of tensile strength and total elongation. This product (TS*El) was considerably higher for the Al-substituted steel than for the conventional TRIP steel. It was also found that the 'n' value of steel A increased steeply to a maximum at the beginning of straining and decreased continuously from a maximum value depending on the annealing. The n value for steel B also reached a maximum. However, this was reached in the beginning of straining and this maximum was maintained during further straining, as observed in Figure 30.

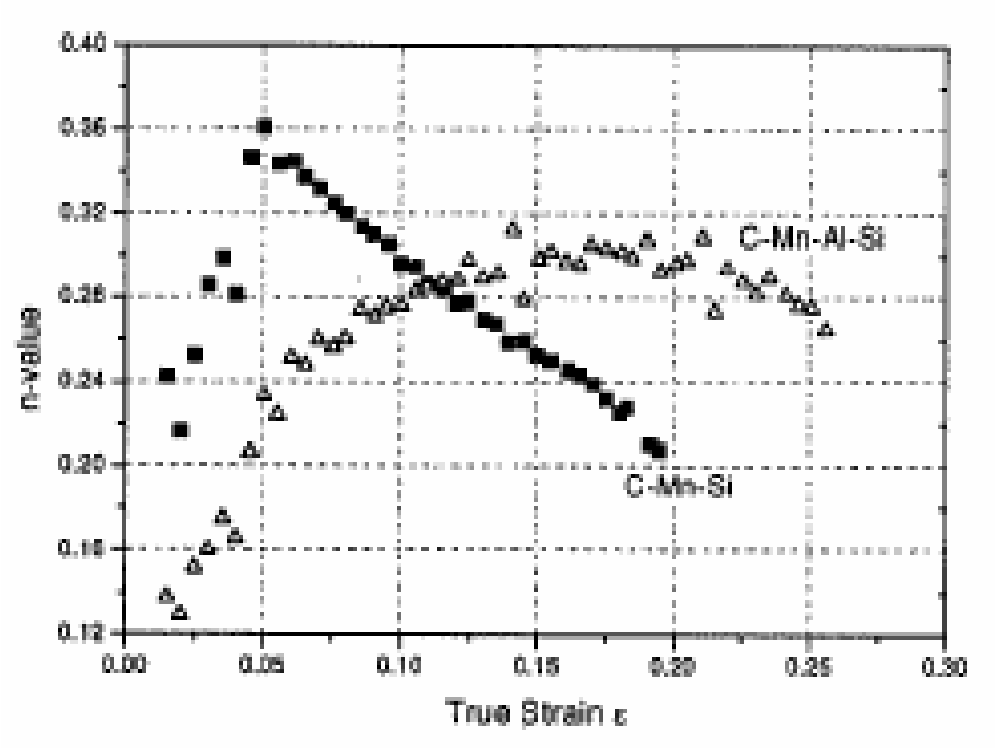

Figure 30 Strain hardening coefficient variation with true strain for Si and Si-Al TRIP steel

A more gradual variation of the strain hardening rate eventually results in a larger uniform elongation. According to Evans et al[37] a higher n value results from a larger amount of retained austenite transforming to martensite during straining. Also, a sharp increase of the n value to a maximum is due to the fast transformation of retained austenite to martensite. The strain induced transformation to martensite occurs more gradually and at a more uniform rate when a slower increase to a maximum 'n' value is observed.

The transformation of retained austenite to martensite during deformation was also studied by DeMeyer and Vanderschueren[36] by interrupted tensile testing, and the results are presented in Figure 31. Although the samples of steel A and B showed a very different strain dependence of the 'n' value, the transformation rate of retained austenite to martensite was

nearly the same for the C-Mn-Si and the C-Mn-Al-Si specimen. These results do not agree with the effects reported by Evans where a sharper increase of the 'n' value corresponds to a faster transformation of retained austenite to martensite.

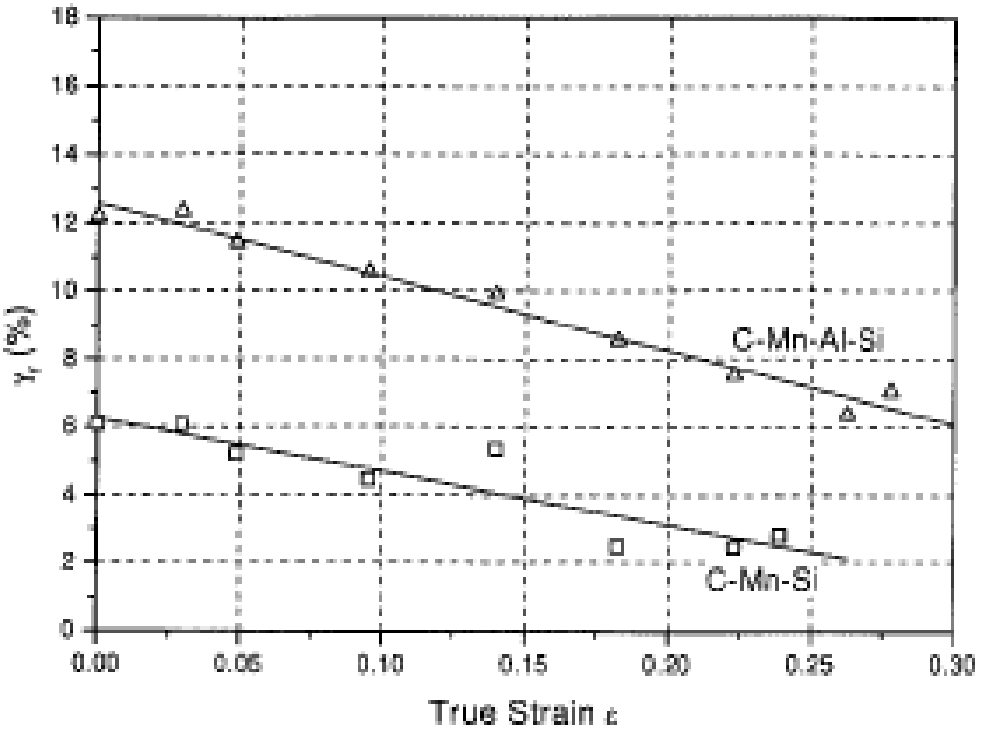

Figure 31 Variation of volume fraction of retained austenite during tensile testing

Micrographs showed that after the same heat treatment (240sec at 770°C + 120-1240sec at 400°C) the amount of fine bainite was larger for steel B than for steel A. Additionally, SEM images revealed that the structure of the second phase ($\gamma_R + \alpha_B$) was much finer in the case of steel B. The higher volume fractions of retained austenite for steel B resulted in the observed higher elongations. Also, it is observed that for steel B the volume fraction of retained austenite always decreased with increasing bainite transformation time. This phenomenon is caused by the

decomposition of the C-enriched metastable retained austenite into a mixture of carbide and ferrite, which occurs after too long isothermal holding. The decomposition of retained austenite already started after 240sec at 400°C for the Al alloyed TRIP steel.

Finally, the C content of the retained austenite was higher for the C-Mn-A1-Si TRIP steel than for the conventional C-Mn-Si steel. As a result of this higher C content, the Ms temperature of the retained austenite is lower for the specimens of steel B than for those of steel A, expressing a greater thermal stability of the retained austenite in the former. However, the larger C content of the retained austenite for the Al alloyed TRIP steel did not result in a slower transformation of the retained austenite during deformation. This is contradictory with the results found by Jacques et al[39], where the retained austenite in the low Si steel, which had a lower C content than the austenite in the conventional TRIP steel, transformed more rapidly during plastic straining. Consequently, the constant high 'n' value obtained for the Al-alloyed TRIP steel cannot be explained by the higher stability due to the C content. Al additions increase the stacking fault energy of austenite, whereas Si decreases the stacking fault energy of the γ phase. In stainless steels the stacking fault energy strongly influences strain hardening, and therefore a similar effect could be related to the characteristic strain dependence of the 'n' value of the Al-alloyed TRIP steel.

It is known that in TRIP aided steels the strengthening of the ferrite matrix by silicon plays an important role in the improvement of the mechanical properties of Si-alloyed TRIP-aided steels. On the other hand, aluminum is not as effective for solid-solution strengthening. Leslie and Pickering[30] proposed a strengthening effect by silicon of the order of 100MPa for 1 wt% of solute while they reported that aluminum exhibits no solid-solution strengthening.

This difference perfectly fits with the change of hardening observed when silicon is substituted by aluminum in TRIP-assisted multiphase steels. The mixed addition of Si and Al in steel Al-Si thus allows a good compromise between the austenite stabilizing effect of both of these elements during the bainite transformation and the solid-solution strengthening effect of the ferritic matrix[39].

2.5.3 Mo

Molybdenum has a strong solute drag effect in steel, resulting in recrystallization and precipitation delays[66,67]. Molybdenum also acts as an austenite stabilizer when added in small quantities, but as ferrite stabilizer at large amounts. Therefore, Mo can have a retardation effect on the transformations to both ferrite and pearlite. This would greatly reduce the cementite formation kinetics facilitating TRIP steel processing[29]. Furthermore, Mo can enhance the effectiveness of both Nb and C in retaining and stabilizing austenite by delaying the precipitation of Nb(C,N) in Nb steels.

2.5.4 Nb

Hanzaki et al[4,28,43] investigated the variations in the bainite characteristics, residual phases and, the state of the retained austenite with the final mechanical properties in two steels with a similar chemical composition (0.20C, 1.50Si, 1.55Mn, 0.024Al) with the difference being only the Nb addition (0.035%) in one of them. Different thermal cycles and deformation schedules were applied to generate different conditions of bainite formation from an austenite with

predetermined characteristics (grain size, substructure, etc). The isothermal holding temperature and duration in the salt bath were varied to produce different bainite characteristics.

The effect of hold time on the amount of retained austenite for a Nb added steel, and for a steel without Nb addition, is shown in Figure 32. It is apparent that, for both steels, increasing the time leads to a maximum retained austenite volume fraction (V_{RA}). The total elongation appears to coincide with the changes in the V_{RA}, but the tensile strength increases continuously with holding time at 400°C.

Increasing the holding duration from 2 to 5 minutes at 400°C, resulted in a decreased lower bainite content. This means that more transformation took place at the holding temperature, decreasing the austenite available either to transform to lower bainite or remain untransformed during subsequent air cooling. A further increase in the holding duration, resulted in a decrease in the retained austenite volume fraction. The maximum retained austenite volume fraction and its carbon concentration coincided with the maximum total elongation. On the contrary, the UTS increased with increasing holding duration.

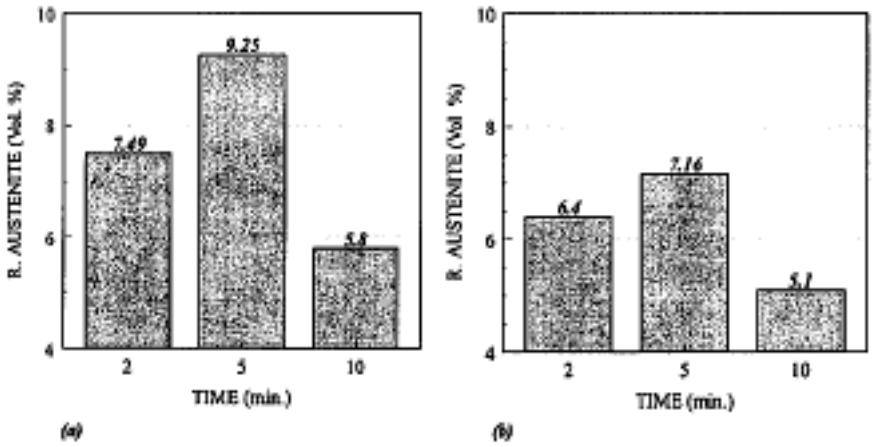

Figure 32 Variation of the V_{RA} with holding time at 400C; (a) Nb added steel, (b) No niobium added

Figure 33 shows the variation of V_{RA} with the temperature of the bainite hold. A change in the bainite hold temperature from 500 to 400°C led to a small change in the retained austenite volume fraction. A significant decrease was seen when the temperature was lowered to 300°C. The tensile strength, however, continually decreased with increasing bainite hold temperature. An increase in the bainite hold temperature resulted in an increase of lath size and interlayer thickness.

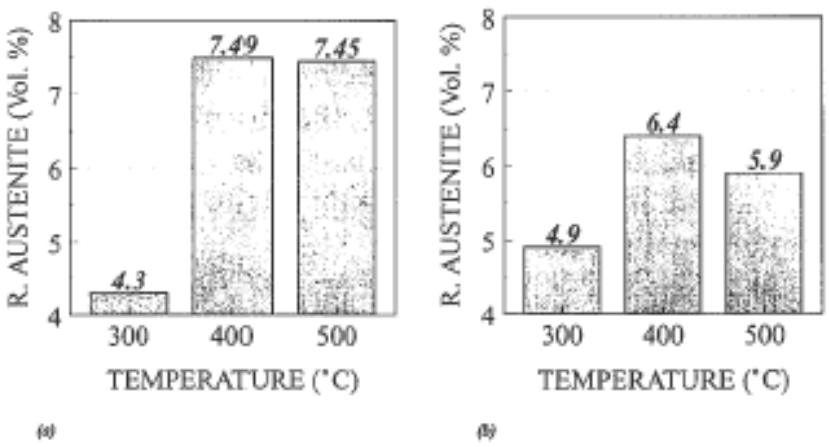

Figure 33 Variation of the V_{RA} with the temperature of bainite formation; (a) Nb added steel, (b) No niobium added

The retained austenite configuration in the specimen treated at 300°C was almost completely in the form of interlayer films between the lower bainite laths. At 500°C, the retained austenite was plate-like, enclosed by the thick upper bainite platelets. The retained austenite stability is influenced by these differences, and this, in turn, dictates the final mechanical properties. In general, isothermal transformation in both the lower and upper bainite temperature ranges resulted in an aggregate of bainitic ferrite and retained austenite. The retained austenite volume fraction, however, was much lower in the case of the lower bainite. The best mechanical properties were found in specimens treated at 400°C. Nearly identical elongations were observed in the higher (500°C) and lower (300°C) temperature specimens. Although the retained austenite volume fraction was lower in the latter case, it had a finer particle size along with a much higher carbon concentration. In other words, the austenite was more stable, and the two structures had comparable ductilities. Also, the austenite in the Nb-added steel had a higher tendency to be retained or stabilized. This was attributed to the inhibiting effect of carbide precipitation and solid solution strengthening of dissolved Nb on the austenite.

3.0 STATEMENT OF OBJECTIVES

There are numerous investigations that have been conducted to obtain a fundamental knowledge on the processing-structure-properties of TRIP steels. Most of them, unfortunately, have used high aluminum and silicon contents (1.5% mass and up). It has already been mentioned that high levels of silicon result in very poor coatability in the galvanizing line, and therefore, are not suitable for production. Also, there are no systematic studies of the kinetics of bainite formation in low Si steels nor a clear understanding of the differences between continuous cooled and isothermally formed bainite in TRIP steels. Similarly, studies on the new ferrite formed during cooling have been widely overlooked. Furthermore, there are no good studies based on simulations of actual continuous galvanizing line (CGL) processing.

This study has the objective of developing a low Si TRIP steel that can be obtained within the ranges of a production line speed observed in a typical CGL or hot dip galvanizing line. Of particular interest in this study, is the evaluation of the influence of prior-hot rolling conditions, that is, coiling temperature, and the variations in the processing parameters in a CGL on the microstructure and properties in a series of low silicon, Al-Mo-Nb added steels.

This research study has two main goals:

1) A systematic study of the austenite formation and recrystallization of ferrite during the intercritical annealing stage, as a function of:

a) Al content

b) Prior coiling temperature during hot rolling

2) A systematic study of the austenite decomposition into “new” epitaxial ferrite, bainite, martensite, etc., during cooling from i) the intercritical annealing temperature and ii) during the isothermal holding temperature, as a function of:

a) Al content

b) Prior coiling temperature

c) Intercritical Annealing Temperature

In addition, it is also of great interest the evaluation of the amount and composition of retained austenite and its stability through its decomposition from the intercritical annealing temperature as a function of a) cooling rate from the T_{IA} to the isothermal holding temperature, b) holding time and c) cooling rate from the isothermal holding temperature to room temperature

Finally, it is necessary to evaluate the tensile properties and correlate the processing routes with the observed microstructures and mechanical properties, in order to provide guidelines to develop a commercial 800 MPa low silicon Al added TRIP steel by CGL processing.

4.0 EXPERIMENTAL PROCEDURE

4.1 MATERIALS / ALLOY DESIGN

In order to successfully meet the objectives of this research work, a series of low Si-Al added steel alloys were chosen in order to study the influence of Al on the behavior of the recrystallization of ferrite and on the austenite decomposition during TRIP steel processing in CG lines. Three TRIP steel alloys were investigated, and their Al content varied from 0.05Al to 1.0Al wt percent. Furthermore, additions of Nb and Mo were added to refine the microstructure and increase strength. The slab chemistry analyses of the three steels used in this research work are shown in Table 1.

Table 1 Chemical composition of TRIP steels used in this research study

Element / Designation	C	Mn	Si	Al	Nb	Mo
0.05Al	0.15	1.52	0.31	0.05	0.03	0.15
0.5Al	0.15	1.52	0.31	0.5	0.03	0.15
1.0Al	0.15	1.52	0.31	1.0	0.03	0.15

4.2 THERMOMECHANICAL PROCESSING (TMP)

Different thermomechanical schedules were performed in order to obtain different starting microstructures in the hot rolled condition. This led to an evaluation of the effect of the prior hot rolled structure on the austenite formation during intercritical annealing. Based on previous work[44,45], it was determined that the variation of coiling temperature was sufficient to obtain a large variation in the starting microstructures. Two coiling temperatures were used: 700°C and 550°C. These coiling temperatures were expected to result in different ferrite microstructures, from polygonal ferrite to non-polygonal, acicular, and bainitic ferrite, as well as clear differences in the carbide phases distribution throughout the ferrite matrix. Table 2 shows the design of the temperatures to be used in the TMP, and Figure 34 shows a schematic representation of the hot rolling processing schedule.

Table 2 Design of thermomechanical processing temperatures

TMP stage	**Temperature**	**Experimental Details**
Reheating Temperature	1250°C	1 hour
Roughing Temperature	1050°C	Two pass @ ε=50% each
Finishing Temperature	950°C	1 pass at ε=50%,
Coiling Temperature	700°C, 550°C	Furnace cooled (30°C/hr)

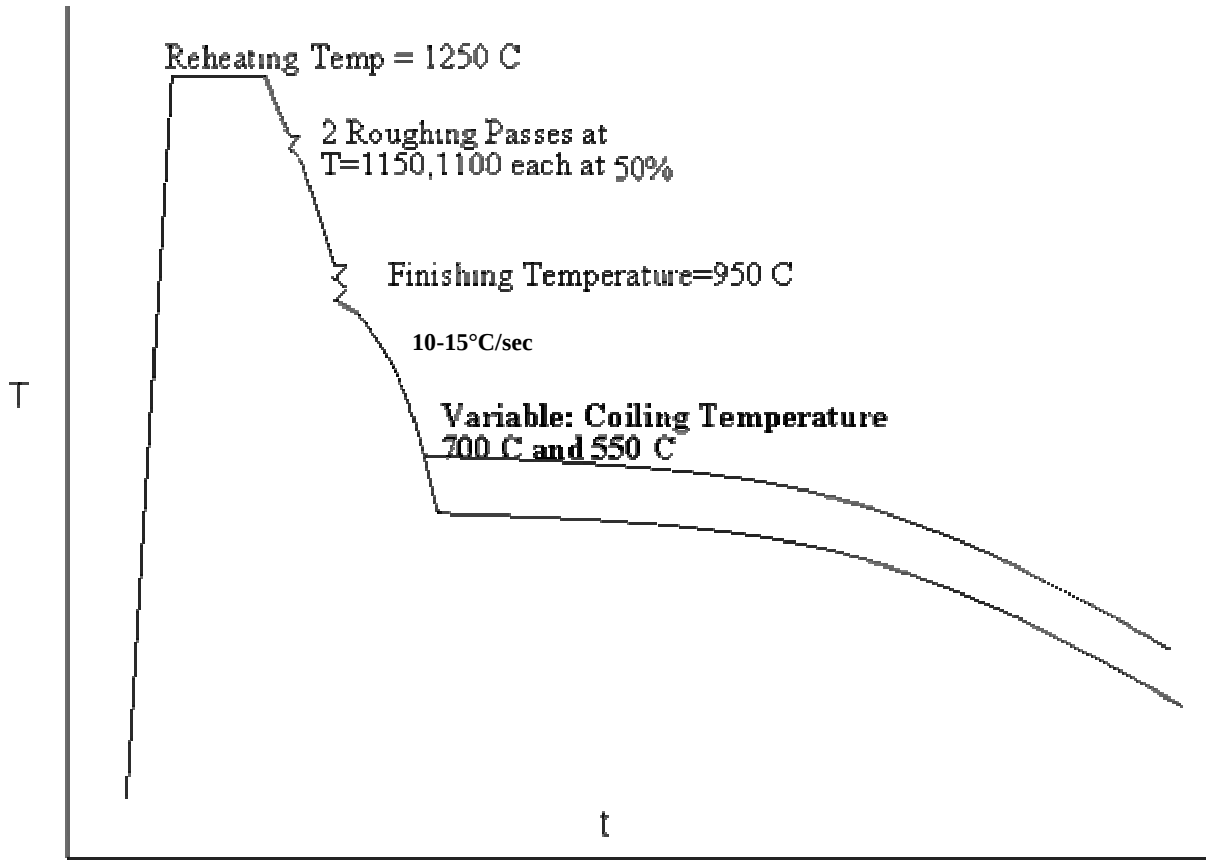

Figure 34 Hot Rolling Variables

4.3 COLD ROLLING

The 0.05Al hot band alloys were cold rolled at US Steel Research Laboratories in several passes from an initial thickness of 0.20" to a final thickness of 0.08" for a total percentage reductions of 60%, whereas the 0.5Al and 1.0Al hot band alloys were cold rolled at POSCO from an initial thickness of 0.25" to a final thickness of 0.1" for a total percentage reduction of 60%.

4.4 INTERCRITICAL ANNEALING HEAT TREATMENTS

JMat-Pro software was used to predict the Ac_1 and Ac_3 temperatures, as well as the austenite volume fraction formation during different intercritical annealing temperatures as a function of Al content. Based on these predictions, a number of intercritical annealing temperatures that would result within a 20-80% initial austenite percent range for the different alloys were chosen. After cold rolling each of the hot band conditions, the samples were heated at 3°C/sec and intercritically annealed for 60 seconds at various temperatures (based on the JMat Pro results) followed by quenching in ice brine solution. The austenite and ferrite volume fractions were then measured to compare the predicted vs observed results.

The austenite (observed as martensite) and ferrite volume fractions, and austenite and ferrite grain size were measured using optical microscopy plus point counting, as well as SEM-EBSD (Image Quality) analysis[62,78]. The ferrite recrystallization behavior was also investigated during the intercritical annealing stage. Optical microscopy plus the Bioquant IV system were used to measure the aspect ratio of the ferrite grains at different intercritical annealing temperatures. It is generally accepted that for a ferrite grain to be considered recrystallized, the aspect ratio should be less or equal to 1.6[79]. Ferrite recrystallization was also quantified by SEM-EBSD, using the Image Quality (IQ) analysis of ferrite grains. Furthermore, microhardness testing was also used to study the extent to which ferrite recrystallizes as a function of time and temperature.

4.5 AUSTENITE DECOMPOSITION STUDY

In order to evaluate the effect of varying intercritical annealing temperatures and cooling rates to the IBT, it was necessary to develop microstructural maps a) during cooling from the T_{IA} to IBT (CCT diagrams) and b) during the isothermal holding temperature IHT. A Theta Dilatronic II Dilatometer and a Gleeble 3500 unit fitted with a laser width sensor were used to study the transformation behavior of austenite during continuous cooling from two intercritical annealing temperatures, those that represent an initial austenite percent of 35% and 55%. The cold rolled samples were heated to the starting intercritical annealing temperature at a constant heating rate of 3°C/sec, and held for 60 seconds before continuous cooling at 1, 15 and 30 °C/sec to room temperature. Based on the CCT diagrams, varying cooling rates from the T_{IA} to the IHT were used to evaluate the austenite decomposition behavior.

Similarly, in order to study and quantify the austenite decomposition products during cooling from the intercritical annealing temperature to the isothermal holding temperature (IHT), interrupted quench experiments were carried out in a MTS-458 unit with a mounted radiation furnace. During these experiments, samples were also heated at a constant rate of 3 °C/sec to the intercritical annealing temperature (equal to 35% and 55% austenite percent), held for 60 seconds and cooled at 5 and 15°C/sec to the isothermal holding temperature of 450 °C, followed by a 2-3 second holding and immediately quenched into iced brine solution. The ferrite and austenite volume fraction were then measured by point counting and the results confirmed by SEM-EBSD (IQ) analysis[62,78].

4.6 ISOTHERMAL HOLDING TEMPERATURE TRANSFORMATION

The variation of the holding time (2s, 30s, 60s, 90, and 120s) at the bainite transformation temperature of 450 °C, temperature at which the galvanizing of the steel sheet takes place, was investigated. The maximum holding time at this temperature was defined by the line speed observed in a typical continuous annealing line or hot dip galvanizing line (up to 120 seconds from the T_{IA} to the exit of the zinc pot). Furthermore, the cooling rate after each holding time was varied in order to study the effect of post-holding on the retained austenite stability. Furthermore, a post-zinc heat treatment was performed in the 1.0Al steel to simulate a galvannealing process and evaluate if it influences the austenite decomposition and/or austenite stability. A qualitative and quantitative analysis of the amount of bainite at each stage was obtained by optical microscopy, SEM-EBSD, TEM and dilatometry analysis. Finally, the retained the austenite was measured by magnetometry and its microstructural appearance was determined by SEM and TEM analysis.

4.7 MICROSTRUCTURAL ANALYSIS

4.7.1 Optical Microscopy

Optical microscopy was used for the initial examination and identification of the different types of microstructures. The samples were sectioned perpendicular to the rolling plane, followed by mounting in bakelite. The specimens were ground using 180, 240, 320, 400 and 600 grit abrasive papers, and polished using 1 um alumina. All samples were then polished on 0.05μm alumina

immediately (i.e., within 15 seconds) before etching to eliminate passivation due to atmospheric exposure.

Parish[38] has made an extensive review on different etching procedures and techniques that are often used to observed the different phases in multiphase steels. Of these techniques, Parish found that only two, LePera's[97,100] and 10% $Na_2S_2O_5$[98,99] techniques, were found to give satisfactory results. The 10% $Na_2S_2O_5$ technique gave moderate metallographic contrast nearly every time, especially when combined with an 8-10 second 3% nital pre-etch. Further, the technique's simplicity resulted in highly consistent etching. LePera's technique was very consistent if care was taken to prevent air contact by storing the sample under alcohol immediately after polishing. LePera's technique gave the best austenite-ferrite contrast. However, LePera's technique was found to give inconsistent etching response in high-bainite-fraction (i.e., >5%) materials. The 10% $Na_2S_2O_5$ technique, however, provided excellent bainite contrast, even if its ferrite-austenite contrast was less pronounced.

Measurements of grain size, aspect ratio and volume fractions of microconstituents were done using a computer controlled Bioquant IV system attached to an optical microscope.

4.7.2 Scanning Electron Microscopy (SEM)/EBSD

A Philips XL30 field emission gun SEM at the University of Pittsburgh was used to examine specimens. Samples prepared for optical microscopy were used for a more comprehensive and detailed identification of microconstituents. Furthermore, thin foils were prepared as described in the following section, and were used for the identification of the different phases, specially the retained austenite phase. Also, Electron Back Scattering Diffraction (EBSD) analysis was used to

determine the crystallographic texture and grain boundary misorientation between the different phases. Furthermore, the image quality approach will also be used to evaluate the different phases[62,78]. The samples used for EBSD analysis were cut parallel to the rolling direction (through thickness), grounded and polished as described in the previous section.

4.7.3 Transmission Electron Microscopy (TEM)

TEM examination of the specimens was conducted using a JEM-200CX electron microscope operated at 200 kV. The analysis included bright field, dark field, and selected area diffraction. The microstructural features that were studied included examination and identification of the different phases and their distribution and morphology, and also for the presence of fine precipitates. The procedure for preparing thin foils was as follows: the samples were sectioned through the thickness (parallel to the rolling direction). A low speed saw was used and the thickness of the slice obtained was close to 0.8 mm. No grinding needed to be used. The samples were chemically thinned to a thickness of 80-90 um. Two separate solutions were used for the chemical thinning. The first solution consisted of 50 ml H_2O, 50 ml H_2O_2 (30%), and 7 ml HF. The second solution consisted of 50 ml H_2O, 30 ml HNO_3, 15 ml HCl, and 10 ml HF. The foils were immersed in the first solution to thin the samples to about 0.1 mm. Then the foils were immersed in the second solution for a few seconds to obtain the final thickness. Finally, 3 mm discs were punched from the foils, and subsequently polished with a twin jet polisher, using an electrolytic solution of 95% acetic acid and 5% perchloric acid at approximately 70 mA.

4.7.4 X-ray diffraction

Careful comparison of the integrated intensities of Bragg peaks for different phases can be used to determine the relative volume fractions. Under the assumption that only ferritic and austenitic phases are present, this relative volume fraction of ferrite to austenite, fα/fγ, can be converted to absolute volume fractions with the identity fα+fγ=1.

This is the so-called "direct comparison method"[42]. As TRIP steels contain only negligible amounts of carbide (if any at all), this assumption should hold. Ratios of volume fractions are calculated from the integrated intensities Iα and Iγ and constants R^{α} and R^{γ}

$$\frac{I^{\gamma}}{I^{\alpha}} = \frac{R^{\gamma} f_{\gamma}}{R^{\alpha} f_{\alpha}}$$

The R-values are constants determined by the particular phase, the particular Bragg reflection and the wavelength of the incident X-rays:

$$R = \left(\frac{1}{\upsilon^2}\right)\left[FF^{*} p\left(\frac{1+\cos^2 2\theta}{\sin^2\theta\cos\theta}\right)\right]\exp(-2M)$$

where ν is the volume of the unit cell, F is the structure factor, F* its complex conjugate, p the multiplicity of the reflection, θ the Bragg angle and exp[-2M] the Debye-Waller temperature factor.

For Cu-Kα radiation of wavelength 0.154 nm, De Meyer et al[80] calculated the following R-values:

Ferrite R values

Peak	(110)	(200)	(211)	(220)
Rhkl	250	36	71	25

Austenite R values

Peak	(111)	(200)	(220)	(311)
Rhkl	184	83	47	58

Samples for X-ray diffraction were prepared by standard grinding and polishing to 0.05μm alumina. Samples are then chemically polished in 95% H_2O_2 (30% grade) - 5% HF (46- 48% grade) solution to remove deformation imparted by the rough grinding. Diffraction experiments were performed using a Philips X-ray diffractometer using Ni monochromated Cu-Kα radiation. Comparisons were made by the average of the values obtained from the (110), (200), (211) and (220) ferrite peaks and from the (111), (200), (220) and (311) austenite peaks.

A mathematical technique can be used to calculate the value, fγ, associated with every combination of (hkl)α and (hkl)γ listed above, and then obtain an average and standard deviation. Thus, individual fγi,j values can be calculated from a ferrite/austenite peak pair i,j as:

$$f_{\gamma}^{i,j} = \frac{\frac{I_{hkl}^{\gamma}}{R_{hkl}^{\gamma}}}{\frac{I_{hkl}^{\gamma}}{R_{hkl}^{\gamma}} + \frac{I_{hkl}^{\alpha}}{R_{hkl}^{\alpha}}} = \frac{\frac{I_{hkl}^{\gamma}}{I_{hkl}^{\alpha}}}{\frac{I_{hkl}^{\gamma}}{I_{hkl}^{\alpha}} + \frac{R_{hkl}^{\gamma}}{R_{hkl}^{\alpha}}}$$

Or, the average fγ value by:

$$\langle f_v \rangle = \left(\frac{1}{16}\right) \sum_i \sum_j f_{\gamma}^{i,j}$$

For i= (111), (200), (220) and (311) and j= (110), (200), (211) and (220).

The average carbon content of retained austenite, C_γ, can be estimated using X-ray diffraction. From the XRD-determined lattice parameter of austenite, a_γ, carbon content was estimated as:

$$C_{\gamma} = \frac{a_{\gamma} - 3.5467}{0.0467}$$

where a_γ is in angstroms and C_γ is in weight percent[21].

4.7.5 Magnetometry

Ferrite, martensite, bainite and cementite are all ferromagnetic; austenite is paramagnetic. Thus, the volume fraction of austenite can be determined by comparing the magnetic properties of a TRIP steel to that of a non-austenite-bearing steel[81,82].

In general, for saturation magnetizations M_{SAT},

$$f_\gamma = \frac{M_{REF}^{SAT} - M_{TRIP}^{SAT}}{M_{REF}^{SAT}}$$

for two steels, REF and TRIP, of the same bulk composition, where TRIP contains a volume fraction fγ of paramagnetic austenite and REF is fully ferromagnetic.

Magnetometry was performed in a vibrating specimen magnetometer (VSM) at the University of Pittsburgh. Thin (0.8-1mm) 2.5x2.5 specimens were cut from the samples using a low speed saw. Reference samples can be prepared by quenching the samples in liquid nitrogen or liquid helium, or by annealing at 500-600°C for three hours under inert atmosphere followed by slow cooling. In this research, the reference samples were taken directly from the hot bands.

Magnetometry was the preferred method for obtaining retained austenite volume fractions in this study, as it is considered to be the most accurate (especially for textured samples or samples containing austenite particles too small to detect using XRD or optical microscopy) and is the fastest technique.

4.8 MECHANICAL TESTING

In order to evaluate the mechanical properties, specimens were annealed in the Gleeble 3500 unit. This Gleeble unit uses specialized annealing grips that produce excellent temperature uniformity. Samples of cold-rolled sheet 25cm long and 5cm wide (parallel to the rolling direction) were used. The temperature has been reported to vary by less than 10°C in a region more than 5 centimeters long and across the sample's full 5 centimeter width. This region is located in the middle of sample length. This allows two ASTM sub-size tensile samples to be taken from each annealed sheet's uniform area, as well as samples for metallography. Mechanical testing was performed on a MTS 880 unit using ATSM sub-size tensile specimens of 25.4mm nominal gauge length and 6.4mm nominal width. The strain rate used was 2mm/min. Figure 35 shows a schematic representation and dimensions of the tensile specimens used.

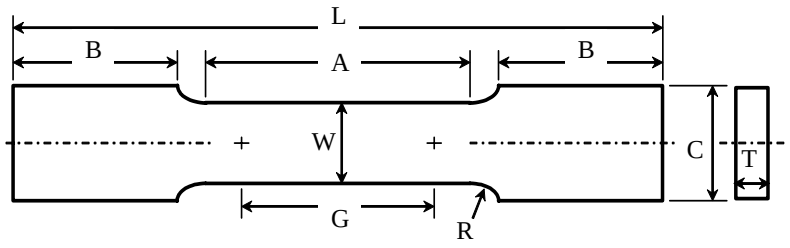

R	Gage length	1.0”
W	Width	0.25”
T	Thickness	Material
R	Radius of fillet	0.25”
L	Overall length	4”
A	Length reduced section	1.25”
B	Length grip section	1.25”
C	Width of grip section	0.5”

Figure 35 Schematic representation of the sub-size tensile specimens used for tensile testing

5.0 RESULTS

The addition of solute Al in this low-Si TRIP steel had a profound impact on the microstructural characteristics of this alloy during the hot band processing. In the 0.05Al alloy, the variation in the coiling temperature from 700 °C to 550 °C resulted in a change from polygonal ferrite + pearlite to acicular ferrite + fine carbides, as observed in Figure 36. Increasing the Al content to 0.5 wt% and 1.0 wt% drastically reduced the effect of the variation in the coiling temperature on the type of ferrite, and as a result polygonal ferrite is mainly observed, as shown in Figure 37 and Figure 38. In addition, the intensity of the carbon segregation to the Mn banded regions is reduced with increasing Al additions and similarly, the banding intensity decreases in the specimens coiled at 550°C. Furthermore, the variation in coiling temperature changes the distribution of the pearlite from banded to a finer and more homogeneous distribution.

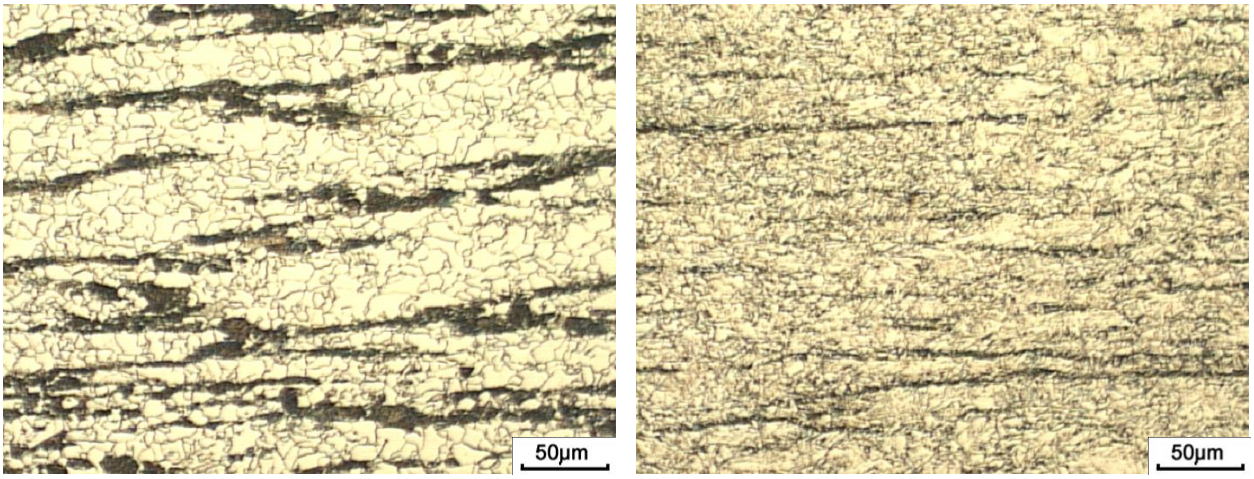

(a) 700 C **(b) 550 C**

Figure 36 Effect of the variation in coiling temperature (a) 700°C and (b) 550°C on the microstructure of the 0.05Al TRIP steel. Ferrite: light, pearlite: dark, etchant=Nital 2%

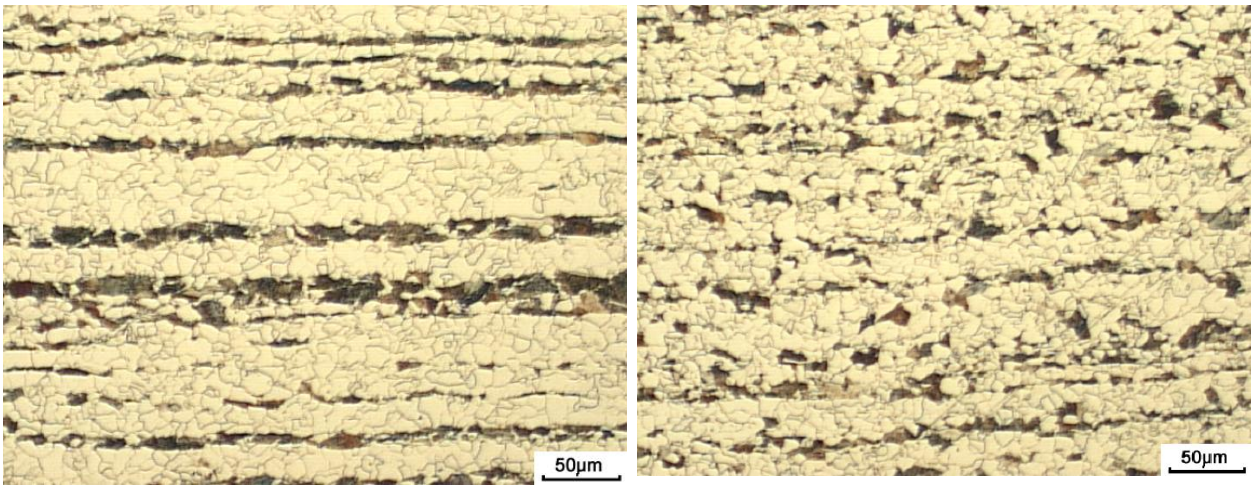

(a) 700 C **(b) 550 C**

Figure 37 Effect of the variation in coiling temperature (a) 700°C and (b) 550°C on the microstructure of the 0.5Al TRIP steel. Ferrite: light, pearlite: dark, etchant=Nital 2%

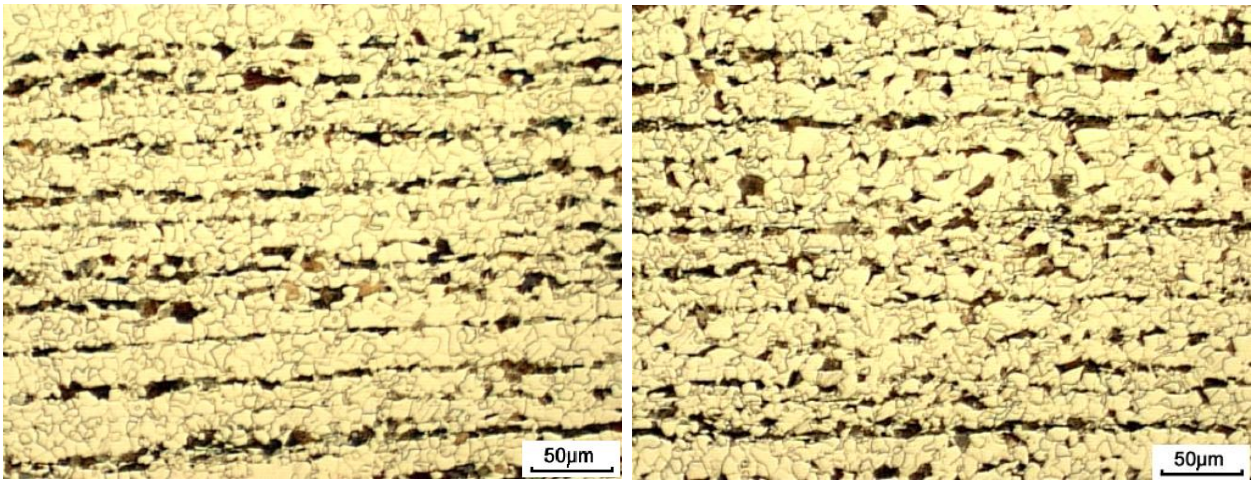

(a) 700 C **(b) 550 C**

Figure 38 Effect of the variation in coiling temperature (a) 700°C and (b) 550°C on the microstructure of the 1.0Al TRIP steel. Ferrite: light, pearlite: dark, etchant=Nital 2%

5.1 STAGE I - INTERCRITICAL ANNEALING

Two events take place during the intercritical annealing: recrystallization of the cold rolled ferrite and the formation of austenite. The temperature used during intercritical annealing can have a large effect on a number of microstructural features in the austenite and ferrite phases. On heating, as soon as the Ac_1 temperature is reached, austenite begins to form and the volume fraction increases according to the level rule until it reaches completion at the Ac_3 temperature. Similarly, the ferrite grains at any given temperature will vary from non-recrystallized grains to fully recrystallized grains. This study shows that the variation of Al content has indeed a large effect on the microstructural characteristics of the austenite and ferrite at any given temperature during intercritical annealing.

5.1.1 Recrystallization of ferrite

The aspect ratio of ferrite grains can indicate the extent to which ferrite has recrystallized, where a grain with an aspect ratio of 1.6 or less is needed for that grain to be considered recrystallized[79]. A ferrite grain with an aspect ratio larger than 1.6 is considered to be non-recrystallized. The effect of Al content on the aspect ratio of the ferrite grains at different intercritical annealing temperatures shows that in the case of the 0.05Al and 0.5Al alloys, a temperature where as much as 75% austenite can be formed, 825°C and 850°C respectively, is needed to obtain 50% of ferrite grains with aspect ratio equal or less than 1.6, as shown in Figure 39 and Figure 40. On the contrary, for the 1.0Al alloy, a temperature where only as little as 27% austenite is formed, 725°C, is needed to reach 50% of ferrite grains with aspect ratio equal or less than 1.6, as shown in Figure 41. The average aspect ratio of the different alloys as a function of intercritical annealing temperature is shown in Table 3.

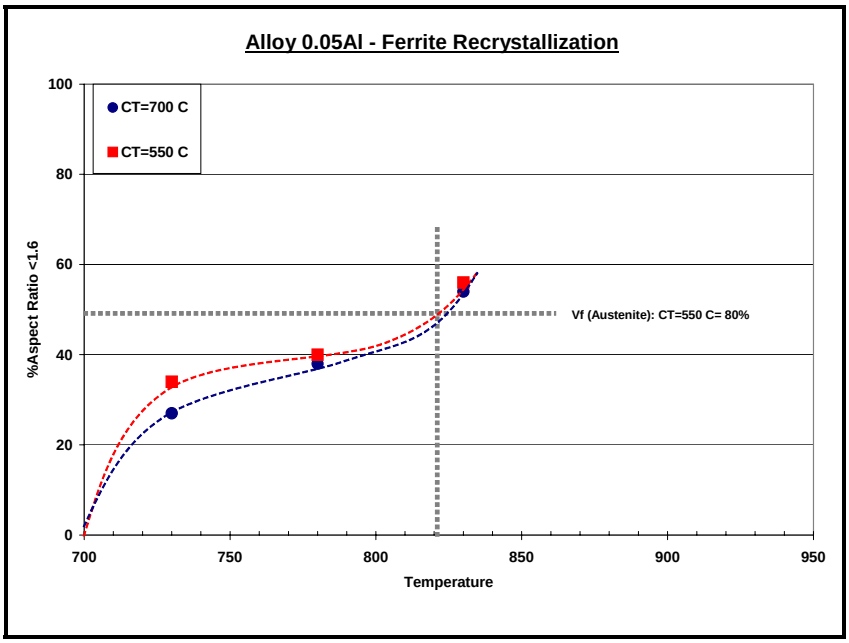

Figure 39 Percent of ferrite grains with aspect ratio <1.6 as a function of intercritical annealing temperature and prior coiling temperature, 0.05Al alloy

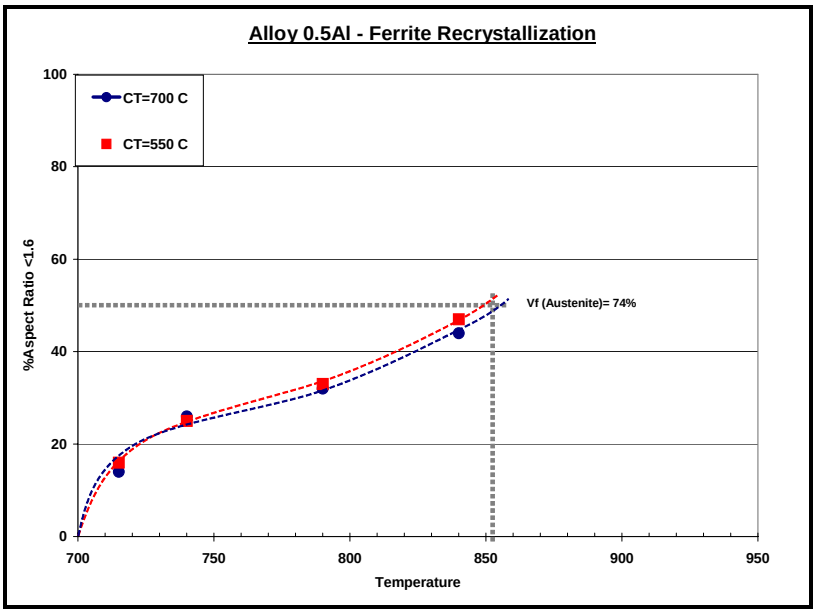

Figure 40 Percent of ferrite grains with aspect ratio <1.6 as a function of intercritical annealing temperature and prior coiling temperature, 0.5Al alloy

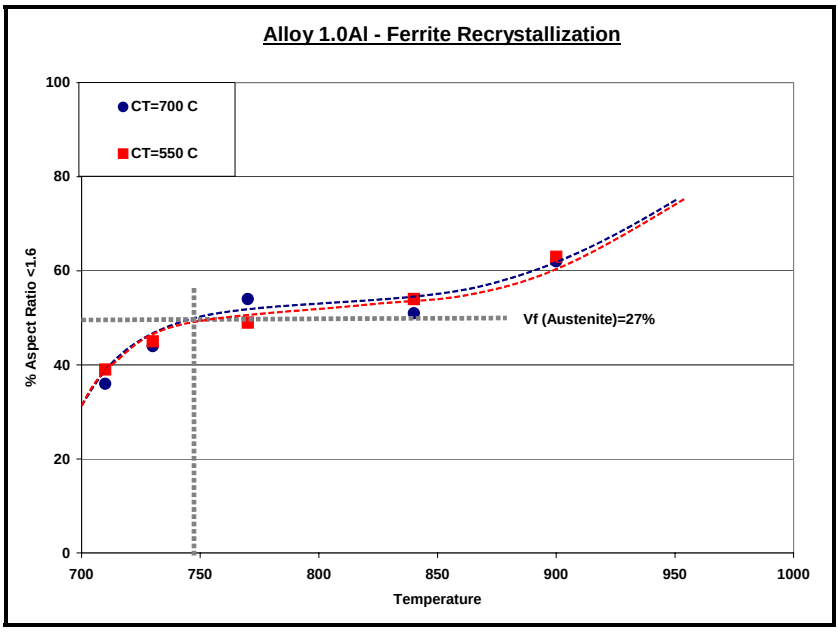

Figure 41 Percent of ferrite grains with aspect ratio <1.6 as a function of intercritical annealing temperature and prior coiling temperature, 1.0Al alloy

Table 3 Average aspect ratio of ferrite grains as a function of intercritical annealing temperature and prior coiling temperature

T_{IA} / Alloy + T_{coil}	690°C	730°C	780°C	830°C	-	HOT BAND
0.05Al-550	2.298	2.172	1.996	1.734		1.808
0.05Al-700	2.286	2.290	2.03	-		1.566
T_{IA} / Alloy + T_{coil}	715°C	740°C	790°C	840°C	-	HOT BAND
0.5Al-550	2.90	2.67	2.12	1.838		1.647
0.5Al-700	2.87	2.44	2.42	1.85		1.33
T_{IA} / Alloy + T_{coil}	710°C	735°C	770°C	840°C	900°C	HOT BAND
1.0Al-550	2.06	1.845	1.823	1.79	1.620	1.40
1.0Al-700	2.01	1.664	1.742	1.715	-	1.478

The EBSD/Image Quality (IQ) technique can also be used to measure in a more accurate and quantitative way the amount of ferrite recrystallization. Figure 42 and Figure 43 show a multi-peak analysis of the IQ values from ferrite grains for the 0.05Al alloy at two different intercritical annealing temperatures, 750°C (35%γ) and 790°C (55% γ) respectively. Note that the IQ results for austenite (34.03%, 50.54%) are very close to the values observed by point count method (35% and 55% respectively) and therefore the use of IQ analysis is validated for the quantitatively analysis of the microstructures. It is observed that at 750°C only 36% ferrite (from a total 65% ferrite at this temperature) has recrystallized, and similarly, intercritical annealing at 790°C results in 28% recrystallized ferrite (from a total of 49% ferrite at this temperature). In both cases, the normalized volume fraction of recrystallized ferrite is ~55%, as

shown in Table 4. This indicates that the variation in the intercritical annealing temperature in the range of 750°C to 790°C has essentially no effect on the percent of ferrite recrystallization. Increasing the Al content from 0.05 wt% to 1.0 wt% increased the volume fraction of recrystallized ferrite. The IQ values from the ferrite grains in the 1.0Al-550 alloy show that for the same percentage of total ferrite formed as in the 0.05Al alloy, a larger ferrite fraction is found to be recrystallized. In fact, the percent of recrystallized grains is already 75% at a very low intercritical annealing temperature, 770°C, as shown in Figure 44 and Figure 45. Also note that the IQ results for austenite (30.2%, 57.5%) are very close to the values observed by point count method (35% and 55% respectively). Furthermore, note that also in this 1.0Al alloy, despite the large difference in temperature to obtain 35%γ and 55%γ during intercritical annealing, there is essentially no difference in the volume fraction of recrystallized ferrite at the two given temperatures. This is because ferrite is already recrystallized at low temperatures during heating and therefore increasing the temperature has no significant effect.

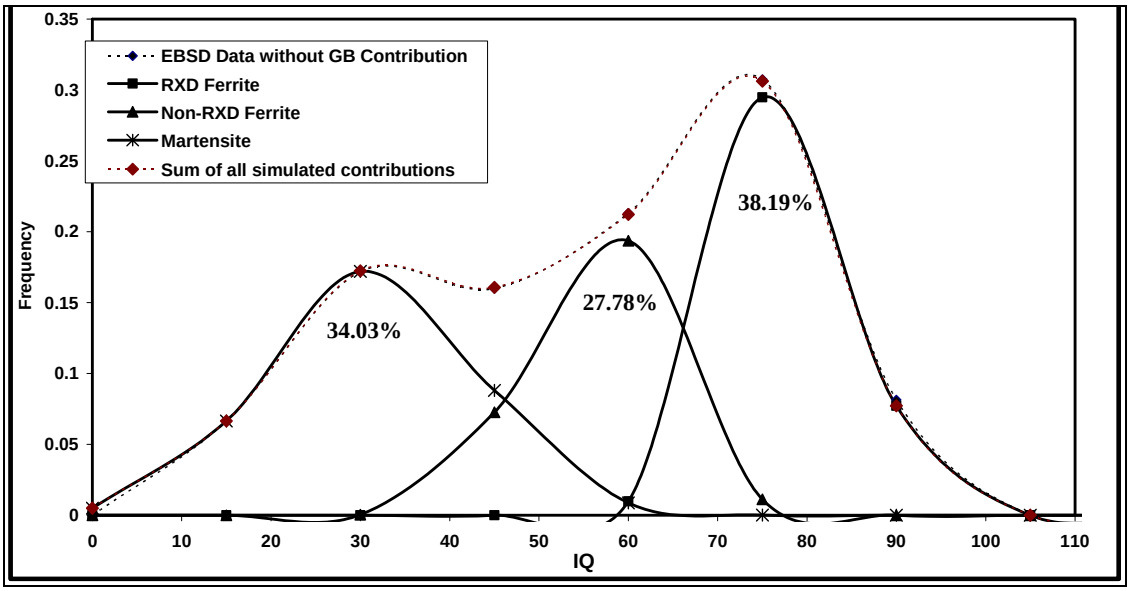

Figure 42 IQ Analysis without grain boundary data in the 0.05Al-550 alloy, T_{IA}=750°C (35%γ), held 60 seconds and quenched

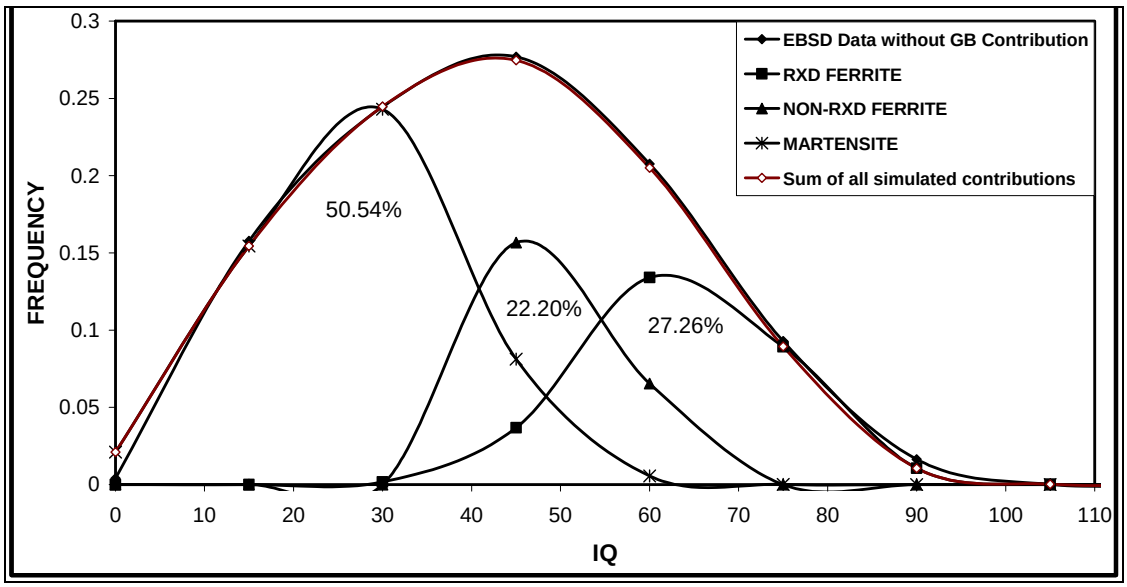

Figure 43 IQ Analysis without grain boundary data in the 0.05Al-550 alloy, T_{IA}=790°C (55%γ), held 60 seconds and quenched

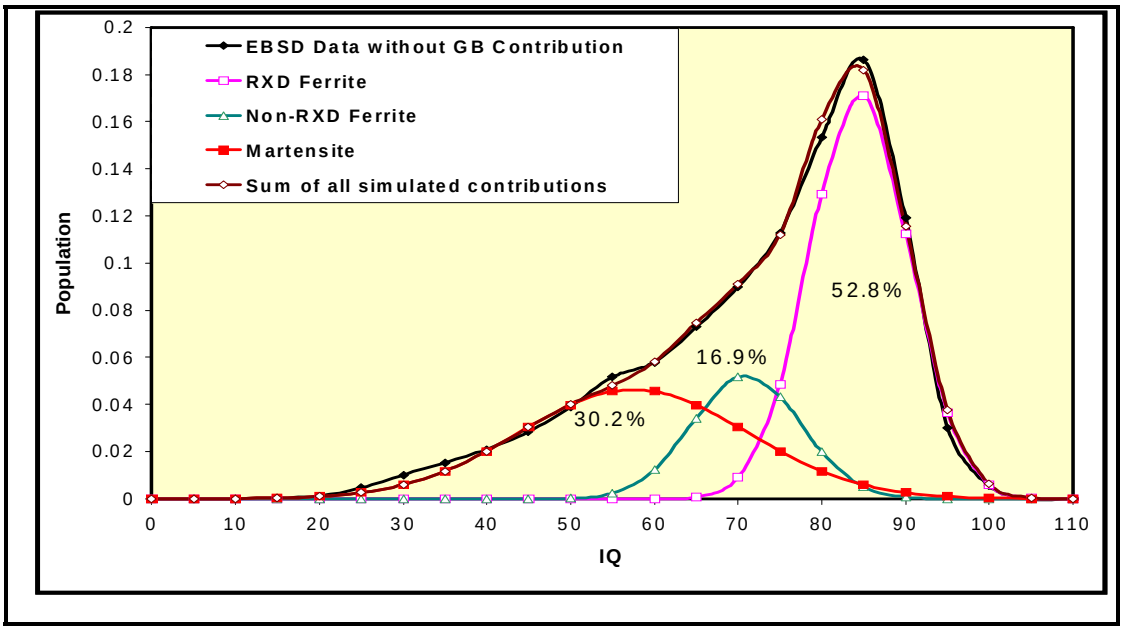

Figure 44 IQ Analysis without grain boundary data in the 1.0Al-550 alloy, T_{IA}=770°C (35%γ), held 60 seconds and quenched

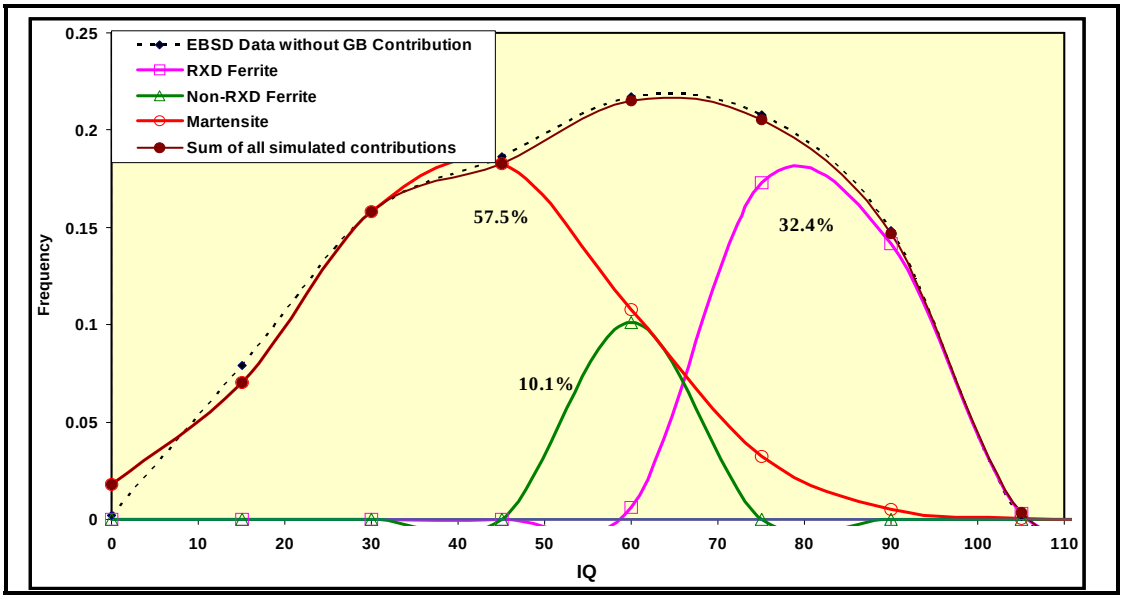

Figure 45 IQ Analysis without grain boundary data in the 1.0Al-550 alloy, T_{IA}=860°C (55%γ), held 60 seconds and quenched

Table 4 shows the amount of austenite, non-recrystallized and recrystallized ferrite at various temperatures for the 0.05Al and 1.0Al alloys. Similarly, the normalized recrystallized ferrite, which is the amount of recrystallized ferrite divided by the total amount of ferrite at any given temperature, is shown in this table.

Table 4 Quantitative microstructural IQ analysis of specimens intercritically annealed to obtain an initial γ=35% and γ=55%, followed by quench, 0.05Al-550 and 1.0Al-550 alloys

Alloy + T_{IA} / Microstructures	0.05Al-550		1.0Al-550	
	750 C, 60s, Quench (35%γ, Point Count)	790 C, 60s,Quench (55%γ, Point Count)	770 C, 60s, Quench (35%γ, Point Count)	860 C, 60s, Quench (55%γ, Point Count)
Austenite (Martensite) %	34.03	50.54	30.2	57.5
RXD Ferrite, %	36.82	27.26	52.8	32.4
Non-RXD Ferrite, %	27.78	22.20	16.9	10.1
Normalized RXD Ferrite (RXD Ferrite/Total Ferrite) %	**56.9**	**55.11**	**75.7**	**76.2**

5.1.2 Austenite Formation

The effect of Al content and the effect of prior-processing hot band coiling temperature on the austenite formation behavior were studied by both OM and SEM-EBSD analysis.

A theoretical calculation using the JMat-Pro software shows that increasing the Al content from 0.05% to 1.0% has the effect of raising the Ac_1 and Ac_3 temperatures of the phase diagram, as shown in Figure 46. Similarly, ThermoCalc suggests that the addition of Al also expands the two-phase region, therefore changing the percent carbon for any given percent austenite in the three alloys, as observed in Figure 47.

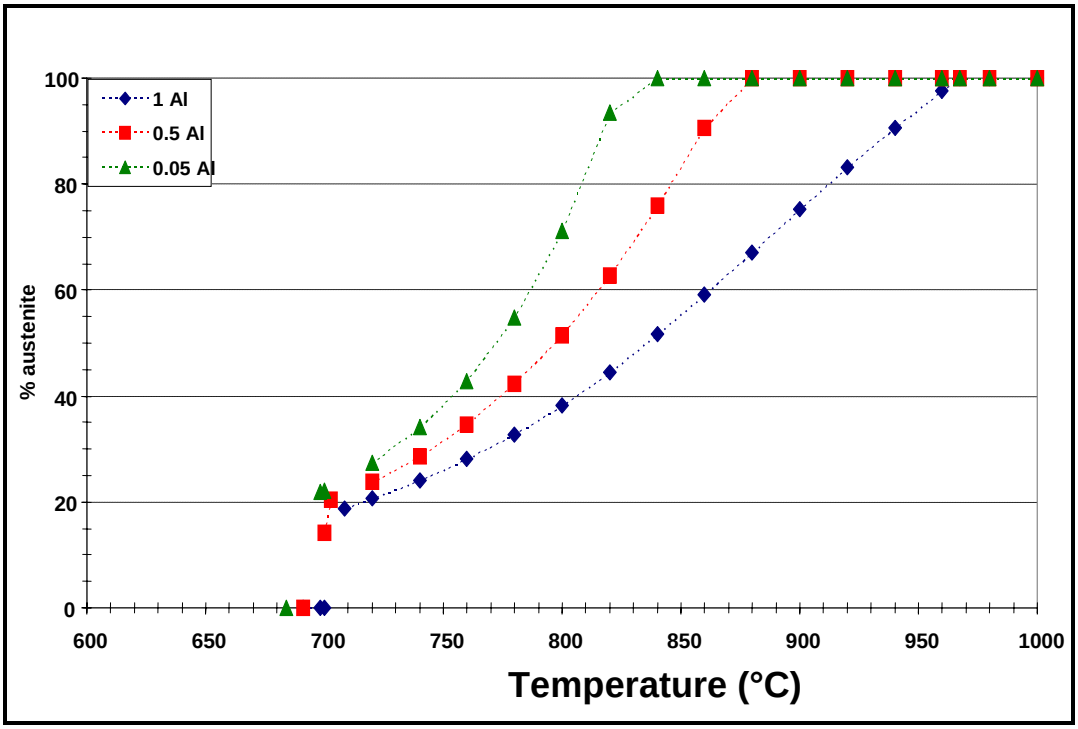

Figure 46 J-Mat Pro simulation of the effect of Al wt% on the austenite volume fraction

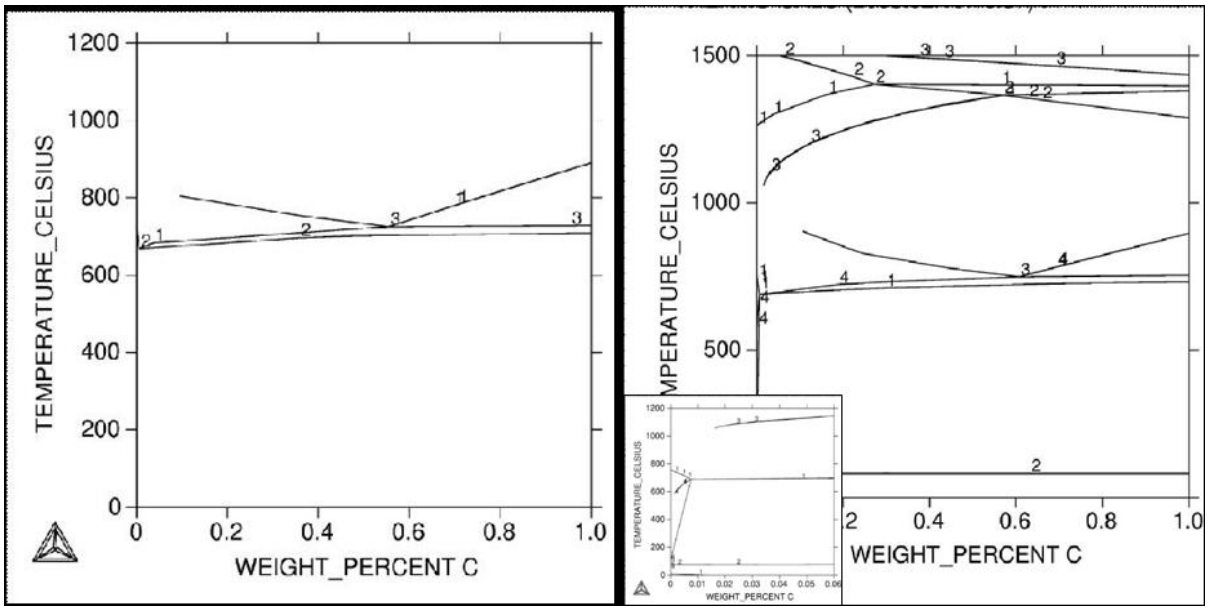

(a) 0.05Al (b) 1.0Al

Figure 47 Effect of Al wt% on the Fe-C Phase Diagram. Addition of Al rises the Ac_1 and Ac_3 temperature, and above 1.0 wt% Al, a loop in the γ-phase is obtained

Figure 48 shows the effect of prior coiling temperature during the hot band processing on the volume fraction of austenite found at different temperatures after holding for 60 seconds in alloy 0.05Al. It is observed that a prior coiling temperature of 550 °C results in a ~15% (absolute value) larger volume fraction of martensite (austenite) when annealed at 780°C compared to the sample coiled at 700°C. Also, in Figure 49 it can be observed that the distribution of austenite throughout the microstructure is more dispersed when the coiling temperature was 550°C, whereas coiling at 700°C results in a more banded austenite structure.

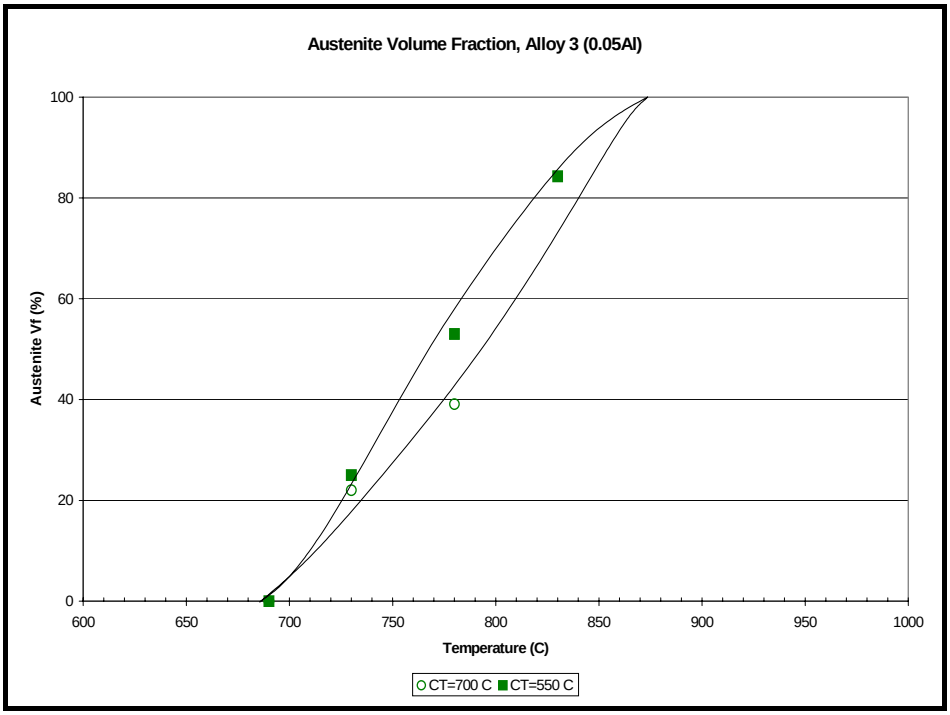

Figure 48 Austenite volume fraction vs intercritical annealing temperature (after 60 sec), 0.05Al alloy

0.05Al-550

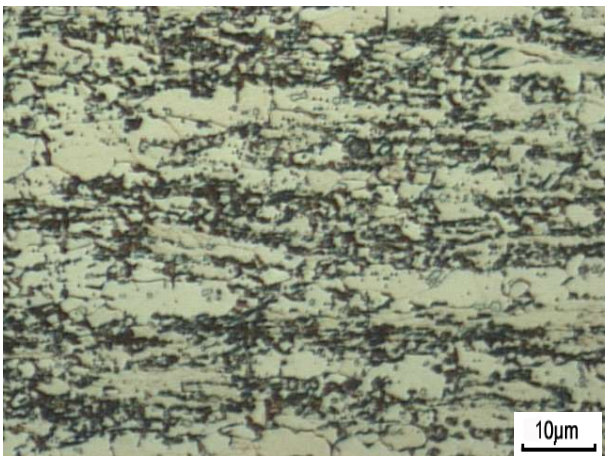

(a) 730°C

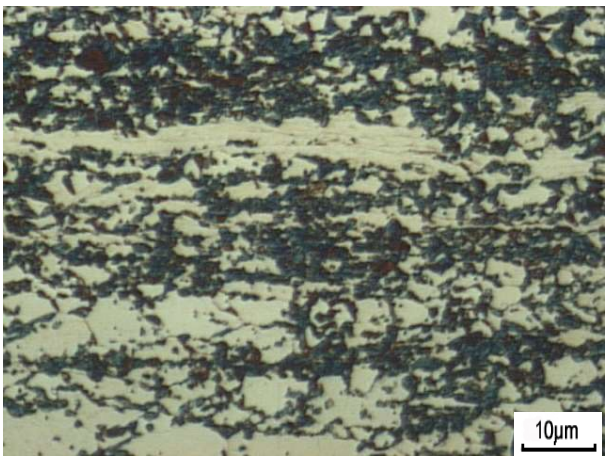

(b) 780°C

0.05Al-700

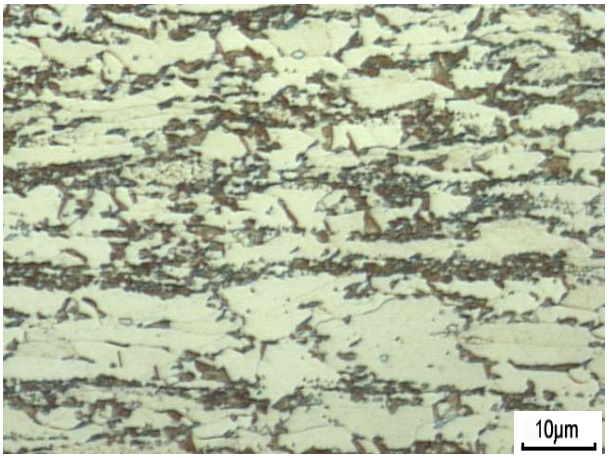

(c) 730°C

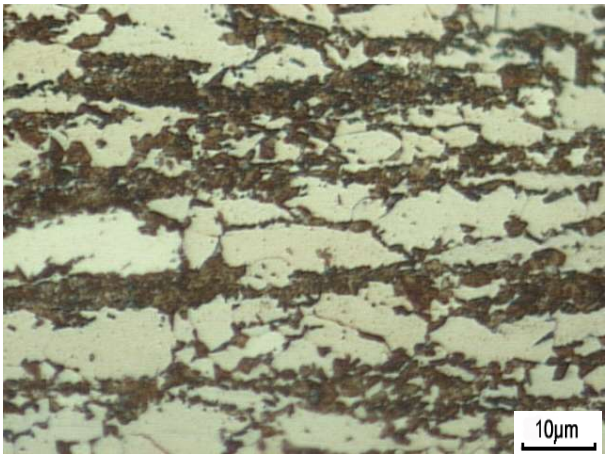

(d) 780°C

Figure 49 Optical micrographs of ferrite (light) and austenite (dark) distribution after intercritical annealing at 730°C and 780°C for 60 seconds followed by quench. (a) and (b) 0.05Al alloy prior-coiled at 550°C, (c) and (d) 0.05Al alloy prior-coiled at 700°C (etchant: 3%Nital + 10% $Na_2S_2O_5$)

The effect of prior coiling temperature on the austenite volume fraction is notably reduced with an increase in Al addition to 0.5 and 1.0 wt%, as shown in Figure 50 and Figure 51. Note that the variation of the coiling temperature in the difference in the austenite volume fraction is less than 5%. Similarly, it is also clear that an increasing Al content increases the Ac_3 temperature, and hence higher intercritical annealing temperatures must be used to obtain similar austenite volume fractions. Figure 51 and Figure 52 show the typical distribution of austenite found in the 0.5Al and 1.0Al alloys, respectively. In the latter, it can be observed that the austenite distribution differs from the 0.05 and 0.5Al alloys, and has shifted from a banded distribution into a necklace type distribution around the ferrite grains.

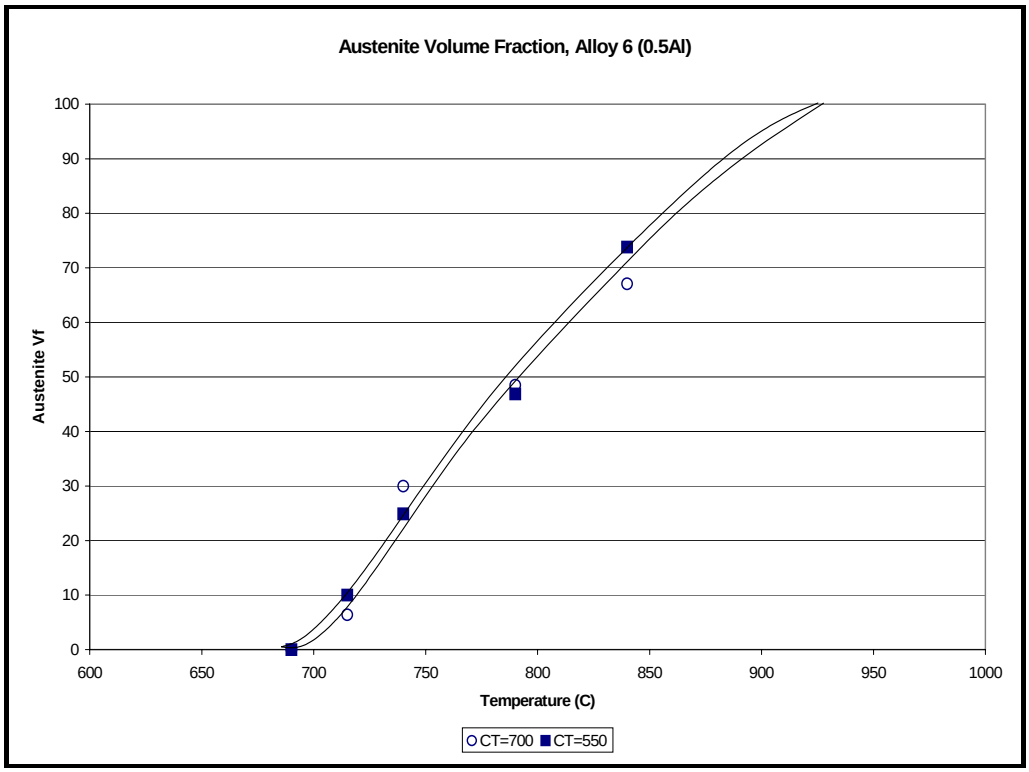

Figure 50 Austenite volume fraction vs intercritical annealing temperature (after 60secs), 0.5Al alloy

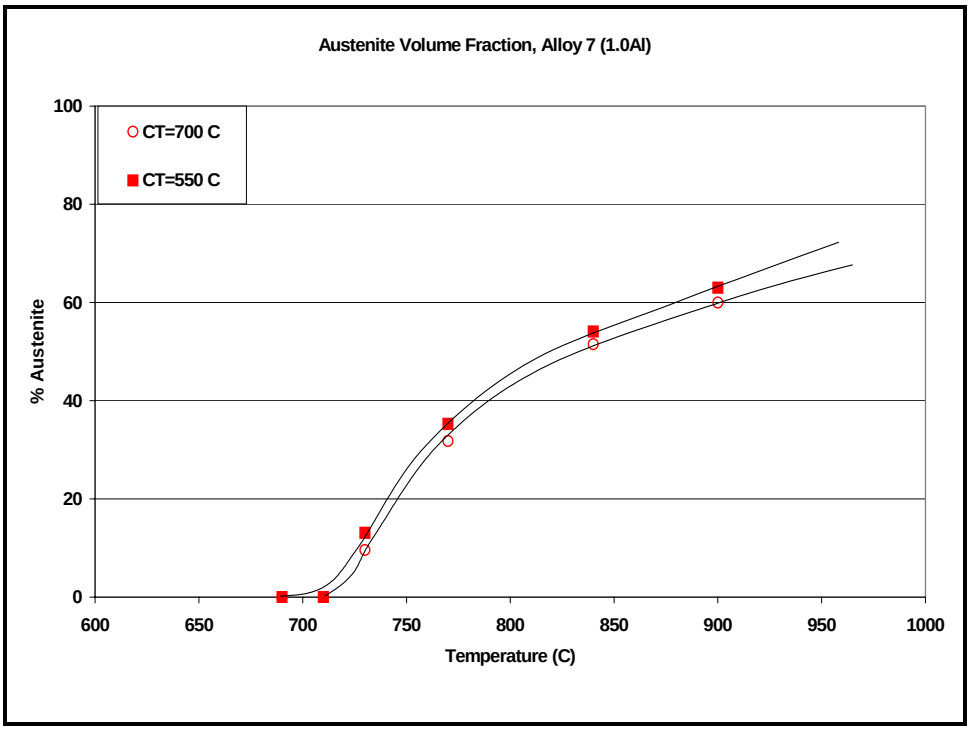

Figure 51 Austenite volume fraction vs intercritical annealing temperature (after 60secs), 1.0Al alloy

0.5Al-550

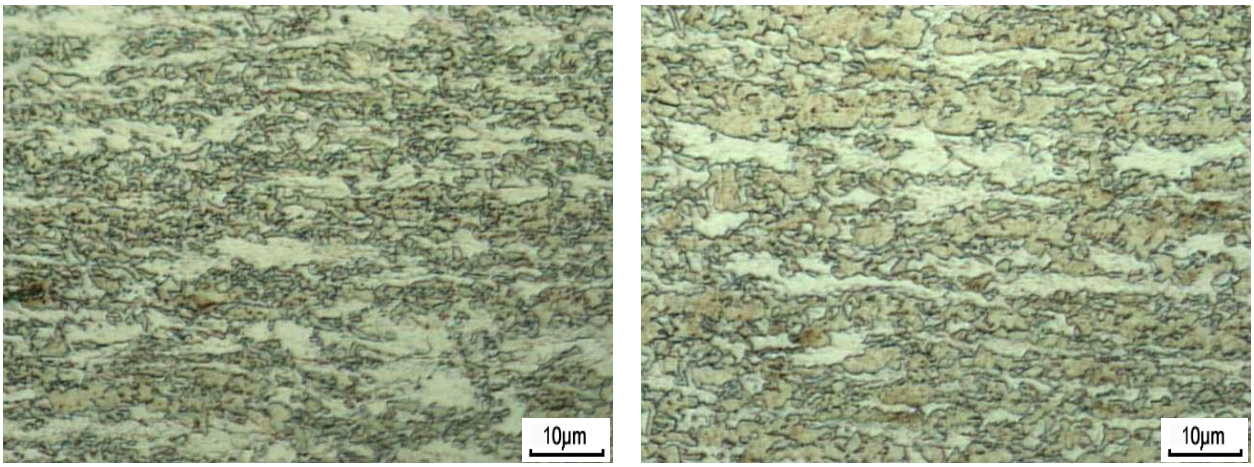

(a) 760 C **(b) 810 C**

0.5Al-700

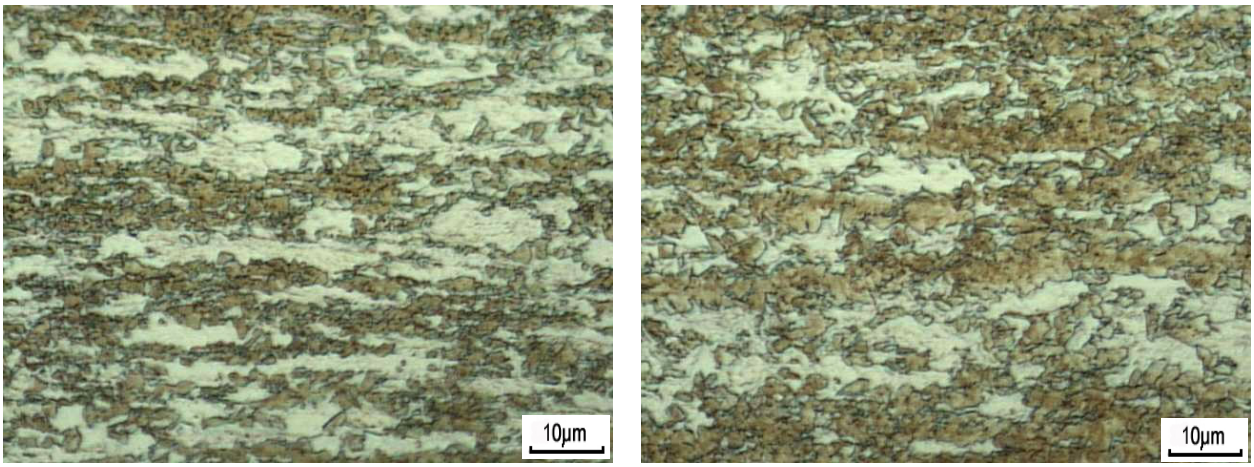

(c) 760 C **(d) 810 C**

Figure 52 Optical micrographs of ferrite (light) and austenite (dark) distribution after intercritical annealing at 760°C (35%γ) and 810°C (55%γ) for 60 seconds followed by quench. (a) and (b) 0.5Al alloy prior-coiled at 550°C, (c) and (d) 0.5Al alloy prior-coiled at 700°C (etchant: 3%Nital)

1.0Al-550

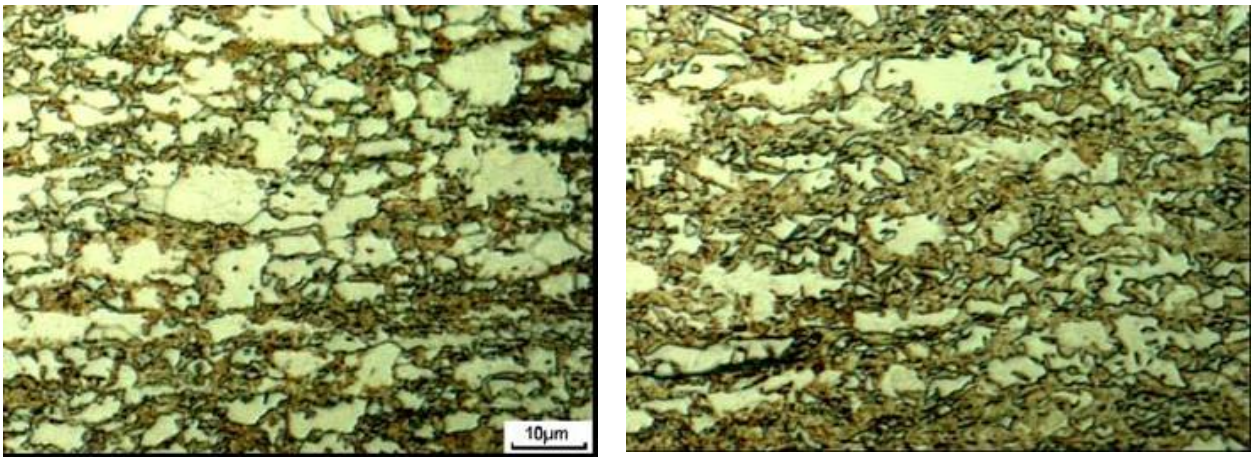

(a) 770 C **(b) 860 C**

1.0Al-700

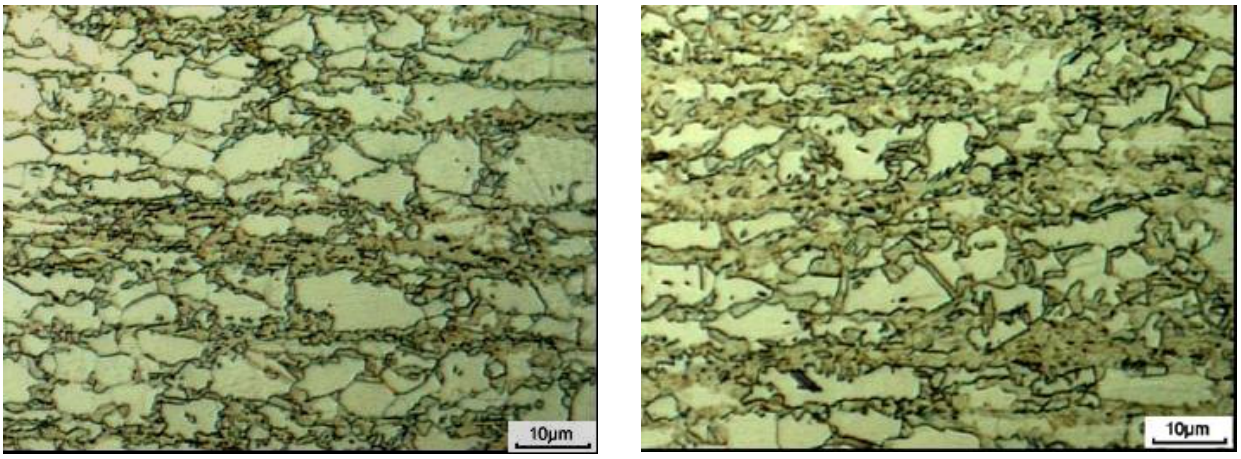

(c) 770 C **(d) 860 C**

Figure 53 Optical micrographs of ferrite (light) and austenite (dark) distribution after intercritical annealing at 770°C (35%γ) and 860°C (55%γ) for 60 seconds followed by quench. (a) and (b) 1.0Al alloy prior-coiled at 550°C, (c) and (d) 1.0Al alloy prior-coiled at 700°C (etchant: 3%Nital)

5.2 STAGE II - AUSTENITE DECOMPOSITION DURING COOLING FROM THE INTERCRITICAL ANNEALING TEMPERATURE (T_{IA}) TO THE ISOTHERMAL HOLDING TEMPERATURE (IHT)

5.2.1 CCT diagrams

The austenite decomposition behavior during cooling was studied in the three Al-bearing TRIP steels. The effects of annealing temperature (initial austenite percent) and prior coiling temperature on the behavior during cooling at different rates to room temperature, as well as cooling to the isothermal bainitic (holding) temperature were investigated.

Figure 54 and Figure 55 show the continuous cooling transformation diagrams (CCT) of the 0.05Al-550, for an initial austenite percent of 35% (750°C) and 55% (790°C) respectively. In the first case, it is observed that epitaxial or "new" ferrite is formed during cooling in the temperature range of 705°C and ceases at ~620°C at essentially all cooling rates. Ferritic bainite forms at a temperature close to 460°C at both 15 and 30°C/sec, and this start temperature increases to 540°C at slower cooling rates, 1°C/sec. Furthermore, granular bainite is also observed when cooling at 1 °C/sec. When cooling from an initial γ=55% condition, both ferrite and bainitic ferrite start temperatures increased. Also, no granular bainite was found when cooling at 1°C/sec. Furthermore, there appears to be a low temperature phase transformation, presumably a martensitic phase transformation at both 30°C/sec and 15°C/sec in the range of 350°C - 250°C. The observed typical microstructures after different cooling rates from T_{IA}=790°C (55%γ) are shown in Figure 56. Similarly, the effect of a higher prior coiling temperature, 0.05Al-700, on the CCT diagram, i.e., new ferrite and bainitic ferrite start and finishing temperatures is shown in Figure 60 for an initial austenite percent of 35% (765°C).

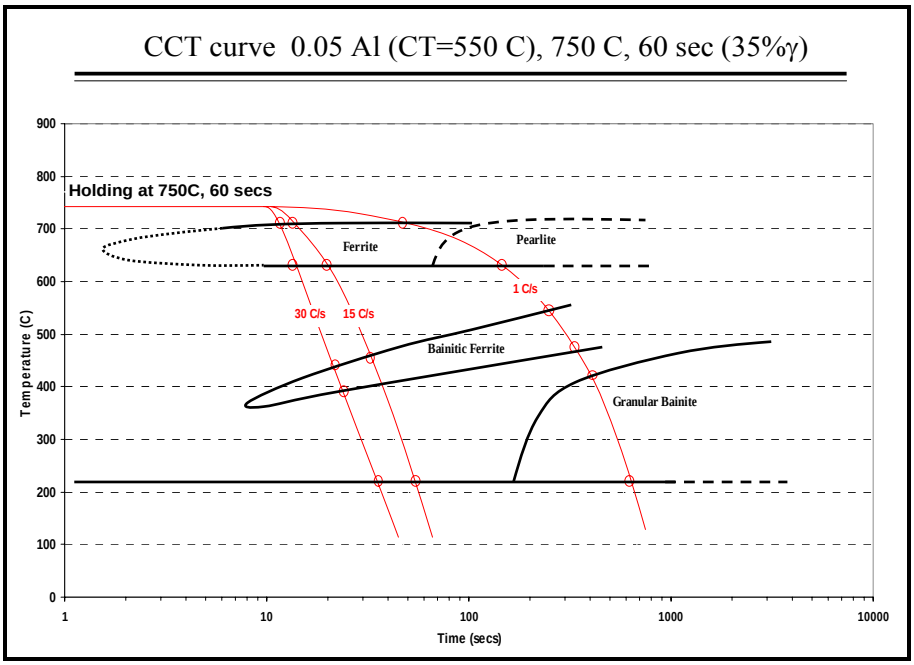

Figure 54 CCT diagram from T_{IA}=750°C (35%γ), 0.05Al-550 TRIP steel

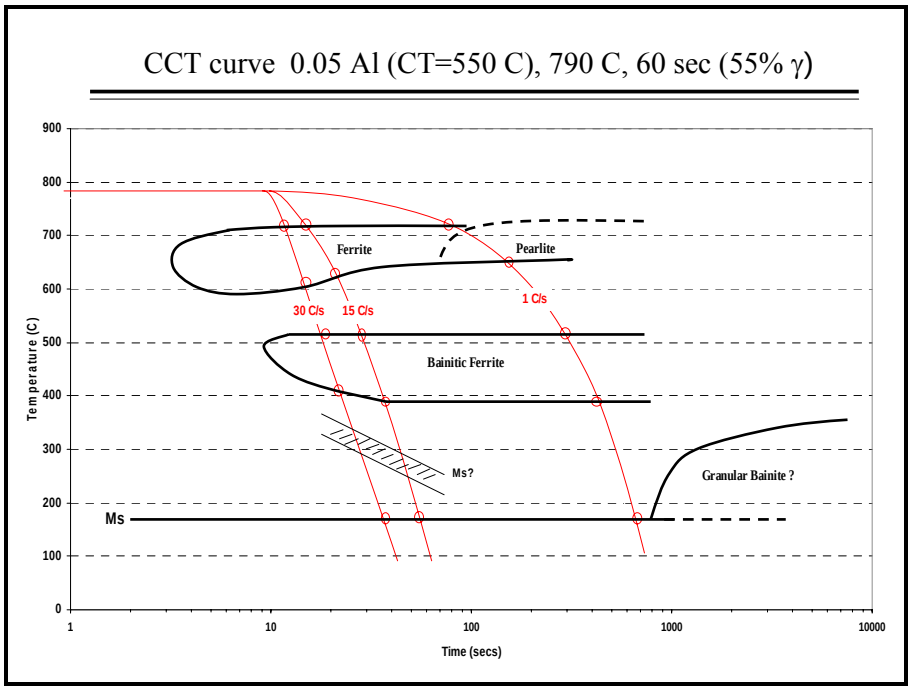

Figure 55 CCT diagram from T_{IA}=790°C (55%γ), 0.05Al-550 TRIP steel

0.05Al-550

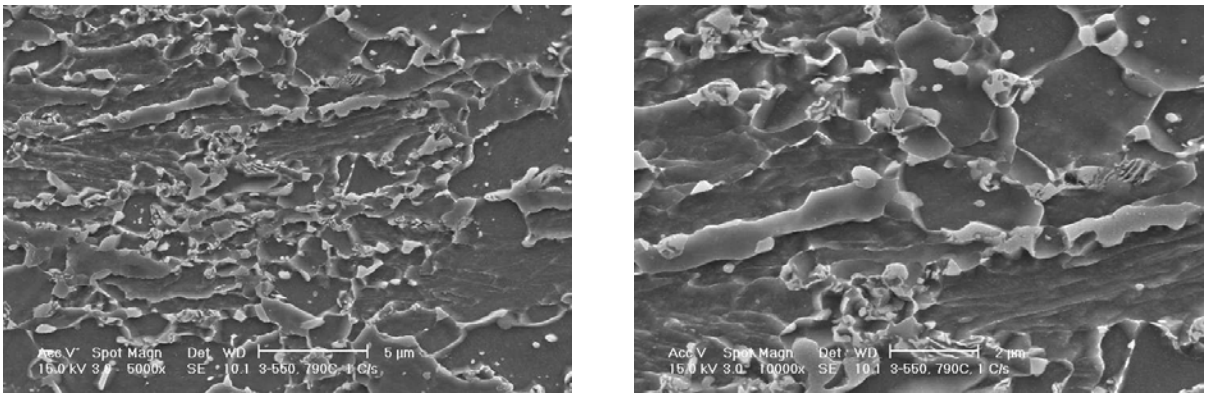

(a) 1 C/sec

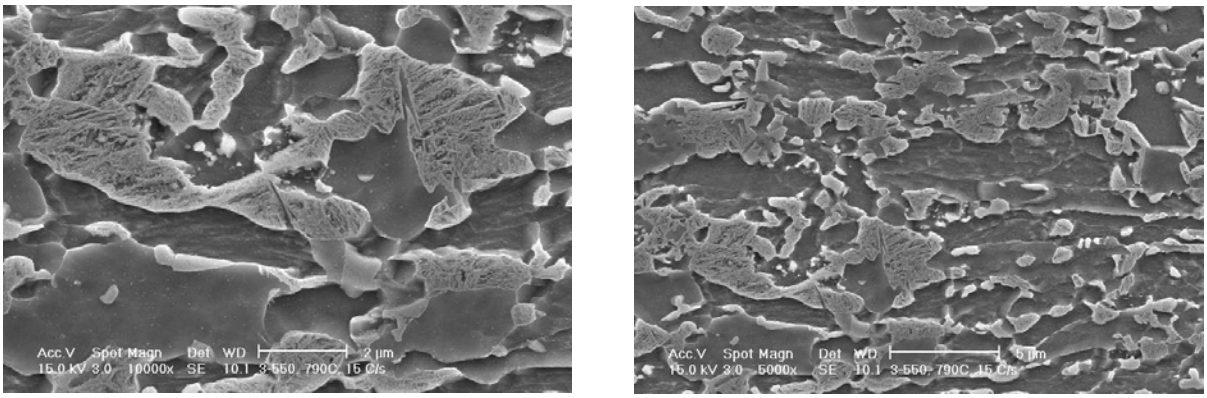

(b) 15 C/sec

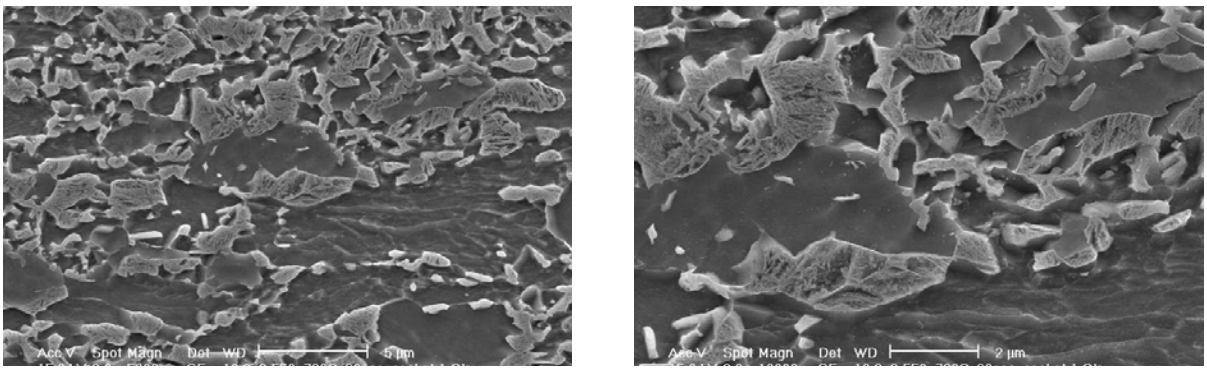

(c) 30 C/sec

Figure 56 SEM micrographs of microconstituents observed after intercritical annealing at 790°C (55%γ) in 0.05Al-550 TRIP steel and cooling to room temperature at various rates: a) 1 °C/sec, b) 15°C/sec, c) 30 °C/sec

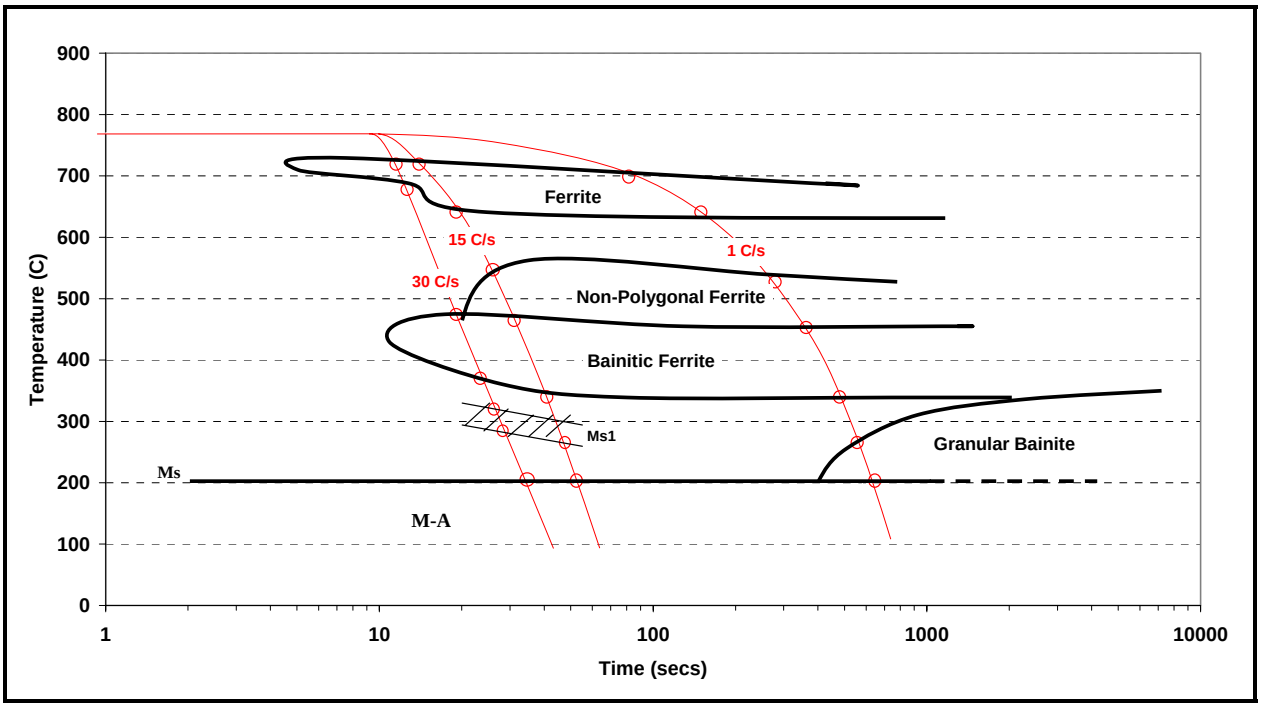

Figure 57 CCT diagram from T_{IA}=765 C (35%γ), 0.05Al-700 TRIP steel

An increase in the Al content to 0.5% lowers the bainitic ferrite start temperature as shown in Figure 58. Also, the temperature region where ferrite and bainitic ferrite form is significantly reduced. Furthermore, granular bainite forms at ~300°C when cooling at 1°C/sec, and on the other hand, pearlite was not observed.

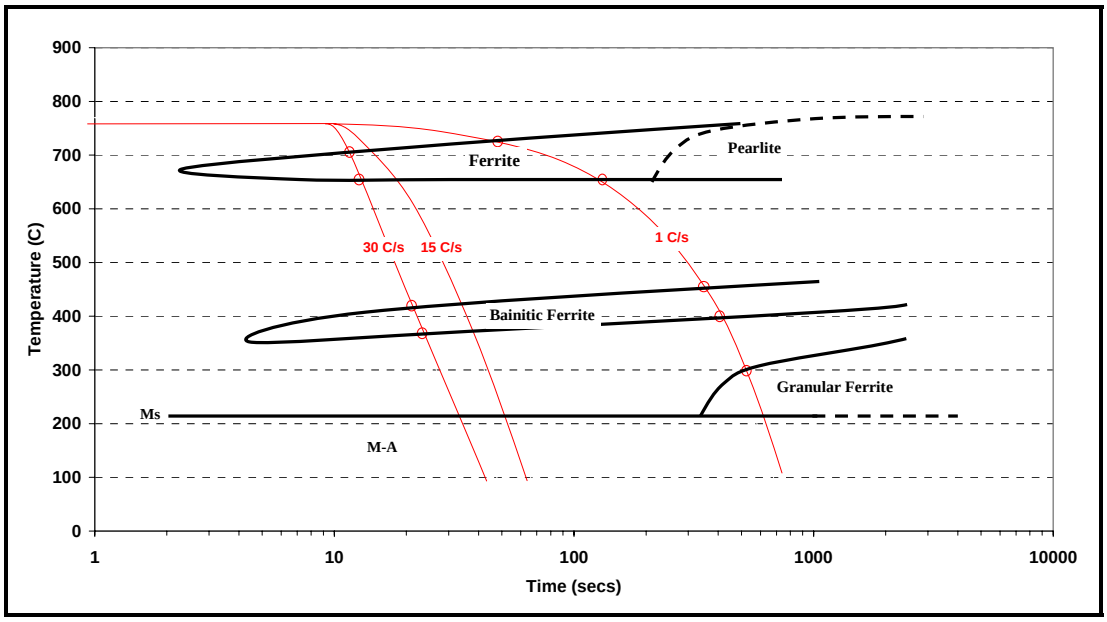

Figure 58 CCT diagram from T_{IA}=760 C (35%γ), 0.5Al-550 TRIP steel

Finally, increasing the Al content to 1.0% eliminates the bainitic ferrite region, and only a "new" ferrite region is observed, regardless of prior coiling temperature. It appears that when an initial austenite percent (35%) is used (T=770C), the epitaxial or "new" ferrite formation immediately begins on cooling as observed in Figure 59. When a larger austenite percent is used (55%, T=860C), an undercooling is necessary before the formation of new ferrite can be observed, as shown in Figure 60. Moreover, note that there is no pearlite formation even at a slow cooling rate of 1°C/sec, however, granular bainite can be observed at this slow cooling rate. Figures 61 and 62 show SEM micrographs of the typical microstructures found in both 1.0Al-550 alloys at both intercritical annealing temperatures of 770°C (35%γ) and 860°C (55%γ). It must be pointed out that a tempering treatment at 200°C for 2 hours was given to these specimens in order to reveal the martensite structure[101], however, no martensite was found and therefore the second phase in these micrographs is retained austenite.

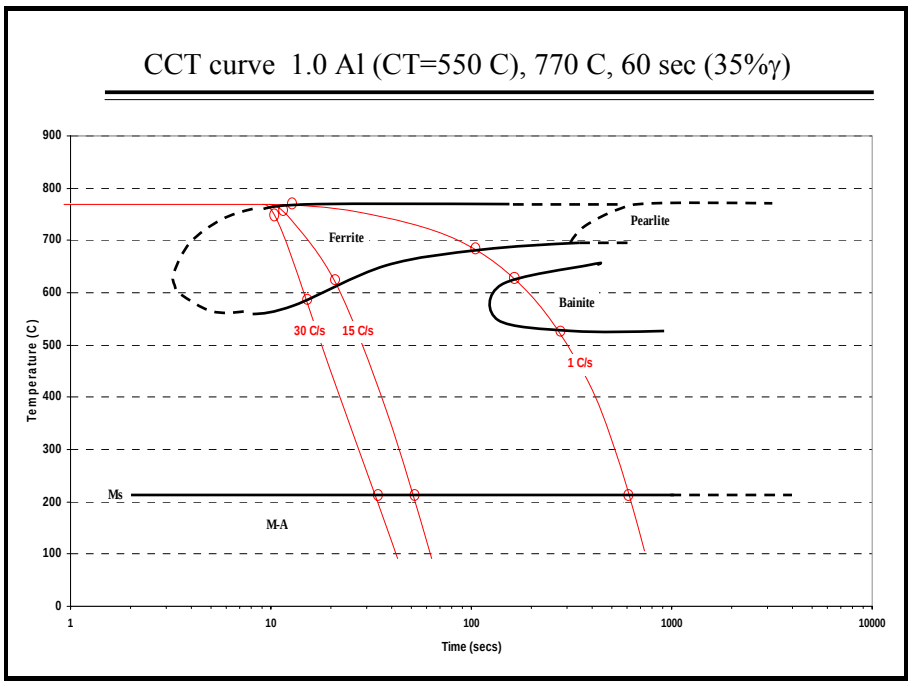

Figure 59 CCT diagram from T_{IA}=770°C (35%γ), 1.0Al-550 TRIP steel

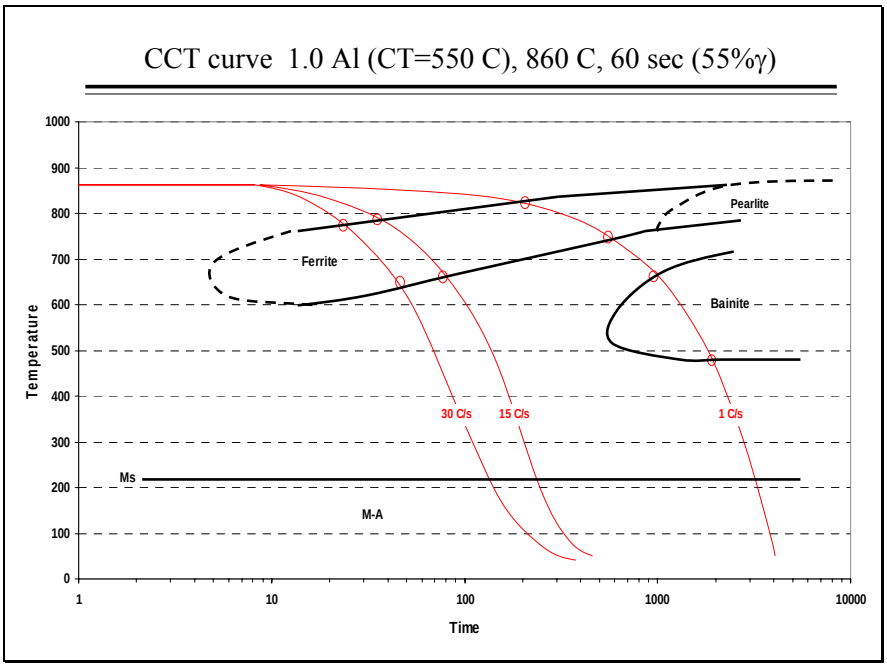

Figure 60 CCT diagram from T_{IA}=860 C (55%γ), 1.0Al-550 TRIP steel

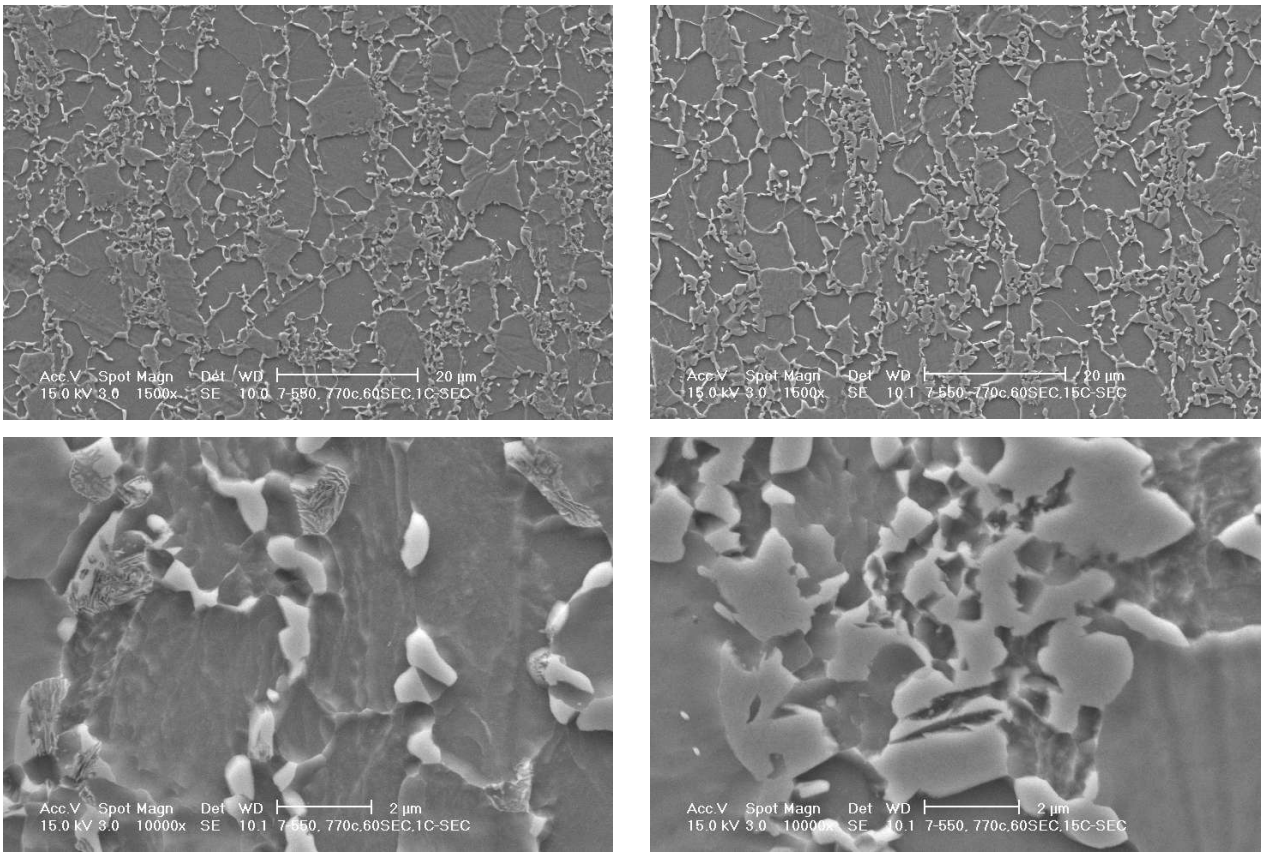

(a) 1°C/sec **(b) 15°C/sec**

Figure 61 SEM micrographs of microconstituents observed after intercritical annealing at 770°C (35%γ) in 1.0Al-550 TRIP steel and cooling to room temperature at various rates: a) 1 °C/sec, b) 15°C/sec. In a) second phase is mostly granular bainite, whereas in b) second phase is retained austenite

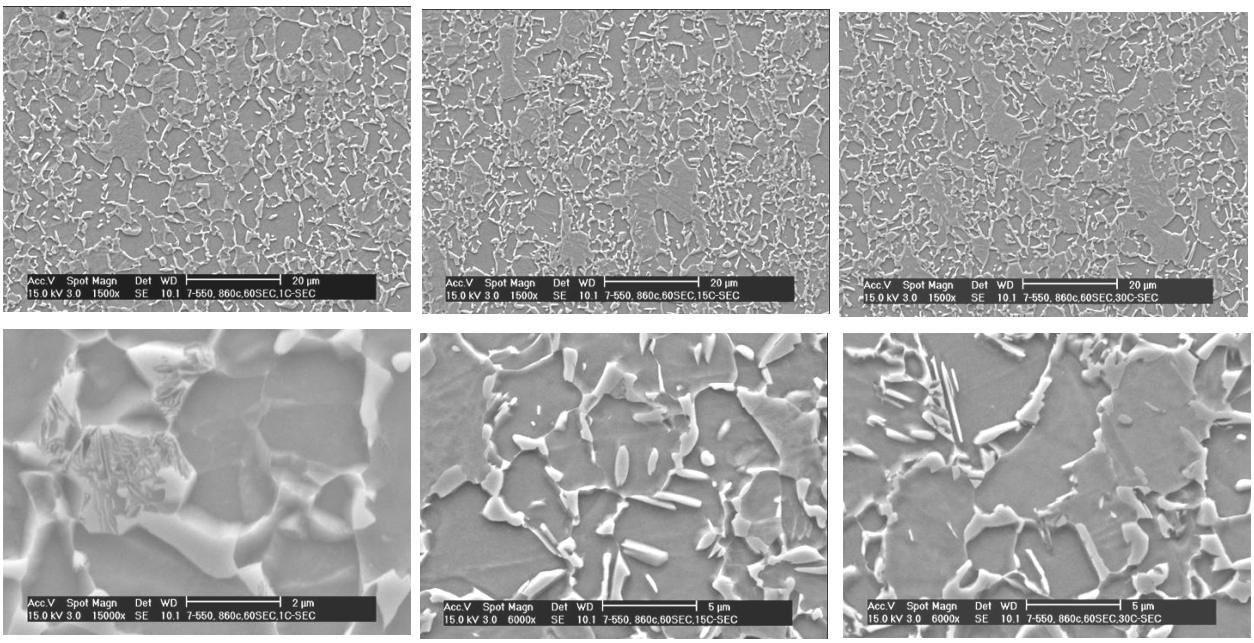

Figure 62 SEM micrographs of microconstituents observed after intercritical annealing at 860°C (55%γ) in 1.0Al-550 TRIP steel and cooling to room temperature at various rates: a) 1 °C/sec, b) 15°C/sec, c) 30°C/sec

5.2.2 Austenite Decomposition after cooling to IBT=450°C

It has been observed that a large percent of the austenite formed during intercritical annealing can transform to ferrite during cooling from the intercritical annealing temperature to the isothermal holding temperature. The effect was observed by OM analysis in the three steels studied under all circumstances and the total amount of transformed ferrite was found to be most influenced by both the Al content and the initial austenite percent at the intercritical annealing temperature (and therefore largely influenced by the carbon content of the austenite). This effect is observed in Figure 63, where the Al content in the alloy is plotted vs volume fraction of the phases observed after cooling at 15°C/sec to 450°C from an intercritical annealing temperature

equal to an austenite volume fraction of 35%. In addition, Figure 64 clearly shows that a larger initial austenite volume fraction during intercritical annealing will result in a larger volume fraction of new ferrite after cooling to the IHT. The M-A volume fraction corresponding to the 1.0Al-550 alloy intercritically annealed at the two temperatures equal to 35% and 55% γ is shown in the OM micrographs in Figure 65, where the M-A microconstituent appears white, and ferrite appears brown or tan (etched in LePera's solution).

In addition, it was observed that the variation in the cooling rate from 15°C/sec to 5°C/sec to the IHT=450°C in the 1.0Al-550 alloy, has a negligible effect on the variation in the volume fraction of transformed austenite, as shown in Figure 66. OM micrographs corresponding to these results are shown in Figure 67, and it can be observed that the M-A volume fraction (white region) is nearly equal (specimens etched in LePera's solution), whereas the ferrite grains appear to have a more polygonal characteristic when cooled at 5°C/sec compared to those ferrite grains observed after cooling at 15°C/sec.

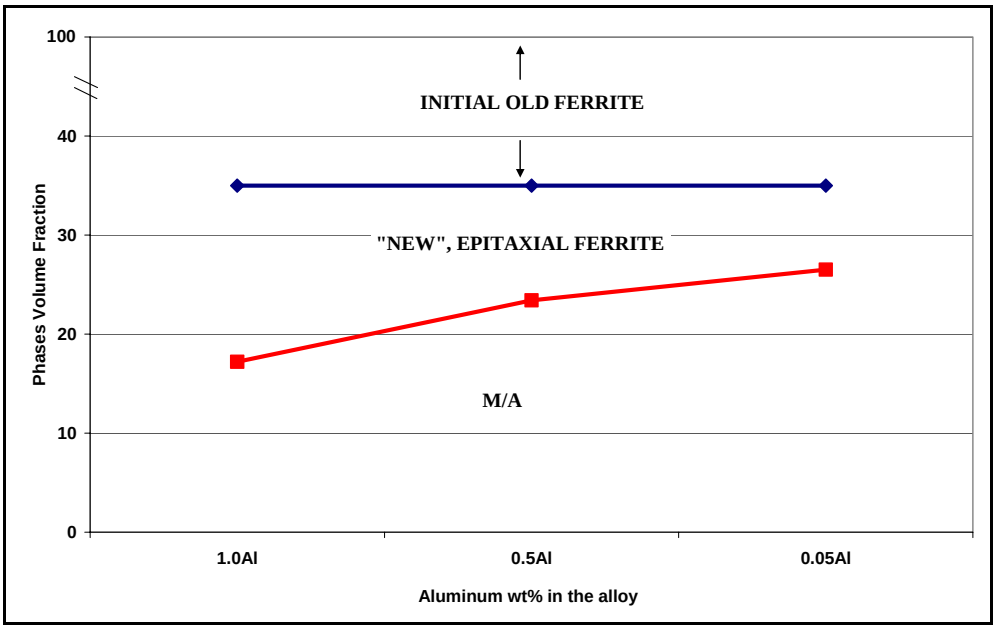

Figure 63 Effect of Al addition on the volume fraction of new ferrite formed during cooling at 15C/sec from T_{IA}= 35%γ to IHT=450°C, followed by quench

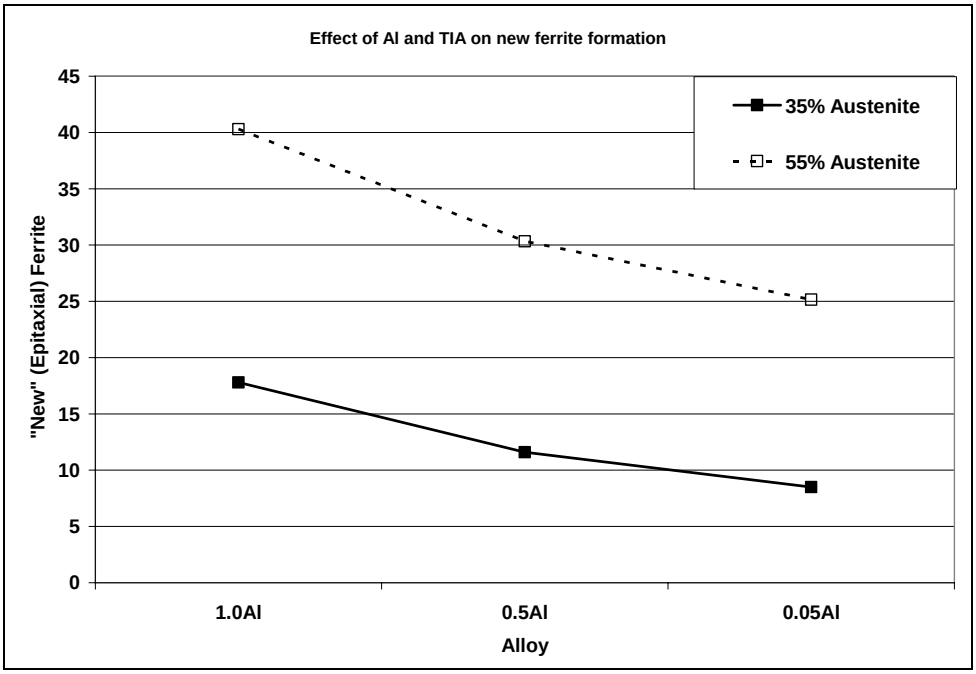

Figure 64 Effect of Al addition and intercritically annealed austenite on the volume fraction of new ferrite formed during cooling at 15C/sec from T_{IA}= 35%γ and T_{IA}= 55%γ to IHT=450°C, followed by quench

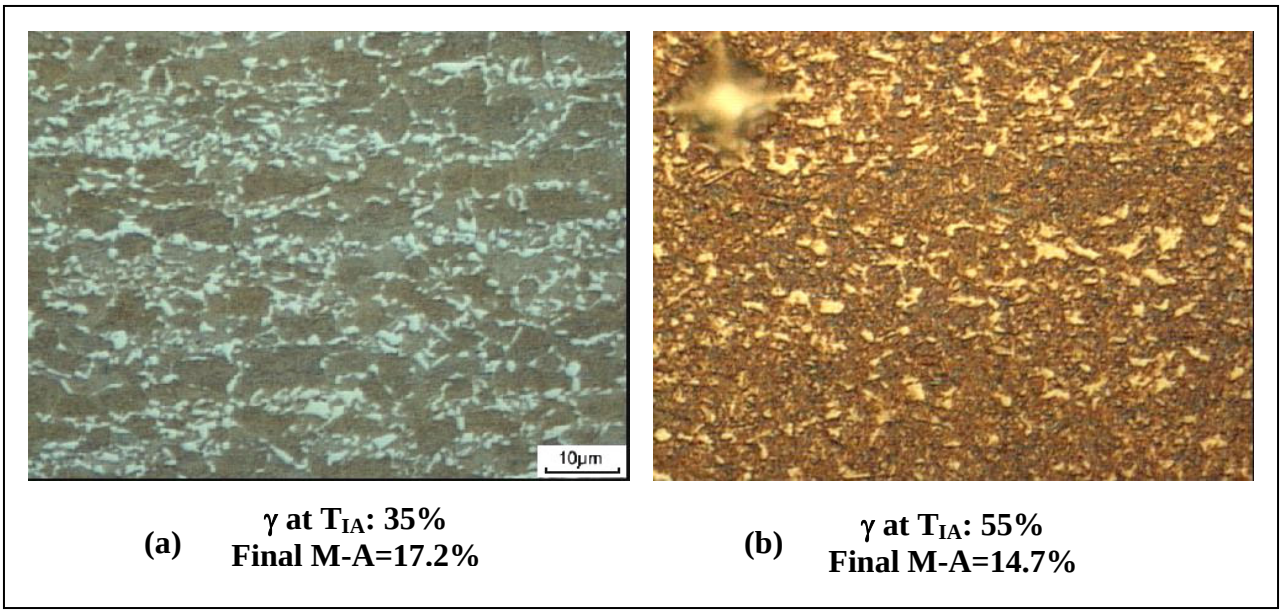

Figure 65 Optical micrographs showing the typical microstructure of the 1.0Al-550 alloy intercritically annealed at (a) 35%γ and (b) 55%γ and cooled at 15C/sec to 450°C followed by quench. White regions show the M-A microconstituent and dark, brown regions show the overall ferrite microconstituent

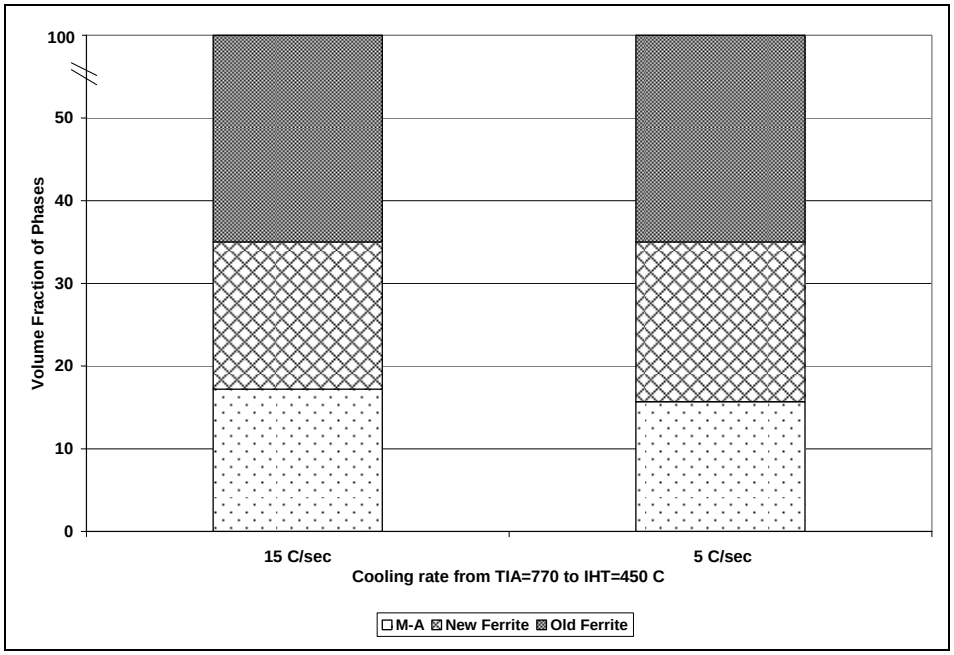

Figure 66 Effect of the variation in cooling rate from T_{IA}= 35%γ to 450°C on the volume fraction of new ferrite

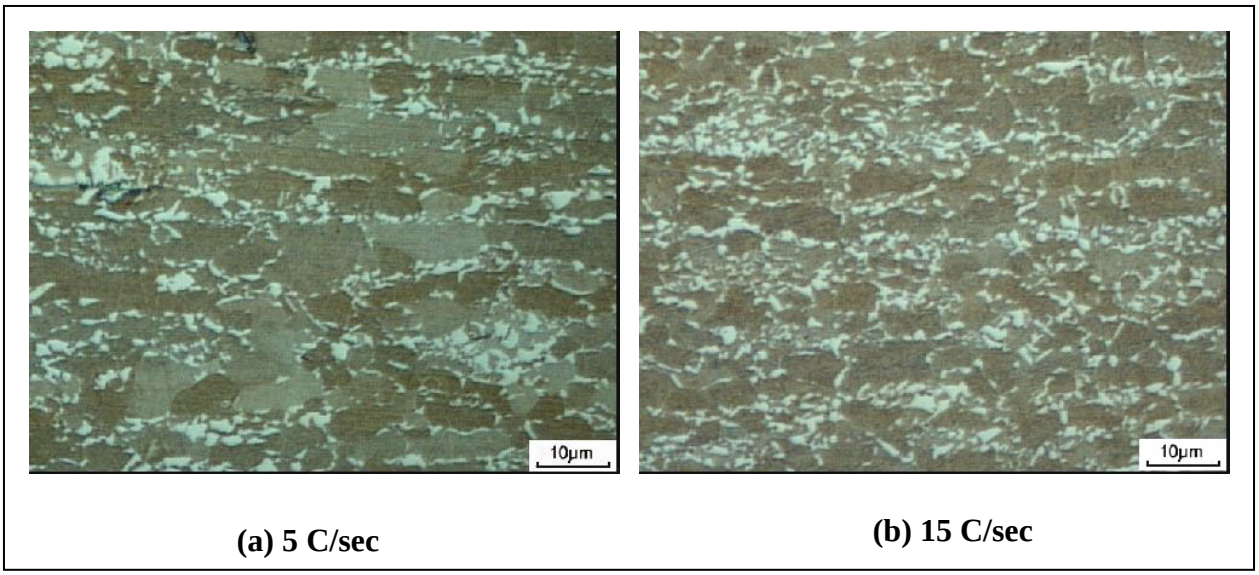

Figure 67 Optical micrographs showing the typical microstructure of the 1.0Al-550 alloy intercritically annealed at 35%γ and cooled at (a) 5°C/sec and (b) 15°C/sec to 450°C followed by quench. White regions show the M-A microconstituent and dark, brown regions show the overall ferrite microconstituent

SEM-EBSD (IQ) analysis has confirmed the observations made by OM analysis. Figure 68 shows the IQ comparison of the 1.0Al-550 alloy after intercritical annealing for an initial austenite volume fraction of 35%(770°C, 60sec → quench) and the IQ analysis after cooling at 15°C/sec from 770°C and held for 2-5 seconds at the IHT (450°C) followed by water quench.

Note that the IQ value of the new ferrite overlaps that of the non-recrystallized ferrite and therefore the total volume fraction of new ferrite must be calculated by subtracting the difference from the percent peak from the non-recrystallized + new ferrite (after cooling from the T_{IA}) to the non-recrystallized peak after only intercritical annealing, as shown earlier in Table 3. Also, it can be observed that a new low IQ peak appears corresponding to a small volume fraction of less than 4%, which was identified to be retained austenite and later confirmed by magnetometry analysis. Alternatively, the new ferrite can be simply obtained by subtracting the volume fraction of martensite + bainite + retained austenite observed after cooling to 450°C followed by quench

from the volume fraction of austenite observed at any given intercritical annealing temperature. Following this analysis, the M-A volume fraction after cooling to 450°C from 770°C is found to be ~20.2%, which after subtracting from an initial 35%γ gives a new ferrite percent of ~14.7%. This latter analysis was used to calculate the new ferrite shown in the subsequent IQ figures. Furthermore, the Tables A,B,and C in Appendix A show the data obtained from these figures.

Figure 69 shows an IQ analysis in the 1.0Al-550 alloy after intercritical annealing at a higher temperature, equal to an austenite volume fraction of 55% (860°C, 60sec → quench). It is obvious that a larger volume fraction of new ferrite is formed during cooling from an initial 55%γ as in comparison with the specimen cooled from an initial 35%γ, and the total volume fraction of M-A observed after quenching from 450°C is very similar to that obtained by intercritical annealing at 770°C (35%γ), although it appears that an additional 4-5% ferrite forms when cooling from 860°C (55%γ). Furthermore, the IQ analysis of the 1.0Al-700 alloy intercritically annealed to obtain an initial 35%γ (T_{IA}=770°C 60 sec), then cooled at 15°C/sec to 450°C + quench is shown in Figure 70, and it appears that a prior coiling temperature of 700°C results in approximately 6.7% additional ferrite being formed during cooling, which causes the total M-A volume fraction to be reduced to only to 13.5% upon cooling to 450°C.

As previously mentioned, smaller Al additions result in less new ferrite formation. Figure 71 shows the IQ analysis of the 0.5Al-550 alloy intercritically annealed at 810°C and held for 60 seconds (equal to 55%γ), cooled at 15°C/sec to 450°C followed by brine quench. It can be observed that the M-A volume fraction equals ~24.7%, which corresponds to a new ferrite formation of 30.3% during cooling to 450°C. Therefore, reducing the Al content from 1.0wt% to

0.5wt% reduces the new ferrite formation from 41.8% to 30.3% (approximately a 11.5% reduction) during cooling from an initial 55%γ to 450°C.

Moreover, the IQ analysis of the austenite decomposition in the 0.05Al-550 alloy is shown in Figure 72. It can be observed that the new ferrite formed after cooling to 450°C from an intercritical annealing temperature equal to an initial 35%γ (750°C), is much less (~8.4%) than the new ferrite formed in the 0.5Al and 1.0Al alloy, and therefore, a larger volume fraction of M-A constituent is observed, 26.5%. Also, cooling from 790°C (55%γ) also results in a small volume fraction of new ferrite, (or in other words, a large M-A volume fraction) as observed from the IQ analysis in Figure 73. Following the same analysis used previously, it was determined that the volume fraction of new ferrite in this case results in 25.1%, which is much less than the amount observed in the higher Al-bearing alloys. Finally, the effect of the prior coiling temperature on the new ferrite formed during cooling from an initial 35%γ (750°C in the 0.05Al-550 and 765°C in the 0.05Al-700 alloy) to 450°C was also analyzed using IQ analysis. Figure 74 shows that the M-A volume fraction is 26.9%, which in turn results in ~8.1% new ferrite formation. This is not very different from the volume fraction of new ferrite observed when the prior coiling temperature was 550°C, and therefore, the variation in the coiling temperature appears to have no significant effect on the new ferrite formation in this 0.05Al alloy.

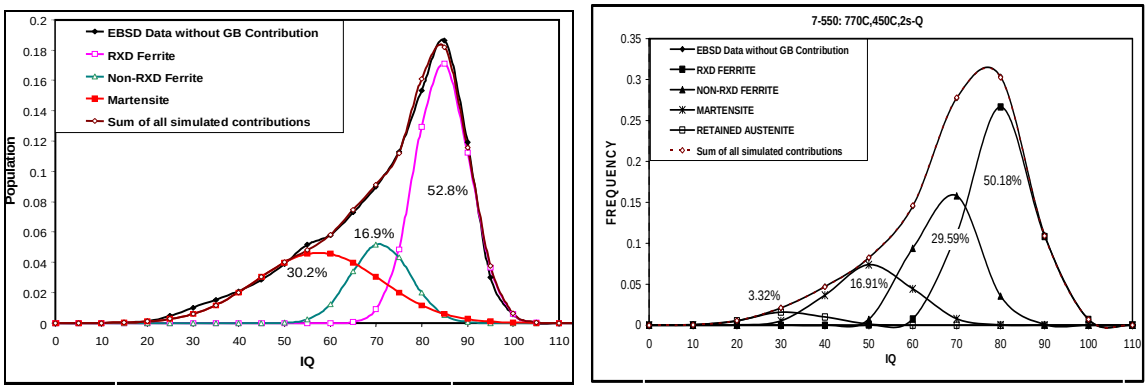

(a) 770°C (60sec) + Q (b) 770°C, cool to 450°C + Q

Figure 68 IQ multi-peak quantitative analysis of the microconstituents in the 1.0Al-550 alloy after (a) T_{IA}=770°C (35%γ), held 60s followed by quenched, and (b) T_{IA}=770°C (35%γ), held 60s followed by cooling at 15°C/sec to 450°C and immediately quenched

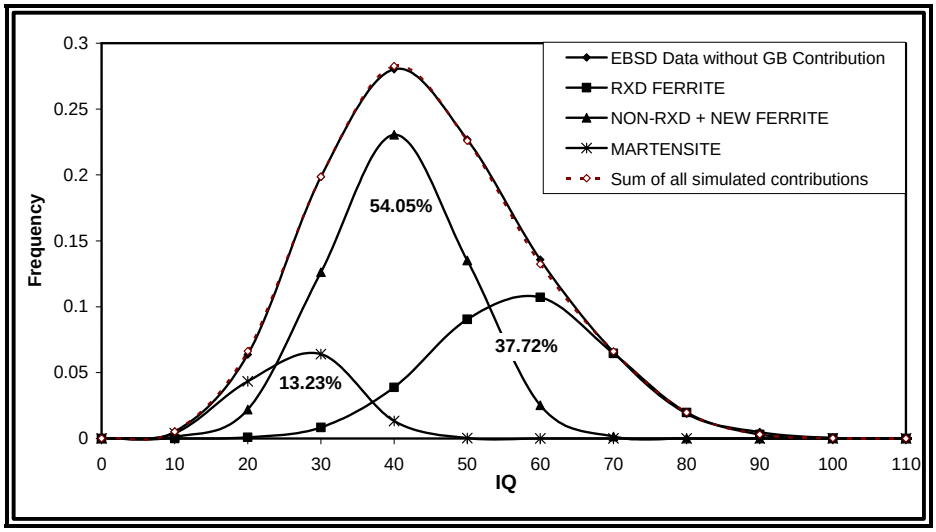

Figure 69 IQ multi-peak quantitative analysis of the microconstituents in the 1.0Al-550 alloy after T_{IA}=860°C (55%γ), held 60s followed by cooling at 15°C/sec to 450°C and immediately quenched

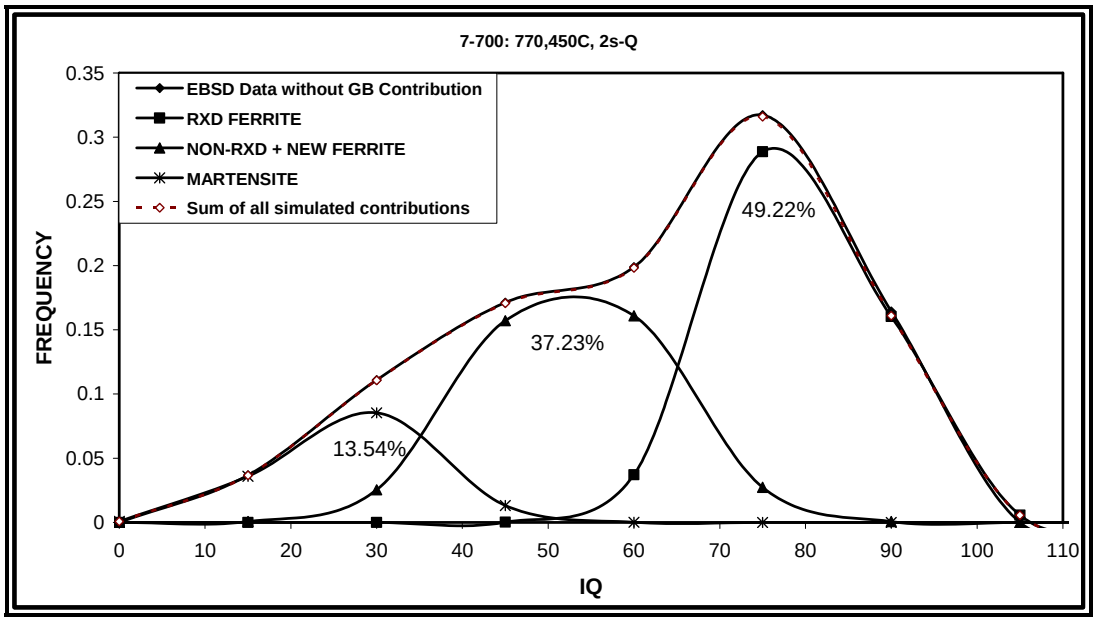

Figure 70 IQ multi-peak quantitative analysis of the microconstituents in the 1.0Al-700 alloy after T_{IA}=770°C (35%γ), held 60s followed by cooling at 15°C/sec to 450°C and immediately quenched

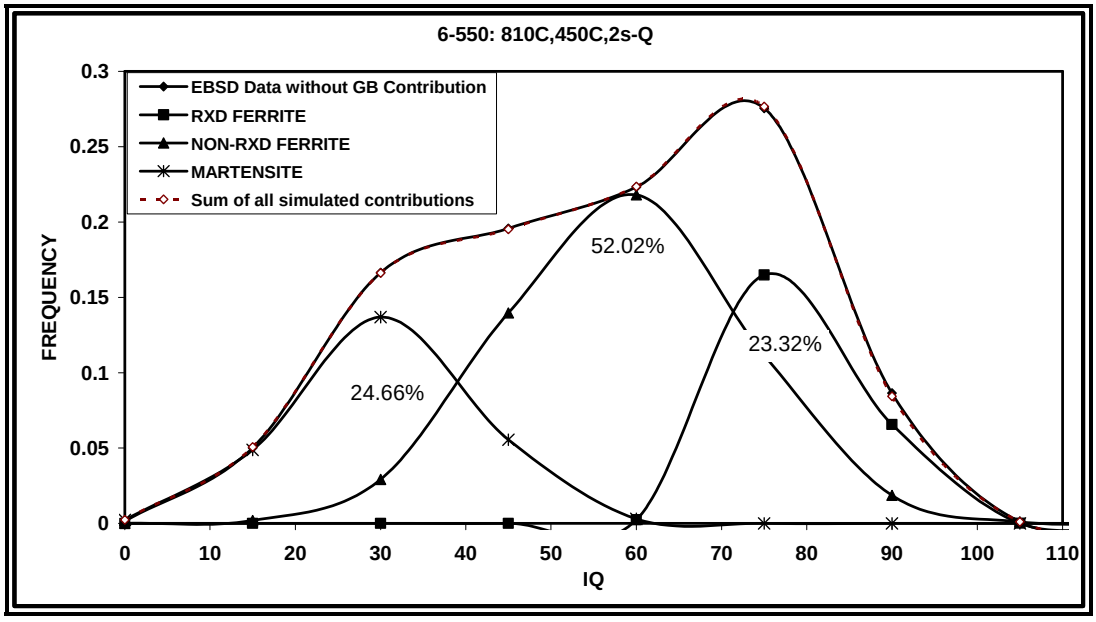

Figure 71 IQ multi-peak quantitative analysis of the microconstituents in the 0.5Al-550 alloy after T_{IA}=810°C (55%γ), held 60s followed by cooling at 15°C/sec to 450°C and immediately quenched

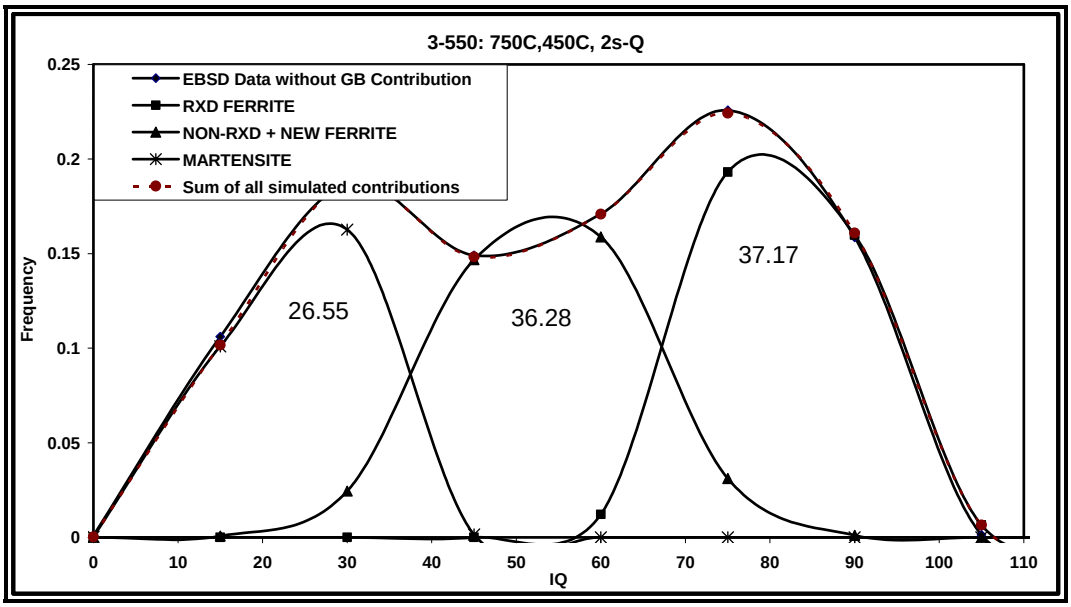

Figure 72 IQ multi-peak quantitative analysis of the microconstituents in the 0.05Al-550 alloy after T_{IA}=750°C (35%γ), held 60s followed by cooling at 15°C/sec to 450°C and immediately quenched

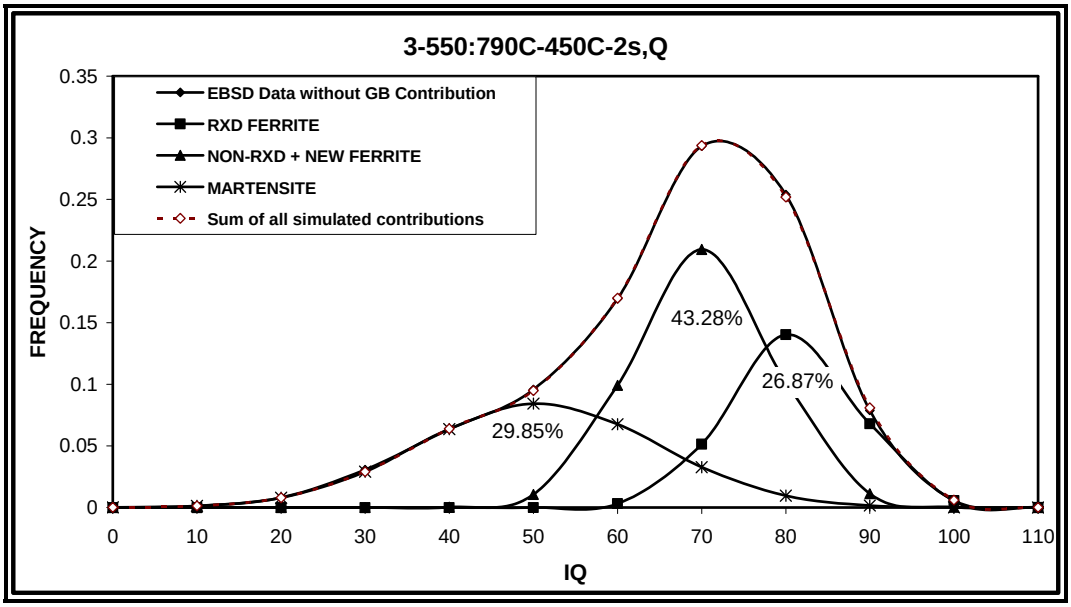

Figure 73 IQ multi-peak quantitative analysis of the microconstituents in the 0.05Al-550 alloy after T_{IA}=790°C (55%γ), held 60s followed by cooling at 15°C/sec to 450°C and immediately quenched

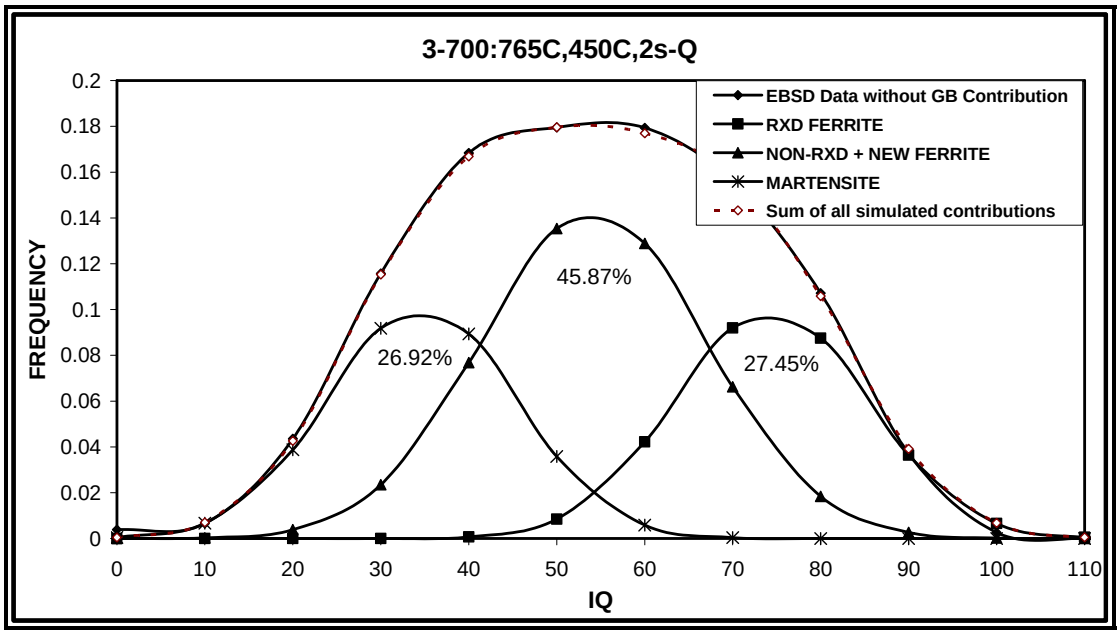

Figure 74 IQ multi-peak quantitative analysis of the microconstituents in the 0.05Al-700 alloy after T_{IA}=765°C (35%γ), held 60s followed by cooling at 15°C/sec to 450°C and immediately quenched

5.3 STAGE III - AUSTENITE DECOMPOSITION DURING ISOTHERMAL HOLDING AT 450 C

5.3.1 Austenite Decomposition Maps

The austenite decomposition during isothermal holding at 450°C was studied in the three Al bearing alloys, and it was observed that in all cases the volume fraction of austenite to bainite transformation during this holding period is relatively small, i.e., only about 2-14% after holding for two minutes, independent of initial volume fraction of austenite, cooling rate from the intercritical annealing temperature to the isothermal holding temperature (450°C) or prior coiling temperature conditions. The volume fraction percent of the different phases observed at different time intervals at 450°C is shown in Tables A,B and C in Appendix A.

These results are shown in Figure 75 for the 1.0Al-550 alloy, where the volume percent of the different phases are plotted at different time intervals during holding at 450°C. In this case, the annealing temperature corresponds to an initial austenite volume fraction=35%, then cooled at 5 and 15°C/sec to 450°C. It can be observed that the variation in the cooling rate has no significant effect on the total volume fraction of the final phases. However, it was observed that cooling at 5°C/sec resulted in a peak in the amount of retained austenite at short holding times, whereas cooling at 15°C/sec no peak is observed, at least during the time interval investigated, and the volume fraction of retained austenite increased with holding time. It can be observed that the amount of martensite gradually decreases and disappears shortly after 60 seconds. Similarly, the maximum volume fraction of bainite after 120 seconds is ~3%. An additional 2% is obtained during cooling from the IHT to RT (room temperature), as observed from the difference in the 2sec+AC and 2sec+quench specimens. A similar analysis is shown in Figure 76 for an initial

austenite volume fraction of 55% (860°C). Note that the maximum amount of bainite is approximately 1%. Also, very little martensite is observed. Furthermore, a similar analysis was undertaken in the 0.5Al-550 alloy intercritically annealed at 760°C (35%γ), Figure 77. Note that the amount of retained austenite is less than that obtained in the 1.0Al-550 alloy, and the volume fraction of martensite is larger. Similarly, the maximum volume fraction of bainite in this 0.5Al-550 alloy is 6.1% and an additional 2.6% is obtained during cooling. Finally, Figure 78 shows a similar analysis for the 0.05Al-550 alloy intercritically annealed to obtain an initial 35%γ. After holding for 30 seconds at 450°C, the volume fraction of bainite reaches 10.3% and the volume fraction of austenite is only 2%. Holding for 120 seconds, increases the bainite volume fraction to 14% and the retained austenite volume fraction is increased to 4.1%.

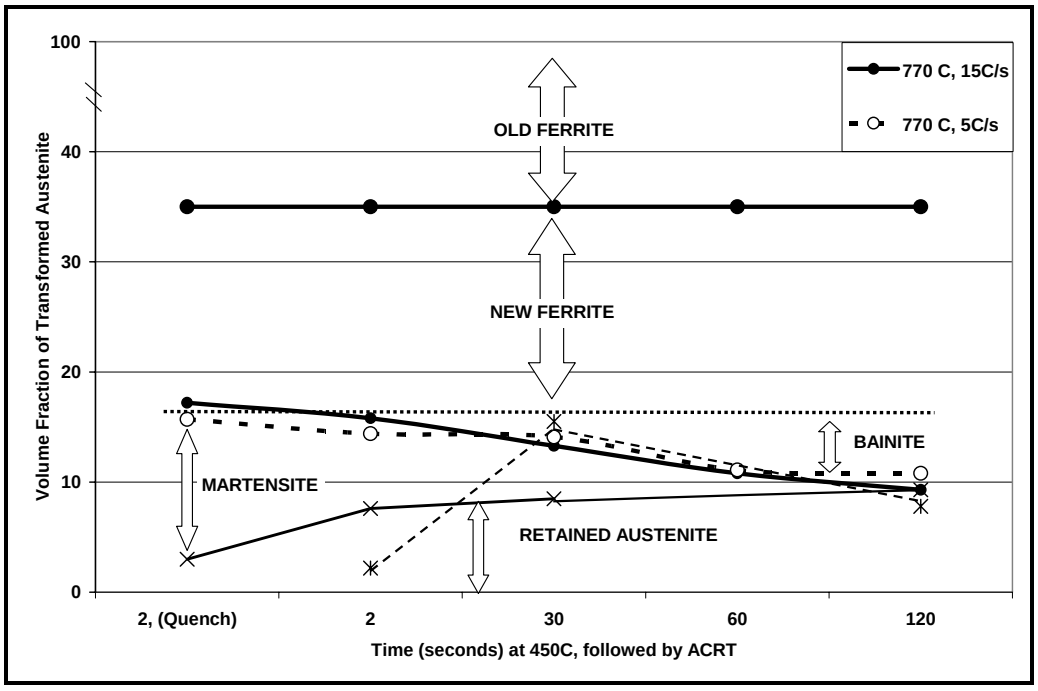

Figure 75 Austenite decomposition behavior during isothermal holding at 450°C after cooling from T_{IA}=35%γ, 1.0Al-550 TRIP steel

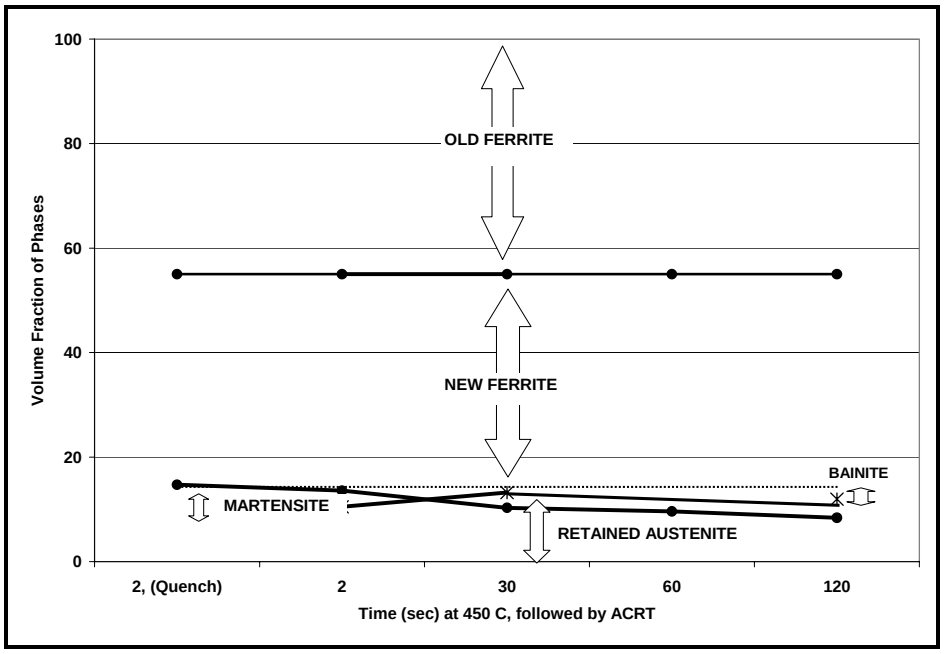

Figure 76 Austenite decomposition behavior during isothermal holding at 450°C after cooling from T_{IA}=55%γ, 1.0Al-550 TRIP steel

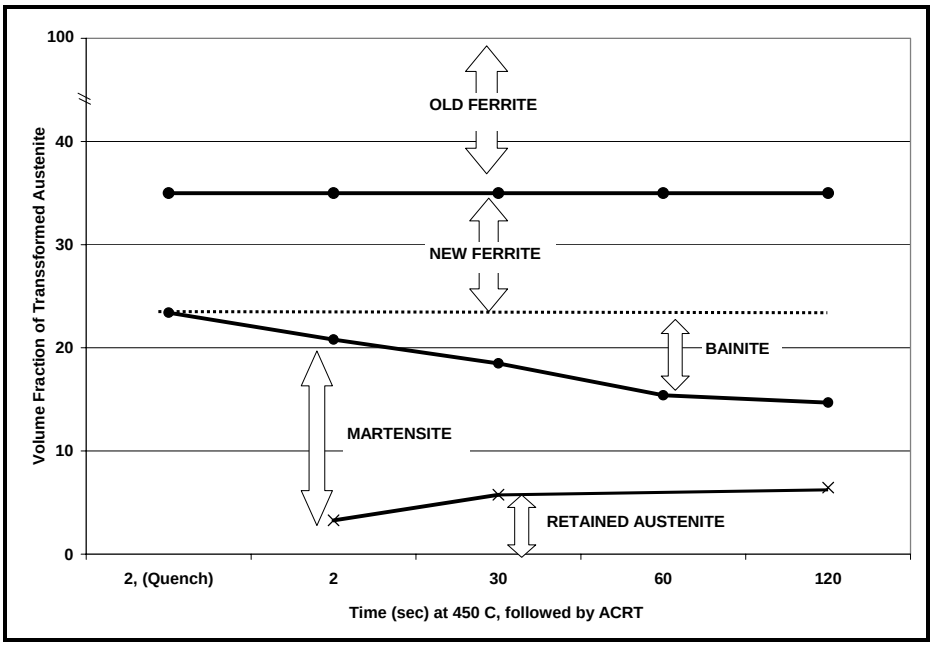

Figure 77 Austenite decomposition behavior during isothermal holding at 450°C after cooling from T_{IA}=35%γ, 0.5Al-550 TRIP steel

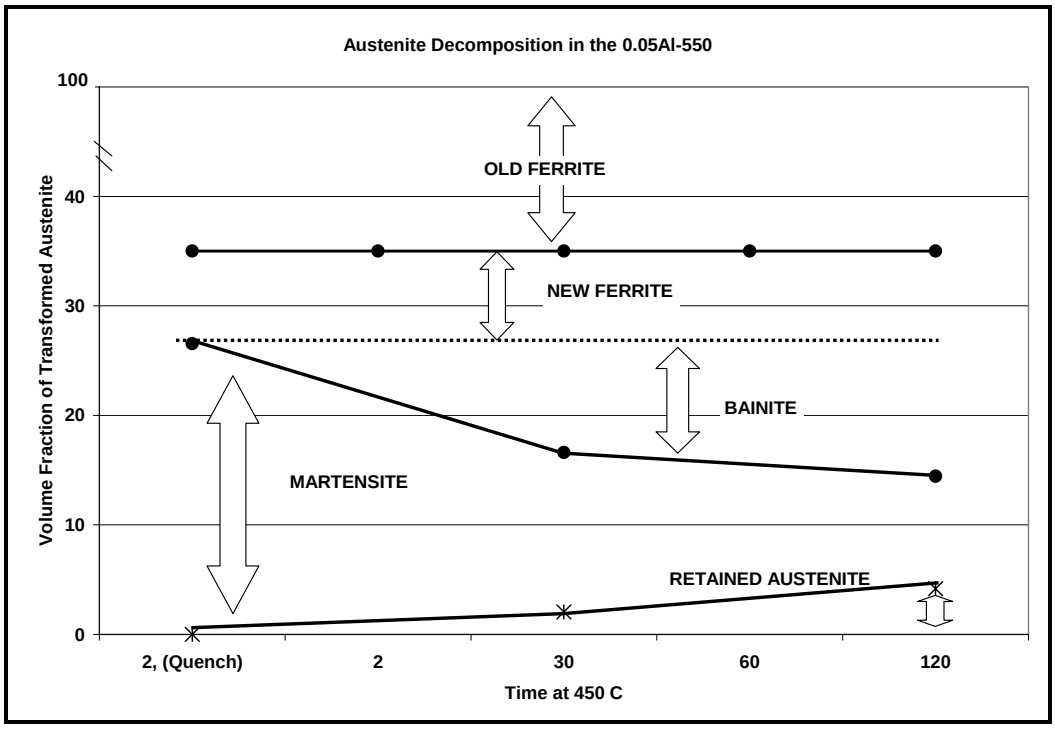

Figure 78 Austenite decomposition behavior during isothermal holding at 450°C after cooling from T_{IA}=35%γ, 0.05Al-550 TRIP steel

Figure 79 shows OM and SEM micrographs showing the microstructure evolution during the holding time at 450°C for the 1.0Al-550 alloy. LePera's etchant was used and the white features show the M-A (Martensite+Retained Austenite) constituent, whereas the brown features show the ferrite. Futhermore, TEM analysis has confirmed the existence of the phases that developed during the IHT holding (see discussion section).

Finally, the IQ multi-peak quantitative analysis showing the microstructure evolution in the 1.0Al-550 alloy is shown in Figure 80 thru Figure 82, and similarly, IQ analysis for the 0.05Al-550 and 0.05Al-700 alloy is observed in Figures 83 thru Figure 88 for an initial austenite volume fraction of 35% austenite.

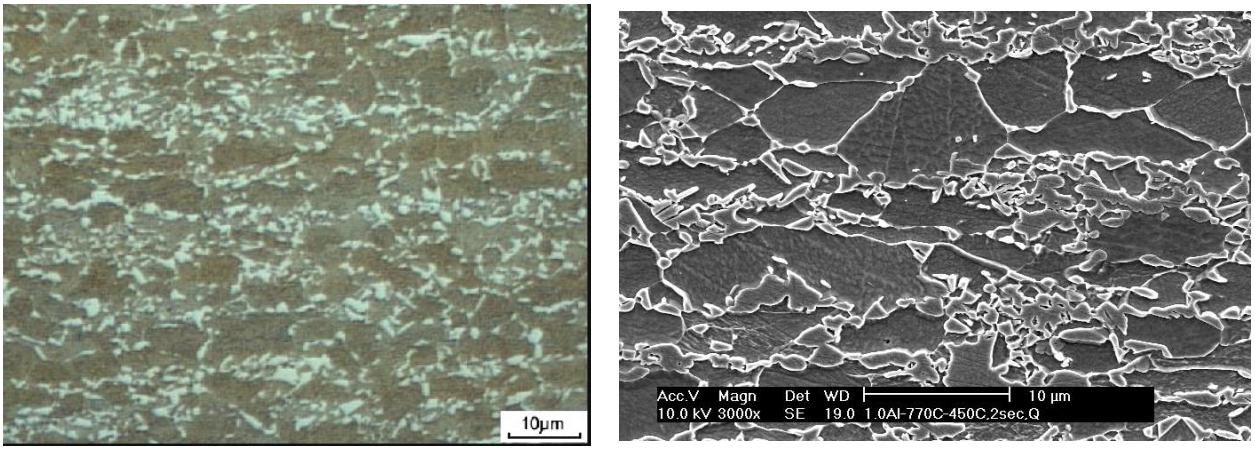

(a) 2 sec, Quench

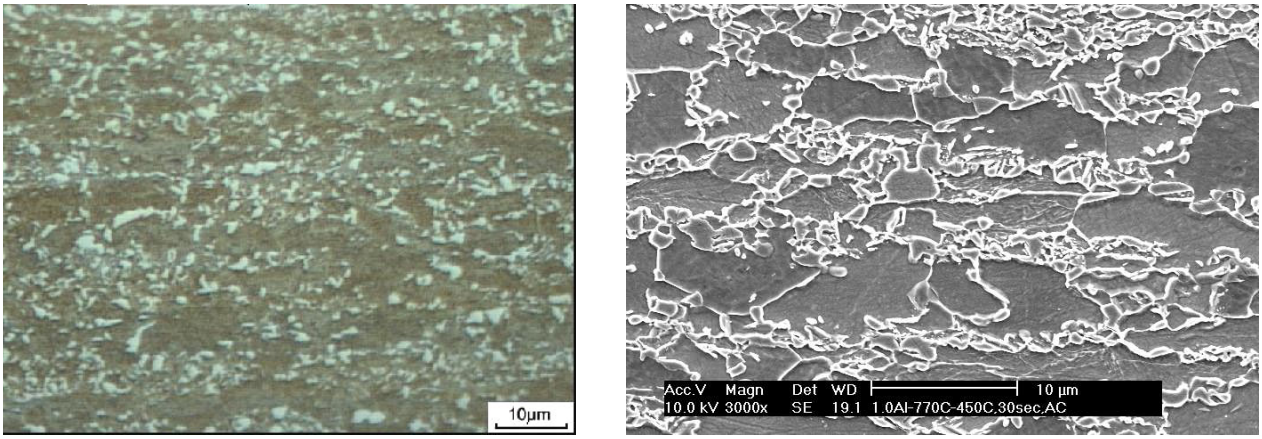

(b) 30 sec, ACRT

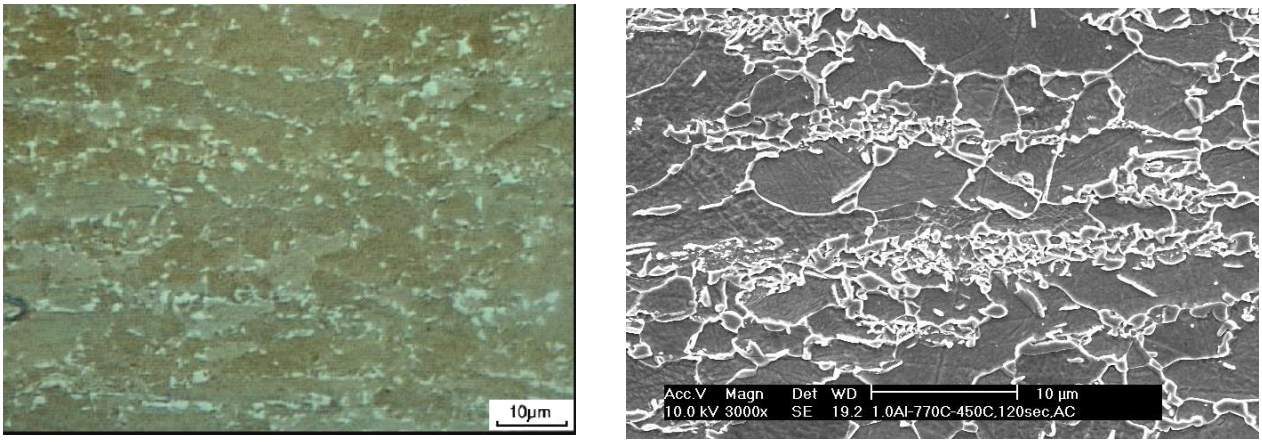

(c) 120 sec, ACRT

Figure 79 Optical and SEM micrographs of typical microstructure in the 1.0Al-550 TRIP steel after cooling from T_{IA}=770°C (35%γ) at 15C°/sec to IHT=450°C, and held at: (a) 2s + Q, (b) 30s + AC, and (c) 120 + AC

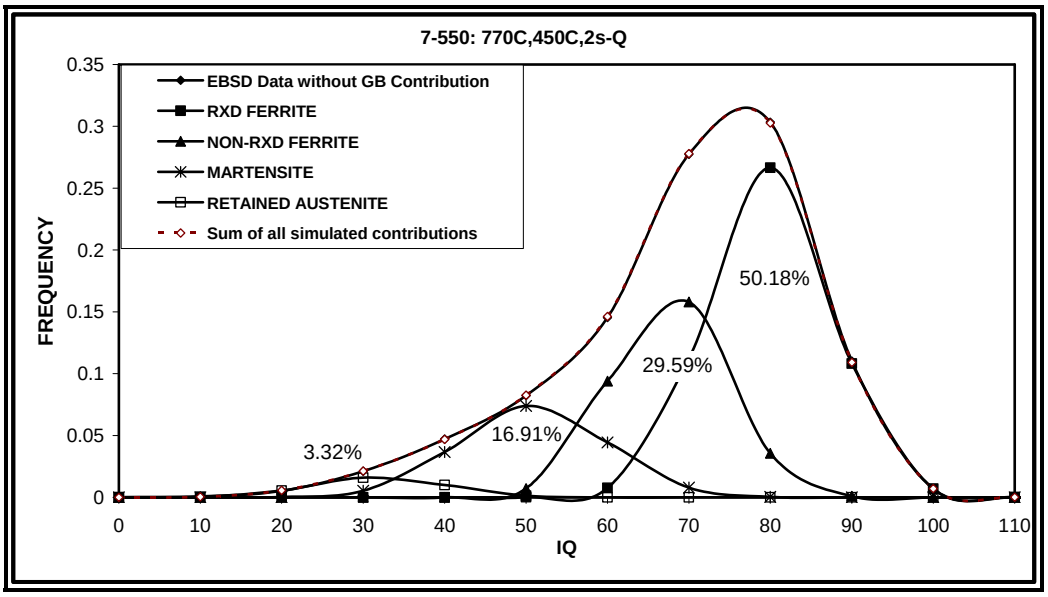

Figure 80 IQ multi-peak quantitative analysis of the microconstituents in the 1.0Al-550 alloy after T_{IA}=770°C (35%γ), cooled at 15°C/sec to 450°C and immediately quenched

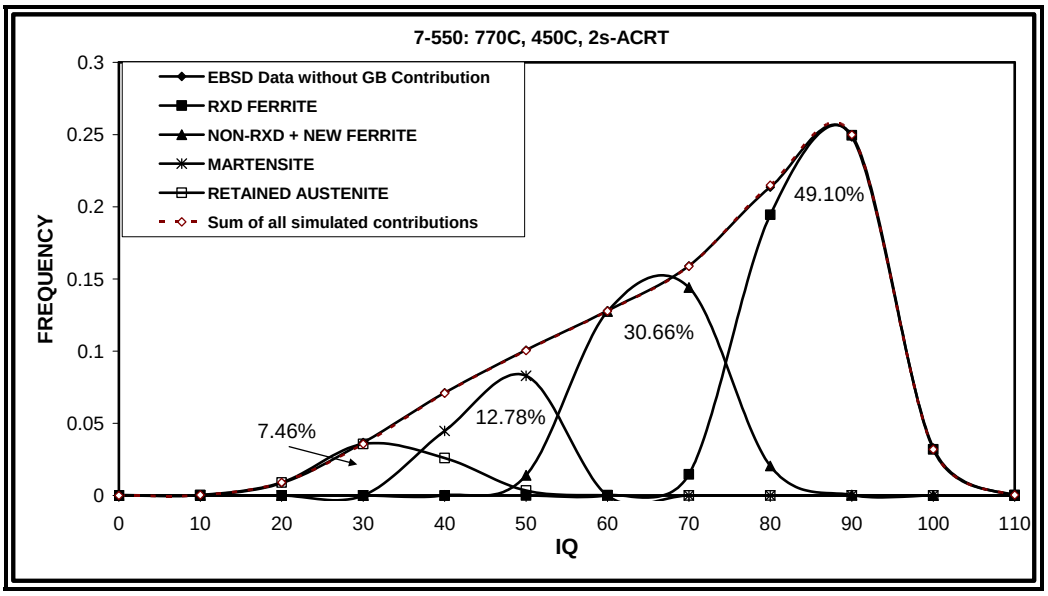

Figure 81 IQ multi-peak quantitative analysis of the microconstituents in the 1.0Al-550 alloy after T_{IA}=770°C (35%γ), cooled at 15°C/sec to 450°C and then air cooled to room temperature (ACRT)

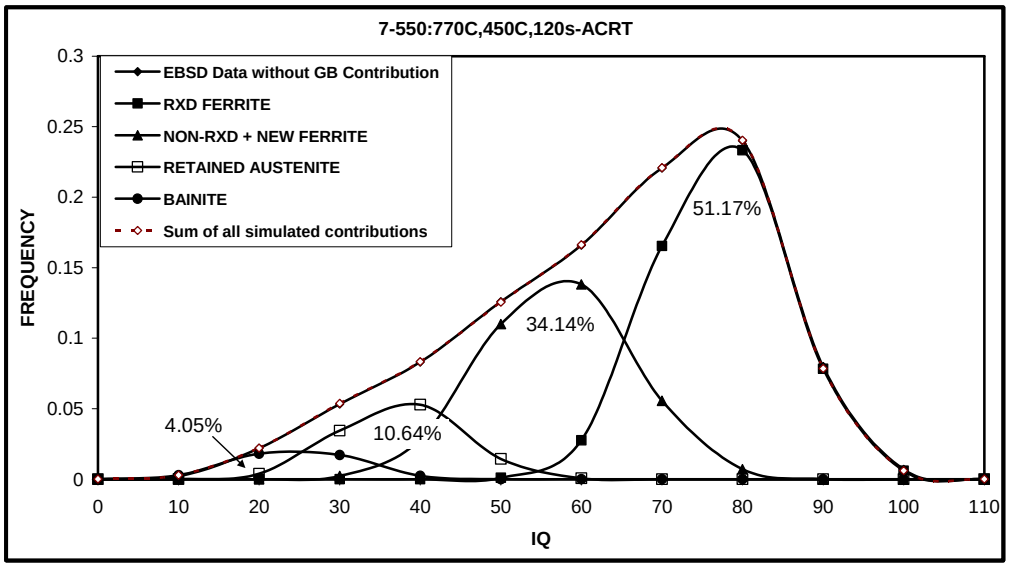

Figure 82 IQ multi-peak quantitative analysis of the microconstituents in the 1.0Al-550 alloy after T_{IA}=770°C (35%γ), cooled at 15°C/sec to 450°C, held 120 seconds and then ACRT

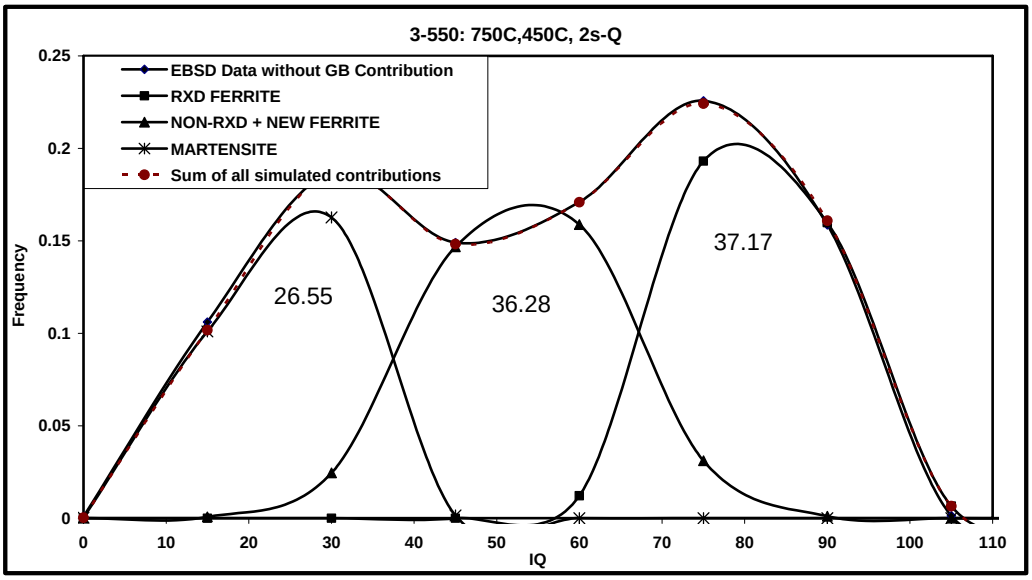

Figure 83 IQ multi-peak quantitative analysis of the microconstituents in the 0.05Al-550 alloy after T_{IA}=750°C (35%γ), cooled at 15°C/sec to 450°C and immediately quenched

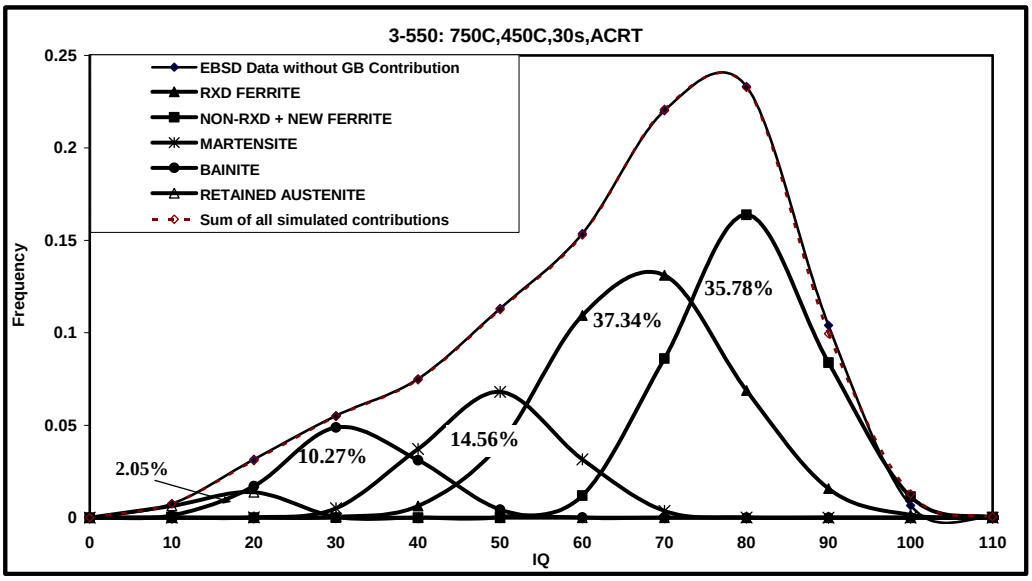

Figure 84 IQ multi-peak quantitative analysis of the microconstituents in the 0.05Al-550 alloy after T_{IA}=750°C (35%γ), cooled at 15°C/sec to 450°C, held 30 seconds and then ACRT

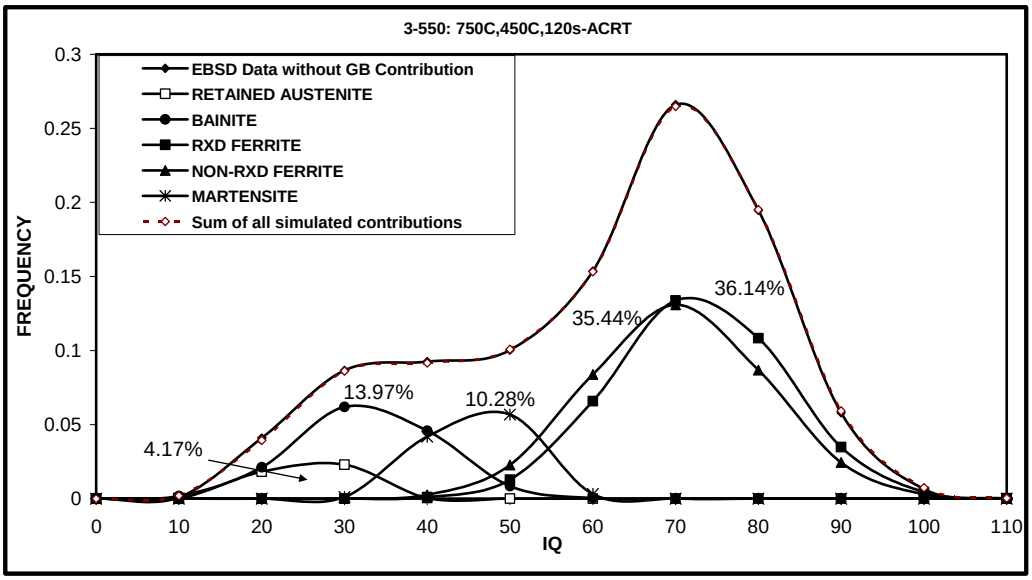

Figure 85 IQ multi-peak quantitative analysis of the microconstituents in the 0.05Al-550 alloy after T_{IA}=750°C (35%γ), cooled at 15°C/sec to 450°C, held 120 seconds and then ACRT

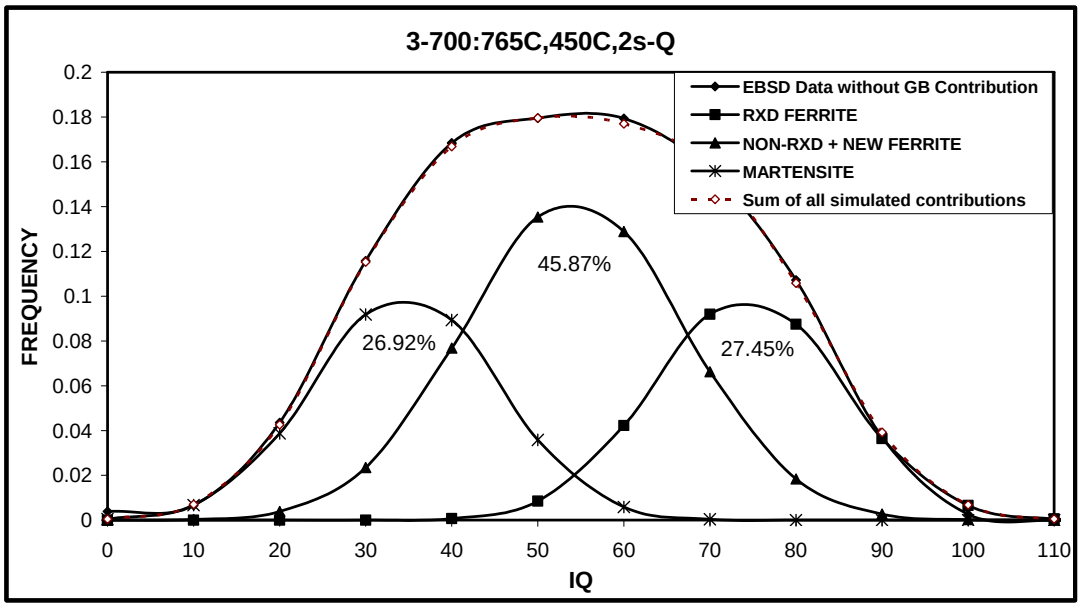

Figure 86 IQ multi-peak quantitative analysis of the microconstituents in the 0.05Al-700 alloy after T_{IA}=765°C (35%γ), cooled at 15°C/sec to 450°C and immediately quenched

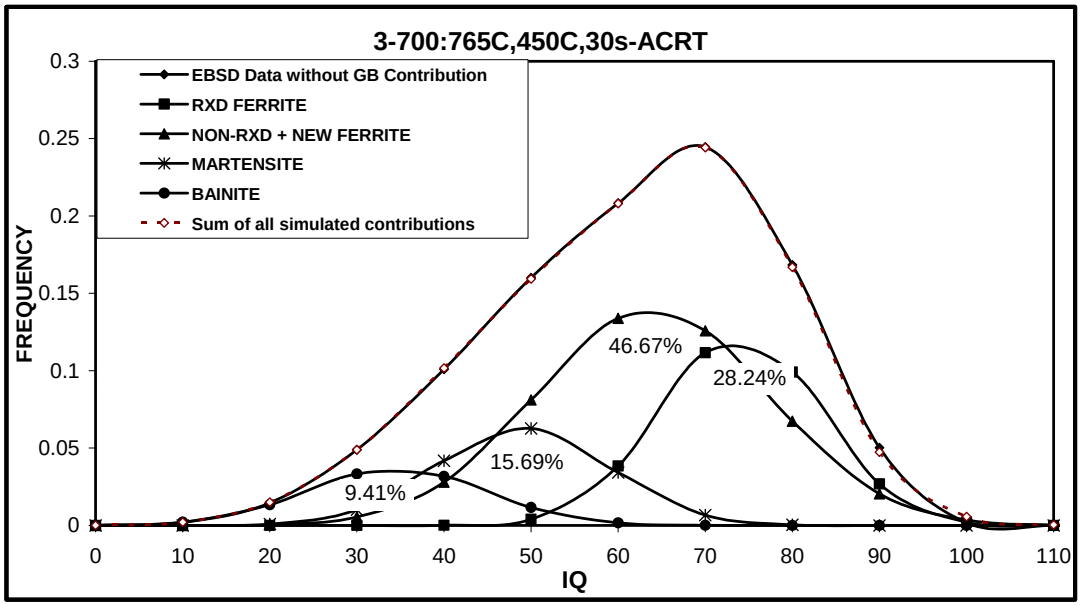

Figure 87 IQ multi-peak quantitative analysis of the microconstituents in the 0.05Al-700 alloy after T_{IA}=765°C (35%γ), cooled at 15°C/sec to 450°C, held 30 seconds and then ACRT

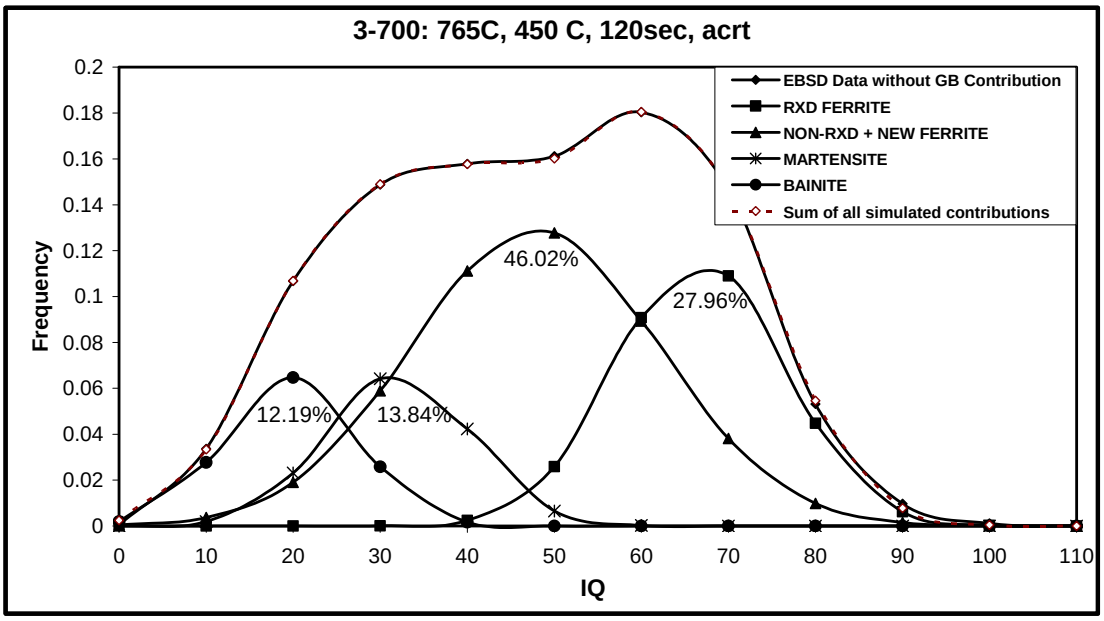

Figure 88 IQ multi-peak quantitative analysis of the microconstituents in the 0.05Al-700 alloy after T_{IA}=765°C (35%γ), cooled at 15°C/sec to 450°C, held 120 seconds and then ACRT

The cooling rate after holding at different time intervals during the isothermal holding at 450°C was varied and it was observed that the stability of the retained austenite changes as a function of the cooling rate after any given holding during the IHT. Figure 89 shows the effect of cooling rate after holding at 450°C on the amount of retained austenite for the 1.0Al-550 alloy. It can be observed that a systematic variation in the amount of retained austenite with varying cooling rates exists. Air cooling after holding at 450°C resulted in the largest amount of retained austenite, whereas quenching resulted in the smallest amount of retained austenite. Also, note that the percent of retained austenite increases with holding time, up to a maximum of 10.5% when air cooling is used, and up to 5% if quenching is used after IHT.

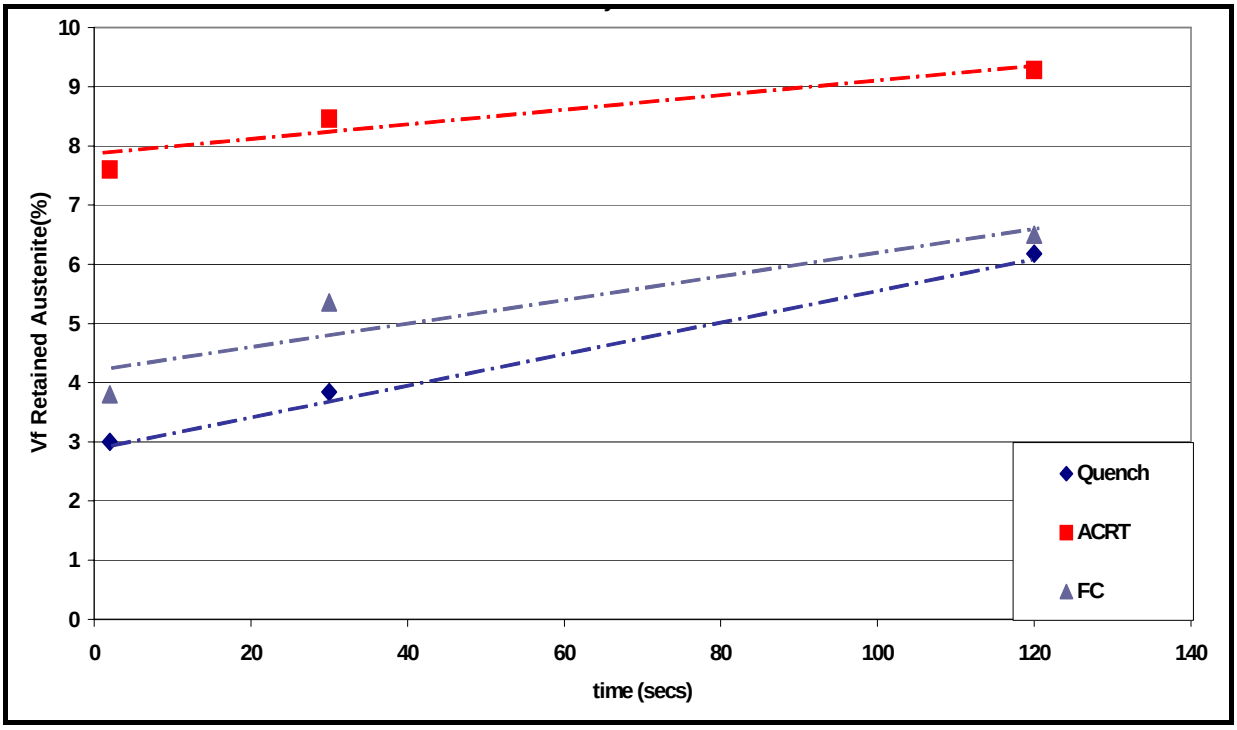

Figure 89 Effect of the cooling rate from IHT=450°C to RT after holding for various times on the volume fraction of retained austenite in the 1.0Al-550 TRIP steel

Also, the prior coiling temperature has a significant effect on the retained austenite content. Figure 90 shows that a prior coiling temperature of 700°C results in less than 2% retained austenite after holding for 30 seconds, and further holding decreases the volume fraction of retained austenite to essentially zero. On the other hand, a prior coiling temperature of 550°C results in 8.5% retained austenite and this increases with further holding time. This evidently indicates that the variation in coiling temperature has a large influence on the composition and stability of the untransformed austenite during TRIP steel processing.

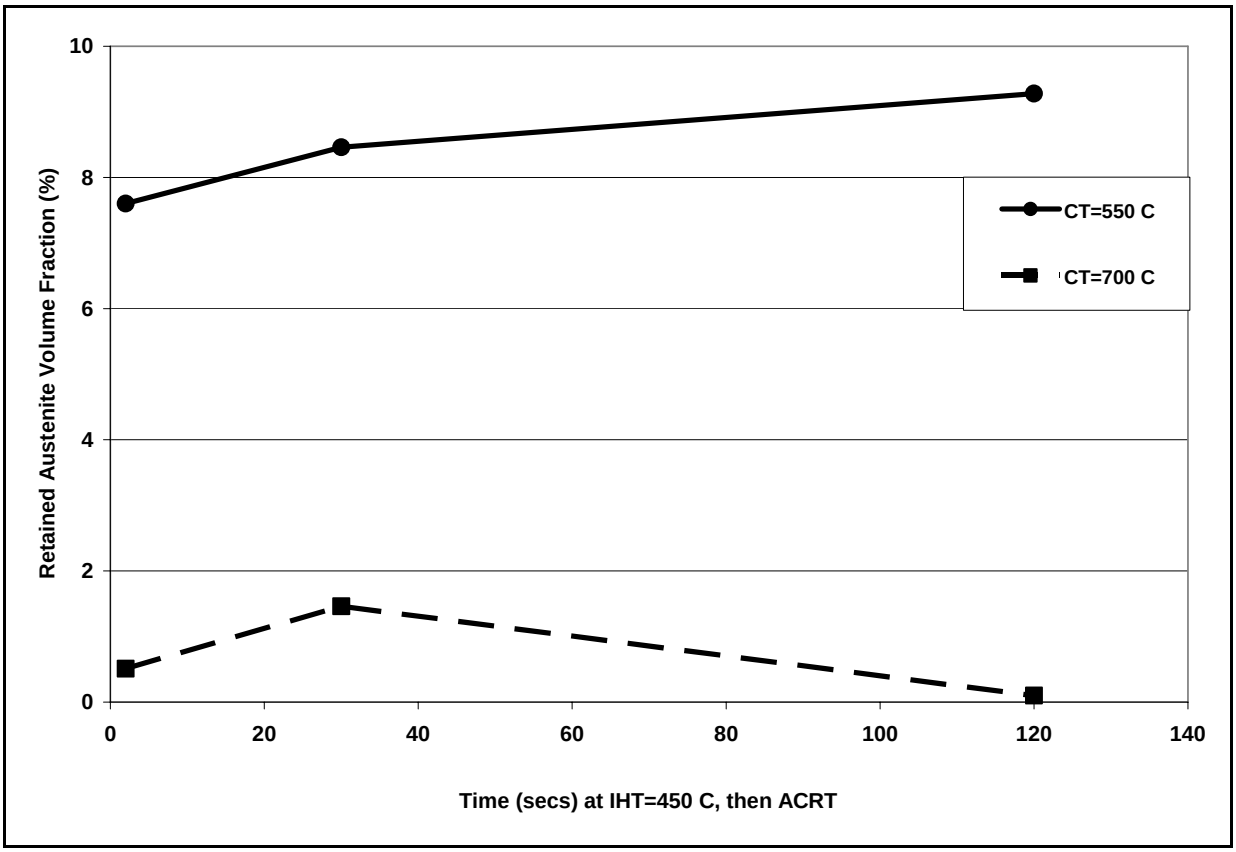

Figure 90 Effect of prior coiling temperature on the volume fraction of retained austenite after holding at various times (followed by air cool) at IHT=450°C, 1.0Al steel

5.4 MECHANICAL PROPERTIES

The tensile properties for selected alloys and selected processing conditions were evaluated. These consisted of: Yield stress (or lower yield point), UTS, uniform strain, total elongation, and UTS x Total Elongation. Appendix B shows the tensile test results for the different alloys and processing conditions that were selected for the mechanical testing.

5.4.1 Yield Stress

Figure 91 shows the yield and/or lower yield point stress values for the 0.5Al-550 and 1.0Al-550 as a function of holding time during the IHT. These samples were both intercritically annealed at a temperature equal to 35% initial percent austenite, 760°C and 770°C, respectively. They were subsequently cooled at 15°C/sec to 450°C, and held at different time intervals, followed by air cooling. It is observed that the YS and/or LYP increases with holding time during the IHT in both alloys. Moreover, the 0.5Al-550 alloy resulted in larger yield stress values than the 1.0Al-550 alloy for identical processing conditions. Holding for a very short time, 5 seconds, resulted in continuous yielding behavior, where as increasing the holding time changed the yielding behavior from continuous to discontinuous yielding, and hence an UYP, LYP and a yield point elongation was observed.

The variation of the cooling rate after holding at 450°C and its effect on the yield stress was also examined. The 0.5Al-550 and 1.0Al-550 alloys were intercritically annealed at a temperature equal to 35% initial percent austenite, 760°C and 770°C, respectively. They were subsequently cooled at 15°C/sec to 450°C, and held for 30 seconds, followed by varying cooling rates to room temperature. The cooling rates used were: a) quench (in water), b) air cooling, and

c) furnace cooling. Figure 92 shows the yield stress results for both 0.5Al-550 and 1.0-550Al alloys. The 0.5Al-550 alloy has a larger yield stress value than the 1.0Al-550 alloy for identical processing conditions. Also, it was observed that a fast cooling rate results in continuous yielding, whereas cooling at slower rates result in a shift from the continuous yielding to a discontinuous yielding. Note that the furnace cooling rate after holding for 30 seconds and the holding condition of 120 seconds at 450°C followed by air cooling result in the largest yield point elongations, 2.5% and 2.9%, respectively, whereas quench conditions and short holding times at 450°C result in continuous yielding behavior.

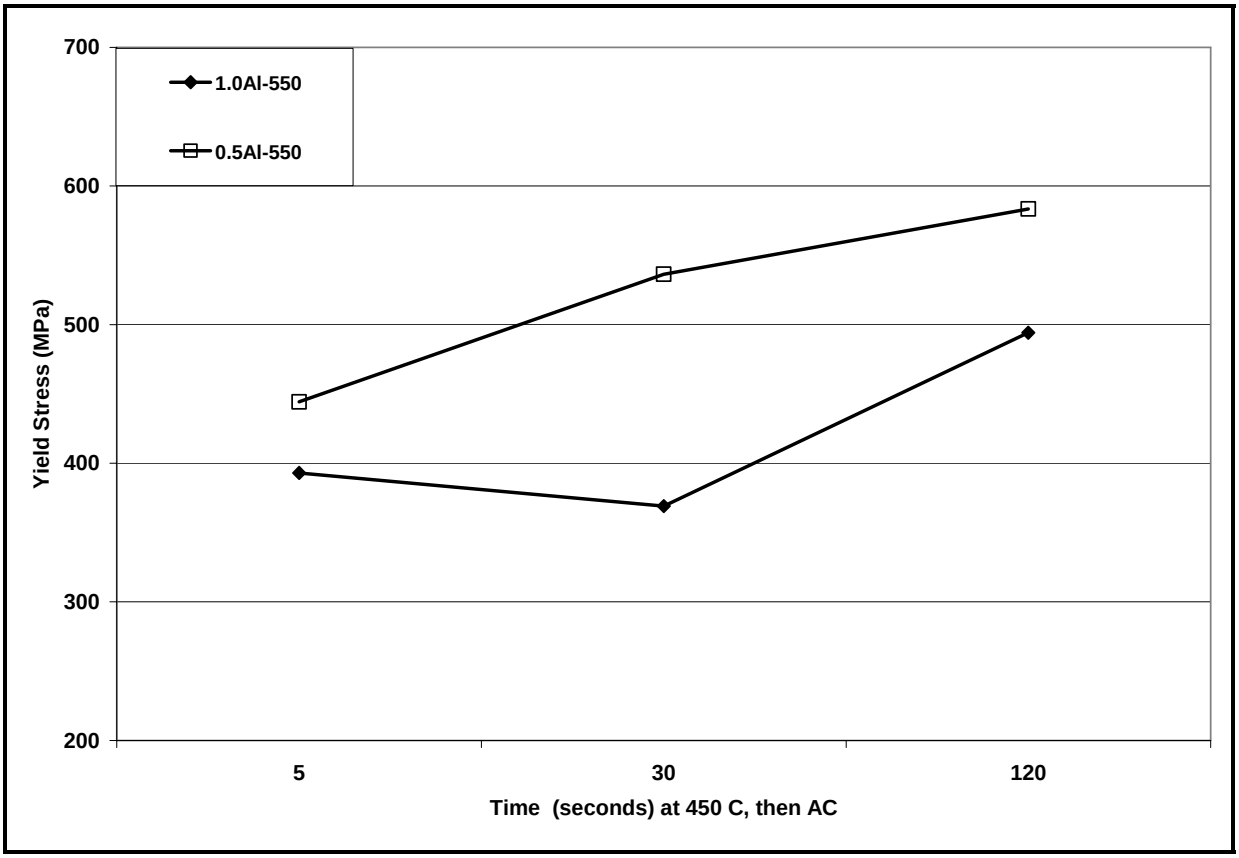

Figure 91 Effect of holding time at IHT=450°C followed by air cooling in the yield stress in the 1.0Al-550 and 0.5Al-550 TRIP steels

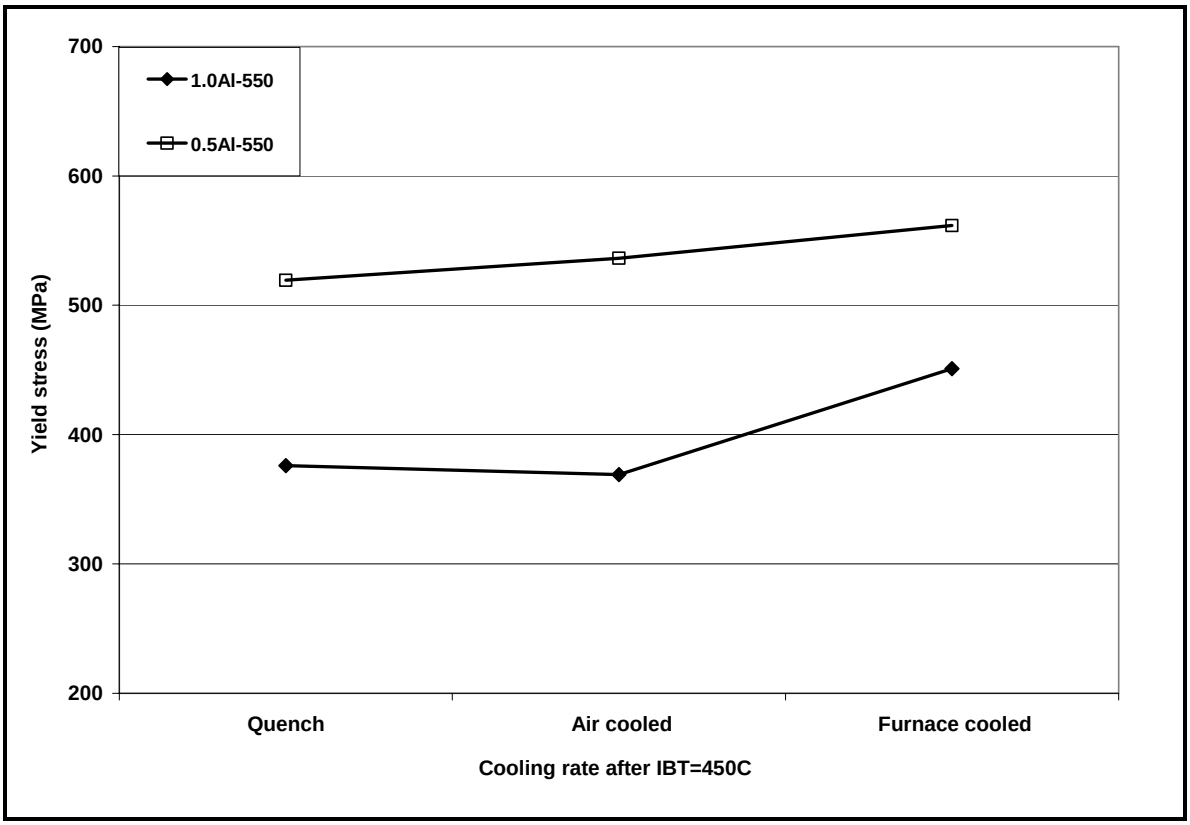

Figure 92 Effect of the cooling rate from IHT=450°C (30 seconds hold) to room temperature in the yield stress in the 1.0Al-550 and 0.5Al-550 TRIP steels

5.4.2 UTS

The UTS values for the 0.5Al-550 and 1.0Al-550 alloys as a function of holding time during the IHT are shown in Figure 93. These samples were both intercritically annealed at a temperature equal to 35% initial percent austenite, 760°C and 770°C respectively, subsequently cooled at 15°C/sec to 450°C and held at different time intervals, followed by air cooling. It can be observed that the UTS decrease with holding time during the IHT in both alloys. Moreover, the 0.5Al-550 alloy resulted in larger UTS values than the 1.0Al-550 alloy for identical processing

conditions. Holding for a very short time, 5 seconds, results in 895 MPa and 871 MPa for the 0.5Al-550 and 1.0Al-550 alloys respectively, whereas increasing holding time to 120 seconds results in 830 and 757 MPa, respectively.

The variation of the cooling rate after holding at 450°C and its effect on the UTS is shown in Figure 94. The 0.5Al-550 and 1.0Al-550 alloys were held for 30 seconds during the IHT, followed by varying cooling rates to room temperature. The 0.5Al-550 alloy has larger UTS values than the 1.0Al-550 alloy for identical processing conditions. Note that furnace cooling results in the lowest UTS values whereas air cooling results in the largest UTS values.

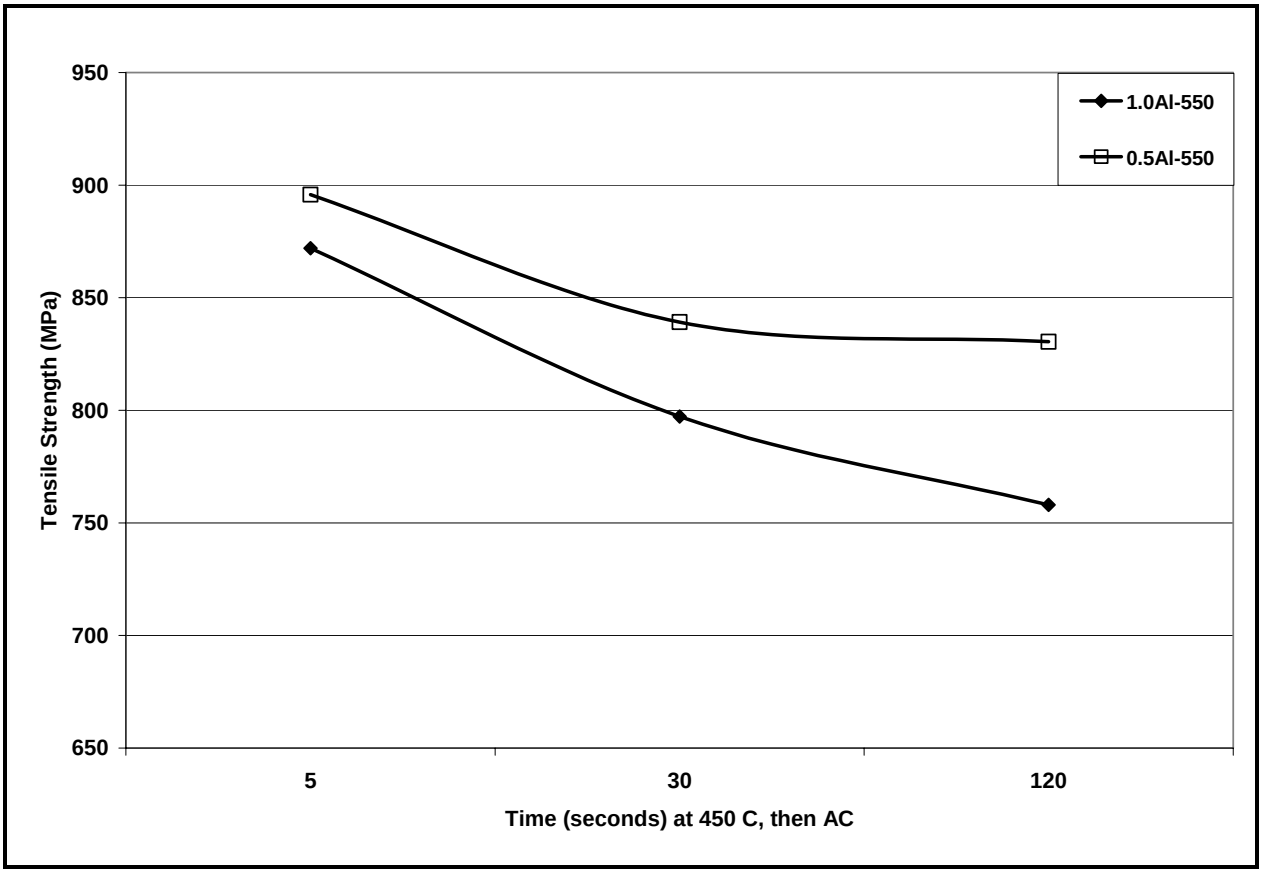

Figure 93 Effect of holding time at IHT=450°C followed by air cooling in the UTS in the 1.0Al-550 and 0.5Al-550 TRIP steels

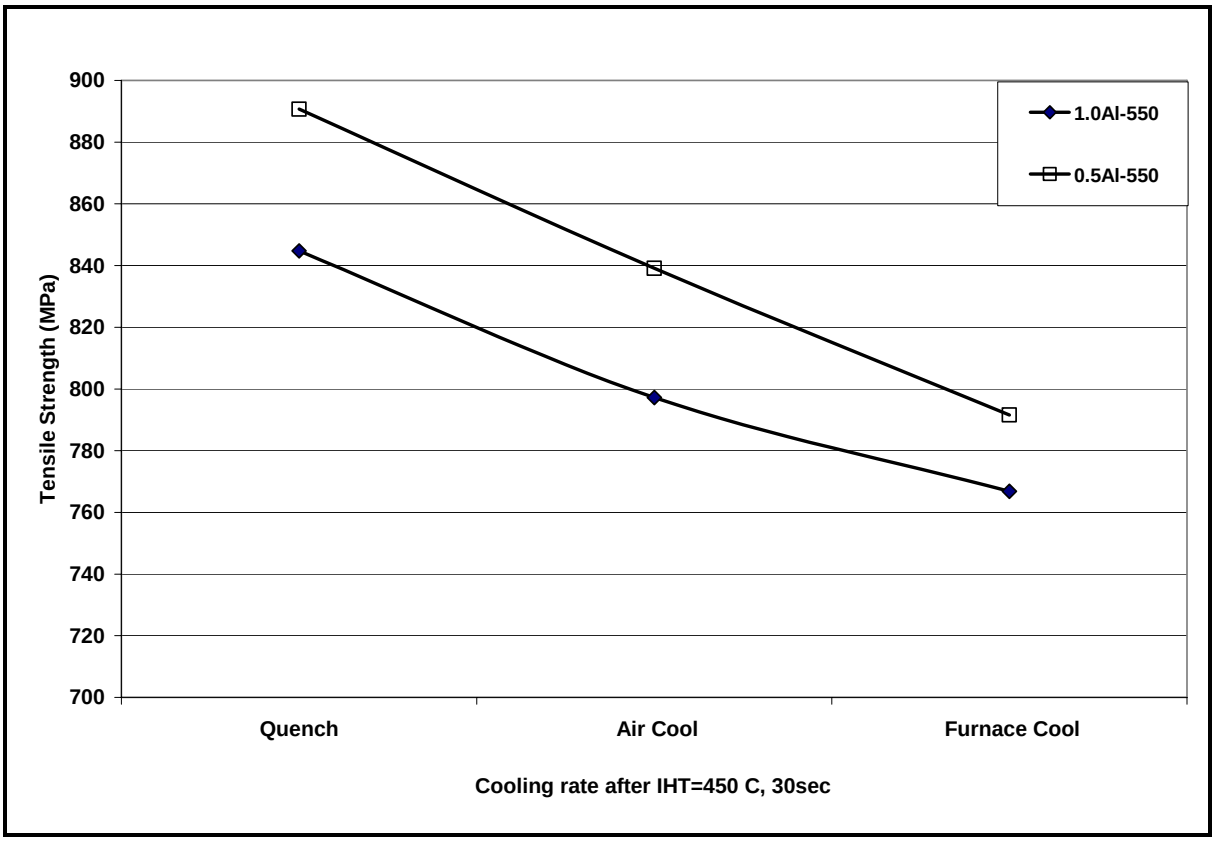

Figure 94 Effect of the cooling rate from IHT=450°C (30 seconds hold) to room temperature in the UTS in the 1.0Al-550 and 0.5Al-550 TRIP steels

5.4.3 Total Elongation

Figure 95 shows the total elongation values for the 0.5Al-550 and 1.0Al-550 as a function of holding time during the IHT. These samples were both intercritically annealed at a temperature equal to 35% initial percent austenite, 760°C and 770°C, respectively. They were subsequently cooled at 15°C/sec to 450°C, and held at different time intervals, followed by air cooling. Note that the total elongation increases with holding time during the IHT in both alloys. Also, the

1.0Al-550 alloy resulted in larger total elongations than the 0.5Al-550 alloy for identical processing conditions. Holding for a very short time, 5 seconds, resulted in the smallest elongation, 22% and 27% for the 0.5Al-550 and 1.0Al-550 alloys respectively, whereas increasing the holding time to 120 seconds changed the total elongation values to 26% and 32% respectively.

The total elongation as a function of the cooling rate to room temperature after holding at 450°C for 30 seconds is shown in Figure 96. The 1.0Al-550 alloy has larger total elongation values than the 0.5Al-550 alloy for identical processing conditions. The smallest total elongations were observed when the cooling rate used was equal to water quenching, and the largest total elongations were obtained for slow cooling rate conditions such as furnace cooling.

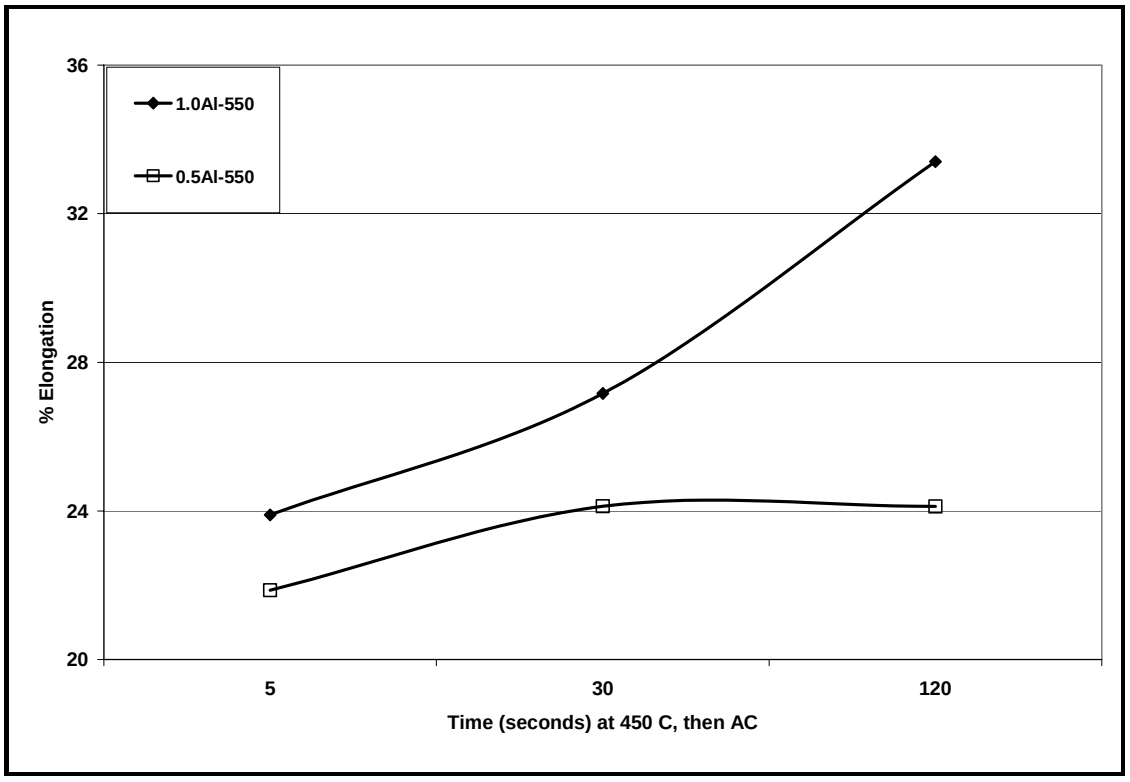

Figure 95 Effect of holding time at IHT=450°C followed by air cooling in the total elongation (%) in the 1.0Al-550 and 0.5Al-550 TRIP steels

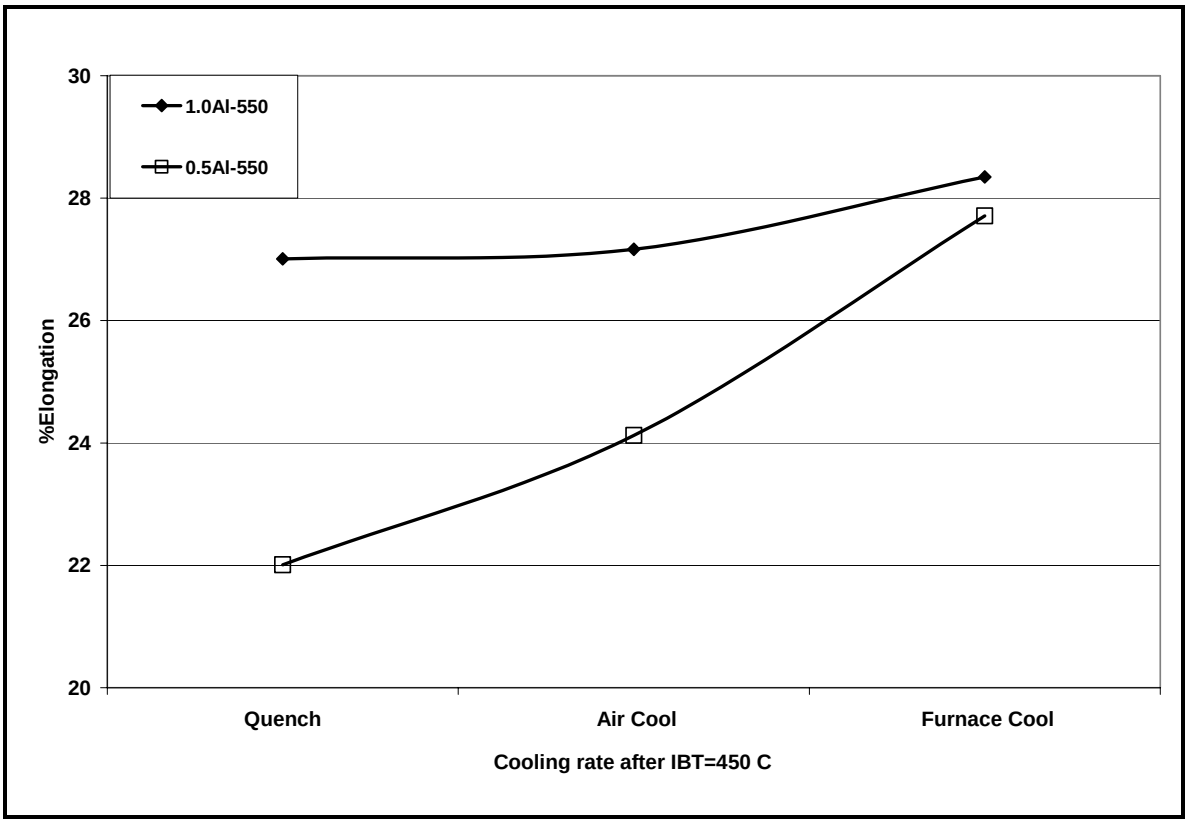

Figure 96 Effect of the cooling rate from IHT=450°C (30 seconds hold) to room temperature in the total elongation (%) in the 1.0Al-550 and 0.5Al-550 TRIP steels

5.4.4 UTS x Total Elongation

In TRIP steels, tensile properties are usually described by the product of the tensile strength and the total elongation. When the value of this product is above 20,000 (MPa x %), the TRIP steel is considered to have acceptable mechanical properties. Figure 97 and Figure 98 shows the resulting values for both 0.5Al-550 and 1.0Al-550 with processing conditions as described in sections 5.5.1 thru 5.5.3. It can be observed that optimum values of at least 20,000 (MPa x %)are obtained at essentially all processing conditions.

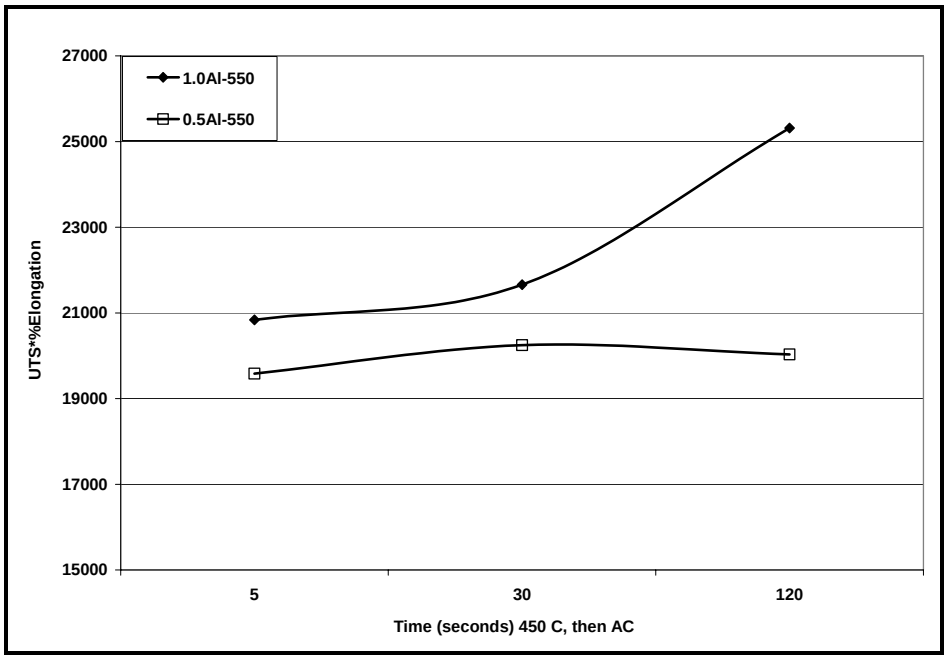

Figure 97 Effect of holding time at IHT=450°C followed by air cooling in the product of UTS x Total Elongation in the 1.0Al-550 and 0.5Al-550 TRIP steels

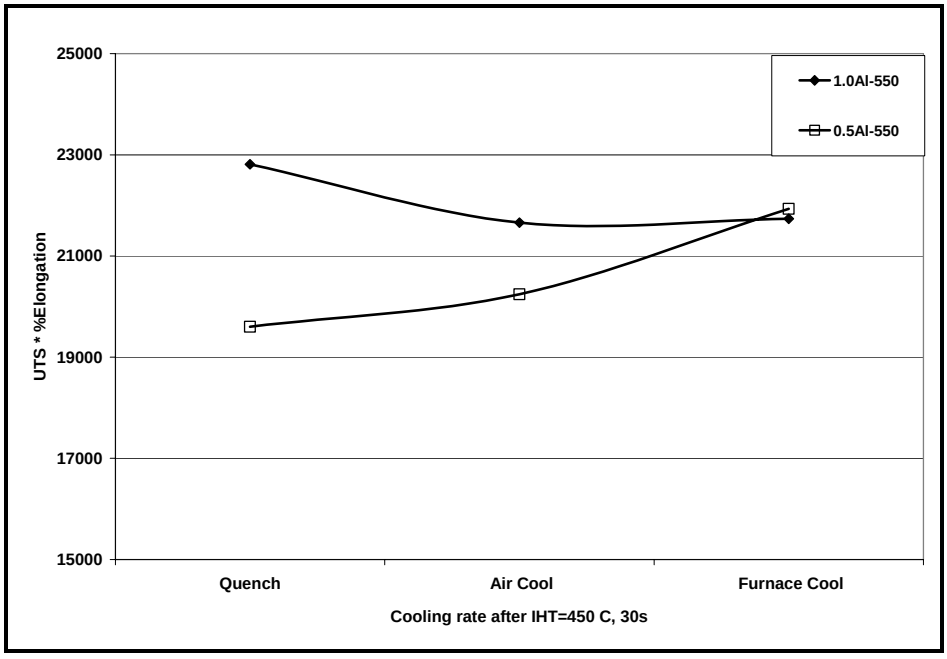

Figure 98 Effect of the cooling rate from IHT=450°C (30 seconds hold) to room temperature in the product of UTS x Total Elongation in the 1.0Al-550 and 0.5Al-550 TRIP steels

6.0 DISCUSSION

6.1 MICROSTRUCTURAL BEHAVIOR DURING INTERCRITICAL ANNEALING

The recrystallization of ferrite and the austenite formation are two important metallurgical phenomena that occur during the intercritical annealing of TRIP steels. It was observed that increasing the Al content from 0.05% to 1.0% wt increased the rate of recrystallization.

However, the effect of prior coiling temperature did not influence the recrystallization behavior in the 1.0% and 0.5%, whereas at lower aluminum content, 0.05% there was a small effect of the prior coiling temperature. The rate at which ferrite recrystallizes is largely influenced by the amount of stored energy, or cold deformation of the material. In the case of the 0.05%Al alloy, the variation of coiling temperature from 700 C to 550 C resulted in a shift from mainly polygonal ferrite to acicular ferrite. The stored energy of the acicular ferrite is much larger than the stored energy of the polygonal ferrite as shown by Garcia-Gonzalez[44,45] in an earlier study on the effect of the type of ferrite on the dislocation density. It was shown that the dislocation density of acicular ferrite varies from 3.5E10 cm^{-2} to 5.6E10 cm^{-2} whereas the dislocation density of polygonal ferrite varies from 6.3E9 cm^{-2} to 8.4E9 cm^{-2}. The difference in stored energy on the 0.05Al alloy was only reflected at low temperatures in the $\alpha+\gamma$ region, up to 780 C. Intercritical annealing at higher temperatures, however, resulted in a similar rate of ferrite recrystallization. The effect of coiling temperature on the type of ferrite was minimized with Al additions of 0.5% and 1.0%. The microstructure observed at both prior coiling temperatures was

polygonal ferrite. As a result, the driving force for the recrystallization of ferrite at both coiling temperatures is expected to be very similar. In fact, this was observed to be the case, since it was shown that the coiling temperature did not have any effect on the amount of the recrystallization of ferrite at different temperatures in the $\alpha+\gamma$ region. According to the aspect ratio of the ferrite grains, it must be noted that 50% of ferrite recrystallization in the 0.05Al and 0.5Al alloy only occurred at relatively high temperatures in the two phase region, equal to an 80% and 74% of austenite percent, respectively. However, in the 1.0Al alloy, 50% of ferrite recrystallization occurred at a very low temperature in the two phase region, equal to 27% austenite. The mechanism by which additions larger than 1.0% wt Al accelerate the recrystallization of ferrite is not yet understood.

However, it is possible that Al prevents the solute atoms to migrate to the ferrite boundaries, thereby decreasing the energy necessary for boundary migration. It is known that an increase in solute content retards the mobility of grain boundaries. Brandt[83] has shown this effect by studying the suppression of epitaxial ferrite during cooling. It was observed that cooling rates close to 120°C/sec were necessary to suppress epitaxial ferrite formation in a 1.2%Mn steel, and about 50°C/sec in a 2.4%Mn steel. Higher manganese contents inhibit epitaxial ferrite formation by the solute-drag-like effect[85,86] and the same effect would be expected with regard to the mobility of grains boundaries during recrystallization. Manganese decreases the activity of carbon in austenite and it also segregates to the austenite-ferrite interface. Because of this, the driving force for diffusion of carbon away from the interface into the austenite is reduced (i.e., manganese segregation attracts carbon to the interface, whereas the reaction requires the carbon diffuse away from the interface), slowing the kinetics of the transformation. Thus, smaller additions of manganese would result in less carbon being attracted

to the interface, leading to an increase in the rate of grain boundary migration. The addition of Al is known to cause an increase in the activity of carbon in the austenite, and therefore the driving force for diffusion of carbon away from the interface is increased. It appears that the critical Al content for a significant reduction of carbon segregation towards this interface is about 1.0 wt%, and in consequence, the mobility of the grain boundaries increases. This would in fact explain why the addition of 1.0%Al results in much faster rates of recrystallization. Moreover, this also explains why the variation in coiling temperature has essentially no effect in the type of ferrite (due to the lack of carbon build up at the α/γ when lowering the transformation temperature) and similarly, the reduced effect of carbon decorating the Mn banding in the 1.0Al steel.

Perhaps this explains the "saturation effect" that Leslie observed in 1961[87]. He found that the retardation of the grain boundary migration increases as solute content increases. However, as more solute is added a critical concentration is reached at which the retarding effect is reversed. This critical concentration varies for each solute element, some being much more effective than others. Figure 99 describes this saturation effect as a function of Mo content. The rate of grain boundary migration is reduced with Mo additions up to about 0.05 at% Mo, where the rate of grain migration increases again. Unfortunately, no data is available for Al additions, but it is possible that this mechanism occurs at about 1.0 wt% Al, as suggested from the observed results.

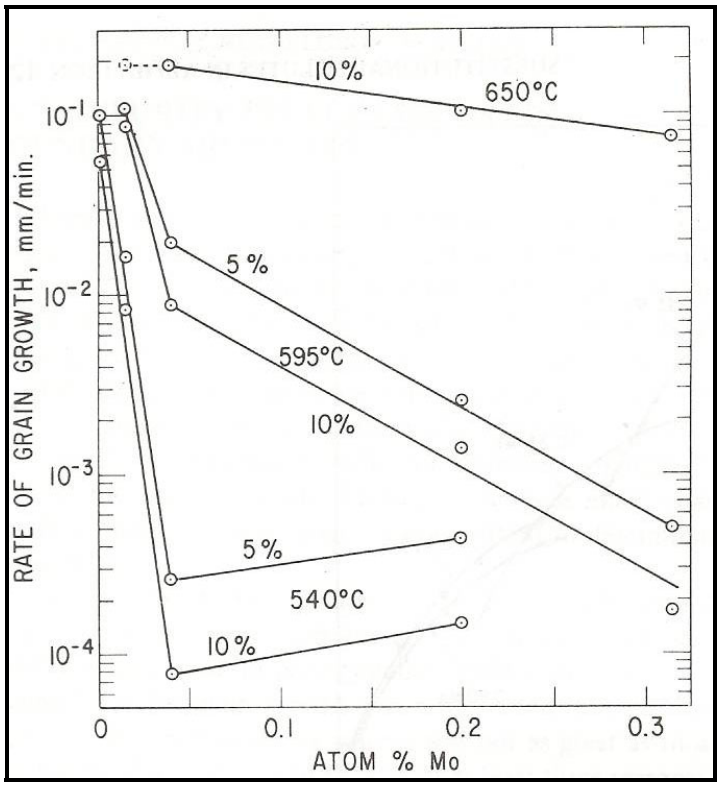

Figure 99 Effect of molybdenum on the rate of growth of recrystallized grains in iron (After W.C. Leslie, 1961)

A very important effect of the addition of Al from 0.05 wt% to 1.0 wt% is the increase in the Ac_3 temperature from 825 C to 970 C, as shown by the J-Mat Pro simulation in Figure 47 (results section). It was observed that the effect of the prior coiling temperature on the variation in the volume fraction of austenite after holding for 60 seconds at different intercritical annealing temperatures was not significant in the 0.5% Al and 1.0%Al alloy, since no more than 5% volume fraction difference existed at any given temperature. However, in the 0.05%Al, there variation in coiling temperature resulted in an increase of as much as 15% volume fraction for the coiling temperature of 550 C. At any given temperature, coiling at 550 C resulted in a higher volume fraction than when the coiling temperature was 700 C. A possible explanation for the

observed increased in the kinetics of austenite formation at 550 C could be attributed to the change in the type of ferrite from polygonal ferrite to acicular ferrite when coiling at 550 C and to the fine distribution of carbides throughout the matrix, which spheroidize before dissolving much faster than pearlite colonies. Also, the initial carbon content in these fine carbides at the early stages of intercritical annealing is larger than a large pearlite colony and therefore an increase in the rate of austenite formation is expected. The fact that the variation in coiling temperature in the 0.5%Al and 1.0%Al resulted in no change in the type of ferrite in the hot band, and that no significant variation on the rate of austenite formation was observed, indicates that the initial type of ferrite has indeed an effect on the rate on austenite formation.

Simultaneous analysis of the austenite formation and the recrystallization of ferrite show that there is a relation between these two metallurgical phenomena. It was observed in the 1.0Al alloy that the rate of recrystallization was much faster than the austenite formation at temperatures above $[(Ac_1+Ac_3)/2]$, where as in the 0.05Al and 0.5Al alloy the rate of recrystallization and austenite formation were similar. In the latter, the simulated (equilibrium) and the measured volume fraction of austenite were very similar, Figure 100; however in the 1.0Al alloy, a significant deviation from equilibrium is observed after 850 C, Figure 101. This suggests that the rate of austenite formation from cold rolled-unrecrystallized ferrite grains is very rapid, and the rate of austenite formation decreases once the recrystallization of ferrite has been completed. Militzer et[76] al observed this behavior in a 0.06C-1.86Mn-0.155Mo steel intercritically annealed at 1 C/sec and 100 C/sec to 750 C, and holding for 100 seconds. The fast heating rate condition resulted in unrecrystallized ferrite grains whereas the slow heating rate conditions resulted in recrystallized ferrite grains. It was observed that after heating at 100 C/sec the austenite formed at an increased rate and reached 30% whereas heating at 1C/sec resulted in

only 16%. In the latter case, the austenite phase was rearranged into a necklace around the ferrite grains, where as a plate-like austenite morphology without any marked austenite formation at the grain boundaries was observed after fast heating. Militzer[76] suggests that the simultaneous ferrite recrystallization and the associated movement of ferrite grain boundaries make it difficult for the austenite to nucleate at these boundaries. Hence, the difference in the nucleation modes and resulting growth appears to be responsible for the differences in the austenite formation rates.

Similarly, years earlier Garcia and DeArdo[51] also observed this behavior in a series of low carbon, 1.5%Mn steels where the rate of austenite formation increased from cold rolled ferrite than from recrystallized ferrite.

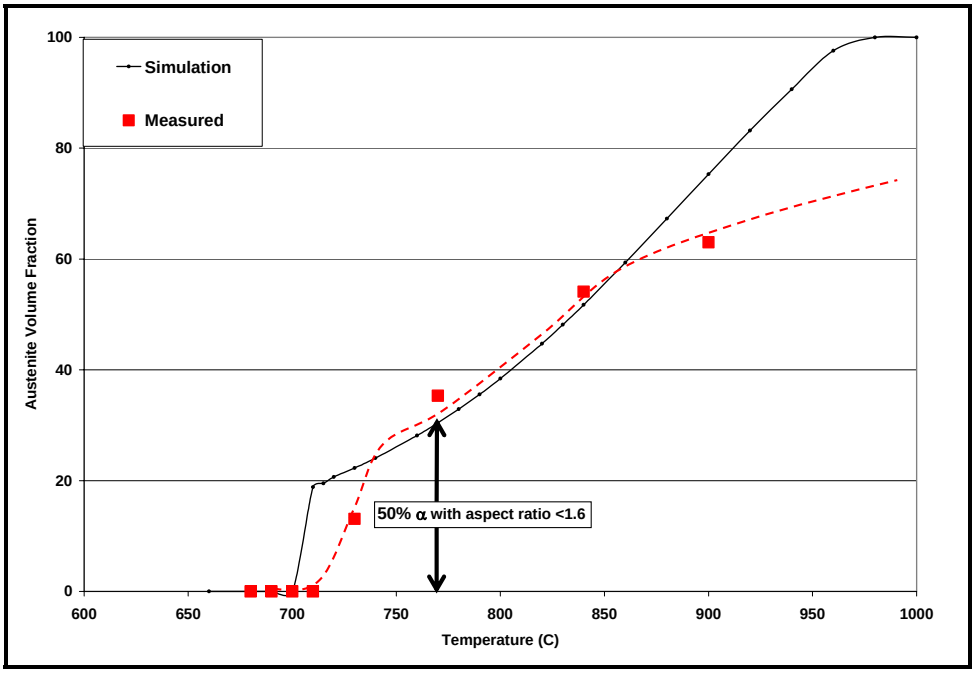

Figure 100 Austenite volume fraction vs temperature using both JMat Pro simulation and measured observations in the 1.0Al-550 TRIP steel. Arrow shows the temperature at which 50% of recrystallized ferrite grains are observed, and at~60%γ the observed and simulated results do not correlate with each other

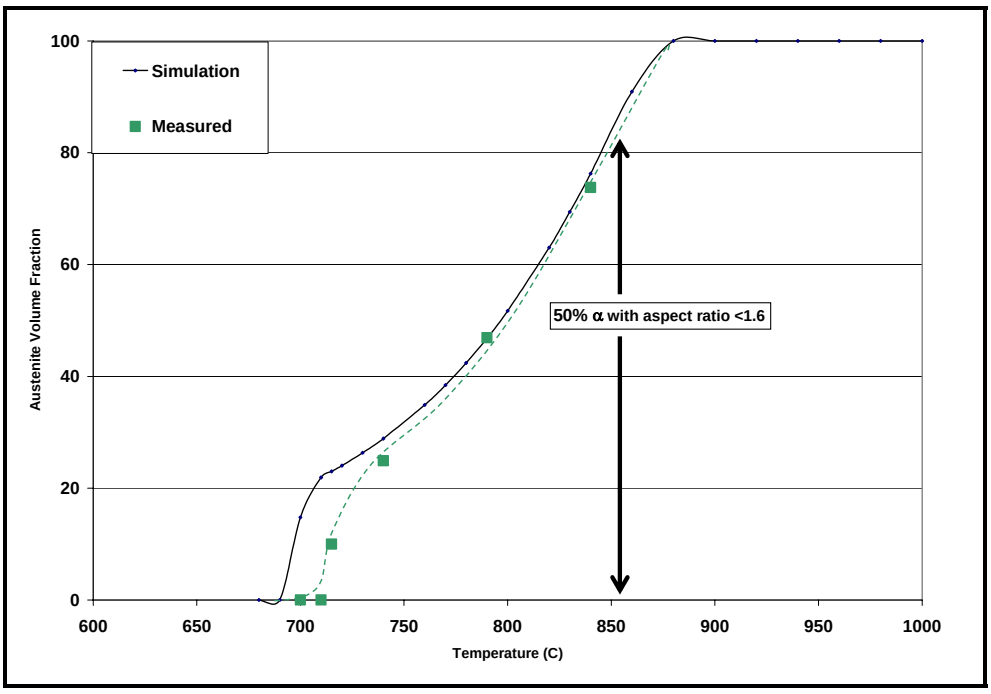

Figure 101 Austenite volume fraction vs temperature using both JMat Pro simulation and measured observations in the 0.5Al-550 TRIP steel. Arrow shows the temperature at which 50% of recrystallized ferrite grains are observed, and note that the observed and simulated results correlate well with each other up to that temperature

6.2 COOLING RATE FROM THE INTERCRITICAL ANNEALING TEMPERATURE TO THE ISOTHERMAL HOLDING TEMPERATURE

The variation of the cooling rate in the range that is typically observed in a CGL does not have a significant effect on the austenite decomposition behavior. In the 0.5% and 1.0%Al alloy the variation of the cooling rate from 15 C/sec to 5 C/sec from an intercritical annealing temperature equal to 35% initial austenite to 450 C resulted in essentially the same volume fraction M-A. Furthermore, when the intercritical annealing temperature of the 1.0Al alloy was varied from 770 C (35%γ) to 860 C(55%γ), the volume fraction of M-A after cooling to 450 was observed to be very similar. This suggests that the M-A volume fraction is independent of the intercritical annealing temperature. Similarly, the measured volume fractions of M-A after continuous cooling from both intercritical annealing temperatures to room temperature did not vary significantly with the variation in cooling rate from 1 C/sec to 30 C/sec. As a result, this obviously indicates that the amount of new ferrite formed during cooling is strongly influenced by the initial austenite volume fraction (and therefore strongly influenced by its carbon content) formed during intercritical annealing, and is not sensitive to the variation in the cooling rate between the ranges of 1 C/sec to 30 C/sec.

This austenite decomposition behavior was observed by Eldis in 1979[56]. He found that there was no effect of cooling rate (~10C/sec or less) after intercritical annealing on the volume fraction of M-A. Furthermore, the volume fraction of M-A was found to be also independent of the intercritical annealing temperature. Eldis[56] suggested that as the temperature is decreased from the T_{IA} at moderate cooling rates (10C/sec) and/or slower, the austenite quickly reverts back to polygonal ferrite, as shown in the CCT diagram in Figure 102. Nucleation of ferrite is not

required, and it is only necessary that the austenite/ferrite interface advance into the austenite. Also, the diffusion of carbon is rapid enough relative to the ferrite growth rate that there is no great accumulation of carbon at the austenite/ferrite interface. That is, the carbon gradient in the austenite remains relatively small. In consequence, near equilibrium is maintained on cooling with the average carbon content of the austenite following closely the composition of the $\alpha+\gamma/\gamma$ boundary of the equilibrium diagram, Figure 103. Hence, the amount of austenite present at any given temperature is a function of temperature rather than cooling rate and below approximately 625 C, the transformation of austenite to polygonal ferrite ceases. At faster cooling rates such as water quench, there still exists some γ to α transformation as the γ/α interface advances with decreasing temperature. However, a large carbon gradient arises at the γ/α interface as carbon is rejected into the austenite by the rapidly growing ferrite. As a result, a substantial amount of austenite having a low average carbon content is undercooled to temperatures below 600 C, where the driving force for acicular or non-polygonal ferrite is strong. Therefore, the amount of austenite is not completely "frozen in" even under water quench conditions and there will be some amount of reversion back to ferrite, both polygonal and acicular, depending on the cooling rate[56,87].

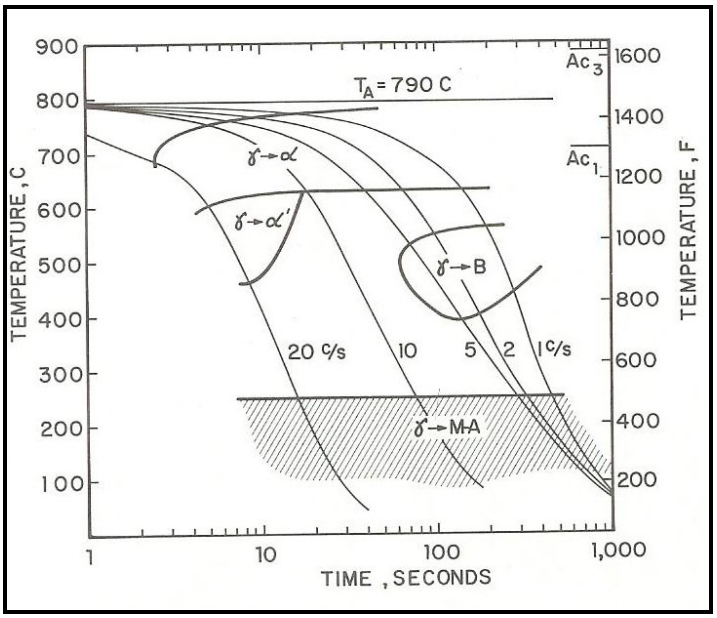

Figure 102 CCT curve of a 0.12C-1.28Mn-0.5Si-0.13Mo steel cooled from the intercritical region. γ=austenite, α=polygonal ferrite, α'=acicular ferrite, B=bainite, M-A=martensite-austenite constituent (After Eldis, 1979)

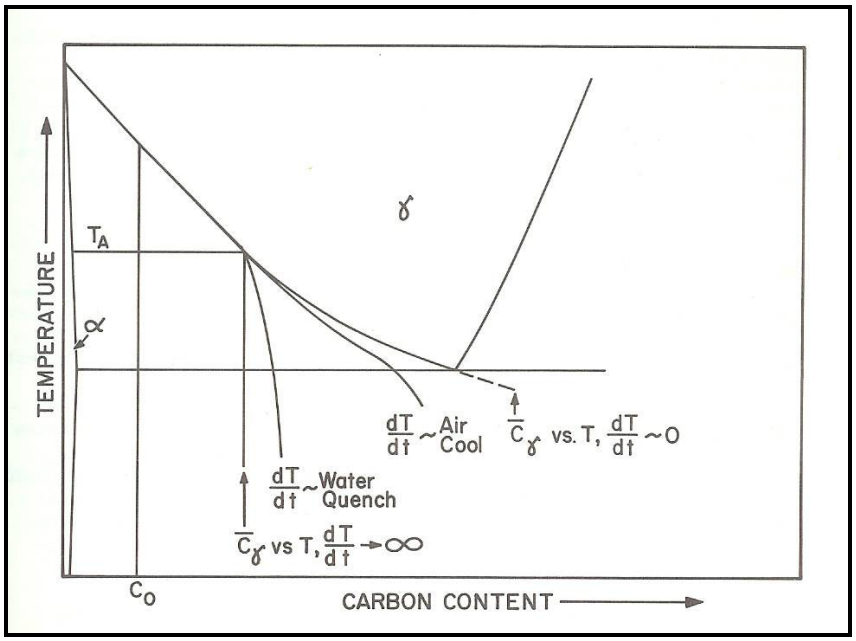

Figure 103 Schematic illustration of the effect of cooling rate on the average carbon content of austenite during cooling from intercritical temperatures (After Eldis, 1979)

Moreover, this was supported by observations of Lawson et al[50] in a 0.06C-1.5Mn-0.25Si dual phase steel. Figure 104 shows that the volume fraction of "new" or epitaxial ferrite increases with larger volume fraction of austenite formed during intercritical annealing.

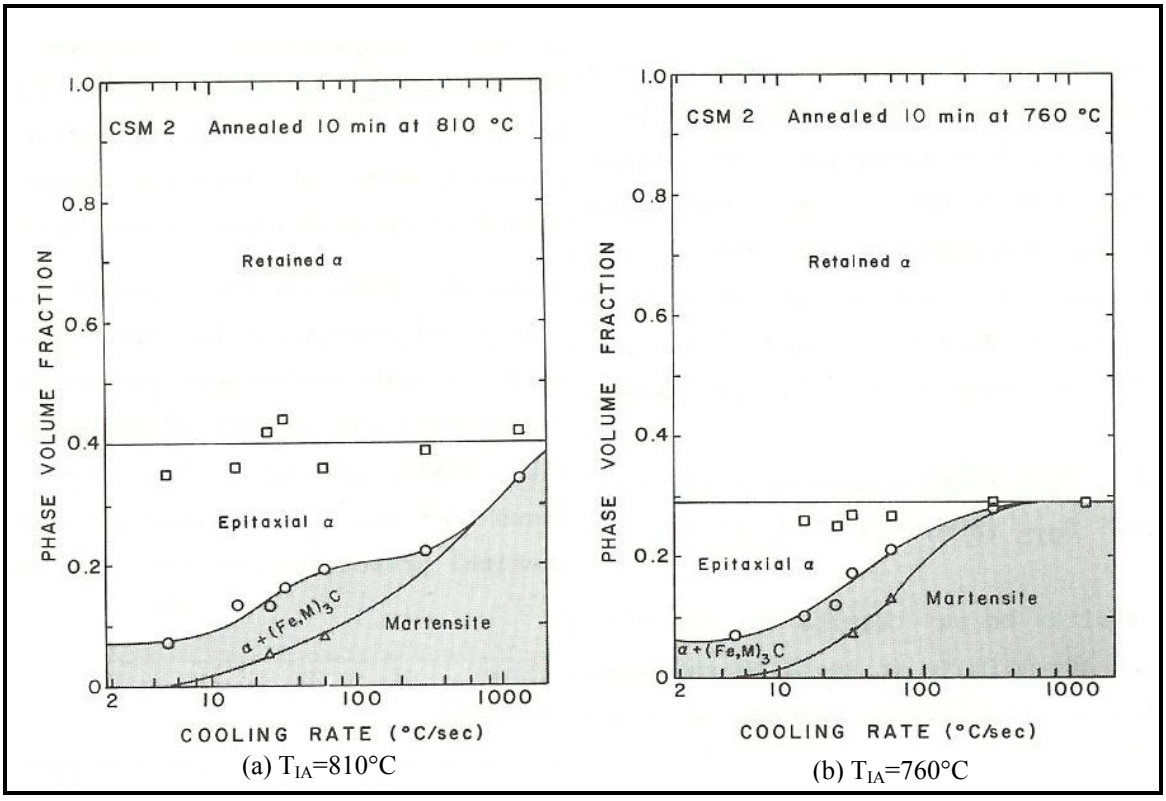

Figure 104 Effect of cooling rate and intercritical temperature on the volume fraction of epitaxial ferrite in a 0.06C-1.5Mn-0.25Si steel, (a) T_{IA}=810°C, and (b) T_{IA}=760°C

The large influence of the intercritical annealing temperature on the volume fraction of new ferrite can also be explained in terms of the austenite hardenability A reduction in the intercritical annealing temperature will result in a smaller fraction of intercritical austenite, with higher carbon content and therefore higher hardenability. In consequence, this will lead to a slower epitaxial ferrite reaction. As the epitaxial ferrite reaction will be diffusion controlled, a

higher carbon concentration will require more time to deplete the transformation-front diffusionally. Figure 105 shows the carbon distribution in austenite and ferrite as the γ/α advances (adapted from Porter and Easterling[88]). Cα is the carbon content in ferrite, Cγ in the intercritical austenite, and Cαγ at the interface. ΔC_0 is Cαγ - Cγ. Particle half-width is X, and growth rate is ν. Making the assumption that the diffusionally enriched zones have not yet begun to impinge on each other, austenite away from the interface will be of the carbon content Cγ, inherited from the intercritical state, and will not yet have been enriched.

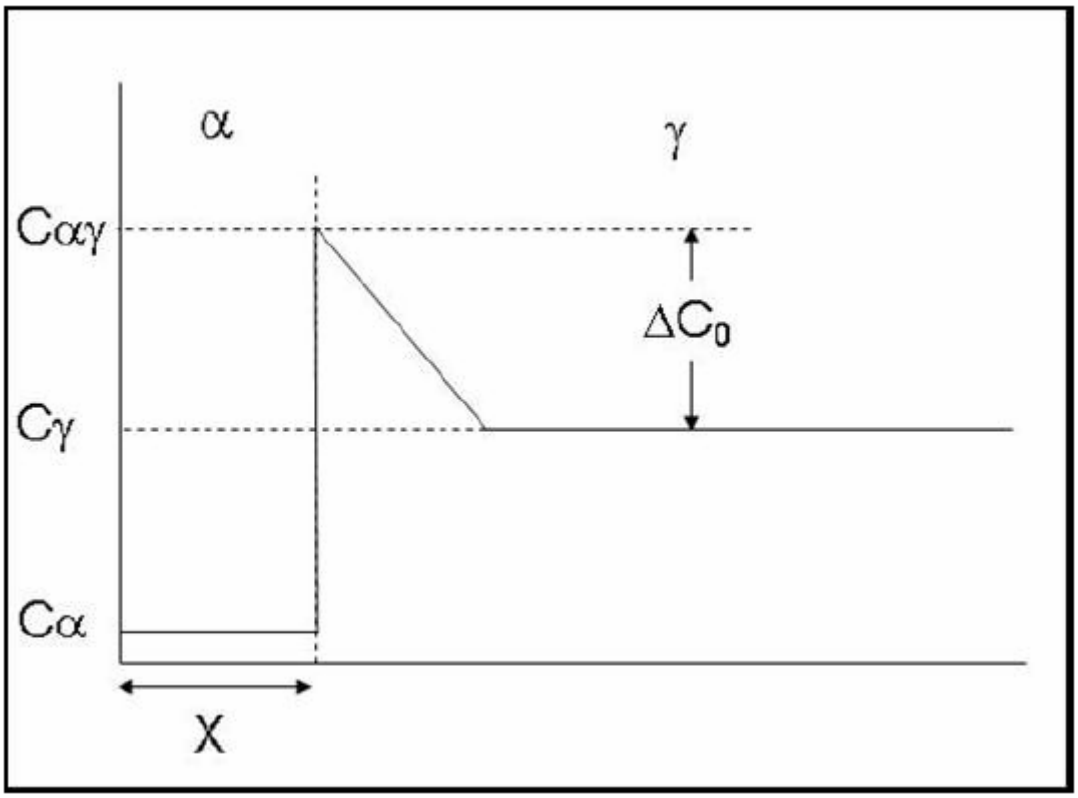

Figure 105 Diagram of ferrite growing into austenite (Adapted from Porter and Easterling)

Following Parish's adaptation of Porter and Easterling's equation for diffusion-controlled growth rate of a planar incoherent interface, when translated into Cα, Cγ, Cαγ and ΔC_0 terminology becomes:

$$v = \frac{D(\Delta C_0)^2}{2(C_\alpha - C_{\alpha\gamma})(C_\alpha - C_\gamma)X}$$

If the intercritical temperature is lower, Cγ will increase, ΔC_0 will decrease (ΔC_0^2 will decrease strongly), Cα - Cγ will become more negative, and X will increase. All of these variations will lead to slower growth (ν decreasing). Further, as Cγ increases, the driving force (difference between Cγ and the carbon content described by the T_0 line) for the bainitic reaction during holding at the IHT will be reduced.

Despite the fact that the range of cooling rates used in this research study only varied from 1°C/sec to 30°C/sec, it is expected that epitaxial ferrite forms at even higher cooling rates, as observed by Parish[38] in a 0.2C-1.8Mn-1.0Al-0.5Si steel. Parish observed that the epitaxial ferrite C-curve was cut by any cooling curve up to about 100°C/sec, as shown in Figure 106. Similarly, Brandt[83] showed that cooling rates close to 120°C/sec were necessary to suppress epitaxial ferrite formation in a 1.2%Mn steel, and about 50°C/sec in a 2.4%Mn steel.

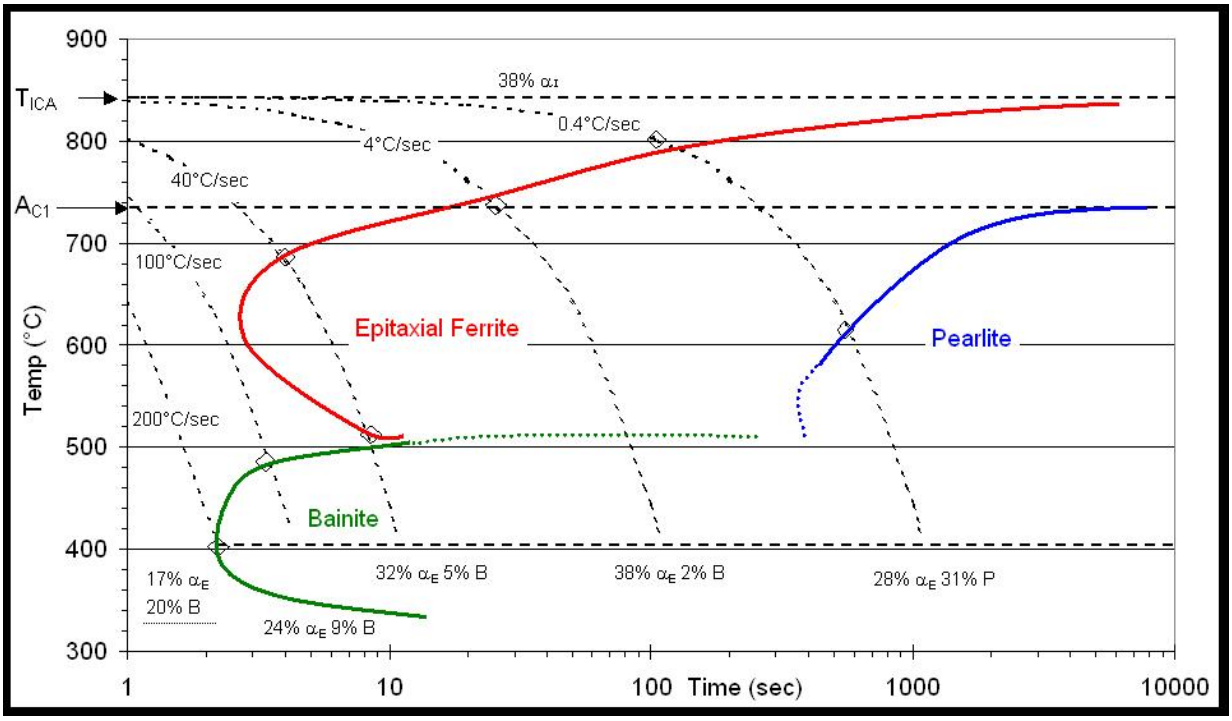

Figure 106 CCT diagram of a 0.2C-1.8Mn-1.0Al-0.5Si steel intercritically annealed at 840°C (60%γ). (After Parish, 2003)

Speich and Miller[84], in a similar result showed that the final volume fraction of martensite in a dual-phase steel was relatively insensitive to intercritical temperature at cooling rates of 1.4 or 10°C/sec. Only at 115°C/sec did the fraction of martensite increase with increasing intercritical temperature, as shown in Figure 107.

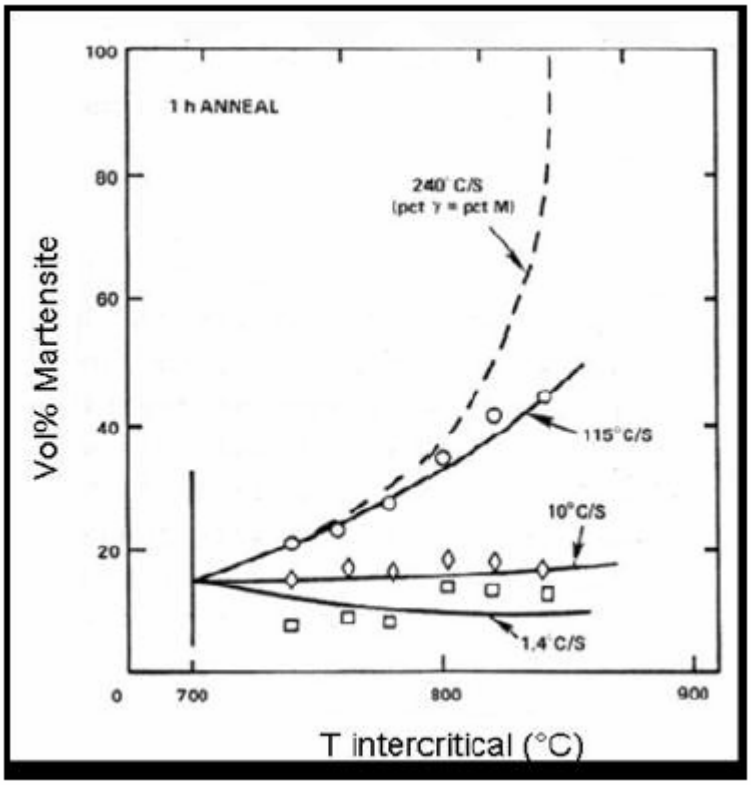

Figure 107 Effect of intercritical annealing temperature and cooling rate to room temperature on the volume fraction of M-A constituent (After Speich and Miller)

Finally, it was observed that the amount of new ferrite formed during cooling appears to depend on the alloy content. In the 0.05Al alloy, cooling from 750 C (35%γ) to 450 C results in ~8.5% new ferrite whereas in the 1.0Al alloy the new ferrite formed is ~18%. This supports the suggestion that the addition of 1.0%Al to this alloy system increases the mobility of grain boundaries by reducing the carbon segregation to the grain boundaries as discussed previously in section 6.1. Also, note that this agrees with the equation relating ΔC_0 £ ν. It was shown previously (using Thermo-Calc) that in the 1.0Al TRIP steel the carbon content for any given austenite volume fraction is larger than for the 0.05Al TRIP steel. Therefore, Cαγ increases in the 1.0Al TRIP steel and, in consequence, ΔC_0 increases. Moreover, the addition of Al also has

an influence on the solubility of C in ferrite, and therefore, the ($C\alpha - C\gamma$) term is also affected and hence the mobility increases. Furthermore, it is possible that the addition of Al greatly affects the self-diffusion coefficient of Fe.

TEM examination reveals that there was no change in the precipitation characteristics after intercritical annealing from that observed in the initial hot band. Nevertheless, analysis of the martensitic pools in those specimens quenched from 450 C after 2-5 second holding, revealed that a very fine (nano) twin structure exists in the martensite particles, Figure 108. This indicates that during cooling from the intercritical annealing to the IHT, the untransformed austenite became enriched in carbon as the austenite/ferrite advanced to at least 0.6 wt% C. In addition, no lath or mixed martensite structure was observed, and therefore it is expected that the % wt C in martensite is as large as 1.2%wt, resulting in the twinned martensite structure that was observed by TEM analysis.

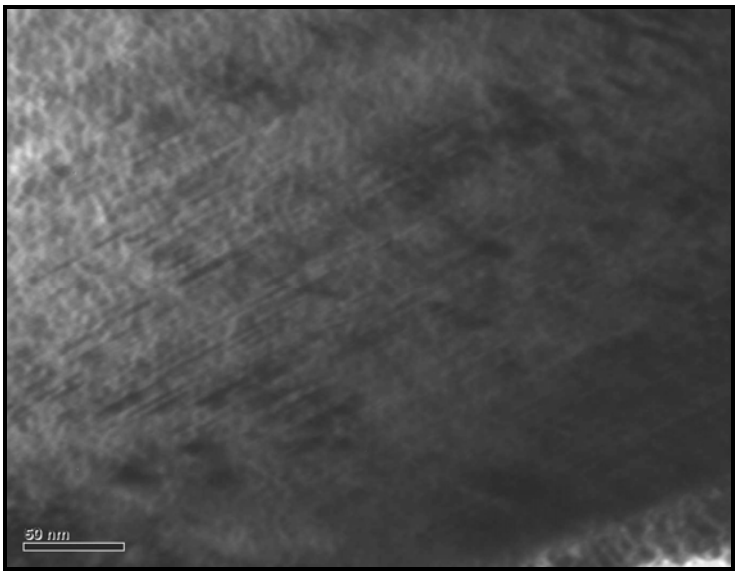

Figure 108 Twinned Martensite in the 1.0Al-550 alloy after intercritical annealing at γ=35%, IHT=450°C and immediately quench

6.3 ISOTHERMAL HOLDING TEMPERATURE

The extent to which the bainite reaction occurs during the isothermal holding region is strongly influenced by the Al content in the alloy. It was shown that the bainite volume fraction that forms during holding is less than 4% in the 1.0Al alloy, whereas the volume fraction found in the 0.05Al almost reached 14%.

Figure 109 shows the dilatometric data obtained during the isothermal holding temperature, and it displays a number of important points for describing the metallurgical phenomena that occur during isothermal holding at 450 C. It can be observed that the reactions begin very rapidly through their first few seconds, and then the reactions slow and level off, having been mostly completed after about 60 seconds for T_{IBT}=450°C in the 1.0Al and 0.5Al alloy, whereas in the 0.05Al alloy the reaction continues even after 300 seconds. This is believed to be due to the difference in the carbon content in the austenite at 450 C. As the temperature drops from the intercritical annealing temperature, the “new” (epitaxial) ferrite growth occurs and the residual austenite becomes enriched in carbon. Once the carbon concentration reaches the T_O line, the reaction is arrested, Figure 110. As the T_O line is approached, the reaction will slow; this is because the driving force for the reaction is reduced as the austenite increases in carbon content. Recall that T_O is defined as the carbon content, at some given temperature, at which the ferrite and austenite have the same free energy. This reduction in driving force/kinetic rate likely explains the "leveling off" shape of the IHT dilatometry curves, Figure 109. In the 1.0Al alloy, it was earlier suggested that the activity of carbon in austenite is increased, and carbon segregation to the γ/α interface is reduced, so that most of the carbon diffuses into the austenite. This would result in a more carbon enriched austenite than that found in the 0.5Al

and/or 0.05Al alloy. In consequence, the driving force for the bainite reaction is reduced and the carbon concentration rapidly reaches the T_0 line. On the other hand, because the carbon content in the austenite in the 0.05Al alloy is low, it requires a longer time to reach the T_0 line and there is a larger driving force for the bainite reaction.

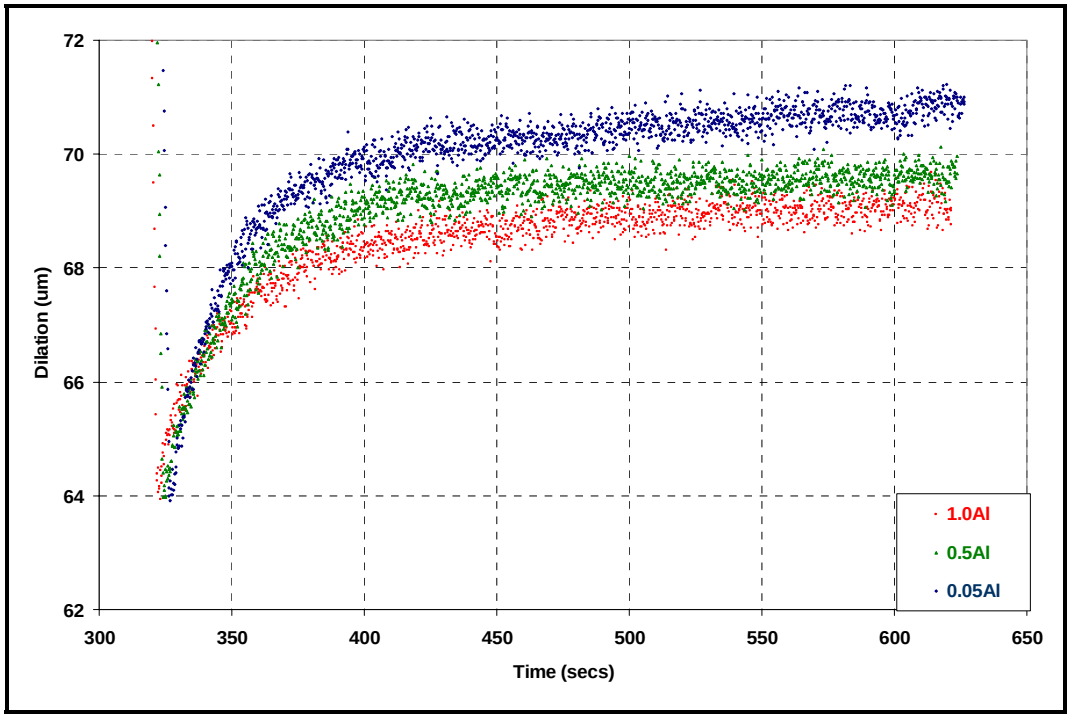

Figure 109 Dilatometry curves for the 0.05Al, 0.5Al and 1.0Al TRIP steels after intercritical annealing at γ=35%, IHT=450°C, and held for 5minutes

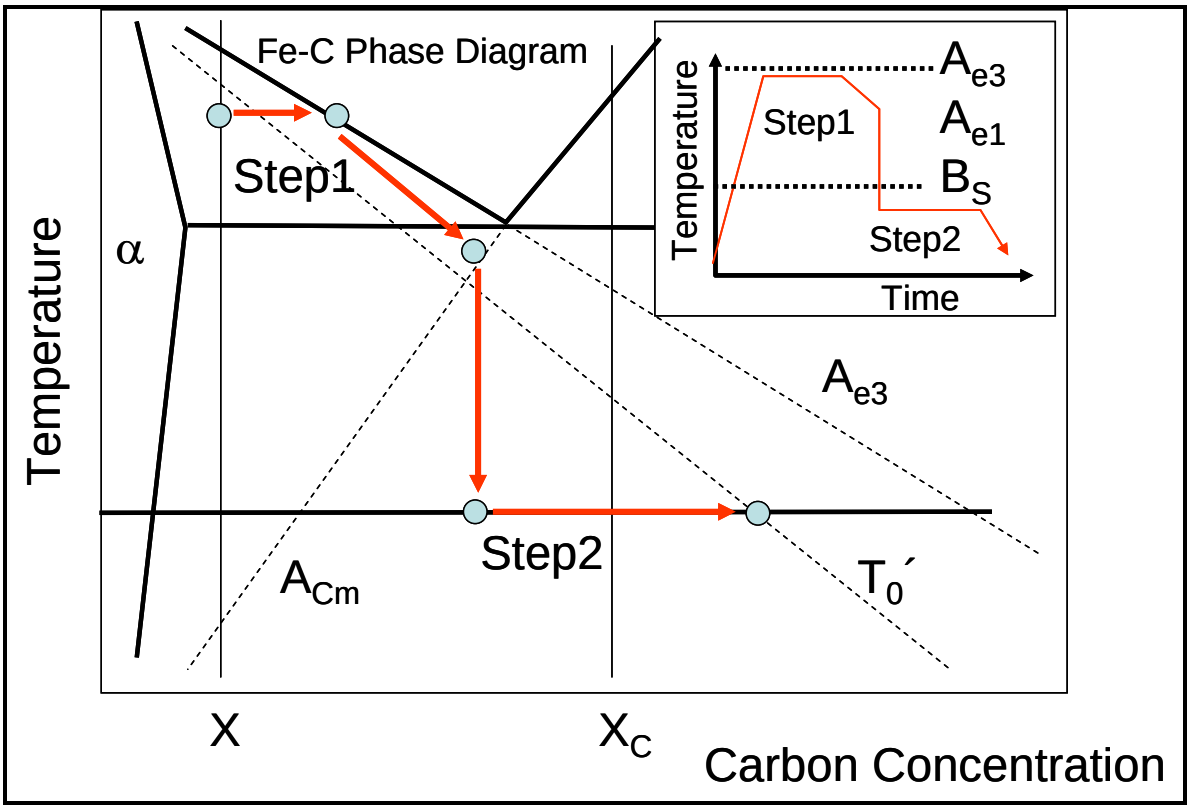

Figure 110 Schematic illustration of carbon enrichment with TRIP steel processing

It was also observed that the retained austenite increased with holding time. The amount and the type of retained austenite were influenced by the Al content in the alloy. In the 1.0Al alloy, a plate-like retained austenite was observed, whereas decreasing the Al addition shift the morphology from plate into an interlath shape. Rigsbee et al.[59] have also observed that the shape of the retained austenite particles depends on the type of ferrite that is in the matrix. Interlath retained austenite films were found in bainite regions, whereas essentially equiaxed or plate retained austenite particles were associated with polygonal ferrite formed during intercritical annealing, as shown in the TEM micrographs in Figures 111 and 112.

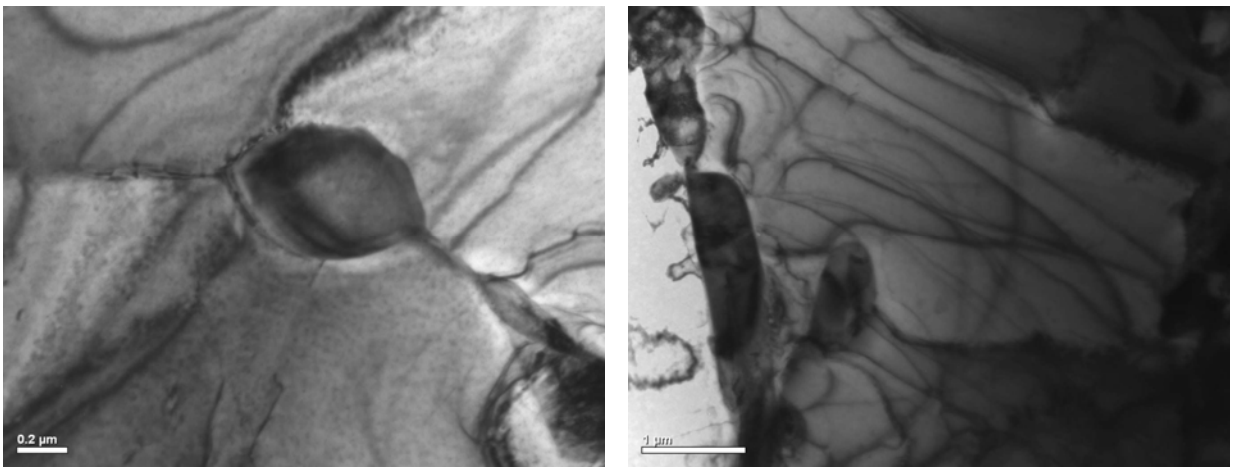

Figure 111 Typical retained austenite particles observed in the 1.0Al-550 alloy after holding for 30 seconds or more at IHT=450°C. Note that the retained austenite is present as isolated particles inside the ferrite grains and along grains boundaries. No association of retained austenite with bainite was observed

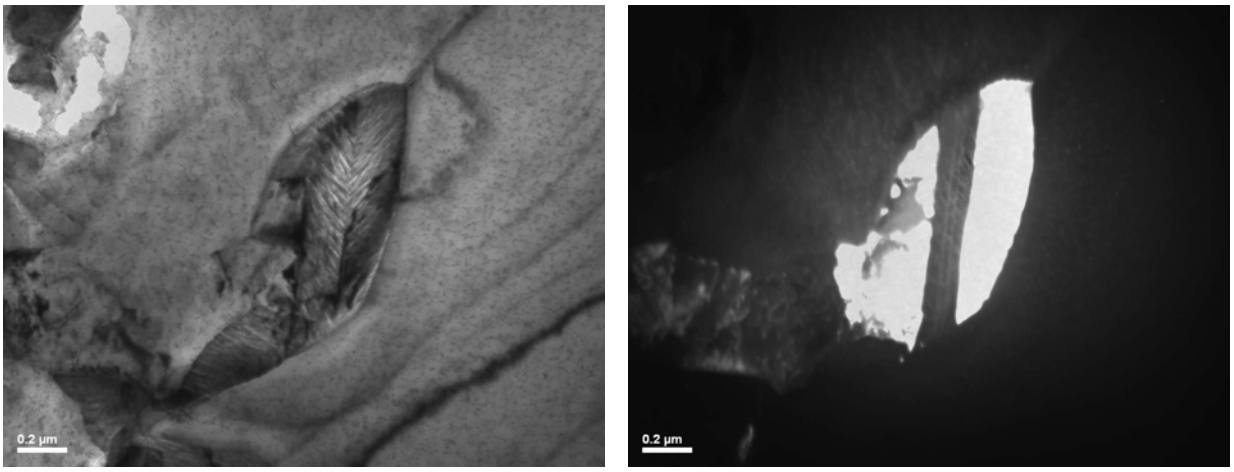

Figure 112 Twinned retained austenite particle observed in the 1.0Al-550 alloy after holding for 30 seconds or more at IHT=450°C. This type of retained austenite was frequently observed along grain boundaries

6.4 MECHANICAL PROPERTIES DISCUSSION

The tensile properties of the three Al-bearing alloys have very similar trends. Increasing the holding time at the isothermal holding temperature resulted in an increase in yield strength, yield point elongation, uniform elongation and total elongation. On the other hand, tensile strength decreased with holding time.

DeMeyer[11,35] observed a similar trend in a 1.5%Al TRIP steel, and similarly, Parish[38] observed in a 0.2C-1.8Mn-1.0Al-0.5Si steel that the tensile strength decreased with increasing length of IBT time; while the total elongation, yield stress and yield-point elongation increased.

6.4.1 Yield Stress (Continuous and Discontinuous Yielding)

It was observed that the specimens held a few seconds at 450 C followed by air cool, as well as those specimens quenched from 450 C after holding for 2-30 seconds, resulted in a continuous yielding behavior and low yield strength. Increasing the holding time and/or decreasing the cooling rate to room temperature after holding at 450 C changed the yielding behavior into discontinuous, increased the yield strength and the yield point elongation with holding time as well as with decreasing cooling rate, as shown in Figure 113 and Figure 114.

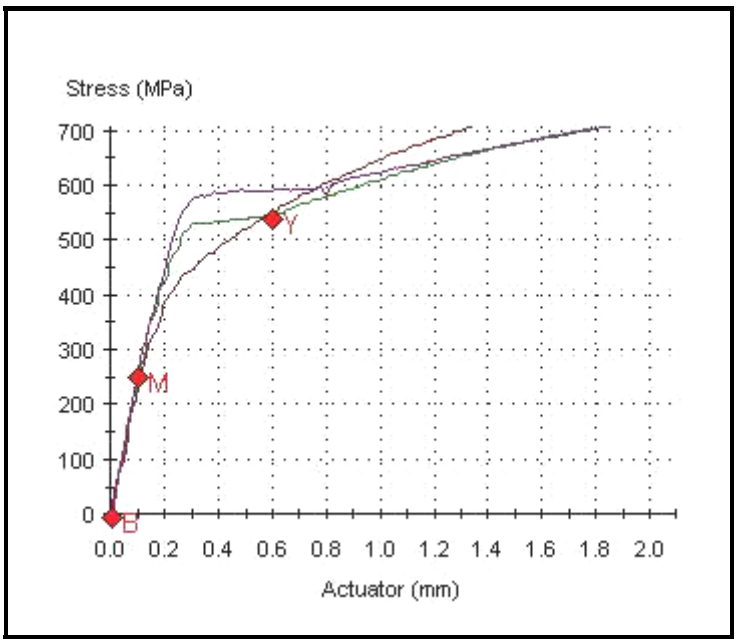

Figure 113 Yielding behavior in the 0.5Al-550 alloy. Curves shift from continuous yielding to discontinuous yielding as holding time increases at IHT=450°C

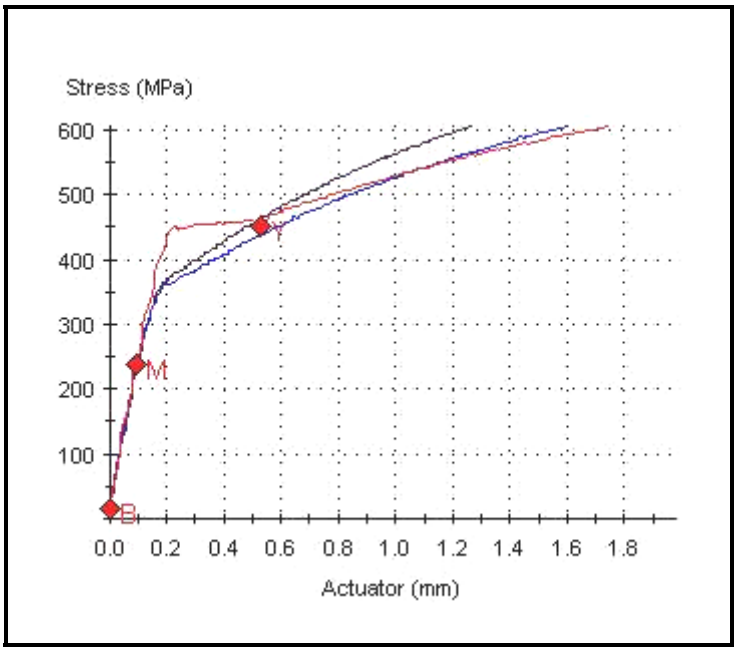

Figure 114 Yielding behavior in the 1.0Al-550 alloy. Curves shift from continuous yielding to discontinuous yielding as holding time increases at IHT=450°C

The decrease in yield strength associated with the continuous yielding behavior has been attributed to the presence of mobile dislocations produced inhomogeneously in the ferrite due to the austenite to martensite transformation within the constraints of the ferrite matrix or to residual stresses developed during transformation[49,54]. If we consider an initial sinusoidal distribution of residual stresses as in Figure 115, this will depress the yield stress by an amount equal to the residual stress and the general yielding will result in a rounding of the stress-strain curve[55].

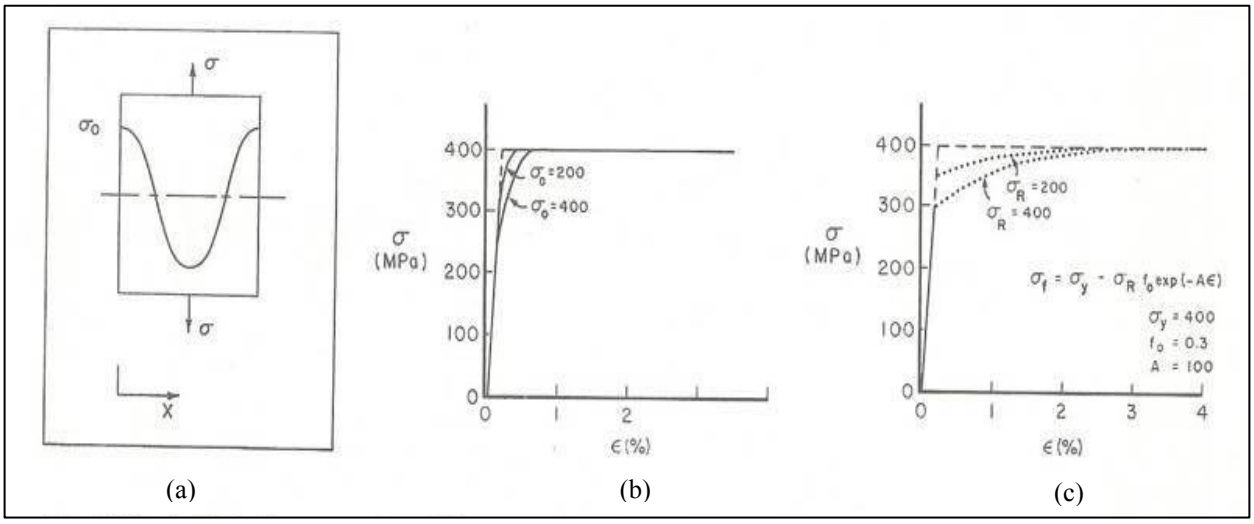

Figure 115 Effect of residual stress on the yielding behavior, (a) Initial distribution of residual stress, (b) rounding of a yield point due to the residual stress distribution in (a), and (c) rounding of a yield point due to non-homogeneous deformation of ferrite grains, containing the residual stress distribution in (a), and a gradual decrease with strain of the number of grains containing the residual stress

The return of discontinuous yielding after holding at 450 C and after slow cooling rates to room temperatures are believed to be due to solute C migrating to the grain boundaries. Furakawa et al.[58] in an internal friction study showed that there is less solute carbon in the ferrite matrix of samples air cooled from 750 C compared to those which were water quenched, Figure 116. Also, they suggest that the solute carbon content in a furnace cooled specimen is even less than the air cool specimen. Similar suggestions by Rigsbee[59] and Speich[48] have been made.

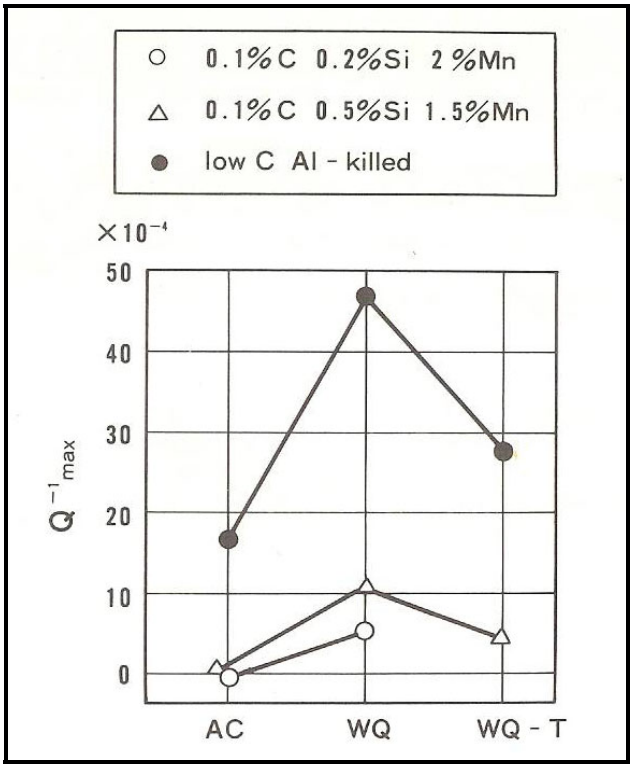

Figure 116 Effect of cooling rate from T_{IA}=750°C on internal friction, AC= air cooled, WQ=water quench, WQ-T=water quenched and tempered at 250°C for 1 minute.

6.4.2 UTS

It was observed that the UTS decreased with holding time during the IHT. However, the tensile properties became almost steady after just one minute of IHT time. This can be explained in terms of the leveling-off of the IBT dilatometry curves before the one minute mark is reached; that is, because the reaction is arrested shortly after a minute, and therefore, they result in very similar mechanical properties.

The large jump in mechanical properties between the specimens held for 5 seconds and the specimens held for 30 can be explained in terms of the rapid reaction at short IBT times shown in Figure 109. The specimen held for 5 seconds experienced only a small bainitic reaction whereas the specimen held for 30 seconds experienced most of the bainite reaction during the holding, in addition to the post-cooling stage.

Dilatometry showed that the first few seconds of the reaction are the most profound, so it comes as no surprise that even a short treatment in the bainitic temperature regime would cause a large difference in mechanical properties than, for example, the difference experienced the specimens held at 60 seconds and 120 seconds.

Furthermore, hardness (Vickers) measurements in the 1.0Al-550 steel agree with the shape of the dilatometry curve. Figure 117 shows that during the first few seconds of isothermal holding there is a clear change in hardness (independent of initial austenite percent), and after 30 seconds, the hardness values remain essentially constant. Obviously, the drop in hardness is associated with the decrease in M-A volume fraction, rather than the bainite formed during this holding period (which is less than 4%).

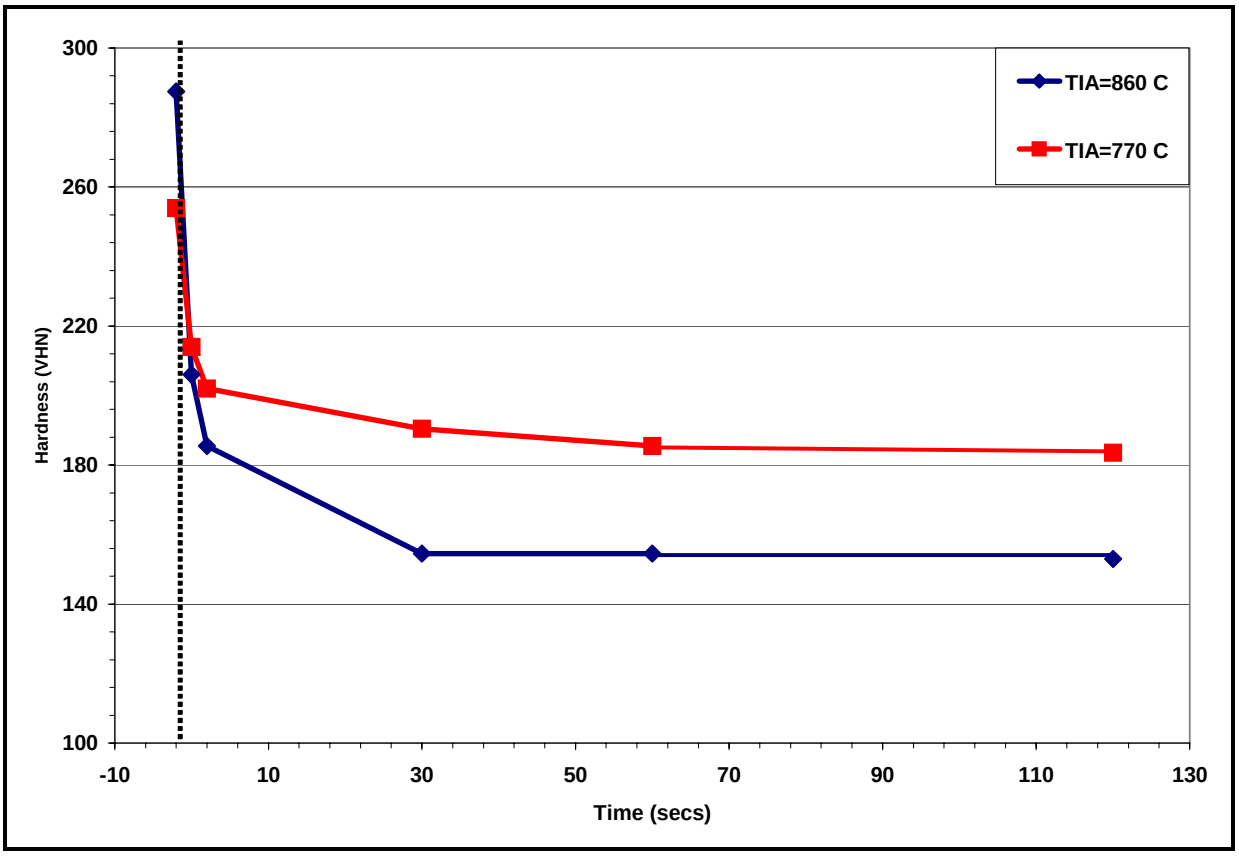

Figure 117 Effect of holding time at 450°C after cooling at 15 C/sec from T_{IA}= 770°C and 860°C on the hardness (Vickers) of the 1.0Al-550 steel

Despite the fact that the hardness remains almost constant after holding for 30 seconds, the tensile strength and elongation values are observed to change with holding time. Given the relatively small magnitude of the bainite reaction in the 1.0Al alloy, equal to about 4% volume fraction, it is surprising to observe such changes in tensile strength and total elongation. Almost identical results were observed by Parish. As suggested in his research work[38], rather than austenite enrichment, a homogenization of carbon is taking place. Using Brande's[90] values of carbon diffusion in austenite, and extrapolating to 416°C, a diffusion constant D_C=5x10^{-4} μm^2/sec is calculated. A diffusion distance calculation[91,92] indicates diffusion distances of

170nm for C in austenite after 1 minute at 416°C, and 390nm after 5 minutes. Because the dimensions of retained austenite in these steels are on the order of 200-600 nm, this indicates that simple homogenization is a possible mechanism of the stabilization between zero IHT and 2 minutes IHT. If, for example, an austenite island present at the start of the IHT had a steep carbon gradient, in which the boundaries were enriched, it might be possible that the boundary area would have an Ms well below room temperature, while the center of the particle still had Ms > RT. Thus, upon cooling, the center of the particle would necessarily transform to martensite. However, after carbon homogenization, the areas of high-carbon-content would have been depleted in carbon while the lower carbon areas were enriched. If this pushed all regions of the particle below Ms, the particle would necessarily be retained upon cooling to room temperature. Figure 118 shows schematically this hypothetical situation, both before (a) and after (b) the homogenization during the holding period. Thus, although there is little dilatometrically observable transformation, the IHT stage would still show a significant effect upon room-temperature properties.

This mechanism of carbon homogenization appears to be valid, since TEM observations in specimens held for 30 seconds at 450 C confirmed retained austenite and martensite coexisting within the same particle, Figure 119 and Figure 120. Furthermore, XRD measurements showed that the carbon content of the retained austenite decreased with holding time, suggesting that at short holding times the austenite was highly enriched, and as homogenization occurred, carbon diffused into the remaining particle, and in consequence, the average austenite particles resulted in lower carbon content, Figure 121.

Also, note that when the cooling rate from the intercritical annealing temperature (770°C) to the IHT=450°C was reduced from 15C/sec to 5C/sec, the carbon content of the austenite does not appear to change with holding time, Figure 122. This suggests that slow cooling rates allow carbon to diffuse away from the α/γ interface and carbon homogenization occurs during cooling and/or at very short times during the IHT.

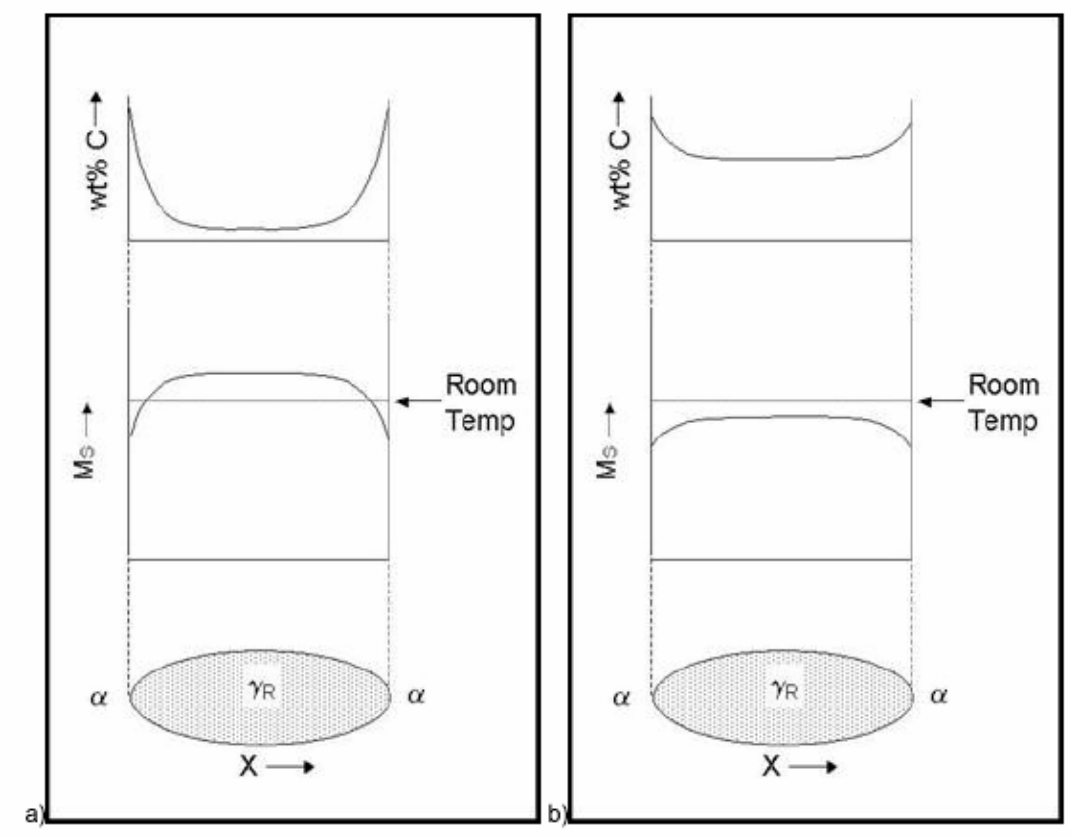

Figure 118 Hypothetical effect of IHT on carbon distribution within austenite islands, (a) no holding time at IHT, (b) after holding at Δt during IHT

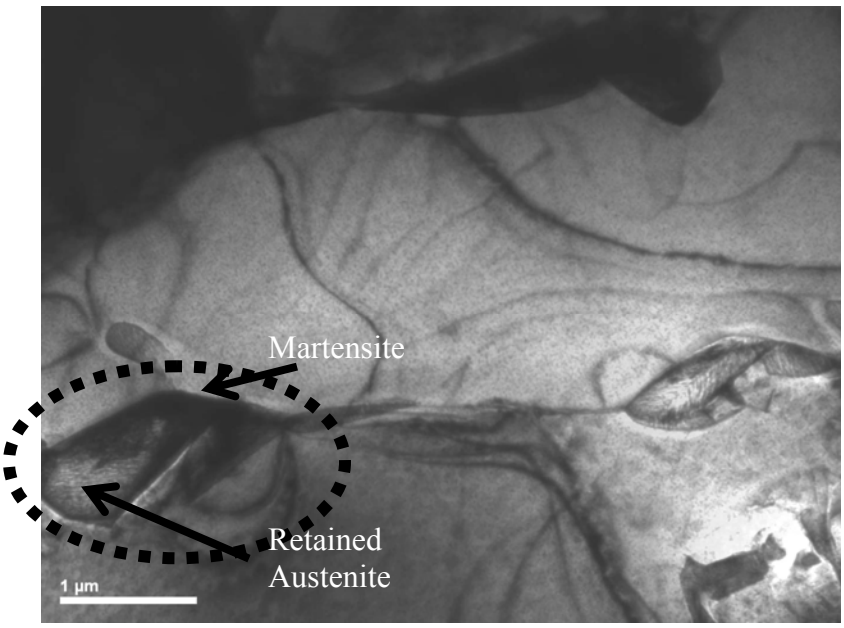

Figure 119 TEM micrographs showing retained austenite and martensite coexisting in the same grain, 1.0Al-550 alloy, after holding 30 seconds at IHT=450°C

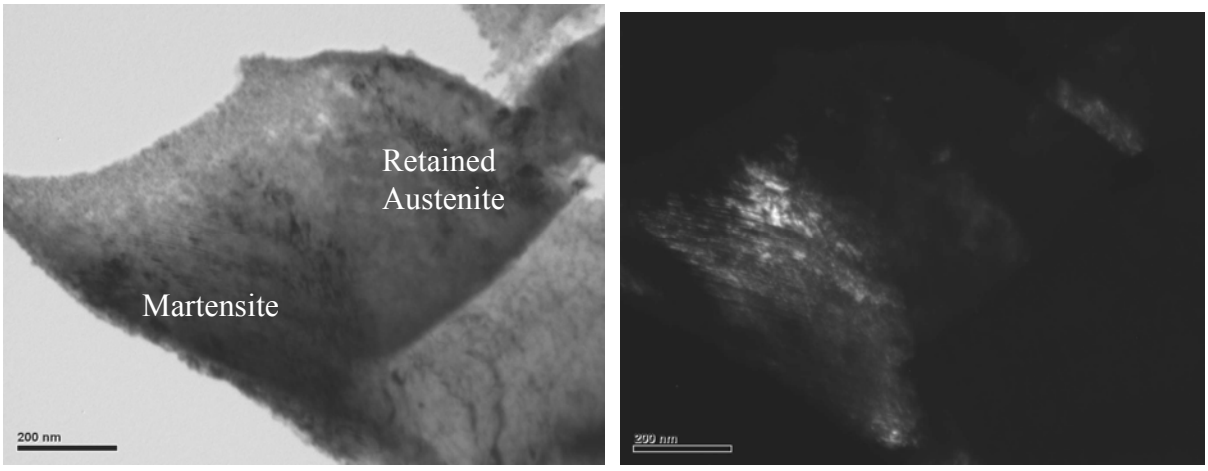

Figure 120 Bright field and dark field TEM micrographs showing retained austenite and martensite coexisting in the same grain, 1.0Al-550 alloy, after holding 30 seconds at IHT=450°C

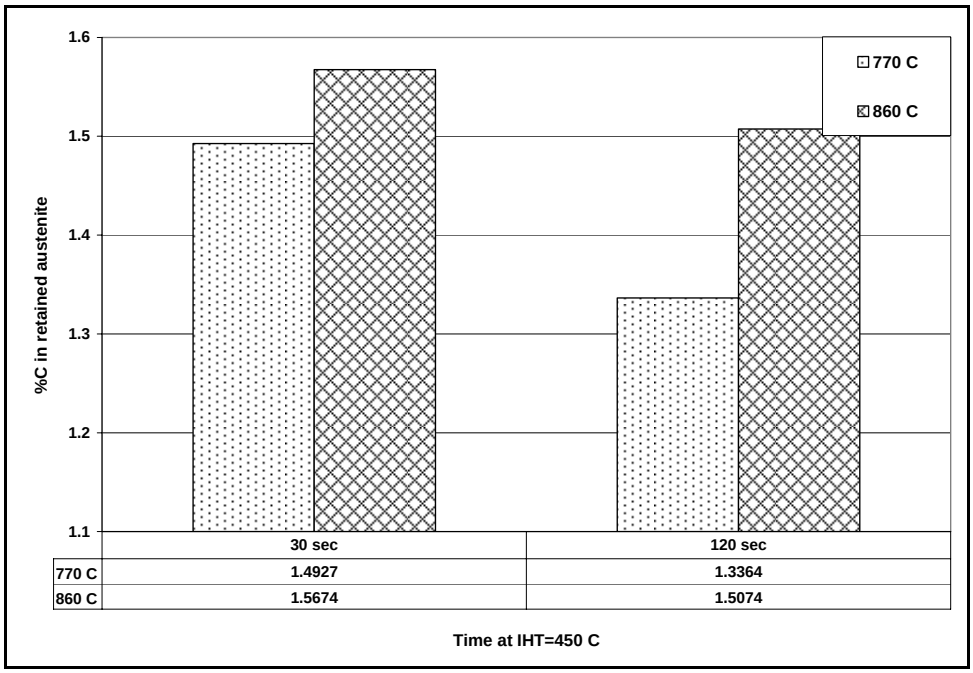

Figure 121 Percent carbon in retained austenite after holding for 30 and 120 seconds at 450°C, for both T_{IA}=770°C and 860°C, with cooling rate from T_{IA} to IHT= 15 C/sec

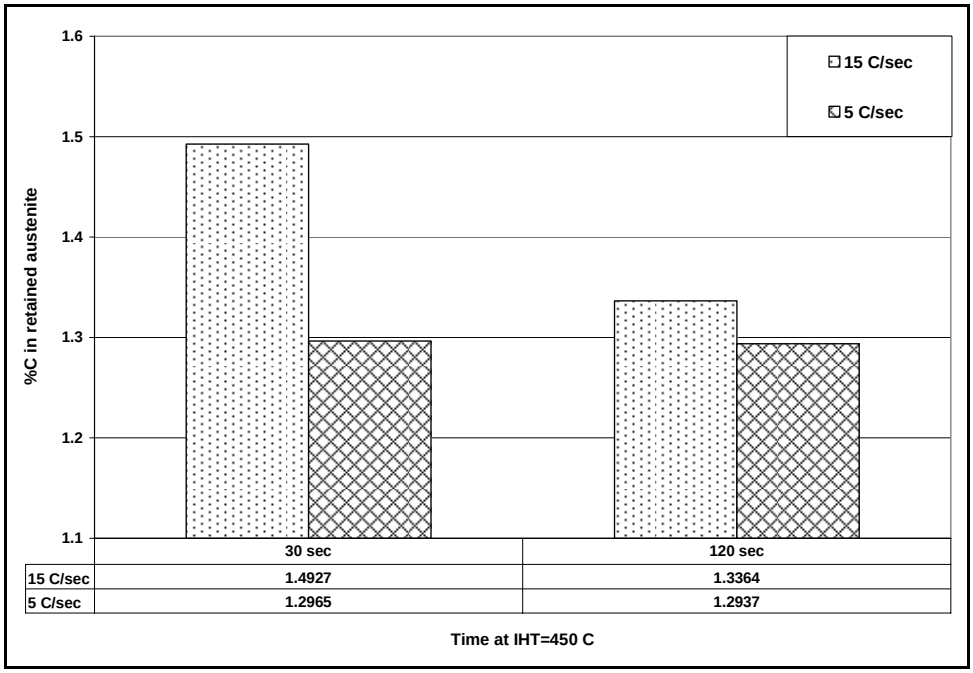

Figure 122 Percent carbon in retained austenite after holding for 30 and 120 seconds at 450°C, for T_{IA}=770°C, with cooling rate from T_{IA} to IHT= 15 C/sec and 5C/sec

Parish[38] observed that the variations in the galvannealed (GA) parameters had a very small effect on final mechanical properties. Based on dilatometry results, it was suggested that the properties/microstructure should be locked-in by the time the bainite reaction levels off at about two-minute hold, so that a short GA step after a two minute holding will have only minimal effects on the stabilized structure. This obviously agrees perfectly with the results shown in this research work. The bainite reaction in the 1.0Al alloy was observed to level off at approximately 60 seconds at 450 C and, in the same way as Parish pointed out, it was observed that a galvannealing treatment after holding for 60 seconds at the IHT resulted in no change in the tensile properties.

Rigsbee[59] has shown in a 0.15C-1.45Mn-0.47Si-0.02Nb-0.05V that bainite content has a minor role on strengthening and that the important factor for strength is the martensite-austenite second-phase constituent. Figure 123 shows that the initial increase in UTS at low bainite content is much larger than the general strengthening trend for bainite, and this increase in UTS is due to the increase in M-A constituent from 0% to 13%. Bainite was found to have a strengthening effect of 1.5 ksi per 10% volume fraction, whereas the M-A was found to have 20 ksi per 10% volume fraction. Furthermore, it was observed that the formation of bainite was detrimental to both uniform and total elongation. Similar analyses of the results obtained in this research study also suggest that bainite is detrimental to both uniform and total elongation. Furthermore, it appears that increasing volume fraction of bainite in fact results in a decrease in tensile strength, as shown in Figure 124. This is likely because the volume fraction of martensite decreases at the expense of bainite formation and retained austenite. In fact, the numbers in parenthesis in Figure 124 clearly show that there is a strong effect of the volume fraction of M-A on the tensile strength.

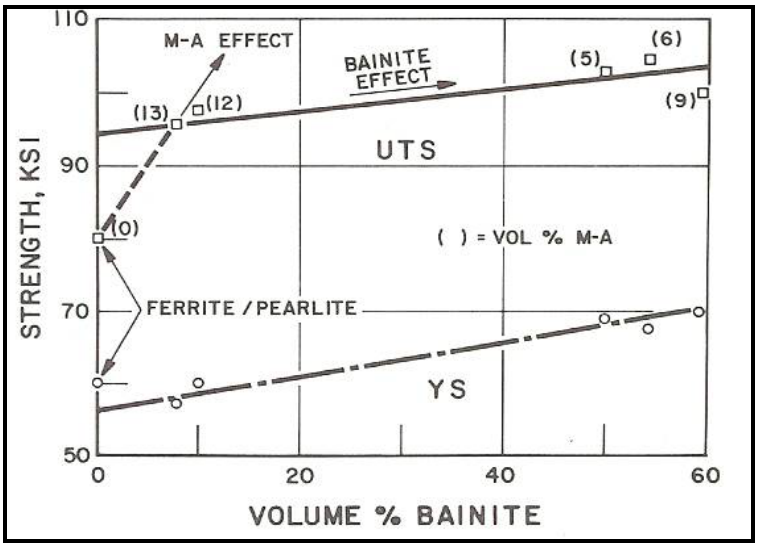

Figure 123 Variation of yield and UTS versus % bainite. Bainite strengthening effect is ~1.5ksi per 10% bainite volume fraction

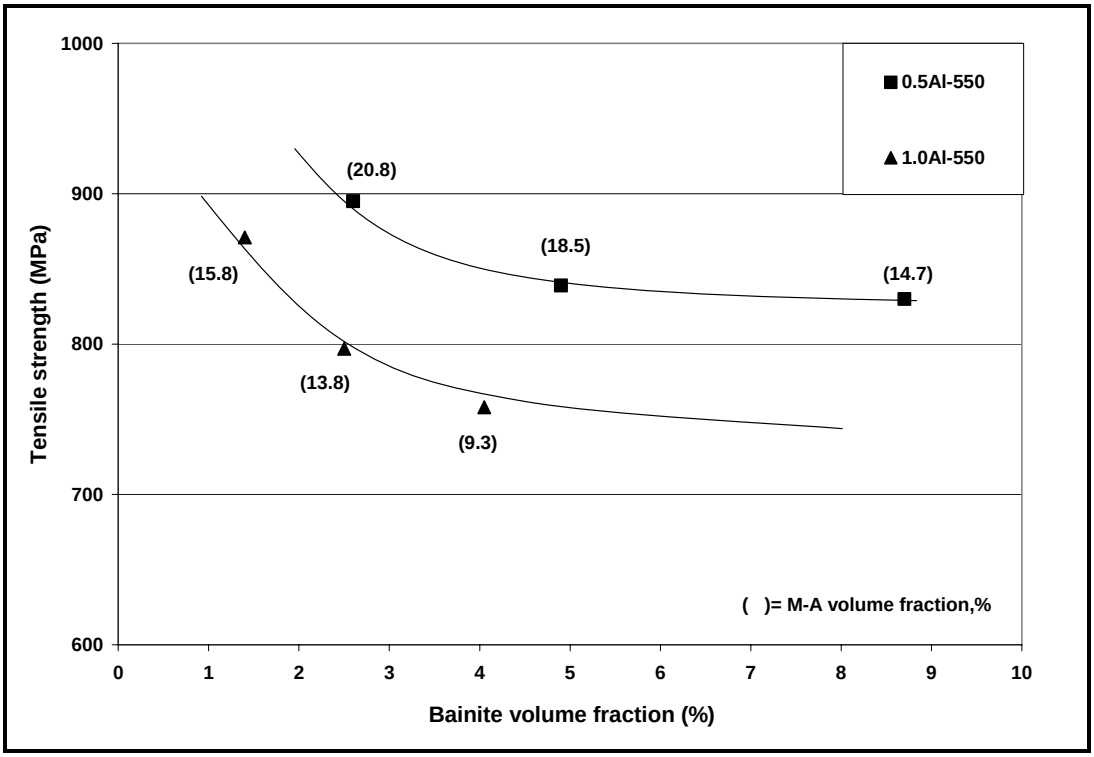

Figure 124 Variation of UTS versus % bainite in the 0.5Al-550 and 1.0Al-550 TRIP steel. The corresponding M-A volume fraction is also shown in parenthesis

6.4.3 Uniform and Total Elongation

The work hardening rate depends on the volume fraction of retained austenite. The continuous strain-induced transformation of the austenite to martensite generates additional dislocation structure in the ferrite during deformation. Since it has been shown the flow stress in steel is linearly proportional to the square root of the dislocation density, it is understandable that a relationship exists between the amount of retained austenite and the work hardening rate.

Similarly, a relationship between the retained austenite and the uniform elongation exists. The improved uniform elongations result from the transformation induced increase in work hardening rate which, according to the Considere criterion[47,93] delays the onset of necking. Plots of instantaneous work hardening vs strain are usually used to describe the behavior of retained austenite during straining. An initial, high work hardening at low strains followed by a continuous decrease in work hardening as strain progresses, is typical of a dual-phase steel or a TRIP steel with unstable retained austenite. On the other hand, an initial high instantaneous work hardening, which is maintained with further strain, is typical of a TRIP steel with stable retained austenite.

The steady instantaneous work hardening is due to the transformation of austenite into martensite, which locally increases the work hardening and ultimately delays the onset of necking. The comparison of this behavior is shown in Figure 125 for the 1.0Al-550 and 0.Al-550 TRIP steels, intercritically annealed for an initial γ=35%, cooled at 15C/sec to IHT=450°C, and held 30 seconds followed by air cooling. Note that the 1.0Al-550 TRIP steel maintains a steady

instantaneous work hardening at larger strains (due to the presence of stable retained austenite), and by preventing an early onset of necking, ultimately, results in a larger total elongation. In the 0.5Al-550 alloy, the retained austenite is not as stable, transforms into martensite too quickly and in consequence, a smaller total elongation is observed.

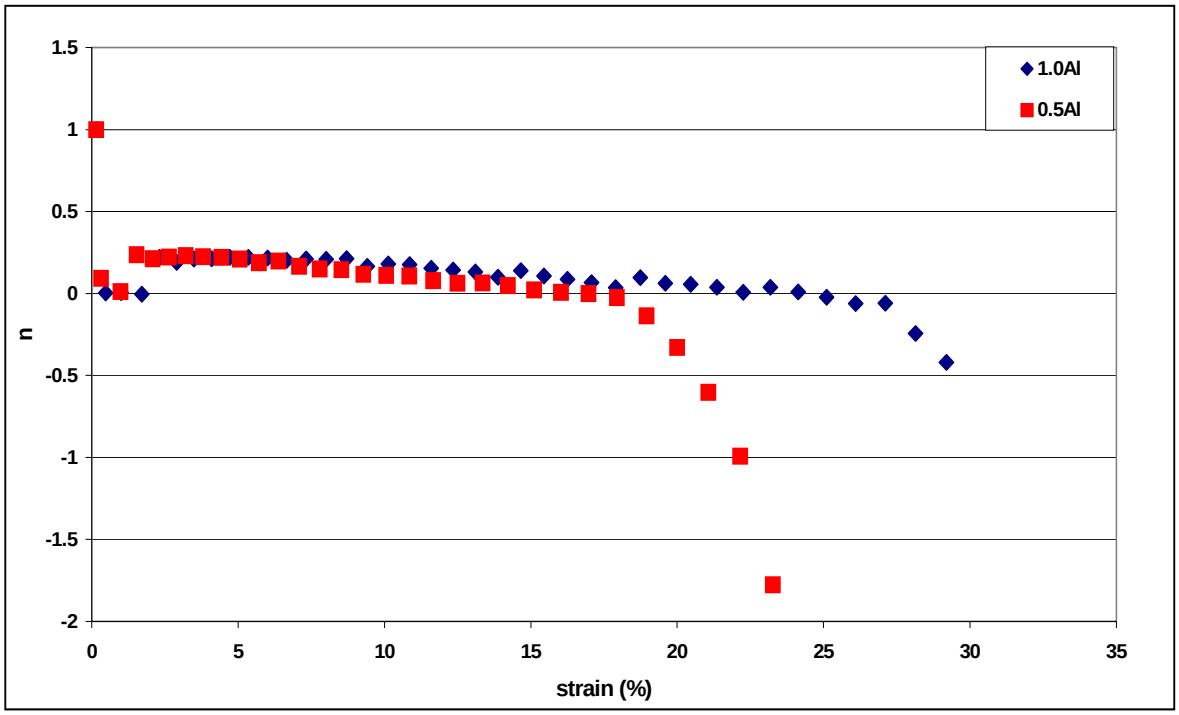

Figure 125 Instantaneous work hardening behavior versus strain in the 1.0Al-550 and 0.5Al-550 TRIP steel. Specimens were intercritical annealed at γ=35%, cooled at 15C/sec to IHT=450°C and held for 30 seconds followed by ACRT

7.0 CONCLUSIONS

It was established that it is possible to obtain TRIP steels with excellent mechanical properties under conventional CGL processing parameters by using Al, Nb-Mo additions. It was observed that the best TRIP steel was the 1.0Al-550 alloy, which achieved tensile strengths of 800MPa and elongations larger than 25%.

The following important conclusions were observed:

a) STAGE I. Intercritical Annealing: It was observed that Al additions greatly affect the Fe-C phase diagram, expanding the $\alpha+\gamma$ region, and increasing both the Ac1 and Ac3 temperature. Additions of 1.0Al wt% increased the Ac3 temperature close to 1000 C. Also, it was observed that the rate of ferrite recrystallization was substantially increased and fully recrystallized grains in the 1.0Al alloy were observed at temperatures well below intercritical annealing temperatures equal to 35%γ or higher. In addition, Al additions >0.5%wt eliminated the effect of prior coiling conditions on the volume fraction of austenite during intercritical annealing and on the recrystallization of ferrite.

b) STAGE II. Cooling from TIA to IHT: It was observed that the volume fraction of “new” epitaxial ferrite is strongly influenced by both the Al additions and the intercritical annealing temperature. More “new” epitaxial ferrite is formed with increasing Al additions and higher

intercritical annealing temperatures. Also, it was observed that increasing the Al content to 1.0%wt eliminated the bainite curve in the CCT diagrams, and retained austenite was observed rather than martensite. No significant effect of prior coiling conditions on the volume fraction of new epitaxial ferrite was observed.

c) STAGE III. Isothermal Holding Temperature: It was observed that the bainite reaction does not occur extensively in Al added Nb-Mo TRIP steels. Only about 4% was present and only after holding for 2 minutes in the IHT=450°C. Also, it was clearly observed that the stability of the retained austenite is not associated with the bainite formation. Retained austenite particles were observed along grain boundaries and inside ferrite grains. Furthermore, stable retained austenite was obtained at short holding times, and therefore long isothermal holding times are unnecessary. In addition, the cooling rate after IHT can have a significant effect on the amount and stability of the retained austenite. It was observed that the optimum cooling rate is air cooling. Faster cooling rates result in a larger amount of martensite, whereas slower cooling rates result in carbon depletion towards the grain boundaries (as observed from the yield point elongation in the tensile curves). Finally, essentially no retained austenite was observed when the specimens where prior-coiled at 700 °C.

d) Mechanical Properties: A lower initial austenite percent during intercritical annealing results in better tensile and elongation properties. Tensile strength decreased and elongation increased with holding time during the IHT. The goal of UTS=800 MPa and %El=25-30% was achieved with the 1.0Al-550 TRIP steel using heat cycles normally observed in a CGL, eliminating the necessity of long IBT holding sections.

APPENDIX A

VOLUME FRACTION OF MICROCONSTITUENTS OF THE TRIP STEELS

Table A1 0.05Al TRIP steel

Alloy 0.05Al-550 T_{IA}=750°C (35%γ)	750C, (60s) + Q	IHT= 450C, 2s + Q	IHT= 450C, 30s + AC	IHT=450C, 120s + AC
OLD FERRITE (RXD + NON-RXD)	65.97	65.97	65.97	65.97
RXD FERRITE	38.19	38.19	38.19	38.19
NON RXD FERRITE	27.78	27.78	27.78	27.78
NEW FERRITE	-	8.45	8.45	8.45
MARTENSITE	34.03	26.55	14.56	10.28
RETAINED AUST	0	0	2.05	4.17
BAINITE	0	0	10.27	13.97

Table A2 0.05Al TRIP steel

Alloy 0.05Al-550 T_{IA}=790°C (55%γ)	790C, (60s) + Q	IHT= 450C, 2s + Q	IHT= 450C, 30s + AC	IHT=450C, 120s + AC
OLD FERRITE (RXD + NON-RXD)	49.46	49.46	49.46	49.46
RXD FERRITE	27.26	27.26	27.26	27.26
NON RXD FERRITE	22.2	22.2	22.2	22.2
NEW FERRITE	-	25.15	25.15	25.15
MARTENSITE	50.54	29.85		
RETAINED AUST	0	0		
BAINITE	0	0		

Table A3 0.05Al TRIP steel

Alloy 0.05Al-700 T_{IA}=765°C (35%γ)	765C, (60s) + Q	IHT= 450C, 2s + Q	IHT= 450C, 30s + AC	IHT=450C, 120s + AC
OLD FERRITE (RXD + NON-RXD)	65	65	65	65
RXD FERRITE	27.45	27.45	27.45	27.45
NON RXD FERRITE	37.55	37.55	37.55	37.55
NEW FERRITE	-	8.08	8.08	8.08
MARTENSITE	35	26.92	15.69	13.84
RETAINED AUST	0	0	0	0
BAINITE	0	0	9.41	12.19

Table B1 0.5Al TRIP steel

Alloy 0.5Al-550 T_{IA}=760°C (35%γ)	760C, (60s) + Q	IHT= 450C, 2s + Q	IHT= 450C, 30s + AC	IHT=450C, 120s + AC
OLD FERRITE (RXD + NON-RXD)	65	65	65	65
RXD FERRITE	-	-	-	-
NON RXD FERRITE	-	-	-	-
NEW FERRITE	-	11.6	11.6	11.6
MARTENSITE	35	23.4	12.74	8.25
RETAINED AUST	-	0	5.76	6.45
BAINITE	-	0	4.9	8.7

Table C1 1.0Al TRIP steel

Alloy 1.0Al-550 T_{IA}=770°C (35%γ)	770C, (60s) + Q	IHT= 450C, 2s + Q	IHT= 450C, 30s + AC	IHT=450C, 120s + AC
OLD FERRITE (RXD + NON-RXD)	69.7	69.7	69.7	69.7
RXD FERRITE	52.8	52.8	52.8	52.8
NON RXD FERRITE	16.9	16.9	16.9	16.9
NEW FERRITE	-	14.77	14.77	14.77
MARTENSITE	30.2	16.91	4.8	0
RETAINED AUST	0	3.32	8.5	10.64
BAINITE	0	0	2.5	4.05

Table C2 1.0Al TRIP steel

Alloy 1.0Al-550 T_{IA}=860°C (55%γ)	860C, (60s) + Q	IHT= 450C, 2s + Q	IHT= 450C, 30s + AC	IHT=450C, 120s + AC
OLD FERRITE (RXD + NON-RXD)	42.5	42.5	42.5	42.5
RXD FERRITE	32.4	32.4	32.4	32.4
NON RXD FERRITE	10.1	10.1	10.1	10.1
NEW FERRITE	-	41.77	41.77	41.77
MARTENSITE	57.5	13.23	0	0
RETAINED AUST	0	0	13.2	11.95
BAINITE	0	0	1.5	2.75

Table C3 1.0Al TRIP steel

Alloy 1.0Al-700 T_{IA}=770°C (35%γ)	770C, (60s) + Q	IHT= 450C, 2s + Q	IHT= 450C, 30s + AC	IHT=450C, 120s + AC
OLD FERRITE (RXD + NON-RXD)	65	65	65	65
RXD FERRITE	49.22	49.22	49.22	49.22
NON RXD FERRITE	15.78	15.78	15.78	15.78
NEW FERRITE	-	21.46	21.46	21.46
MARTENSITE	35	13.54	-	-
RETAINED AUST	0	0.51	1.46	0.1
BAINITE	0	0	-	-

APPENDIX B

MECHANICAL PROPERTIES OF THE TRIP STEELS

Table D1 1.0Al-550 TRIP steel

Alloy 1.0Al-550 TIA=770°C (35%γ)	IHT= 450C, 2s + AC	IHT= 450C, 30s + Q	IHT= 450C, 30s + AC	IHT= 450C, 30s + FC	IHT= 450C, 60s + AC	IHT= 450C, 60s + GA*	IHT= 450C, 90s + AC	IHT=450C, 120s + AC
YS (0.2%), LYP	393	376	369					494
Yield Point Elongation	no	no	no	yes	yes	yes	yes	Yes
UTS	871	844	797	766	780	779	764	758
Uniform Strain	0.1612	0.2037	0.2095	0.2198	0.1894	0.1889	0.2230	0.2456
Total Elongation	23.9	27.0	27.16	28.34	27.53	26.87	31.73	33.4
UTS x Total Elongation	20835	22814	21657	21735	21473	20931	24241	25316

Table D2 0.5Al-550 TRIP steel

Alloy 0.5Al-550 TIA=760°C (35%γ)	IHT= 450C, 2s + AC	IHT= 450C, 30s + Q	IHT= 450C, 30s + AC	IHT= 450C, 30s + FC	IHT= 450C, 60s + AC	IHT= 450C, 60s + GA	IHT= 450C, 90s + AC	IHT=450C, 120s + AC
YS (0.2%), LYP	444	519	536	561				583
Yield Point Elongation	no	no	yes	yes				yes
UTS	895	890	839	791				830
Uniform Strain	0.1531	0.1480	0.170	0.1969				0.1762
Total Elongation	21.86	22.0	24.12	27.70				24.12
UTS x Total Elongation	19584	19603	20243	21934				20030

Table D3 1.0Al-550 and 1.0Al -700TRIP steel

Alloy	1.0Al-550		1.0Al-700
Processing / Tensile Properties	T_{IA}=770°C (35%γ) IHT= 450C, 30s + AC	T_{IA}=860°C (55%γ) IHT= 450C, 30s + AC	T_{IA}=770°C (35%γ) IHT= 450C, 30s + AC
YS (0.2%), LYP	369		399
Yield Point Elongation	no	yes	Yes
UTS	797	723	736
Uniform Strain	0.209	0.2419	0.212
Total Elongation	27.16	31.61	28.65
UTS x Total Elongation	21657	22854	21100

APPENDIX C

IMAGE QUALITY ANALYSIS

Measuring the degree of lattice imperfection of the grain centers of the ferrite and other microconstituents is one way of first identifying, then grouping, and finally quantifying, the different types or forms of microstructures. In EBSD analysis, an index to distinguish the degree of lattice imperfection is the image quality (IQ). The IQ is proportional to the sharpness of the Kikuchi Pattern, which is related to the presence of crystalline defects. An elastically distorted lattice will have a smeared Kikuchi Pattern and a low IQ, Figure C1.

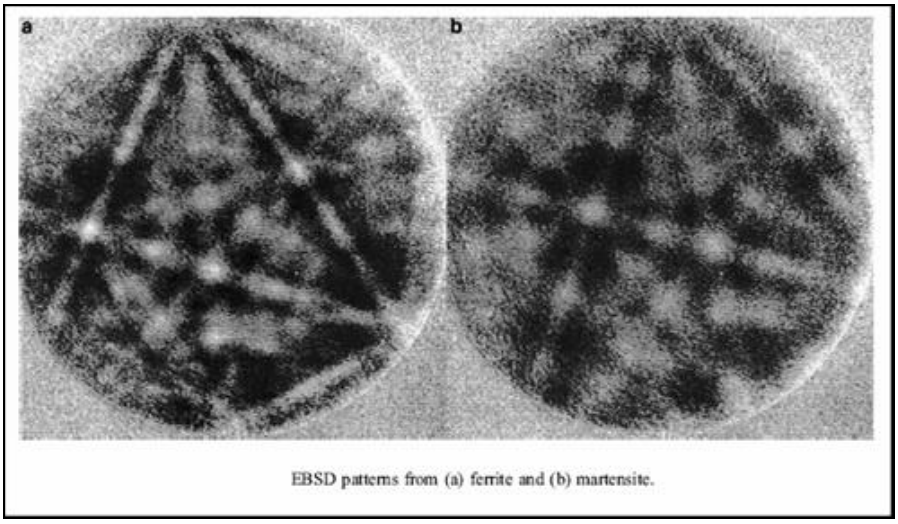

Figure C1 The image quality parameter, IQ, describes the quality of an electron backscatter diffraction pattern. The greatest effect on IQ is the perfection of the crystal lattice in the diffracting volume. Strain, dislocation and all kind of defects associated with the lattice could significantly affect the pattern quality, which can be used to identify and quantify different microconstituents

The new approach of using IQ to characterize microstructures eliminates the contribution from grain boundaries to the total IQ distribution[62,78]. Depending upon the transformation behavior during cooling, it is not uncommon for different microconstituents to co-exist in one specimen. These different types of microconstituents are often readily discernable in optical microscopy and SEM. However, measuring their volume fractions is not easily accomplished using conventional quantitative metallographic techniques. Since the types of microcosntituents and the IQ level of the individual grains vary with their defect structure, such as dislocation density, the measurement of the spectrum of IQ values in a given samples is necessary.

To take full advantage of the new IQ approach, the effects of image processing on the IQ values is minimized through a normalization procedure. Also, a program is used to eliminate the effects of grain boundaries on the IQ distribution curve and a multi-peak model for analyzing multi-component microstructures is also employed [62,78].

BIBLIOGRAPHY

1. **Senuma T**., "Physical Metallurgy of Modern High Stregth Steel Sheets", ISIJ International, Vol 41, 2001. No.6 pp 520-532

2. **Jacques P., Ladriere J**., "On the influence of interactions between phases on the mechanical stability of retained austenite in transformation-induced plasticity multiphase steels", Metallurgical and Materials Transactions A, vol 32A, November 2001, pp2759-2768

3. **Jacques P., Girault E**., "The development of cold-rolled TRIP assisted multiphase steels. Low Si TRIP assisted multiphase steels", ISIJ International, vol 41, No.9, 2001, pp1061-1067

4. **Hanzaki A., Hodgson P**., "The influence of bainite on retained austenite characteristics in Si-Mn TRIP steels", ISIJ International, vol. 35, No.1, 1995, pp79-85

5. **Samajdar I., Girault E.,** "Transformations during intercritical annealing of a TRUP-assisted steel", ISIJ International, vol 38, No.9, 1998, pp998-1006

6. **Garcia C.I., DeArdo A.J.,** "Formation of austenite in low alloy steels", Proceedings of an International Conference on Solid-Solid Phase Transformations, AIME, 1982, pp 855-860

7. **Park, Y.J., Eldis G.T.,** "A dilatometric study of the transformation behavior of intercritically annealed molybdenum and vanadium containing dual phase steels" Proceedings of a symposium on Metallurgy of Continuous Annealed Sheet Steel, AIME, 1982, pp 321-331

8. **Lee C.G., Kim S.J.,** "Effects of heat treatment and Si addition on the mechanical properties of 0.1wt%C TRIP aided cold rolled steels", ISIJ International, Vol.42, No.10, 2002, pg 1162-1168

9. **Tsukatani I., Hashimoto S**., "Effects of silicon and manganese addition on mechanical properties of high-strength hot rolled sheet steel containing retained austenite" ISIJ International, vol 31, No.9, 1991, pp992-1000

10. **Jacques P., Girault E**., "The development of cold-rolled TRIP assisted multiphase steels. Al alloyed TRIP assisted multiphase steels", ISIJ International, vol 41, No.9, 2001, pp1068-1074

11. **DeMeyer M., Vanderschueren D**., "The influence of Al on the properties of cold rolled C-Mn-Si-TRIP steels", Iron and Steel Making, February 2000, pp55-63

12. **Ohmori Y**., "Bainitic Transformations in extremely low carbon steels", ISIJ International, vol 35, No.8, 1995, pp962-968

13. **Vetters H**., "Transformation of austenite into bainitic ferrite and martensite", Steel Research, vol 67, No.10, 1996, pp408-411

14. **Eberle K., Harlet Ph**., "New thermomechanical strategies for the realization of multiphase steels showing a transformation induced plasticity effect", Iron and Steel Making, February 1999, pp 23-27.

15. **Matsumara O., Sakuma Y**., Scripta Materialia, vol 21, 1987, pp1301

16. **Grange R., Stewart H**., "The temperature range of martensite formation", Transactions of the AIME, vol 167, 1946, pp467-490

17. **Speich G., Demarest**., Metallurgical Transactions, vol 12A, 1981, 1419

18. **Bhadeshia H., Edmonds D**., "The mechanism of bainite formation in steels", Acta Metallurgica, vol 28, 1980, pp1265-1273

19. **Bhadeshia H.K., Waugh A**., "Bainite: an atom probe study of the incomplete reaction phenomenon" Acta Metallurgica, vol 30, 1982, pp778-784

20. **Itami A., Takahashi M**., "Plastic stability of retained austenite in the cold-rolled 0.14%C-1.9%Si-1.7%Mn sheet steel", ISIJ International, vol 35, No.9, 1995, pp1121-1127

21. **Sugimoto K., Usui N**., "Effects of volume fraction and stability of retained austenite on ductility of TRIP-aided dual phase steels", ISIJ International, vol 32, No.12, 1992, pp1311-1318

22. **Skrotzki B., Wiech U**., "Influence of austenite strength on martensite start temperature Ms", Steel Research, vol 64, No. 10, 1993, pp509-512

23. **Haidemenopoulos G., Vasilakos A**., "Modelling of austenite stability in low-alloy triple phase steels", Steel Research, vol 67, No.11, 1996, pp513-519

24. **Haidemenopoulos G., Papadimitriou K**., "Retained austenite and mechanical properties in bainite transformed low alloy steels", Steel Research, vol 66, No.10, 1995, pp 433-438.

25. **Sugimoto K., Misu M**., "Effects of second phase morphology on retained austenite morphology and tensile properties in a TRIP-aided dual phase steel sheet", ISIJ International, vol 33, No.7, 1993, pp775-782

26. **Radcliffe S., Schatz M**., Acta Metallurgica, vol 10, 1962, pp201

27. **Vasilakos A., Papamantellos K**., "Experimental determination of the stability of retained austenite in low alloy TRIP steels", Steel Research, vol 67, No.11, 1996

28. **Zarei-Hanzaki A., Yue S**., "Ferrite formation characteristics in Si-Mn TRIP steels", ISIJ International, vol 37, No.6, 1997, pp583-589

29. **Jiao S., Hassani F**., "The effect of processing history on a cold rolled and annealed Mo-Nb microalloyed TRIP steel", ISIJ International, vol 42, No.3, 2002, pp299-303

30. **Leslie WC**, The Physical Metallurgy of Steels, Techbooks, 1981, P295-296

31. **Matsumura O., Sakuma Y**., "Retained austenite in 0.4C-Si-1.2Mn steel sheet intercritically heated and austempered", ISIJ International, vol 23, No.9, 1992, pp1014-1020

32. Reference 18 in: **Sugimoto K., Usui N**., "Effects of volume fraction and stability of retained austenite on ductility of TRIP-aided dual phase steels", ISIJ International, vol 32, No.12, 1992, pp1311-1318

33. **Baik S., Kim S**., "Effects of alloying elements on mechanical properties and phase transformations of cold rolled TRIP steel sheets", ISIJ International, vol 41, No.3, 2001, pp290-297

34. **Tsukatani I., Hashimoto S**., "Effects of silicon and manganese addition on mechanical properties of high-strength hot rolled sheet steel containing retained austenite" ISIJ International, vol 31, No.9, 1991, pp992-1000

35. **DeMeyer M., Vanderschueren D**., "The influence of the substitution of Si by Al on the properties of cold rolled C-Mn-Si- TRIP steels", ISIJ International, vol 39, No.8, 1999, pp813-822

36. **DeMeyer M., Vanderschueren D**., "The influence of Al on the properties of cold rolled C-Mn-Si-TRIP steels", Iron and Steel Making, February 2000, pp55-63

37. **Evans P., Crawford L**., Ironmaking and Steelmaking, vol 24, No.5, 1997, pp361

38. **Parish Chad**, "Fundamental study of phase transformations in Si-Al TRIP steels" M.Sc. Thesis, University of Pittsburgh, 2003

39. **Jacques P., Girault E**., "The development of cold-rolled TRIP assisted multiphase steels. Al alloyed TRIP assisted multiphase steels", ISIJ International, vol 41, No.9, 2001, pp1068-1074

40. **Mahieu J, Maki J, De Cooman BD**, "Hot-Dip Galvanizing of Al Alloyed TRIP Steels," 43rd MWSP Conf Proc, ISS, 2001, P397

41. **Mahieu J, Maki J, De Cooman BD**, " Hot-Dip Galvanizing of Al Alloyed TRIP Steels," Iron & Steelmaker, V29, June 2002, P29

42. **Cullity BD**, Elements of X-Ray Diffraction, 2nd. ed., Addison-Wesley, 1978, pp 411-417

43. **Zarei-Hanzaki A., Hodgson P. and Yue S.,** "Retained Austenite characteristics in Thermomechanically Processed Si-Mn Transformation-Induced Plasticity Steels," Met Trans A, V28A, 1997, P2405

44. **Garcia-Gonzalez Jose E**, M.Sc. Thesis, University of Pittsburgh, 2002

45. **Garcia-Gonzalez J.E., Wu J.,** "Reducing the variability in HSLA steels", 44th MWSP Conference, ISS, Orlando, Fl, 2002

46. **Leslie WC**, The Physical Metallurgy of Steels, Techbooks, 1981, P130

47. **Speich G.R., Miller R.L., "**Tempering of Ferrite-Martensite steels" Fundamentals of Dual Phase Steels, ed by R.A. Kot and B.L Bramfitt, AIME, 1981, pg 300

48. **Speich G.R., Miller R.L., "**Tempering of Ferrite-Martensite steels" Fundamentals of Dual Phase Steels, ed by R.A. Kot and B.L Bramfitt, AIME, 1981, pg 285

49. **Speich G.R.,** "Physical Metallurgy of Dual-Phase Steels" Fundamentals of Dual Phase Steels, ed by R.A. Kot and B.L Bramfitt, AIME, 1981, pg 3-39

50. **Lawson R.D., Matlock D.K., Krauss G**, "The effect of microstructure on the deformation behavior and mechanical properties of a Dual-Phase steel" Fundamentals of Dual Phase Steels, ed by R.A. Kot and B.L Bramfitt, AIME, 1981, pg 355

51. **Garcia C.I., DeArdo A.J.,** "The formation of austenite in low alloy steels" Structure and Properties of Dual-Phase steels, ed by R.A. Kot and J.W.Morris, AIME, 1979, pg 40

52. **Matlock D.K., Krauss G.,** "A correlation of processing variables with deformation behavior of dual-phase steels", Structure and Properties of Dual-Phase steels, ed by R.A. Kot and J.W.Morris, AIME, 1979, pg 62

53. **Gerbase J., Embury J.D.,** "The mechanical behavior of some dual-phase steels with emphasis on the initial work hardening rate", Structure and Properties of Dual-Phase steels, ed by R.A. Kot and J.W.Morris, AIME, 1979, pg 118

54. **Speich G.R., Miller R.L.,** "Mechanical Properties of ferrite-martensite steels", Structure and Properties of Dual-Phase steels, ed by R.A. Kot and J.W.Morris, AIME, 1979, pg 145

55. **Thomas G., Koo J-Y.,** "Developments in strong, ductile duplex ferritic-martensitic steels", Structure and Properties of Dual-Phase steels, ed by R.A. Kot and J.W.Morris, AIME, 1979, pg 183

56. **Eldis George T.,** "The influence of microstructure and testing procedure on the measured mechanical properties of heat treated dual-phase steels", Structure and Properties of Dual-Phase steels, ed by R.A. Kot and J.W.Morris, AIME, 1979, pg 202

57. **Tanaka T., Nishida M.,** "Formation and properties of ferrite plus martensite dual-phase structures", Structure and Properties of Dual-Phase steels, ed by R.A. Kot and J.W.Morris, AIME, 1979, pg 221

58. **Furukawa T, Morikawa H.,** "Process factors for highly ductile dual-phase sheet steels" Structure and Properties of Dual-Phase steels, ed by R.A. Kot and J.W.Morris, AIME, 1979, pg 281

59. **Rigsbee J.M., Abraham J.K.,** "Structure-processing and structure-property relationships in commercially processed dual-phase steels", Structure and Properties of Dual-Phase steels, ed by R.A. Kot and J.W.Morris, AIME, 1979, pg 304

60. **Sun S., Pugh M.,** "Manganese partitioning in dual-phase steel during intercritical annealing" Materials Science and Engineering A276, 2000, pg 167

61. **Sun S., Pugh M.,** "Properties of thermomechanically processed dual-phase steels containing fibrous martensite", Materials Science and Engineering A335, 2002, pg 298

62. **Wu J., DeArdo A.J.,** "Diffraction Pattern Quality: A new application of EBSD to characterize microstructures"

63. **Hillert M.,** "Solute drag, solute trapping and diffusional dissipation of Gibbs energy", Acta Materialia, Vol 47, No. 18, 1999, pg 4481

64. **Ros-Yanez T., Houbaert Y.,** "Characterization of TRIP-assisted multiphase steel surface topography by atomic force microscopy" Materials Characterization, Vol 47, 2001, pg 93

65. **Traint Sandra, Pichler Andreas,** "The influence of Nb on the phase transformations and mechanical properties in Al and Si alloyed TRIP steels" Austenite Formation and Decomposition, Ed. By E.B. Damm and M.J. Merwin, The Iron and Steel Society and TMS, 2003, pg 577

66. **Fletcher H.A., Aaronson H.I.,** "A STEM method for investigating alloying element accumulation at austenite-ferrite boundaries in a Fe-C-Mo alloy" Scripta Materialia 45, 2001, pg 561

67. **Aaronson H.I., Purdy G.R.,** "Tests of the Zener theory of the incomplete transformation phenomena in Fe-C-Mo and related alloys" Scripta Materialia 44, 2001, pg 2425

68. **Yakubovsky O., Fonstein N.,** "Effect of alloying elements on mechanical properties and coatability of multi-phase steels with ferrite-bainite and ferrite-bainite plus retained austenite microstructure" Galvatech '04 Conference Proceedings, 2004, pg 547

69. **Zaefferer S., Ohlert J.,** "A study of microstructure, transformation mechanisms and correlation between microstructure and mechanical properties of a low alloyed TRIP steel", Acta Materialia 52, 2004, pg 2765

70. **Garcia C.I., Parish C., "**Thermomechanical processing challenges in the cold mill", TMP'04, Liege, Belgium, 2004, pg 442

71. **Godet S., Jacques P.,** "Thermomechanical processing of TRIP-assisted multiphase steels" TMP'04, Liege, Belgium, 2004, pg 341

72. **Erdogan M.,** "Effect of austenite dispersion on phase transformation in dual phase steel", Scripta Materialia 48, 2003, pg 501

73. **Berbenni S., Favier V.,** "Micromechanical modeling of the elastic-viscoplastic behavior of polycrystalline steels having different microstructures", Materials Science and Engineering A372, 2004, pg 128

74. **Al-Abbasi F.M., Nemes J.A.,** "Micromechanical modeling of the effect of particle size difference in dual phase steels", International Journal of Solids and Structures 40, 2003, pg 3379

75. **El-Sesy, I.A., El-Baradie Z.M.,** "Influence of carbon and/or iron carbide on the structure and properties of dual-phase steels", Materials Letters 57, 2002, pg 580

76. **Militzer M., Poole W.,** "A critical comparison of microstructure evolution in hot rolled and cold rolled dual phase steels", AHSSS Proceedings, 2004, pg 219

77. **Sherif M.,** "Strain induced transformation of very strong metal" Master of Philosophy Dissertation Thesis, Dept. of Materials Science and Metallurgy, University of Cambridge, 2003

78. **Wu Jinghui**, PhD Thesis Dissertation, Materials Science and Engineering, University of Pittsburgh, 2004

79. **Garcia C.I.**, Personal Communication, 2003

80. **DeMeyer M., Vanderschueren D.,** "The Characterization of Retained Austenite in TRIP Steels by X-Ray Diffraction", 41st MWSP Conf. Proc, ISS, 1999, pp 483-491

81. **Zhao L, Van Dijk NH**, "Magnetic and X-ray Diffraction Measurements for the Determination of Retained Austenite in TRIP Steels," Mat Sci Eng A, VA313, 2001, pp 145-152

82. **Wirthl E., Pichler A.**, "Determination of the Volume Fraction of Retained Austenite in Small Specimens by Magnetic Measurements," Int. Conf. on TRIP-Aided High Strength Ferrous Alloys, ed BC DeCooman, GRIPS, Ghent, 2002, pp 61-64

83. **Brandt ML**, Ph.D. Thesis, Northwestern University, 1997

84. **Speich G.R. and Miller R.L.**, "Hardenability of Austenite After Intercritical Annealing," Proc. Int. Conf. on Solid-Solid Phase Transformations, ed. HI Aaronson, DE Laughlin,RF Selerka and CM Wayman, TMS-AIME, 1981, P843

85. **Militzer M, Pandi R and Hawbolt EB**, "Austenite to Ferrite Transformation Kinetics During Continuous Cooling", Proc. Int. Conf. on Solid-Solid Phase Transformations, ed. WC Johnson, JM Howe, DE Laughlin and WA Soffa, TMS, 1994, P177

86. **Bradley JR, Shiflet GJ and Aaronson HI**, "A Current View of Alloying Element Effects on Growth Kinetics of Proeuctectiod Ferrite in Fe-C-X Alloys," Proc. Int. Conf. on Solid-Solid Phase Transformations, eds. HI Aaronson, DE Laughlin, RF Selerka and CM Wayman, TMS-AIME, 1981, P824-848

87. **Speer JG and Matlock DK**, "Recent Developments in Low-Carbon Sheet Steels," JOM, V54, 2002, P19-24

88. **Porter and Easterling**, Phase Transformations in Metals and Alloys, 2nd ed., Chapman and Hall, London, Chapter 5

89. **Wilson E.**, "The $\gamma \rightarrow \alpha$ transformation in low carbon irons", ISIJ International, vol 34, No.8, 1994, pp615

90. **Brandes E.A.**, Smithells' Metals References Book, 6th ed., Butterworths, London, 1983, Ch. 13

91. **Porter and Easterling**, Phase Transformations in Metals and Alloys, 2nd ed., Chapman and Hall, London, Chapter 2

92. **Shewmon P**, Diffusion in Solids, 2nd ed., TMS, Warrendale, PA, 1989, Chapter 1

93. **Dieter,** Mechanical Metallurgy, McGraw-Hill, 3rd edition, 1986

94. **Krauss G., Thompson S**., “Ferritic Microstructures in continuously cooled low and ultralow carbon steels”, ISIJ International, vol 35, No.8, 1995, pg 937

95. **Andrews K**., “Empirical formula for the calculation of some transformations temperatures”, Journal of the Iron and Steel Institute, July 1965, pg 721

96. **Traint S., Pichler A., Stiaszny P.**, “Silicon and Aluminum in Low Alloyed TRIP Steels,” 44th MWSP Conf. Proc., ISS, 2002, pg 139

97. **LePera F.S.,** “Improved Etching Technique to Emphasize Martensite and Bainite in High-Strength Dual-Phase Steel,” JOM, V32, March 1980, pg 38

98. **Marder A.R. and Benscoter A.O**., “Quantitative analysis of Dual-Phase steels,” Metallography, V15, 1982, pg 73

99. **Marder A.R.**, "Factor affecting the ductility of Dual-Phase alloys”, Formable HSLA and Dual-Phase Steels, ed. AT Davenport, TMS/AIME, 1979, pg 87-98

100. **Colleluori D**., “Improved etching methods for quantitative analysis of HSLA multi-phase steels”, Praktische Metallographie/Practical Metallography, V20, 1983, pg 546

101. **Girault E., Jacques P., Harlet**, “Metallographic methods for revealing the multiphase microstructure of TRIP-Assisted Steels”, Materials Characterization, V40, 1998, pg 111